A Local Complete Active Space 2nd-Order Perturbation Theory Method

Von der Fakultät Chemie der Universität Stuttgart

zur Erlangung der Würde eines Doktors der

Naturwissenschaften (Dr. rer. nat.) genehmigte Abhandlung

Vorgelegt von

Filipe Miguel Cardoso Micu Menezes

aus S. Sebastião da Pedreira

Hauptberichter: Prof. Dr. H.-J. Werner, Universität Stuttgart

Mitberichter: Prof. Dr. A. Köhn, Universität Stuttgart

Prüfungsvorsitzender: Prof. Dr. J. van Slageren, Universität Stuttgart

Tag der mündlichen Prüfung: 08.12.2016

Institut für Theoretische Chemie

der Universität Stuttgart

2016

Contents

Acronyms

%Ecorr Percentage of correlation energy (Ecorr) recovered. 111, 112, 139–143, 145–148, 150, 158, 162, 183, 189, 190, 196, 200

ACCD Approximate Doubles Coupled Cluster (CCD). 25

ACPF Averaged Coupled Pair Functional. 27

AO Atomic Orbital. 21, 22, 24, 25, 33, 34, 39, 40, 46, 51, 56, 57, 60, 65, 97, 114, 129, 135

aug-cc-pV5Z Dunning's correlation consistent augmented quintuple-ζ basis set. 128, 133, 159–161

aug-cc-pVDZ Dunning's correlation consistent augmented double-ζ basis set. 127, 128, 132, 134, 136, 137, 156–164, 166, 196–201

aug-cc-pVQZ Dunning's correlation consistent augmented quadruple-ζ basis set. 128, 133, 134, 159–161, 198, 199

aug-cc-pVTZ Dunning's correlation consistent augmented triple-ζ basis set. 128, 132, 133, 137, 156–163, 166, 196–199

avg(Pair Natural Orbital (PNO)) Average PNO Domain Size. 110–112, 139–141, 145–150, 153–155, 157, 158, 161, 162, 165–167, 173, 174, 183, 184, 191, 192, 197, 201

B3LYP Becke's 3-parameter, Lee-Yang-Parr Functional. 137

C.I. Conical Intersection. 134, 177

CAS Complete Active Space. 18, 20, 47, 48, 65, 67, 69, 79, 80, 84, 115, 117, 127, 132–137, 165, 167

CASPT Complete Active Space Perturbation Theory. 19, 67

CASPT2 Complete Active Space 2^{nd}-order Perturbation Theory. 6, 8, 9, 11–15, 19–22, 28, 65–69, 72, 74, 75, 78–80, 91, 108–110, 113, 117, 123, 126, 129, 139, 142, 154–156, 165, 167, 169, 176, 178–180

CASPT3 Complete Active Space 3rd-order Perturbation Theory. 20, 78

CASSCF Complete Active Space Self-Consistent Field. 18, 19, 46–48, 65, 67, 69, 70, 97, 117, 125, 127–129, 134, 138, 159, 165–169, 179, 180

CC Coupled Cluster. 17, 24, 26, 27, 38, 39, 44, 46, 69, 156, 165

cc-pVDZ Dunning's correlation consistent double-ζ basis set - cc-pVDZ. 128, 135, 136, 166

cc-pVTZ Dunning's correlation consistent triple-ζ basis set - cc-pVTZ. 128, 135, 166

CCD Doubles Coupled Cluster. 4, 21, 25

CCSD Singles Doubles Coupled Cluster. 6, 21, 24–27, 46, 72, 77, 91, 94, 154–157

CCSD(T) Singles Doubles Coupled Cluster with Perturbative Treatment of Triples. 21, 24–27, 128, 156

CCSDT Singles Doubles Triples Coupled Cluster. 21

CEPA Coupled Electron Pair Approximation. 24–27

CI Configuration Interaction. 17, 23, 26, 27, 38–42, 44, 46–50, 69, 83, 114, 125, 129

CIPT2 Configuration Interaction Perturbation Theory 2. 79

CISD Singles Doubles Configuration Interaction. 8, 21, 25, 27, 40

CISDT Singles Doubles Triples Configuration Interaction. 40

CISDTQ Singles Doubles Triples Quadruples Configuration Interaction. 21

CP Cyclopentadienyl. 135

CSF Configuration State Function. 46, 47, 65, 66, 70–73, 75, 78–80, 83, 110, 115

CW Celani-Werner. 9, 79, 110, 127, 129

def2-tzvp Ahlrichs triple-ζ basis sets with polarization. 128, 132, 135–137, 162–164, 199–201

DF Density Fitting. 20, 26–28, 55–57, 93, 115, 117, 125, 128, 136

DIIS Direct Inversion of the Iterative Subspace. 49, 126

Ecorr correlation energy. 4, 112, 139, 141, 142, 146, 147, 149, 154, 157, 158, 161–164, 173, 175, 192–194, 198, 199

ECP Effective Core Potential. 135

EOM-CCSD Equation of Motion Singles Doubles Coupled Cluster (CCSD). 26

ES Excited State. 17, 21, 37, 40, 45, 49, 112, 129, 133, 135, 137–142, 145–148, 150, 176, 189–191, 193, 194, 196, 197, 200, 201

FCI Full Configuration Interaction. 18, 20, 40, 46–48, 69, 72, 75

FORS Full Optimized Reaction Space. 47

GMP Generalized Møller-Plesset Theory. 66, 72

GS Ground State. 17, 21, 35, 37, 40, 45, 49, 65, 108, 112, 128, 129, 133, 136–142, 145–148, 150, 151, 157, 167, 170, 172, 174–176, 189–193, 196, 197, 200, 201

HF Hartree-Fock. 17, 21, 22, 32–39, 42, 44–47, 50, 60, 127, 128, 136, 137, 165

HOMO Highest Occupied Molecular Orbital. 17, 44, 45

IAO Intrinsic Atomic Orbital. 51, 52

IBO Intrinsic Bond Orbital. 11, 13, 14, 24, 51, 52, 61, 94, 115, 125, 127–129, 135–137, 165, 167, 178

ic-CASPT2 Fully Internally-Contracted Complete Active Space 2^{nd}-order Perturbation Theory (CASPT2). 109, 125, 137–139, 141, 150, 152–154, 156, 159, 164, 168–170, 172–174

ICC Internally-Contracted Configuration. 66, 72–80, 83, 91, 110, 127, 138, 178

ICMRCC Internally Contracted Multireference Coupled-Cluster. 72

ICMRCI Internally Contracted Multireference Configuration Interaction. 72

IEPA Independent Electron Pair Approximation. 26

ITF Integrated Tensor Framework. 7, 29, 109, 110, 113, 114, 118–125

LCAO Linear Combination of Atomic Orbitals. 33

LCASPT2 PNO-Projected Atomic Orbital (PAO) Local Complete Active Space 2^{nd}-order Perturbation Theory. 10–15, 28, 29, 65, 80, 84, 94, 97, 99, 103, 108–115, 118–120, 123–125, 127–131, 135, 136, 139, 141–143, 145, 146, 148, 150–158, 162, 165–175, 178–180

LDF Local Density Fitting. 26, 64, 97

LITF Local Integrated Tensor Framework (ITF). 29, 109, 119, 121, 170, 171

LMO Localized Molecular Orbital. 50–53, 56, 57, 60, 94, 97, 117

LOVO Localized Orthogonal Virtual Orbital. 24, 28

LUMO Lowest Unoccupied Molecular Orbital. 17, 44, 45

LVO Localized Virtual Orbital. 24

MCSCF Multi-Configuration Self-Consistent Field. 18, 21, 28, 44, 46–50, 67, 114, 115, 125, 128, 136

MO Molecular Orbital. 21, 32–35, 39, 42, 49–51, 56, 65, 83, 97, 114, 127, 195

MP Møller-Plesset Perturbation Theory. 17, 18, 25, 42, 44, 67, 89

MP2 Second-Order Møller-Plesset Perturbation Theory. 17, 20, 21, 24–27, 43, 44, 53, 59, 62, 65, 69, 91, 94, 117, 127, 128, 150, 154, 156, 157

MP3 Third-Order Møller-Plesset Perturbation Theory. 21, 27, 44

MP4 Fourth-Order Møller-Plesset Perturbation Theory. 21, 26, 44

MPA Multipole Approximation. 12, 15, 26, 28, 57, 59, 60, 92, 116, 126, 129, 164–170, 179

MPn n^{th}-order Møller-Plesset Perturbation Theory. 24, 42, 44

MR Multireference. 11, 12, 14, 17–20, 22, 27–29, 44–46, 65, 69, 72, 75, 76, 78, 82, 91, 92, 99, 119, 136, 155, 156, 165, 178

MR-MP Multireference-Møller-Plesset. 19, 66

MRCC Multireference Coupled Cluster. 21, 27, 28, 44

MRCI Multireference Configuration Interaction. 20, 22, 24, 27, 28, 44, 70, 72, 75, 78, 79

MRPT Multireference Perturbation Theory. 11, 12, 18–20, 42, 44, 65, 66

MS-CASPT2 Multi-State CASPT2. 20, 70, 72

NEVPT N-Electron Valence state Perturbation Theory. 19, 27, 28, 66, 72, 167

OLED Organic Light-Emitting Diode. 133

OSV Orbital Specific Virtual. 23, 24, 28, 52, 53, 57, 94, 97

PAO Projected Atomic Orbital. 7, 8, 10–15, 23–29, 52, 53, 55–57, 60–65, 94–99, 102, 109, 110, 113–124, 126, 137, 139–144, 146, 151, 154, 157, 166, 168, 170, 173, 175, 178, 190, 192–194

PAO(SC) SemiCanonical PAO. 62, 64, 95, 98, 102, 109, 115, 117, 118

PES Potential Energy Surface. 17, 20, 22, 31, 35, 37, 45, 64, 69, 127, 134, 136, 151, 172–177

PNO Pair Natural Orbital. 4, 7, 8, 10–15, 23, 24, 26–29, 52, 53, 55, 62–65, 82, 84, 91, 93, 94, 96–99, 102, 103, 109–114, 117–124, 126, 137, 139–150, 153–155, 157, 158, 161–163, 165–167, 170, 171, 173, 174, 178, 179, 183, 184, 191, 192, 197, 199, 201, 202

PNO(SC) SemiCanonical PNO. 64, 96, 109, 118

PT Perturbation Theory. 17, 18, 22, 24, 38, 41, 44, 45, 52, 67, 72, 107, 156

QCISD Quadratic Singles Doubles Configuration Interaction (CISD). 21, 25–27

QCISD(T) Quadratic CISD with Perturbative Treatment of Triples. 27

RAS Restricted Active Space. 48

RASSCF Restricted Active Space Self-Consistent Field. 48, 69

RHF Restricted Hartree-Fock. 17, 35

ROHF Restricted Open-Shell Hartree-Fock. 35

RS2C Celani-Werner (CW)-CASPT2. 110–112, 123, 125, 126, 128, 137, 138

RSPT Raylaeigh-Schrödinger Perturbation Theory. 42

SCF Self-Consistent Field. 21, 50

SD Slater Determinant. 33, 39, 45, 70, 71

SR Single-Reference. 11, 12, 14, 17, 18, 20, 22, 27–29, 37, 39, 44, 45, 69, 75, 76, 91, 92, 94, 96, 119, 154–156, 165

TNO Triples Natural Orbital. 27

TS Transition State. 45, 132, 134, 177

UHF Unrestricted Hartree-Fock. 17, 35

WK Werner-Knowles. 78, 79

XMS-CASPT2 eXtended Multi-State CASPT2. 20, 78

Acknowledgements

First and foremost I wish to thank my advisor, Prof. Dr. Hans-Joachim Werner. Being his doctoral student allowed me to take part in the state of the art in method development for theoretical chemistry. His dedication to this work and his knowledge made my experience at the Institute for Theoretical Chemistry of the University of Stuttgart most intellectually enriching. I am also most thankful to Dr. Daniel Kats for all his support and anchoring in many moments of my Ph.D.. Definitely, his knowledge, skills, patience and calm eased all stages of this work, specially in the derivation of all the mathematical expressions and in the whole implementation of the PNO-PAO Local Complete Active Space 2^{nd}-order Perturbation Theory (LCASPT2) method. Without Prof. Dr. Hans-Joachim Werner and Dr. Daniel Kats this work would surely have not been possible. I also wish to give a special thank You to my colleagues Dr. Christoph Köppl, Christine Krause, Oliver Marchetti, Filipe Agapito and David Kreplin. More than just colleagues, I am sure they became friends for life. I wish also to express my gratitude to all my other colleagues at the Institute. To Fundação para a Ciência e Tecnologia I must definitely thank all the financial support provided via the scholarship SFRH/BD/72132/2010.

Secondly I can but only be grateful for all the love, emotional and personal support that my family gave me, namely my beloved wife Alecsandra, whom I met during this Doctoral Program and gave me but joy and happiness in our lives together and our son Patrick; my parents Rui and Rosa, my dear sister Ana and my parents in law Florea and Maria. Without their love and encouragement in the moments of doubt, I would surely have not been here in this moment.

Last but not least I want to thank all my friends and people that were model to me and for my personal development. I want to thank specially Jan Trachte and his family for receiving me at their own home as one long beloved friend, just like for all the nights I spent at Martin Dreizler's: they all offered me their full support and friendship. I am also grateful for all the good and relaxing times I had in the most friendly environment with Jan Trachte, Martin Dreizler and Wasilios Zmitas. This section could not possibly be complete without a special thank Dr. Karl Gfesser, Dr. Stefan Warthmann and Per Protoschill, not only for their unique friendship but especially for the intellectual discussions only they could provide, being surely some of my intellectual role models.

1. Abstract

1.1 English

Ever since the pioneering work of Pulay in local correlation (*1*), a wide spectrum of local variants of Single-Reference (SR) methods appeared. Local methods aim at reducing the computational costs of electron correlation methods with the minimal loss in accuracy possible. Many choices of local virtual orbitals were used and for almost all classes of methods a local variant was implemented. This allowed the significant reduction of the scaling of computational resources with the molecular size. Of particular relevance is the work of Werner and Schütz in the development of the first linear scaling electron correlation methods using Projected Atomic Orbitals (PAOs) (*2, 3*), and the similar work of Neese *et al.* with Pair Natural Orbitals (PNOs) (*4*). On the other hand, local variants of Multireference (MR) methods were barely explored. Even though the scaling of MR and SR methods with the molecular size is affected by the same exponents, the pre-factors of this scaling are larger for MR methods. MR methods are therefore computationally more demanding than SR methods and exploring the effects of local approximations can become more meaningful. This exploration began only recently, and only now are available the first local MR methods. In this work we present the development and implementation of a local linear scaling variant of a Multireference Perturbation Theory (MRPT) method, CASPT2. Our method was named PNO-PAO Local Complete Active Space 2^{nd}-order Perturbation Theory (LCASPT2) and like the parent canonical method can be used to calculate reaction and excitation energies. Because of the reduction of the computational costs, we extended until now the applicability of the CASPT2 level of theory to more than 230 atoms and 4175 basis functions. This molecular size is unthinkable to the canonical method at the current state of the art technology.

The LCASPT2 method uses Intrinsic Bond Orbitals (IBOs) for the closed-shell and active spaces, even though after orthogonalizing the configuration subspaces the localized structure of active orbitals is no longer explored. Two choices of local virtuals are used: all configuration subspaces are initially transformed to the PAO basis; a few of these configuration subspaces are then transformed to the PNO basis. Using PAOs as an intermediate step before generating PNOs contributes to reduce the computational cost of obtaining the PNOs. In both cases we use domain approximations to reduce the size of substitution spaces for each type of configuration. We build specific PAO domains for

each closed-shell orbital but a common PAO domain for all active orbitals. For the case of PNOs, occupation numbers and an energy consistency threshold are used to build the domains. Pair approximations are also employed, and three types of pairs are distinguished: normal pairs, without any kind of approximation; distant pairs, for which it is possible to apply the Multipole Approximation (MPA); very distant pairs, which can be neglected.

Using the default options for the PAO and PNO domains builds local substitution spaces for orbital pairs with typically 40 to 60 PNOs. In these conditions LCASPT2 recovers almost 99.9% of the canonical correlation energy. In average, absolute errors of 2.1 meV are introduced by the local treatment in excitation energies. For reaction energies, LCASPT2 with the default options differs by around 0.42 $kcal.mol^{-1}$ with respect to the canonical case. Smaller domains for both PAOs and PNOs can also be used for larger systems. The accuracy is slightly affected (*e.g.*, smaller PAO domains can double the average absolute errors in excitation energies) and a larger variance is observed in the results.

1.2 Deutsch

Seit der Pionierarbeit von Pulay in lokaler Korrelation (*1*) ist ein weitreichendes Spektrum an lokalen Single-Reference (SR) Methoden erschienen. Lokale Methoden zielen darauf ab, den Rechenaufwand von Elektronenkorrelationsmethoden mit nur einem minimalen Verlust an Genauigkeit zu reduzieren. Dabei wurden viele Arten von lokalen virtuellen Orbitalen entwickelt und für fast alle Methoden wurde eine lokale Variante implementiert. Dadurch wurde die Skalierung der Rechenzeit mit der Molekülgrösse deutlich reduziert. In der Entwicklung der ersten linear skalierenden Elektronenkorrelationsmethoden ist die Arbeit von Werner und Schütz von besonderer Bedeutung (*2,3*), die Projected Atomic Orbitals (PAOs) benutzen, sowie die Arbeit von Neese *et al.* mit Pair Natural Orbitals (PNOs) (*4*). Allerdings wurden lokale Varianten von Multireference (MR) Methoden bislang kaum betrachtet. Auch wenn die Skalierung mit der Molekülgrösse für MR und SR Methoden vom gleichen Exponenten abhängt, so ist doch der Vorfaktor für MR Methoden grösser. Da MR Methoden rechnerisch anspruchsvoller sind, ist es demnach bedeutsam, die Effekte lokaler Näherungen genauer zu betrachten. Damit wurde erst kürzlich begonnen, sodass neuerdings die ersten lokalen MR Methoden verfügbar sind. In dieser Arbeit präsentieren wir die Entwicklung und Implementierung einer lokalen linear skalierenden Variante der Multireference Perturbation Theory (MRPT) Methode, CASPT2. Unsere Methode nennt sich PNO-PAO Local Complete Active Space 2$^{\text{nd}}$-order

Perturbation Theory (LCASPT2) und kann wie die vorrangegangene kanonische Methode verwendet werden, um Reaktions- und Anregungsenergien zu berechnen. Aufgrund der Verringerung des Rechenaufwandes haben wir jetzt die Anwendbarkeit von CASPT2 auf bis zu 230 Atome und 4175 Basisfunktionen erweitert. Diese Molekülgrösse war bis dato mit der kanonischen Methode und dem aktuellen Stand der Technik bis datum unberechenbar.

Die LCASPT2 Methode verwendet Intrinsic Bond Orbitals (IBOs) für den besetzten und aktiven Raum, auch wenn nach Orthogonalisierung des Konfigurationsunterräumes die lokalizierte Struktur der aktiven Orbitale nicht mehr benutzt wird. Dabei wurden zwei Varianten von lokalen virtuellen Orbitalen verwendet: zunächst werden alle Konfigurationsunterräume in die PAO Basis transformiert; dann wird ein Teil der Konfiguratonsunterräume weiter in die PNO Basis übertragen. Mithilfe dieses Zwischenschritts, der Verwendung von PAOs vor dem Erzeugen der PNOs, wird die Rechenzeit reduziert. In beiden Fällen verwenden wir die Domänennäherung, um die Grösse des Anregungsraumes für jedes Orbitalenpaar zu reduzieren. Wir erzeugen für jedes besetzte Orbital spezifische PAO Domänen, aber nur eine gemeinsame PAO Domäne für alle aktiven Orbitale. Im Falle von PNOs werden die Besetztungszahlen und ein Energiekriterium als Grenzwerte für die Domänenselektion verwendet. Außerdem werden Paarnäherungen verwendet. Dabei wird zwischen drei Arten von Paaren unterschieden: *normal pairs*, ohne jede Art von Näherung; *distant pairs*, für die es möglich ist, eine Multipolnäherung (MPA) zu verwenden; *very distant pairs*, welche vernachlässigt werden können.

Durch die Verwendung der *default* Optionen für die PAO und PNO Domänen erhält man normalerweise Unterräume für die Orbitalpaare mit 40 bis 60 PNOs. Unter diesen Umständen gibt LCASPT2 99.9% der kanonischen Korrelationsenergie wieder. Im Durchschnitt beträgt der absolute Fehler bei der lokalen Berechnung von Anregungsenergien 2.1 meV. Für Reaktionsenergien liegt die Abweichung von LCASPT2 mit *default* Optionen zur kanonischen Methode bei 0.42 $kcal.mol^{-1}$. Werden kleinere Domänen für PAOs und PNOs für grössere Systeme verwendet, kann eine grössere Varianz in den Ergebnissen beobachtet werden (z.B. können kleinere PAO Domänen den durchschnittlichen absoluten Fehler in den Anregungsenergien verdoppeln), obwohl die Genauigkeit dadurch nur geringfügig beinträchtigt ist.

1.3 Português

Após o trabalho pioneiro de Pulay no desenvolvimento de aproximações locais em correlação electrónica (*1*) surgiu um amplo espectro de variantes locais de métodos *Single-Reference* (SR). O objectivo destes métodos locais é a redução dos custos computacionais no cálculo de energias de correlação electrónica sem afectar significativamente a exactidão dos resultados. Diversas escolhas para orbitais virtuais locais foram usadas e para quase todas as classes de métodos foi implementada uma variante local que permitiu reduzir consideravelmente o escalar de recursos computacionais com as dimensões dos sistemas a estudar. De especial relevância é o trabalho de Werner e Schütz no desenvolvimento dos primeiros métodos de correlação eletrónica com escalar linear usando para tal orbitais atómicas projectadas (PAOs) (*2, 3*), bem como o trabalho de Neese e colaboradores com orbitais naturais para pares (PNOs) (*4*). No entanto, variantes locais de métodos *Multireference* (MR) permaneceram praticamente inexploradas. Ainda que o escalar de teorias MR e SR com as dimensões moleculares seja influenciada pelos mesmos expoentes, os pré-factores são significativamente maiores para métodos MR. Estes são portanto computacionalmente muito mais exigentes, tornando ainda mais relevante a exploração de aproximações locais. Esta pesquisa teve início recentemente, estando só agora disponíveis as primeiras variantes locais de métodos MR. Neste trabalho apresentamos o desenvolvimento e a implementação de uma variante local da teoria de perturbações de segunda ordem aplicada a uma referência *Complete Active Space* (CASPT2). O método aqui desenvolvido, *PNO-PAO Local Complete Active Space* 2^{nd}*-order Perturbation Theory* (LCASPT2), apresenta escalar praticamente linear para todos os recursos computacionais. Tal como o método parente (com orbitais canónicas), o LCASPT2 pode ser utilizado no cálculo de energias de reacção e de energias de excitação electrónica. Devido à redução significativa do custo computational torna-se possível usar a teoria CASPT2 em sistemas com mais de 230 átomos e 4175 funções de base, dimensões moleculares até à data impensáveis para estes métodos usando a tecnologia actual.

O método LCASPT2 recorre a orbitais intrínsicas de ligação (química), IBOs. Estas são utilizadas tanto para o espaço de orbitais de camada fechada como para o espaço de orbitais activas, ainda que após a ortogonalização dos subespaços de configurações a estrutura localizada das orbitais activas não possa mais ser explorada. Duas escolhas de orbitais virtuais locais são usadas: todos os subespaços de configurações são inicialmente transformados para uma base de PAOs; alguns destes subespaços de configurações são posteriormente transformados para uma base de PNOs. Recorrendo a uma transformação

intermediária para a base de PAOs permite reduzir o custo computacional para gerar a base de PNOs. Tanto no caso das PAOs como para as PNOs utilizam-se aproximações nos domínios das orbitais para diminuir as dimensões dos espaços de substituição de cada tipo de configuração excitada. Para tal, constroem-se domínios de PAOs específicos para cada orbital da camada fechada e um domínio comum para todas as orbitais activas. Para o caso das PNOs os domínios para os pares de orbitais são construídos com base em números de ocupação e num critério de consistência energética. Aproximações nos pares de orbitais são também exploradas. Para tal distinguimos três classes distintas de pares: pares normais, sem qualquer tipo de aproximação; pares distantes, para os quais é possível utilizar a aproximação multipolar (MPA); pares muito distantes, os quais podem ser desprezados do tratamento.

Recorrendo às opções *default* para os domínios de PAOs e PNOs o método LCASPT2 constrói espaços de substituição com tipicamente 40 a 60 PNOs. Nestas condições é possível recuperar quase 99.9% da energia de correlação do respectivo método canónico. Em média observam-se desvios por excesso de 2.1 meV em energias de excitação. Para energias de reacção observámos para as mesmas condições erros de 0.42 $kcal.mol^{-1}$ face ao CASPT2 canónico. Para sistemas maiores é possível reduzir os domínios das PAOs sem grandes consequências na exactidão: erros absolutos em energias de excitação duplicam e a variância aumenta.

The main results of this work were published in:

F. Menezes, D. Kats, and H.-J. Werner, *J. Chem. Phys.*, Vol. 145(12), 124115, **2016**

2. Introduction

In theoretical chemistry, *ab initio* refers to methods built from first principles. The results are independent of any experimental data. These methods involve specific approximations, which determine their accuracy. The field of theoretical chemistry aims at improving theoretical methods while simultaneously minimizing their computational cost.

One of the most popular methods in Single-Reference (SR) theoretical chemistry is Second-Order Møller-Plesset Perturbation Theory (MP2) (*5*). This has mostly to do with its relatively low computational costs (*6, 7*), as it is the most economical SR electron correlation method available. Although not the most accurate of methods (*8*), MP2 estimates well correlation effects. MP2 can be formulated non-iteratively (*9*) and brings together two desired qualities in quantum chemical methods (*6, 10–12*): size consistency and size extensivity. Configuration Interaction (CI), another possibility to treat electron correlation, is neither size consistent nor size extensive and Coupled Cluster (CC) is not variational. Furthermore, both CI and CC are computationally much more expensive than MP2 (*13*). MP2's comfort zone is for non-degenerate Ground States (GSs) of closed-shell systems with a wide HOMO-LUMO gap (Highest Occupied Molecular Orbital (HOMO); Lowest Unoccupied Molecular Orbital (LUMO)) (*14, 15*). The reference is a Restricted Hartree-Fock (RHF) wavefunction. Open-shell systems can also be treated at the MP2 level using an Unrestricted Hartree-Fock (UHF) reference (*16, 17*). The main problem is an undesired spin-contamination already from the reference (*18–22*), which also affects the convergence of UMP2 negatively (*12, 13, 23*). The spin contamination complication can be overcome using spin projected (*24–27*) or spin-adapted formulations (*28–38*). Nevertheless, all MP2 variants are restricted to wavefunctions with strong SR character. When systems gain Multireference (MR) character, the Hartree-Fock (HF) reference becomes less suitable: it no longer is the dominant configuration in the wavefunction. Typical cases range from some GSs (*e.g.* ozone, organometallic complexes) to Excited States (ESs) or to systems at dissociation limits. Since the reference loses its quality, Perturbation Theory (PT) corrections become unreliable (*20, 29, 30, 34, 37, 39, 40*). The result is that the Møller-Plesset Perturbation Theory (MP) series begins to lose its convergence properties (*10*). With multi-configurational references, PT regains its attractive properties and the total electronic correlation is kept balanced over full Potential Energy Surfaces (PESs) (*9, 40–44*), from minima up to dissociation, as well as for any electronic state.

The multi-configurational reference with the basic qualitative description for MR sys-

tems is calculated using the Multi-Configuration Self-Consistent Field (MCSCF) theory (*45–47*). In MCSCF the most relevant configurations to introduce strong correlation in a wavefunction are included. The results are qualitatively correct, but not quantitatively. Even though MCSCF includes many different approaches, now-a-days the most widely used is the Complete Active Space Self-Consistent Field (CASSCF) (*48–52*). Here, orbitals are partitioned into three spaces (*46*): closed-shell, with doubly occupancy; virtual, always empty; active, with variable occupation numbers. A specific combination for the dimensions of these orbital sets builds a Complete Active Space (CAS) reference. The CAS includes all configurations arising from all possible substitutions within the active space. This ansatz may include configurations with minor or negligible contribution to the wavefunction, but due to its Full Configuration Interaction (FCI) character (*45*), special techniques may be used to simplify the computational effort.

The first MRPT methods were developed by Bloch and Horowitz (*53, 54*), (*55*), and Kelly (*56*) in the 50's and 60's. One of the biggest challenges in MRPT was the generalization of the zeroth-order Hamiltonian from MP (*15, 39*). The pillar upon which PT is built, is the search of an approximate solution to a problem having as starting point the exact solution of a similar but simpler problem. The zeroth-order Hamiltonian defines the problem with the exact solution, while the perturbation term allows the calculation of the approximate solution to the problem one wishes to solve. Any ambiguity or ill-definition of the zeroth-order Hamiltonian may determine the lack of success of the method (*9,13,40,57*). And this is indeed the source of most errors (*58*). In MP theory, the zeroth-order Hamiltonian is the sum of one-electron Fock operators (*5*). Attempts were made to outperform this choice, but none actually achieved any improvement (*56, 59–61*). Likewise, when generalizing to the MR case, the zeroth-order wavefunction should be an eigenfunction of the zeroth-order Hamiltonian (*57, 62, 63*). It should furthermore be fast convergent (*39, 58*), equivalent to the MP Hamiltonian for the SR limit (*12, 39, 64*) and it should be orbital invariant (*57, 62, 63*).[1] In general, the zeroth-order Hamiltonian for MR theories is non-diagonal in the configuration basis and built from non-diagonal Fock matrices (*65*). As showed by Pulay and Sæbø (*8*), it is possible to reformulate MP with orbitals other than canonical and with non-diagonal zeroth-order Hamiltonians (*13, 57, 66, 67*). The zeroth-order Hamiltonian is still the sum of one-electron Fock operators (*66*), but the orbitals are no longer in the main diagonal of the Fock matrix. The results are equivalent (*8, 68*) but at the price of a slight increase of the computational cost:

[1] For an orbital invariant method, using two different types of orbitals gives the exact same result.

analytical solutions are no longer directly found (*14*) and the solution must be sought iteratively (*8, 57, 66, 68*). Non-diagonal zeroth-order Hamiltonians can however be brought to block diagonal forms (*14*). For these cases, convergence is rapidly achieved and each iteration has a low computational cost. In contrast, there are also methods with diagonal zeroth-order Hamiltonians. This diagonality stems from diagonal Fock matrices, either in the orbital basis, or from both in the orbital and in the configuration bases. These methods are however not orbital invariant (*57*). For these cases, the methods additionally depend on the definition of the configuration spaces. Given the possible choices for the zeroth-order Hamiltonian in the MR case, different variants of MRPT were proposed and implemented. References for some of the most relevant work in the field can be found in (*9, 12, 13, 23, 40–42, 44, 57, 69–73*).

From the whole spectrum of MRPT methods that were developed, now-a-days only CASPT, N-Electron Valence state Perturbation Theory (NEVPT) and Multireference-Møller-Plesset (MR-MP) are still in use (*63*). Of these, CASPT enjoys perhaps greater popularity (*74*). In this work, local approximations were applied to CASPT2.

The first version of CASPT2 was proposed by Roos in 1982 (*58*). It was built to be a non-iterative reduced perturbative treatment to account for dynamic correlation after a CASSCF calculation (*58*). The wavefunction included initially only pairs (*58*) and the zeroth-order Hamiltonian was built from a Fock operator diagonal in the orbital basis. The latter was multiplied to the left and to the right by projectors to the reference space and its orthogonal complement (*58*). These projections made the zeroth-order Hamiltonian diagonal in the configuration basis. Around equilibrium geometries, the method provided good estimates for basic properties of chemical systems, *e.g.*, excitation energies, but dissociation processes of chemical bonds were poorly represented (*39, 58, 63*). This was related to the absence of singles in the first-order wavefunction (*58, 63*).

In the first improvement the singles and the internals were added to the first-order wavefunction (*39*). The zeroth-order Hamiltonian was also changed from diagonal to block diagonal with respect to configuration subspaces (*39*). Thus, the interaction between different configuration subspaces was neglected, but interactions within each configuration subspace were considered (*39*). The Fock matrix in the zeroth-order Hamiltonian was partitioned in two different terms (*39*): diagonal elements were used in the zeroth-order Hamiltonian; off-diagonal terms were collected in the perturbation operator. This new version of CASPT2 improved total energies but was still not absolutely satisfactory for energy differences (*39*). The method was thus once more improved by skipping the partitioning of the Fock matrix and by making the zeroth-order Hamiltonian non-diagonal in

the configuration basis. This became the modern version of CASPT2 (*64*).

For systems with high SR character, CASPT2 offers but only minor differences with respect to MP2. However, for strong MR cases like Ozone, differences are not negligible (*64*). CASPT2 behaves with fair accuracy when compared to Multireference Configuration Interaction (MRCI) or even FCI (*64*). The great advantage is that CASPT2's computation time can take down to 20% of the calculation time of MRCI (*42*). In the current literature there is already an unsurmountable amount of applications of CASPT2. To mention a few, we can refer the reader to the references (*64, 75–86*). These are but very few examples, including mostly excitation energies, some transition metal chemistry and PES with special focus on avoided crossings. While for the first two cases CASPT2 enjoys success and good potential (*64, 81, 83, 86, 87*), for PES with avoided crossings the performance is somewhat far from ideal (*88–90*). Furthermore, CASPT2 suffers from the intruder state problem. This occurs whenever the state of interest mixes strongly with a state from the secondary CAS, shifting excitation energies or even causing divergence (*57, 63, 91*).

To overcome the liabilities for avoided crossings, Finley, *et al.* proposed a multi-state extension to CASPT2, Multi-State CASPT2 (MS-CASPT2) (*89*). The theory extends CASPT2 to multidimensional reference spaces spanned by $N > 1$ states. In MS-CASPT2 an effective Hamiltonian is perturbed and then diagonalized to allow all the states to interact (*89*). The zeroth-order Hamiltonian is separated into contributions from each reference. The projector to the reference space becomes the sum of projectors to all references, which build a diagonal Fock matrix in each reference space. The diagonal of the effective Hamiltonian gives CASPT2 energies for the N states used. MS-CASPT2 was later generalized to include non-diagonal Fock matrices in the reference space, eXtended Multi-State CASPT2 (XMS-CASPT2) (*74, 92, 93*).

More recently, Cholesky decomposition (*94, 95*) and Density Fitting (DF) approximations (*96*) were applied to CASPT2 to improve both the efficiency and applicability of the method. Finally, the explicitly correlated variants of CASPT2 should be mentioned (*93, 97–100*), which significantly improve the basis set convergence of CASPT2. Explicitly correlated methods aim at overcoming the incompleteness of basis sets by including in the wavefunction terms which depend directly on the inter-electronic distance (*101–106*). However, to improve the inherent accuracy of the method, higher orders in perturbation are required. Complete Active Space 3$^{\text{rd}}$-order Perturbation Theory (CASPT3) is available, but it is already extremely expensive. Even higher orders in MRPT are not frequently mentioned and might not even bring better results (*10*). Alternatively, at a similar cost of CASPT3 but with better accuracy there is still MRCI (*43, 98, 99, 107–120*)

and Multireference Coupled Cluster (MRCC) (*121–130*). Furthermore, analytical gradients are available for CASPT2, both for the single- and multi-state variants of the theory. This allows the geometry optimization and the calculation of first-order properties for both GSs and ESs (*62, 74, 96*).

Electron correlation methods are typically formulated in the canonical or natural orbital bases. Canonical orbitals emerge from Self-Consistent Field (SCF) calculations (HF or MCSCF), and in this basis the closed-shell and the external blocks of the Fock matrix are diagonal. Since no other restriction is imposed, canonical Molecular Orbitals (MOs) are delocalized through molecules (*65, 131, 132*). For pair theories, the correlation energy may be partitioned according to orbital pairs. The number of pairs to correlate scale quadratically with the system's size, and so does the number of orbitals in substitution spaces. This yields a minimum scaling[2] of $\mathcal{O}(M^4)$ for electron correlation methods (*133*). Adding the high tensor rank of the mathematical objects needed, an unphysically steep increase of computational costs with the molecular size is created. The most economical electron correlation method, MP2 (*5*), has a scaling of CPU times already of $\mathcal{O}(M^5)$ with the molecular size M (*1, 2, 6, 132*). These costs arise from the integral transformation to the MO basis (*2*). Using the sparsity of the Atomic Orbital (AO) integral list reduces these costs by almost one order of magnitude (*2*). Other methods including at most double substitutions from the reference[3] scale typically with $\mathcal{O}(M^6)$ (*2, 6, 7, 133–137*), *e.g.*, CISD, CCSD, CCD, Quadratic CISD (QCISD), Third-Order Møller-Plesset Perturbation Theory (MP3), Fourth-Order Møller-Plesset Perturbation Theory (MP4). Any further order of substitution added increases the scaling by two orders of magnitude. Therefore, including triple substitutions raises the scaling to $\mathcal{O}(M^8)$ (*6, 137, 138*) (*e.g.*, Singles Doubles Triples Coupled Cluster (CCSDT)), while introduction of quadruples raises the scaling to $\mathcal{O}(M^{10})$ (*6, 138*) (*e.g.*, Singles Doubles Triples Quadruples Configuration Interaction (CISDTQ)). The exponent of the computational costs due to the introduction of triples can be reduced by one, to $\mathcal{O}(M^7)$, if a perturbative treatment of these is used (*2, 3, 6, 66, 133, 139*). Typical examples are MP4 with triples or quantum chemistry's "Gold Standard", Singles Doubles Coupled Cluster with Perturbative Treatment of Triples (CCSD(T)).[4] Going be-

[2]The scaling of a method is measured from the most expensive tensor contraction operation. These involve typically dimensions of different quantities, *e.g.*, the Atomic Orbital (AO) basis, the orbital spaces. For simplification we transformed these dimensions to a general variable M.

[3]Single substitutions are usually included as their computational costs are negligible when compared to the cost of doubles.

[4]If HF provides a good reference, for large enough basis sets, CCSD(T) can predict reaction energies within chemical accuracy (*3*).

yond triple substitutions for systems with amenable dimensions is not common. Doubling the system's size in a method which includes up to triple substitutions represents 128 to 256 times more computational effort. The introduction of quadruple substitutions represents 512 to 1024 times more computational effort. It is therefore but natural that these methods become prohibitively expensive for canonical theories. For MR theories, similar scalings are observed. For instance, CASPT2 shows a scaling of $\mathcal{O}(M^5)$ and MRCI with up to doubles a scaling of $\mathcal{O}(M^6)$. The difference in the computational costs between SR and MR methods is in the pre-factor for these scalings. In the MR case the pre-factor depends on the size of the active space and is therefore significantly higher.

Amplifying the increase of computational costs in electron correlation methods is the requirement for larger AO spaces (*1, 68*). First, the convergence of the correlation energy with the basis set's dimension is rather slow when using canonical orbitals (*3*). Furthermore, for smaller AO spaces, the effort of going beyond HF is not compensating: the computational effort is too high and the amount of correlation energy recovered is (too) small. Consequently, basis sets of at least double-ζ quality with polarization should be used. Even though the size of the basis set does not influence the power in the scaling of a method, it influences the pre-factors.

All these factors together generate a computatinal scaling wall (*1, 132, 136*) which is rapidly reached. This hinders these methods from routine application, or from being used at all. There is also a problem of disk-storage capacity, as many sets of integrals must be stored and constantly read. For instance, the number of matrices containing two-external exchange integrals increases roughly with the square of the number of correlated orbitals (*66, 136, 140*). This is however just one of the required sets of integrals for electron correlation methods. This very high demand in disk-storage for larger systems brings high demands in I/O, creating bottlenecks hard to overcome (*68*).

Decreasing the computational costs of electron correlation methods requires excluding unnecessary configurations (*134, 135*). The first selection schemes followed PT estimations of the amplitudes (*132*). Since no other criteria was used, this arbitrary configuration selection neglected countless of small contributions, which summed together played a major role. This had a negative impact on PES, which were not smooth (*1, 66, 68, 134, 140*). This configuration selection caused also a dependence on the virtual orbitals (*66*) and had expensive logic (*66, 68, 134*). Another solution performed this truncation already at the orbital level (*140*). The correlation energy calculated through these methods suffered from weak dependences on the virtual space, as well as poor convergence (*140*).

The ideas behind local methods (*141–146*) are not far from orbital and configuration

truncations. They also aim at reducing the computational demands of theoretical methods by truncating the CI expansion at the configuration and orbital levels (*66, 68, 68, 134, 136, 140*). The difference lies in the orbital basis, which is chosen to concentrate efficiently the information, making the truncation always consistent (*66, 140*). This physically motivated configuration selection scheme (*147*) has many consequences: the truncation at two levels has but a minor influence in the calculation of properties (*136, 140*); better convergence with respect to the number of configurations (*136*); the matrix structure of the formalism remains intact, avoiding logic in innerloops (*147*).[5]

Unlike canonical orbitals, which are not easily interpreted (*66, 68, 132*), local orbitals have a clear chemical interpretation and a clear contribution to a particular region of a molecule. Because local orbitals concentrate spatially the correlation effects, these bases allow the exploration of the locality of correlation effects (*13, 68, 132, 148, 149*). Truncation schemes can then be efficiently applied both at the configuration and orbital levels: a large fraction of the configurations in a CI expansion can be neglected based on energy or distance criteria (*66, 68, 132*); excited configurations associated with a specific orbital pair are restricted to a particular subspace of the virtuals (*66, 68, 132*). This truncation alleviates the "scaling-wall" of canonical methods at a (very) small sacrifice in accuracy (*148, 149*), which, if methodical and structure independent, is negligible when compared to other sources of error (*140*).

As the correlation energy rapidly decreases with the distance between orbitals to correlate (it goes with the sixth power of the interelectronic distance) (*66, 68, 136, 148*), orbital pairs can be classified according to their significance to correlation effects (*2, 3, 150*). Separating pairs into classes allows the use of pair approximations (*2, 3, 66, 133, 136*), which handle each class differently: high-level treatment of correlation effects is restricted to the most significant ones; other pairs are treated at lower levels of theory; the least significant pairs are neglected with no loss. The second level of approximations are domain approximations (*2, 66, 136, 148*). In canonical methods, the substitution space of a given orbital (pair) is the full set of virtual orbitals (*132, 136*). Domain approximations restrict the substitution spaces of each orbital m or pair mn to a subset of the virtual space (*136, 140*) in the same spatial region as m or mn.

The most popular choices of local bases for the virtual space are beyond doubt Projected Atomic Orbitals (PAOs) (*1, 8, 66, 132, 136, 140*) and Pair Natural Orbitals (PNOs) (*4, 137, 139, 151–154*). Of particular relevance are also Orbital Specific Virtu-

[5]The fast operations in both workstations and vector computers are matrix multiplications.

als (OSVs) (*131, 155*), Localized Virtual Orbitals (LVOs) (*156–159*) and fragmentation methods. Tables 2.1 and 2.2 summarize the main features and provides references for these and other methods.

Table 2.1: Comparison between different local methods. Table summarizing information about PAOs; PNOs; OSVs; LVOs; LOVOs; the method of Stollhoff, Vasilopulos and Fulde; fragmentation methods; the Laplace-transform method of Scuseria and Ayala.

Method	**Generation**	**Implementation/Accuracy**
PAO (*1, 136*) (*8, 140*) (*66, 68, 132*)	AOs projected onto the virtual space	almost all classes of methods (refer to text); 98-99%/30-70 PAOs
PNO (*151, 160*) (*161, 162*) (*153, 154*)	tensor factorizations MP2 pair amplitudes	mostly CEPA, CC, MPn classes (refer to text); 99.9%/20-40 PNOs
OSV (*131, 155*)	tensor factorizations MP2 intrapair amplitudes	CCSD(T) (*163*); CCSD, MP2 (*155*); CCSDF12, CCSD(T)F12 (*131*); 99.8%/100 OSVs
LVO (*156*)	localized virtual orbitals	large basis set superposition errors (*164–167*); 70% accuracy
LOVO (*157, 158*)	based on Boys' localization	reaches accuracy of PAOs and PNOs with much more LOVOs; applied to MRCI (*168*) and PT (*159*)

PAOs were introduced by Pulay (*1*) and implemented by Pulay and Sæbø (*8, 66, 132, 136, 140*). These are built by spanning the virtual space with non-orthogonal AOs. These AOs are projected onto the virtual space to ensure orthogonality to other orbital spaces. Closed-shell orbitals are localized using Boys' procedure (*169–171*).[6] PAOs domains were

[6]Other methods to localize closed-shell orbitals are, *e.g.*, the Pipek and Mezey method (*172*) and IBOs (*173*).

built for each orbital m by including PAOs located on the same atoms on which m was located (*68, 132, 136*). These domains were later extended to include neighbouring atoms. Domains for pairs mn are built by uniting the domains of the orbitals m and n (*68, 132, 136*). Pairs were divided in three classes based on energy criteria (*66, 134, 136*) and singles were initially omitted from the local treatment.

Table 2.2: Comparison between different local methods. Table summarizing information about the method of Stollhoff, Vasilopulos and Fulde; fragmentation methods; the Laplace-transform method of Scuseria and Ayala.

Method	**Generation**	**Implementation/Accuracy**
Stollhoff, Vasilopulos, Fulde (*175–177*)	local substitution operators	CEPA-0 (*174*)
Fragmentation Methods	partition of molecules in small and local local parts	MP2 (*178–181*)
		MP2, CCSD, CCSD(T) (*182, 183*)
		CCSD, CCSD(T) (*184–186*)
		MP2(F12), CCSD(T)(F12) (*187–189*)
		CCSD, CCSD(T)F12 (*190–193*)
		MP2, CCSD, CCSD(T) (*194–197*)
Ayala, Scuseria (*198*)	AO-Laplace transform (*199–201*)	exact within Laplace transform; MP2

Using PAOs, substancial savings in the computational effort of electron correlation methods were reported (*1, 8, 66, 136, 140*): speed-up factors of 17-40 for a molecule as small as butadiene (*66, 68*). 98-99% of the pair correlation energy is recovered (*68, 136*) using domain sizes of around 30-70 PAOs for double- or triple-ζ basis sets with polarization (*136*). It was also shown that the local treatment contributed to reduce basis set superposition errors (*8, 66, 140, 147, 202–204*).

PAOs were used for local variants of CISD, Coupled Electron Pair Approximation (CEPA)-0, Approximate CCD (ACCD), CEPA-2 and second-, third- and fourth-order MP (*68, 134, 136*).[7] Hampel and Werner implemented PAO variants of CCSD and QCISD (*147*) and analytical gradients for local MP2 (*210*) and CCSD (*211*) were also reported.

[7]The original publications are in the references (*5, 151, 174, 205–209*).

Crawford and Russ implemented also PAO-CC linear response theory (*212, 213*).

Later on, Werner and Schütz used a truncated multipole expansion to approximate exchange integrals for a specifc pair class (*214*). This Multipole Approximation (MPA), together with pair and domain approximations applied to the integral transformation, provided the ground for the first asymptotic linear scaling MP2 method. This allowed the first MP2 calculations for systems with *ca.* 500 correlated electrons and 2000 basis functions on a PC.

Linear-scaling local variants of MP4(SDQ), QCISD, CCSD (*133,215*), CCSD(T) (*216–219*), Equation of Motion CCSD (EOM-CCSD) (*220*) and of CC2 (*221–225*) were also implemented. A DF (*226, 227*) variant was implemented for local CCSD (*3, 228*) and extending the local approximations to the DF evaluation of integrals lead to linear scaling Local Density Fitting (LDF) algorithms as well (*3, 148, 228–235*).

Near linear-scaling local variants of explicitly correlated methods were also implemented: MP2-F12 (*231, 234, 236*); CCSD-F12 (*150, 237*); DF-CCSD(T)-F12 (*238*). The local explicitly correlated treatment reduced not only errors of the basis set incompleteness, but also the errors of domain approximations. Finally, unrestricted variations of the linear scaling local CCSD and CCSD(T) were also implemented, both with and without explicit correlation (*239–241*).

Although PAOs comprised a turning step in computational chemistry, large PAO domains are required for fully converged results (*148, 149*). For triple-ζ basis sets, accuracies of 99.8-99.9% in correlation energy and chemical accuracy in energy differences can be reached with domains containing 400-600 PAOs (*242*). PNOs were introduced by Edmiston and Krauss (*160, 243*) and further investigated by Meyer in the context of CEPA (*151, 152, 244–251*), Ahlrichs and Kutzelnigg in the context of Independent Electron Pair Approximation (IEPA) (*161, 252–256*) and Taylor (*162, 257*). PNOs were built to be a consistent configuration selection method in a CI expansion. They aim to provide a set of pair specific approximate natural orbitals, for which the CI expansion converges most rapidly (*258*). The first use of PNOs in the context of local correlation was due to Neese *et al.* (*4, 137, 139, 153, 154, 259–262*). PNOs offer a very compact description of correlation effects. For the same level of accuracy, same level of theory and same basis set, PNO methods contract pair substitution spaces 6-10 times more than PAO methods (*149*). They offer also good convergence of absolute and relative energies with respect to domain sizes. However, since they are built specifically for each pair, the total number of virtuals that is built is very large, which can translate into high scaling of computational times as well as large memory requirements.

The first PNO implementation in the context of local correlation was the local PNO-CEPA method (*4*). Local PNO-CCSD (*153*), the respective open-shell variant (*261*) and parameterized CCSD (*154, 263*) were also implemented. The problem of these early implementations was a steep scaling with the system's size in the generation of PNO, becoming the methods too expensive for molecules with more than 100 atoms. To reduce this steep scaling, canonical virtuals were first transformed to the PAO basis using large PAO domains and the PAOs were then transformed to the PNO basis (*72, 137, 148, 149, 235, 264–266*). The multipole approximation was also used, along with local DF approximations for the generation of exchange and Coulomb integrals. All these changes reduced the original scaling of $\mathcal{O}(M^6)$ to linear for all computational resources. Losses in accuracy amounted at most to 0.05% for energy differences and at most to 0.1% in the correlation energy being recovered. Errors were dominantely introduced by the PAO domains, even though the use of PNOs contracted substitution spaces to 20-40 local virtuals (in contrast with 300-700 PAOs per domain). This allowed CCSD calculations on systems with more than 1000 atoms and 20000 basis functions (*264*).

Linear scaling local PNO variants of CEPA, variational CEPA, QCISD, parameterized CCSD, CCSD(T) and Quadratic CISD with Perturbative Treatment of Triples (QCISD(T)) were implemented (*137,139*). The last two implementations required the concept of Triples Natural Orbital (TNO) (*139*), a generalization of PNOs to triple substitutions. Explicitly correlated variants of local PNO methods were also implemented: PNO-LMP2-F12 and PNO-LMP3-F12 (*235, 266–268*); PNO-LCCSD-F12 (*269, 270*). These implementations showed that combining PNOs with explicitly correlated methods is particularly advantageous. A PNO doubles correction to the CI method with singles was developed for excited states (*271*), just like PNO linear response theory for CC (*272–274*).

Although local SR methods have been extensively studied for decades, there is still a big gap in implemented local MR methods. To our knowledge there are the implementations of Carter *et al.* (*275–281*) of local MRCI and MR Averaged Coupled Pair Functional (ACPF), Hoyau's (*282*) local variant of (uncontracted) MRCI, the recent work of Neese *et al.* of a mixed PNO-PAO local NEVPT2 (*72*) and the state specific singles and doubles PNO Mukherjee MRCC (*283*). Although not aiming specifically for local correlation methods, Fink and Staemmler also developed a PNO-MRCEPA (*115*). This method can use localized orbitals for the internal orbital spaces, even though a full exploration of the advantages of local approximations is not undertaken. In a similar fashion there is still the implementation of a PNO-MRCI by Taylor (*257*).

In the local variant of NEVPT2, only the closed-shell space is localized (using the

method of Boys). The active space is not localized,[8] and for these orbitals a single domain is built as the union of all the active orbital domains. The virtual space is spanned either with PNOs or PAOs, according to the configuration subspaces. Although not yet defined, we will specify here the the choices for the local NEVPT2, for later reference: for P_0 and S_0 PAOs are employed; PNOs are built for P_2 and P_1; the P_2 PNOs are used for S_2 and S_1 (OSVs or intrapair PNOs). The threshold used for S_1's PNOs was 100 times smaller than the thresholds used in other subspaces, in order to retain the same accuracy for all configuration subspaces. Integrals are built using DF approximations and the MPA is used as a pre-screening for the calculation of two-electron integrals for all configuration subspaces involving at least a closed-shell index. Using the default thresholds, PNO-NEVPT2 recovers 99.9% of the correlation energy. For fixed sizes of the active space, the computational costs scale linearly with the molecular size. The analogous local Mukherjee MRCC (*283*) behaved similarly.

Carter's local MRCI method (*168, 275–279*) explored both LOVOs and PAOs. Pair and domain approximations were also used, yielding a method with a scaling somewhere between third- and fourth-order with the system's size. The accuracy remained by 97% for correlation energies and within 3 $kcal/mol$ from the canonical case for energy differences. The regionally contracted MRCI of Hoyau *et al.* (*282*), brought to MR methods the concepts of fragmentation methods: a molecule is partitioned into many disjoint blocks or fragments, and a set of localized virtuals is assigned to each fragment. A series of MCSCF calculations are then performed on each block and pairs of them to build the ansatz for the wavefunction. The regionally contracted MRCI introduced errors of 1-100 mH in total energies, when compared to the canonical case. The reduction of the computational effort is demonstrated using the relative scaling of the non-local unrestricted MRCI against the scaling of the regionally contracted MRCI.

In this work a mixed PNO-PAO local variant of CASPT2 was derived and implemented. We named our method PNO-PAO Local Complete Active Space 2^{nd}-order Perturbation Theory (LCASPT2). For simplicity, we omitted both the PNO and PAO acronyms in the acronym of the method. Our main objective was the reduction of computational costs without sacrificing the accuracy of the canonical method. Our goal is thus to allow larger molecules to be studied with MR theories. The larger systems we aim at are typically organic molecules or transition metal complexes with a large closed-shell space and a small and local active space. For any other type of chemical system, the local treatment

[8] This is a significant difference towards our LCASPT2 implementation.

using both PAOs and PNOs still allows significant savings in the computational cost. We aimed at asymptotic linear scaling of the computational costs with the molecular size for the cases of small active spaces and large closed-shell spaces in specific. Local approximations were generalized from the SR to the MR case. This required building PNOs from PAOs, as well as using pair and domain approximations in building the two-electron integrals and applying pair approximations to the many configuration subspaces. We explored the properties of both PAOs and PNOs, using these in the most convenient way in view of our goals. We implemented LCASPT2 in the development version of `MOLPRO` , partially using FORTRAN, partially using `MOLPRO` 's Local ITF (LITF) (*111, 284–287*). The latter extends ITF to local cases and was developed by Dr. D. Kats during the course of this work.

3. Theoretical Background

3.1 The Molecular Hamiltonian

In Quantum Mechanics, the energy of a non-relativistic quantum many-body system is given by the Schrödinger equation (*6, 288*). In its time-independent formulation the Schrödinger equation is defined as

$$\hat{H}\Psi = E\Psi \tag{3.1}$$

The Hamiltonian operator, $\hat{H}$, is defined as the sum of both kinetic $\hat{T}_x$ and potential $\hat{V}_{xy}$ contributions. The kinetic operator gives the energy due to the motion of each particle, while the potential operator the energy due to the interaction of particles pairwise. It accounts for interactions between electrons, between nuclei and between electrons with the nuclei. Using the subscript e for electrons and the subscript n for nuclei all these contributions may be specified in the Hamiltonian as

$$\hat{H} = \hat{T}_e + \hat{T}_n + \hat{V}_{ee} + \hat{V}_{nn} + \hat{V}_{en} \tag{3.2}$$

with the operators

$$\hat{T}_x = -\frac{1}{2}\sum_{i=1}^{X}\frac{1}{M_i}\nabla_i^2 \tag{3.3}$$

$$\hat{V}_{xy} = \sum_{i=1}^{X}\sum_{j=1}^{Y}\frac{Z_i Z_j}{r_{ij}} \tag{3.4}$$

In both equations (eqs.) 3.3 and 3.4, X and Y are the total number of particles x and y (which can be electrons or nuclei), M_i is the mass of particle i (1 *a.u.* for electrons), $r_{ij} = |r_i - r_j|$ is the distance between particles i and j and Z_i the charge of the particle.

Neglecting relativistic effects, the Hamiltonian above defined is exact. But being the nuclei much heavier than electrons, the motion of these two types of particles can be considered to occur in different time-frames: the nuclei become fix with respect to the motion of electrons. Consequently, the Hamiltonian and also the wavefunction can be separated into a nuclear and an electronic component. This separability of the nuclear and electronic motion leads to the separation of the Schrödinger equation into nuclear and electronic parts. The electronic equation depends parametrically on the molecular geometry, thus the wavefunction for each electronic state x is a function $\Psi_x(\mathbf{r}, \sigma; \mathbf{R})$ of the coordinates for the electrons $\mathbf{r}$, their spin σ and the nuclear coordinates $\mathbf{R}$. Solving

the electronic Schrödinger equation for many geometries yields a grid for the nuclear motion, and this grid composes a Potential Energy Surface (PES) for a given electronic state. After obtaining PESs from the electronic Schrödinger equation the nuclear part can also be solved for each molecular quantum state k, yielding a nuclear solution associated to each electronic state, $\Theta_{xk}(\mathbf{R})$. The full solution of the Schrödinger equation for the molecular quantum state k is then given by $\Psi_k^{total}(\mathbf{r}, \sigma, \mathbf{R}) = \sum_x \Psi_x(\mathbf{r}, \sigma; \mathbf{R})\Theta_{xk}(\mathbf{R})$. This separability of the Schrödinger equation into nuclear and electronic components is known as the Born-Oppenheimer approximation (*6, 289*).

The Hamiltonian in eq. 3.2 is in an operator form requiring integration, also known as first-quantization. In this formalism one usually keeps track of the behavior of each particle of the system, even if all the particles are indistinguishable. This becomes cumbersome when the number of particles becomes too large and not so practical to be used to solve many-body problems. An equivalent formalism[1] is offered by second-quantization, which no longer keeps track of particles but instead is centered in occupation numbers and many-particle states. This is particularly advantageous for systems with a very large number of particles or systems with a variable number of particles. In second-quantization, a ket spin-orbital ($|\psi_{r,\sigma}\rangle$, where $\psi_{r,\sigma}$ is built as the product of a spatial orbital ϕ_r with the respective spin function σ) is seen as a creation operator, $\hat{a}^\dagger_{r,\sigma}$, which creates a particle in the spatial orbital ϕ_r with spin $\sigma = \alpha, \beta$, when acting on an adequate state. Similarly, a bra spin-orbital ($\langle\psi_{r,\sigma}|$) is seen as an annihilation operator, $\hat{a}_{r,\sigma}$, removing a particle in ϕ_r with spin σ. (Spin-)Orbitals are thus seen as quantum mechanical operators (*65*). These creation and annihilation operators can be used to construct n-particle spatial substitution operators (*65*),

$$n=1 \qquad \hat{E}_{rs} = \hat{a}^\dagger_r \hat{a}_s = \sum_{\sigma=\alpha,\beta} \hat{a}^\dagger_{r\sigma} \hat{a}_{s\sigma} \tag{3.5}$$

$$n=2 \qquad \hat{E}_{pq,rs} = \hat{a}^\dagger_p \hat{E}_{rs} \hat{a}_q = \sum_{\sigma=\alpha,\beta} \hat{a}^\dagger_{p,\sigma} \hat{E}_{rs} \hat{a}_{q,\sigma} \tag{3.6}$$

The operators $\hat{a}^\dagger_r$ and $\hat{a}_r$ are spin-summed. They do not affect the spin of a particle, just its spatial function (orbital), and they are in a true sense creation and annihilation operators. They follow a specific algebra known as the anticommutation rules:

$$\left[\hat{a}^\dagger_r, \hat{a}^\dagger_s\right]_+ = \hat{a}^\dagger_r \hat{a}^\dagger_s + \hat{a}^\dagger_s \hat{a}^\dagger_r = 0 \tag{3.7}$$

$$\left[\hat{a}_r, \hat{a}_s\right]_+ = \hat{a}_r \hat{a}_s + \hat{a}_s \hat{a}_r = 0 \tag{3.8}$$

[1]The expressions in first-quantization are equivalent to the ones in second quantization if finite basis approximations are considered in the former (*6*).

$$\left[\hat{a}_r^\dagger, \hat{a}_s\right]_+ = \hat{a}_r^\dagger \hat{a}_s + \hat{a}_s \hat{a}_r^\dagger = \delta_{rs} \tag{3.9}$$

These rules can be easily derived by applying the operators sequentially to occupation vectors, following the algebraic rules inherent to these. The anticommutation rules can be used to work out specific expressions into workable formulas, which can be implemented in algorithms. These form the core of second quantization in quantum chemistry.

When projected on the left and on the right by the reference state, the one-particle substitution operator generates elements of the first-order density matrix, the quantity bridging the formalisms of first and second quantization.[2] Instead of dealing with the number of particles within the operators, this information is transferred to the wavefunction (*6*). In the second quantization the Hamiltonian may be rewritten as

$$\hat{H} = \sum_{rs} h_{rs} \hat{E}_{rs} + \frac{1}{2} \sum_{pq} \sum_{rs} (pq|rs)\, \hat{E}_{pq,rs} + E_{nuc} \tag{3.10}$$

where indices run over the occupied space. h_{rs} gives the kinetic contribution of electrons, as well as the potential contribution between electrons and nuclei,

$$h_{rs} = \int \phi_r^* (\mathbf{r}_x) \left(-\frac{1}{2}\nabla^2 - \sum_A^{nuc} \frac{Z_A}{|\mathbf{r}_x - \mathbf{r}_A|} \right) \phi_s (\mathbf{r}_x)\, d\mathbf{r}_x \tag{3.11}$$

and $(pq|rs)$ the potential contribution between electrons, *i.e.*, their repulsion.

$$(pq|rs) = \int \phi_p^* (\mathbf{r}_x)\, \phi_q (\mathbf{r}_x) \left(\frac{1}{|\mathbf{r}_x - \mathbf{r}_y|} \right) \phi_r^* (\mathbf{r}_y)\, \phi_s (\mathbf{r}_y)\, d\mathbf{r}_x d\mathbf{r}_y \tag{3.12}$$

As can be seen from eqs. 3.10-3.12, the Hamiltonian $\hat{H}$ becomes independent on the number of electrons but depends instead on the integrals h_{rs} and $(pq|rs)$ in a given orbital basis.

The formulae in this work were developed using the formalism of second-quantization. Any further expression herein will be expressed in terms of n-particle substitution operators. For further information on the formalism and basics of second-quantization we refer the reader to reference (*10*) and references therein.

3.2 Hartree-Fock

One of the most widely used and central methods in quantum-chemistry is Hartree-Fock (HF), an extension of the Molecular Orbital (MO) theory (*10, 290*). The MOs are

[2] In the first quantization, the first order density is obtained by external product of the orbital coefficient matrix with itself.

expressed as a Linear Combination of Atomic Orbitals (LCAO) and the HF wavefunction, a Slater Determinant (SD), is given by

$$\Phi_{\mathrm{HF}} = \frac{1}{\sqrt{N!}} \begin{vmatrix} \psi_1(\mathbf{r}_1) & \psi_2(\mathbf{r}_1) & ... & \psi_m(\mathbf{r}_1) \\ \psi_1(\mathbf{r}_2) & \psi_2(\mathbf{r}_2) & ... & \psi_m(\mathbf{r}_2) \\ ... & ... & ... & ... \\ \psi_1(\mathbf{r}_N) & \psi_2(\mathbf{r}_N) & ... & \psi_m(\mathbf{r}_N) \end{vmatrix} \tag{3.13}$$

SDs are anti-symmetrized products of the one-electron spin-orbitals in compliance with Pauli's principle. For simplicity we represent the r, σ pair of indices from $\psi_{r,\sigma}$ as just one index. SDs describe stationary states of quantum many-body systems with an associated energy, the minimum for single configurations for a particular molecular geometry (*6*).

The HF theory starts with the minimization of the energy expectation value using the variational principle.[3]

$$E_{HF} = \langle \Phi_{\mathrm{HF}} | \hat{H} | \Phi_{\mathrm{HF}} \rangle \tag{3.14}$$

The constraint in this minimization is that the orbitals must remain an orthonormal set ($\langle \psi_{r,\sigma_1} | \psi_{s,\sigma_2} \rangle = \langle \phi_r | \phi_s \rangle \langle \sigma_1 | \sigma_2 \rangle = \delta_{rs}\delta_{\sigma_1\sigma_2}$). This can be easily achieved by building a Lagrangian for the HF energy. The minimization of this Lagrangian is equivalent to solving the Roothaan-Hall equation, given by

$$\mathbf{FC} = \mathbf{SC}\varepsilon \tag{3.15}$$

In eq. 3.15 $\mathbf{F}$ is the Fock operator (see description below), $\mathbf{C}$ the matrix with the MO coefficients, $\mathbf{S}$ the overlap matrix for the basis set and ε the diagonal matrix with the orbitals energies. In practice, solving eq. 3.15 is very time consuming and error prone: in each iteration the Fock matrix must be transformed to the MO basis, a demanding transformation for which numerical errors may accumulate or even amplify. A more convenient approach solves this equation in the AO basis and uses the orthogonalization matrix $\mathbf{X} = \mathbf{S}^{-\frac{1}{2}}$. The matrix $\mathbf{X}$ orthogonalizes the basis of AOs, and transforms eq. 3.15 into 3.16.

$$\mathbf{X}^\dagger \mathbf{F} \mathbf{X} \tilde{\mathbf{C}} = \tilde{\mathbf{F}} \tilde{\mathbf{C}} = \tilde{\mathbf{C}} \varepsilon, \quad \mathbf{C} = \mathbf{S}^{-\frac{1}{2}} \tilde{\mathbf{C}} \tag{3.16}$$

Solving eq. 3.16 consists in solving an eigenvalue problem (*290*), which is equivalent to the diagonalization of the matrix $\tilde{\mathbf{F}}$. When eq. 3.16 is solved one obtains the matrix with the MO coefficients $\mathbf{C}$ and the matrix ε with the orbital energies.

[3] In quantum mechanics the variational principle minimizes the expectation value of an operator using a trial function, which depends on many parameters. The optimization takes place by changing (optimizing) the latter.

The Fock operator, defined from the minimization of the HF energy as the sum of effective one-electron Hamiltonians, is given by

$$\hat{F} = \sum_{rs} f_{rs} \hat{E}_{rs} \tag{3.17}$$

$$\begin{aligned} f_{rs} &= h_{rs} + \sum_{pq}^{occ} \left[(pq|rs) - \frac{1}{2} (rq|ps) \right] \langle \Phi_{\mathrm{HF}} | \hat{E}_{pq} | \Phi_{\mathrm{HF}} \rangle \\ &= h_{rs} + \sum_{pq}^{occ} \left[J_{rs}^{pq} - \frac{1}{2} K_{rs}^{pq} \right] \langle \Phi_{\mathrm{HF}} | \hat{E}_{pq} | \Phi_{\mathrm{HF}} \rangle \end{aligned} \tag{3.18}$$

In the latter, $\langle \Phi_{\mathrm{HF}} | \hat{E}_{pq} | \Phi_{\mathrm{HF}} \rangle$ corresponds to the element pq of the first-order density matrix, $D_{pq}^{(1)}$ (*10, 65, 290*). By definition, $\hat{F}$ is a N-electron operator built as the sum of one-electron operators. These describe: the energy of each electron in each spin-orbital ψ_i when moving in the field defined by the nuclei (h_{rs}); the repulsion to all other electrons (J_{rs}^{ij} and K_{rs}^{ij}). The repulsive component comes through the Coulomb (J_{rs}^{ij}) and the exchange (K_{rs}^{ij}) terms. The Coulomb operator has a classical interpretation, it gives the electrostatic component of an electron in the field generated by the wavefunction (*13*). The exchange operator is non-classical and gives the energy of exchanging electrons in such field. Through the $\hat{F}$ operator an electron sees all other electrons as a (mean) field and not as independent particles. Consequently, the electron-electron repulsion is averaged and one electron sees only the whole as an electronic cloud (*10, 65, 290*). Since $\hat{F}$ is a mean-field operator, HF is a mean-field theory.

Finally, because the Fock operator both depends and determines the MOs, the HF equations are non-linear and must be solved iteratively.

Limitations of Hartree-Fock

To the HF two main limitations are usually pointed out. The first limitation comes with the fact that the AO basis is incomplete. The basis set may be improved, but this error due to the AO incompleteness is reduced only up to a certain point: the HF limit. No matter how much one improves the AO basis, the HF energy will always be an upper bound of the true energy of the system. This is related to the second and most restrictive limitation: the approximation on the electron-electron repulsion interaction. Because there are no explicit electron-electron interactions, HF always under-evaluates the electronic repulsion energy: not only are energies predicted by excess, but also the electronic cloud is broader (than the exact one) (*290*).

The HF method can in principle treat all kinds of systems, from closed- to open-shell.[4] But different systems require distinct treatment, according to the nature of the MOs searched: Restricted Hartree-Fock (RHF) searches for spatial orbitals, and it is used for closed-shell systems; Unrestricted Hartree-Fock (UHF) searches for spin-orbitals, and is valid for both closed- and open-shell molecules; in Restricted Open-Shell Hartree-Fock (ROHF) all β electrons are paired with α electrons in the same spatial orbital, and if there still remain α electrons unpaired these are treated as being open-shell (*6*).

When searching for the GS of a closed-shell system the UHF wavefunction usually collapses into the RHF solution. For open-shell systems UHF lowers the energy of the respective RHF, if the latter is even possible to calculate. At dissociative bond lengths the RHF solution breaks down, because it always forces double occupation. This is inconsistent with most bond breaking processes and unable to describe the di-radical nature of most systems. However the effects of RHF's forced double occupancy are felt allover in a PES, not just at dissociative limits (*65*): i) energies are too high; ii) bond distances are too small; iii) PESs become steeper than they actually are; iv) minima are misplaced; v) wavefunctions have an excessive ionic character, increasing the norms of the dipole moment vectors. The UHF provides better descriptions at dissociative bond distances, as it allows the breaking in two radicals (*290*). However, this wavefunction is usually unphysically contaminated with higher-order spins states, and therefore restricted solutions are preferred around minima. At sufficiently large bond lengths unrestricted solutions should be searched, where the RHF solution is no longer a minimum. At intermediate bond lengths both methods prove themselves qualitatively inadequate: The RHF double occupation imposition overshoots the energy, while UHF suffers from contamination of states with higher spin. Even though UHF can qualitatively describe energy profiles of bond dissociation processes, its wavefunctions are poor descriptors of these processes. This becomes even more crucial when predicting other molecular properties, *e.g.* the total spin (*290*), since UHF is not an eigenfunction of the total spin $\hat{S}^2$.

To remove the undesired spin contamination, whose relevance grows with the atomic distances, the wavefunction is changed to a linear combination of configurations. This keeps the qualitatively correct description of UHF, while still allowing to preserve the correct spin state. The adoption of a multi-determinant nature of the wavefunction gives rise to post-HF methods (for further details, *cf.* reference (*290*), pages 225-229).

There are many examples illustrating the inadequacy of HF wavefunctions in describ-

[4] A closed-shell system has an even number of electrons, all paired. An open-shell system does not have all electrons paired.

ing both the chemistry and properties of molecular systems. For instance, in the hypersurface of disilyne (Si_2H_2), a new local minimum was discovered with post-HF methods, inexistent in any HF study (*291*). There is also the example of carbon monoxide (CO) for which the dipole moment is qualitatively wrong, pointing to the wrong direction (*292*).

3.3 Correlation Energy

In HF, electrons avoid an electronic cloud instead of feeling each other electron as a singular entity. Since the Hamiltonian is a sum of two-electron operators (terms with $(r_{ij})^{-1}$), the real wavefunction, in compliance with the Schrödinger equation, should attend the condition (*65*)

$$\lim_{r_{ij}\to 0} \hat{H}\Psi\left(\mathbf{r}_1, \mathbf{r}_2, ..., \mathbf{r}_N\right) = E\Psi\left(\mathbf{r}_1, \mathbf{r}_2, ..., \mathbf{r}_N\right) \tag{3.19}$$

The limit in eq. 3.19 exists and is the energy of the system, a constant. But the function $\hat{H}\Psi$ has a pole for all $\mathbf{r}_i = \mathbf{r}_j$, the Coulomb singularity. This brings a contradiction in the equations because the local energy is a constant and it cannot possess singularities. This singularity needs thus to be canceled out by another term in the Schrödinger equation. Because electrons do not necessarily have to be close to nuclei, the other singularity can but only occur in the kinetic energy (*65*). Expanding the wavefunction in terms of its Maclaurin series of $\mathbf{r}_{ij}$ and putting it in the Schrödinger equation, it is possible to derive an expression that shows the requirement to remove the pole, eq. 3.20. This has to further assume that electron pairs have singlet spin multiplicity, thus also that angular terms can be ignored at low order (*65*).

$$\frac{\partial}{\partial \mathbf{r}_{ij}}\Psi\left(\mathbf{r}_{ij} = 0\right) = \frac{1}{2}\Psi\left(\mathbf{r}_{ij} = 0\right) \tag{3.20}$$

Around the coalescence between the two electrons, the exact wavefunction has the shape of a cusp due to the Coulomb hole, as depicted in Figure (Fig.) 3.1 (*65*). Thus electrons avoid the instantaneous position of other electrons, making correlation a local effect. Instead of being ignorant of the whereabouts of other electrons, each electron rather avoids the field of every other electron. Furthermore, whichever direction is taken from $\mathbf{r}_{ij} = 0$, the wavefunction increases linearly (*65*). For triplet states, equivalent cusp conditions exist, but as the electrons are already kept apart by the Pauli principle,[5] the effects of neglecting the correlation energy are not as relevant (*65*).

[5]Two fermions cannot occupy the same quantum state.

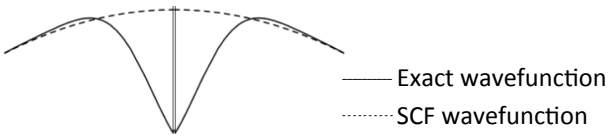

Figure 3.1: The interelectronic cusp adapted from reference (*65*). Wavefunctions plotted against $z = z_2 - z_1$, for $x = x_2 - x_1 = 0$ and $y = y_2 - y_1 = 0$.

The HF wavefunction does not respect the cusp condition 3.20, as its first derivative zeroes for $\mathbf{r}_{ij} = 0$ (*65*). Consequently, with its mean-field character, HF does not describe the correlation of electrons.[6]

The analysis above defined a short-range type of correlation between electrons, also known as dynamic or instantaneous correlation (*6, 65*). Dynamic correlation is responsible for the correct description of the electronic cusp and is dominant closer to minima. This effect arises from electrons occupying the same spatial orbital and whenever chemical bonds are close to dissociation, it is minimized. It happens that electron correlation is not just a concept around minima in a PES. The correct bond dissociation profile defines yet another type of correlation, known as static or non-dynamic correlation (*6, 65*). Static correlation becomes significantly more important at molecular dissociation, *i.e.*, when $r_{ij} \to +\infty$. For most chemical systems, bond dissociation processes occur in an even fashion. This means that whenever a bond is broken, the two electrons making up the former bond are distributed over the two newly-formed fragments. This is the case for almost all covalent bonds. Static correlation is thus the effect responsible for the correct description of bond dissociation processes. There is yet another type of electron correlation effects. Whenever there is more than just one dominant configuration in a correlated wavefunction, strong correlation effects arise. Both dynamic and static correlation occur in specific regions of a PES. On the other hand, strong correlation effects are felt globally over PES, from minima up to dissociation. Strong correlation is usually more significant for ESs, even though there are several characteristic examples of molecules with already strong correlation character in the GS. Since in the regime of strong correlation there is more than just one leading orbital configuration, Single-Reference (SR) electron correlation methods are inappropriate: wrong energies and wrong properties are predicted.

All types of correlation effects can be introduced by including all excited configurations of the HF reference. Even though there is only a small overlap in the definitions of dynamic, static and strong correlation, it is not possible to clearly point exactly where each

[6]HF contains however exchange correlation.

effect begins. As mentioned above, one can however identify the domain where each effect is predominant. Nevertheless, the calculation of one always introduces some character of the other types of correlation, even if just to minor extent (*6, 63*). Both dynamic and static effects can be accounted for by extremely large wavefunction expansions. Strong correlation by definition admits more than just one leading configuration, and can be accounted for by methods which allow the calculation of multi-configurational functions. This means that the multideterminant character is already introduced at the reference level. Since correlation effects are described by the same kind of expansion (just to different extents), a mathematical distinction between them cannot be introduced. Correlation energy, E_{corr}, comprises thus simultaneously dynamic, static and strong effects and is defined as the difference between the exact and non-relativistic energy of a system, ϵ,[7] and the HF energy, E_{HF}.

$$E_{\text{corr}} = \epsilon - E_{\text{HF}} \tag{3.21}$$

Because HF offers an upper bound to the exact energy, for other variational methods correlation lowers the exact energy with respect to HF. The correlation energy takes thus negative values (*65*).

Since obtaining the exact energy ϵ is not always possible, this quantity might be substituted by the energy of a method X. Furthermore, HF might not be used as reference and instead the energy of the reference method can be used, E_{ref}. This yields the general expression for the correlation energy of the method X, which is in practice used,

$$E^{\text{X}}_{\text{corr}} = E^{\text{X}} - E_{\text{ref}} \tag{3.22}$$

Making use of the adequate methods this definition allows to estimate the contributions of dynamic, static or strong correlation effects.

The correlation energy comprises typically at most 1% of the total energy of a system (*40*). Nevertheless, its magnitude matches the amplitude of the energies associated to chemical or physical processes. The introduction of these effects is thus of utter relevance to account for the chemistry and the physics of a system.

3.4 Single Reference Methods

The introduction of dynamic correlation is achieved mainly through three different theories: Configuration Interaction (CI), Perturbation Theory (PT) and Coupled Cluster

[7] The Born-Oppenheimer approximation is usually also considered.

(CC). These methods are not suitable to treat strong correlation (*23*), since they add large expansions of configurations with only minor contributions each. The next sections are dedicated to the first two of these methods for the SR case. For readers interested in the CC theory, we refer them to, *e.g.*, references (*10, 138, 293*).

3.4.1 Configuration Interaction

The full set of unique configurations built from HF's MOs forms a suitable basis of N-electron functions to expand multiconfiguration wavefunctions. Including these, wavefunctions relax around minima and at dissociation limits: electrons are allowed to avoid each other better by occupying other orbitals.[8] The full set of configurations is complete within an AO basis and includes not only the HF determinant but also all possible excited configurations. A Configuration Interaction (CI) wavefunction takes a set of these excited configurations as an ansatz. The wavefunction is thus written as

$$\Psi_{\mathrm{CI}} = a_0\Phi_{\mathrm{HF}} + \sum_{i=1} a_i\Phi_i = a_0\Phi_0 + \sum_{i=1} a_i\Phi_i \tag{3.23}$$

Here, Φ_i, $i > 0$, is an excited SD and the a_i, $i \geq 0$, are amplitudes in the wavefunction (*6*). Excited configurations are obtained by removing electrons from occupied HF orbitals and putting these in virtual HF orbitals, a task performed directly by substitution operators (eqs. 3.5 and 3.6). In the CI method the coefficients for this expansion are determined using the Schrödinger equation and the variational principle. This optimization takes place by minimizing the Rayleigh Quotient

$$\bar{E} = \frac{\langle\Psi_{\mathrm{CI}}|\,\hat{H}\,|\Psi_{\mathrm{CI}}\rangle}{\langle\Psi_{\mathrm{CI}}|\Psi_{\mathrm{CI}}\rangle} \tag{3.24}$$

subject to the restriction that Ψ_{CI} remains orthonormal. This can once more be achieved by zeroing the derivatives of the respective Lagrangian with respect to the expansion coefficients a_i. The residual equations of CI are thus given by (*65*)

$$R^i = \langle\Phi_i|\left(\hat{H} - E\right)|\Psi_{\mathrm{CI}}\rangle = 0 \tag{3.25}$$

Alternatively, the diagonalization of the electronic Hamiltonian in the basis of configurations yields all eigenvalues and eigenvectors of $\mathbf{H}$. These correspond, respectively, to

[8] The typical example illustrating this feature is molecular hydrogen, H_2 (*42, 292*): With only one configuration, both electrons are always forced to be paired, even at the dissociation limit where each electron should populate each hydrogen atom; allowing a second configuration to contribute to the wavefunction enables the spatial separation of the electrons, essential for the correct description of the dissociation process.

energies and wavefunctions of many electronic states. The method allows thus not only to study GSs but also ESs, as they are also eigenstates of the electronic Hamiltonian (*65, 292*).

If the full basis of configurations is used in the ansatz for Ψ_{CI}, the result is exact for the N-electron subspace spanned by the determinants within the AO basis and other approximations taken.[9] This energy is still an upper bound to the exact one, but for any AO basis, the Full Configuration Interaction (FCI) energy is the closest possible to the exact energy that can be calculated (*292*). Unfortunately, the total number configurations in FCI grows too fast,[10] and only (very) small molecules can be treated at this level of theory. Consequently, CI is commonly used in truncated formulations. Truncated CI schemes on the other hand limit configuration spaces to maximal orders of substitution, including for each order all the possible determinants: CISD - includes all the possible single and double substitutions; Singles Doubles Triples Configuration Interaction (CISDT) additionally includes all triples. Any other order of substitution is neglected. Despite the truncation, the Hamiltonian matrix can still easily reach dimensions of $\left(10^6\right)^2 = 10^{12}$ (*6, 65, 292*). This restricts CI to be only solved for a few states of interest, usually through algorithms like Davidson's (*294*).

Any truncated CI scheme has a severe drawback, the lack of both size consistency and size extensivity (*6, 65, 292*). Size consistency is the property ensuring a consistent energy behavior when two particles cease interacting. Thus for a non-interacting size consistent system $E_{\mathrm{AB}} = E_{\mathrm{A}} + E_{\mathrm{B}}$ (*6, 10*). Size extensivity consists on the proper (linear) scaling of the energy with the number of particles, ensuring that the amount of correlation energy recovered is independent on the system's size. From the definition, size extensivity implies size consistency and these methods allow the direct comparison of calculations between systems with changeable number of electrons (*295*). These are thus very important properties in electron correlation methods. Keeping size consistency and extensivity can be usually achieved at the cost of losing variationality in the optimization. The immediate consequence is that one does not know anymore whether the energy is being over- or underevaluated.

[9] Namely the Born-Oppenheimer approximation and/or neglecting relativistic effects.

[10] For an N-electron system with $2m$ orbitals and n excited electrons there are $\sum_{n=0}^{N} \binom{N}{n} \binom{2m-N}{n}$ configurations (*292*).

3.4.2 Single Reference Perturbation Theory

Perturbation Theory (PT) offers a non-variational, size extensive and size consistent alternative to CI. In PT, the Hamiltonian $\hat{H}$ is partitioned into a zeroth-order component, $\hat{H}^{(0)}$, and a small perturbation, $\lambda\hat{V}$. The perturbation term corrects the zeroth-order approximation, making it exact (*6, 10, 11, 65*).

$$\hat{H} = \hat{H}^{(0)} + \lambda\hat{V} \tag{3.26}$$

The key concept in PT is that the perturbation is small. The rationale underneath PT is to consider the real solution to differ only slightly from one previously found (*6, 10, 11*). The exact energy and wavefunction are expanded as the Maclaurin series of the perturbation, λ. This variable can in principle be chosen freely, even though it will in practice only assume the values of zero (unperturbed or zeroth-order expressions) and one (perturbed system). For small perturbations (*40*), the perturbation series convergences rapidly and only the first few orders of perturbation need to be considered.

$$E = \sum_{n=0} \lambda^n E^{(n)} \tag{3.27}$$

$$\Psi = \Phi_0 + \sum_{n=1} \lambda^n \Psi^{(n)} \tag{3.28}$$

Using both 3.27, and 3.28 in the Schrödinger equation, an expression with infinite order on λ is obtained.

$$\begin{aligned} &\hat{H}^{(0)}\Phi_0 + \lambda\left(\hat{H}^{(0)}\Psi^{(1)} + \hat{V}\Phi_0\right) + \lambda^2\left(\hat{H}^{(0)}\Psi^{(2)} + \hat{V}\Psi^{(1)}\right) + ... \\ &= E^{(0)}\Phi_0 + \lambda\left(E^{(0)}\Psi^{(1)} + E^{(1)}\Phi_0\right) + \lambda^2\left(E^{(0)}\Psi^{(2)} + E^{(1)}\Psi^{(1)} + E^{(2)}\Phi_0\right) + ... \end{aligned} \tag{3.29}$$

Since 3.29 is valid for any $\lambda \in \mathbb{R}$, for every power of λ an equation can be built. This separation of the Schrödinger equation into different orders of λ leads to the set of equations describing perturbation theory:

$$\hat{H}^{(0)}\Phi_0 = E^{(0)}\Phi_0, \quad n = 0 \tag{3.30}$$

$$\hat{H}^{(0)}\Psi^{(n)} + \hat{V}\Psi^{(n-1)} = \sum_{i=0}^{n} E^{(i)}\Psi^{(n-i)}, \quad n \geq 1 \tag{3.31}$$

It is worth noting that according to eq. 3.31, the n^{th} order equation depends on all the $n-1$ orders below, but not on any order above. This feature allows the perturbation series to be truncated at a specific order n, without requiring knowledge about any order

above. It can be shown that knowing $\Psi^{(n)}$ allows the calculation of the energy up to the $(2n+1)^{\text{th}}$ order. This is known as Wigner's $(2n+1)$ rule (*6, 10*).

In the formalism of Raylaeigh-Schrödinger Perturbation Theory (RSPT) $\Psi^{(i)}$ is spanned using the CI ansatz (eq. 3.23). To make the theory applicable one needs only to define the perturbation and the zeroth-order Hamiltonian. The choice of the latter is of uttermost relevance, since this partitioning of the full Hamiltonian in a zeroth-order Hamiltonian and a perturbation determines the performance of the method (*40*). To keep size consistency and extensivity, the zeroth-order Hamiltonian is set to the sum of one-electron Fock operators. This choice has two other significant advantages: $\hat{H}^{(0)}$ is diagonal in the canonical MO basis; $\Psi^{(0)}$ is an eigenfunction of $\hat{H}^{(0)}$. The first-order equations can thus be easily solved. The perturbation remains as the difference between the Hamiltonian and the Fock operator (*6, 11*).

$$\hat{H}^{(0)} = \sum_{rs} \hat{E}_{rs} f_{rs} \tag{3.32}$$

$$\hat{V} = \hat{H} - \hat{H}^{(0)} = \hat{H} - \hat{F} \tag{3.33}$$

This choice of the zeroth-order Hamiltonian and perturbation comprises the premises of Møller-Plesset Perturbation Theory (MP), giving rise to the family of n^{th}-order Møller-Plesset Perturbation Theory (MPn) methods.[11] With this choice, the HF wavefunction remains an eigenfunction of the zeroth-order Hamiltonian and the HF energy comes as the sum of the first two orders of energy, *i.e.*, $E_{\text{HF}} = E^{(0)} + E^{(1)}$. This means that correlation corrections can only arise after the second-order in perturbation (*6, 10, 11*). Projecting the reference on eq. 3.31 for $n = 2$ and rearranging in terms of $E^{(2)}$ defines the expression for the second-order energy

$$E^{(2)} = \sum_{i \neq 0} \frac{\langle 0 | \hat{V} | \Phi_i \rangle \langle \Phi_i | \hat{V} | 0 \rangle}{E_0^{(0)} - E_i^{(0)}} \tag{3.34}$$

Projecting each contribution to $\Psi^{(1)}$ on eq. 3.31 for $n = 1$ gives the residual equations, which must once again zero. Alternatively, the residuals may be obtained by differentiation of the Hylleraas energy.[12] The full set of excited configurations essential to solve the n^{th}-order residuals forms the first-order interacting space. This is composed by all

[11] Note that originally $\hat{H}^{(0)}$ was a diagonal operator since canonical orbitals were used. We decided to follow here the generalization of MP theory to a non-diagonal $\hat{H}^{(0)}$ (*8*), as this proves more useful for the understanding of MRPT. The difference between canonical and non-canonical MP theory is that the latter requires solving the residual equations iteratively, since there is no analytical solution. The results are however equivalent.

[12] More details on the Hylleraas functional are given in section 4.11.

non-zero Φ_{pq}^{rs} configurations (*65*). The residual equations determining each excited configuration's amplitude in MP2's wavefunction are given by:

$$R^i = \langle \Phi_i | \hat{F} \left| \Psi^{(1)} \right\rangle - E_0^{(0)} \left\langle \Phi_i | \Psi^{(1)} \right\rangle + \langle \Phi_i | \hat{V} | \Phi_0 \rangle = 0 \tag{3.35}$$

In these expressions, $E_0^{(0)}$ is the sum of the energies of all occupied orbitals in the reference, and $E_i^{(0)}$ is the sum of energies of occupied orbitals in the excited configuration i (*6*). For convenience, intermediate normalization of $\Psi^{(1)}$ is assumed, *i.e.*, $\left\langle 0 | \Psi^{(1)} \right\rangle = 1$.

Since the Hamiltonian is built as a sum of at most two-electron operators then for second-order perturbation theory substitutions higher than double have no contribution. Additionally, due to Brillouin's theorem, singly excited configurations also zero. The first-order wavefunction is thus left as a linear combination of doubly excited configurations, which can be generated from the substitution operators 3.6 (*65*). This leads to the ansatz

$$\Psi^{(1)} = \frac{1}{2} \sum_{ij} \sum_{ab} \Phi_{ij}^{ab} c_{ab}^{ij} \tag{3.36}$$

with

$$\Phi_{ij}^{ab} = \hat{E}_{ai,bj} \Phi_0 \tag{3.37}$$

Note that since $\hat{E}_{ai,bj} = \hat{E}_{bj,ai}$ also $T_{ab}^{ij} = T_{ba}^{ji}$, which accounts for the factor $\frac{1}{2}$ in 3.36.

Using this framework, and assuming the use of canonical orbitals the amplitudes can be derived from eq. 3.35 as

$$c_{ab}^{ij} = -\frac{K_{ab}^{ij}}{\epsilon_a + \epsilon_b - \epsilon_i - \epsilon_j} \tag{3.38}$$

with the second-order energy thus defined as

$$E^{(2)} = -\sum_{ij} (2 - \delta_{ij}) \sum_{ab} \frac{K_{ab}^{ij} \left(2K_{ab}^{ij} - K_{ba}^{ij} \right)}{\epsilon_a + \epsilon_b - \epsilon_i - \epsilon_j} \tag{3.39}$$

For non-canonical orbitals the expressions 3.38 and 3.37 differ by the fact that the closed-shell Fock matrix is no longer diagonal, thus $f_{ij} \neq \epsilon_i \delta_{ij}$. The virtual block of the Fock matrix can however be made diagonal. The amplitudes are in this case calculated using a perturbative update instead. In iteration *iter* the amplitude $c_{ab}^{ij(iter)}$ is defined as

$$c_{ab}^{ij(iter)} = c_{ab}^{ij(iter-1)} - \frac{R_{ab}^{ij(iter)}}{\epsilon_a + \epsilon_b - f_{ii} - f_{jj}} \tag{3.40}$$

where $c_{ab}^{ij(iter-1)}$ is the value of the same amplitude in the previous iteration ($c_{ab}^{ij(0)} = 0$), and $R_{ab}^{ij(iter)}$ is the value of the residual equation for that same pair for the iteration *iter*.

At low orders, PT recovers a significant percentage of dynamic correlation (*8, 41*). Second-order MP (MP2) recovers typically 80 to 120% of the correlation energy. This is also the least expensive post-HF method, scaling with $\mathcal{O}(M^5)$. Third-Order Møller-Plesset Perturbation Theory (MP3) accounts for typically 90 to 110% of the correlation energy, scaling with $\mathcal{O}(M^6)$. The accuracy of Fourth-Order Møller-Plesset Perturbation Theory (MP4) can go up to 98 to 102% of the correlation and the method scales with $\mathcal{O}(M^7)$ (*208,209*). Calculations beyond MP4 are rare. Although MP4 improves over MP3, which in its turn improves over MP2 (*10*), there is no guarantee that the perturbation series is convergent. There are indeed many examples showing otherwise. Furthermore, now-a-days, only MP2 and MP3 are still in use, since for equivalent computational costs, CC methods offer more accuracy and better results (*6*).

In PT it is not ensured that the calculated energy ceils the exact energy of the system. As PT considers the perturbation of a system to be rather small, if HF meagers as a reference, the equations acquire inferior convergence until divergence occurs. This is indeed the case when the HOMO-LUMO gap becomes too small, causing the energy to diverge. Everytime bonds are stretched to dissociation, MPn methods are typically doomed to fail, mostly due to the quality of the reference wavefunction (*6, 10*). This liability can only be overcome by generalizing the theory to multiconfiguration references.

3.5 Multireference Methods

Whenever correlation effects take a purely dynamic character, HF offers a proper zeroth-order approximation. SR methods will be accurate enough for both correlation energies and correlated wavefunctions. For systems with high strong correlation character the HF wavefunction is only one of the leading contributions. It no longer is a satisfactory starting point and consequently SR methods are no longer adequate. A method improving the reference wavefunction for such cases is the Multi-Configuration Self-Consistent Field (MCSCF). The MCSCF provides a reference with multiconfigurational character, and unlike CI, PT or CC will not aim for dynamic correlation. Instead, a balanced and qualitatively correct wavefunction is searched. For quantitative solutions one may apply on top of the MCSCF the CI formalism (yielding Multireference Configuration Interaction (MRCI) theories), Perturbation Theory (giving rise to Multireference Perturbation Theory (MRPT)), or even Coupled Cluster (Multireference Coupled Cluster (MRCC) methods). As their name already suggest, these methods are labeled Multireference (MR).

Typical examples of strong MR cases are diradicals like Ozone, benzynes or carbenes.

For these molecules, energies and properties are not correctly predicted using SR methods. ESs belong also to the class of typical MR systems (*63*). In a truly simplistic approximation, the lowest ESs may be described by one excited SD. This means that we restrict the transition to single excitations, *e.g.*, $n \rightarrow \pi*$ or $\pi \rightarrow \pi*$. Such cases are rarely true, and as the ESs move energetically farther from the GS (*e.g.* Rydberg states) the density of states of states increases and different electronic states will mix. Large systems with extended conjugation with an almost vanishing HOMO-LUMO gap (*63*) and organometallic compounds are also typically MR. As a consequence of the high strong correlation character of these systems, they show variable occupation patterns. It is still worth mentioning the cases of avoided crossings, when two electronic states come energetically close enough for some particular geometries. These are common for photorelaxation processes (*93*). Cases like these can only be treated with purely MR wavefunctions (*47*).

PES in general and partially broken/formed bonds in particular, like Transition States (TSs), are also cases which might require a MR treatment. Around stable minima the HF solution is usually the leading configuration in a wavefunction, acting thus as a good reference. But closer to the dissociation limits of chemical bonds, higher spin multiplicities start having a significant weight in the wavefunction. Therefore single-determinant based solutions do not provide accurate enough results, sometimes not even correct dissociation profiles. The dissociation of F_2 calculated with Perturbation Theory using both SR and MR methods is presented below. Using MR methods is possible to obtain a balanced global description of PESs (*43*), not only for the description of dissociation processes but also of the many electronic states.

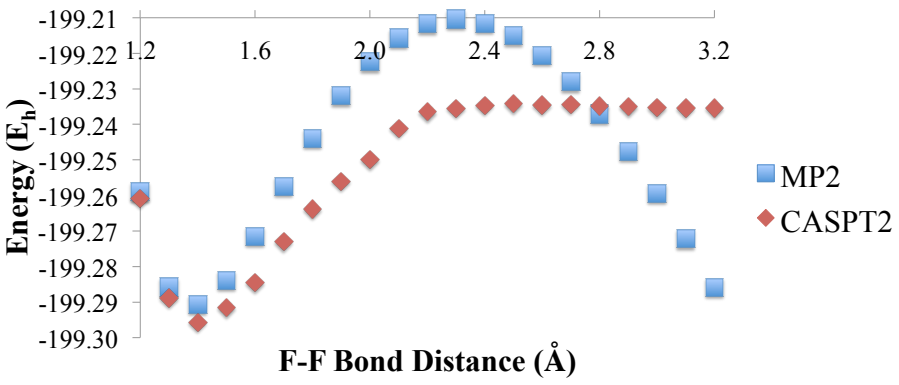

Figure 3.2: PES for the F_2 molecule from 1.1 to 3.5 Ångstrom.

This does not mean though that SR methods cannot predict excitation energies with some accuracy, nor give correct dissociation profiles. We can surely mention the exam-

ples of CC2 (*221, 222, 224, 225, 296*)[13] or equation of motion CC methods (*297–301*), successful in the calculation of excitation energies. The recently introduced Distinguishable Cluster method is also particularly efficient when studying multiple bond breaking processes (*302*). In any case, a general treatment of any MR system and its chemistry (not simply properties like excitation energies) requires a reliable theoretical description of properly adapted methods (*14, 126*).

The next section provides a short introduction on the multi-configurational reference using Multi-Configuration Self-Consistent Field (MCSCF).

3.5.1 Multi-Configuration Self-Consistent Field

In a very simplistic way, Multi-Configuration Self-Consistent Field (MCSCF) is an extremely reduced truncated formulation of the CI method. Here, both the orbitals and a wavefunction containing only the leading configurations from the FCI expansion are optimized.

$$\Psi_{\mathrm{MCSCF}} = \sum_{R} c^{R} \Phi_{R} \tag{3.41}$$

The configurations $|\Phi_R\rangle = |R\rangle$ are typically Configuration State Functions (CSFs) (these are detailed in section 4.2) describing pure spin states. This ensures that resulting wavefunctions are eigenfunctions of the total spin. Since the aim of MCSCF is to introduce strong correlation, the wavefunction expansion comprises a significantly reduced number of configurations, just enough to give the wavefunction a multi-configuration character. Furthermore, in MCSCF, the orbitals are also optimized, being thus possible to let them relax. The most detailed description possible of the orbitals is of utmost importance, as the MCSCF is especially built to provide reference wavefunctions for more refined electronic correlation treatments. The full optimization is performed variationally, such that the HF solution appears as a restriction of MCSCF to single determinant cases. Hence, for any given AO basis, the MCSCF energy will always lie between HF's and FCI's (*45, 48*).

$$E_{\mathrm{HF}} \geq E_{\mathrm{MCSCF}} \geq E_{\mathrm{FCI}} \tag{3.42}$$

The description given above is mostly general, and indeed several MCSCF formulations are possible. A first difficulty is the selection of configurations to span the wavefunction (*47*). Of the possible formulations, the Complete Active Space Self-Consistent Field

[13] An approximated CCSD method based on linear response theory

(CASSCF) provides the most simple selection procedure (*48–50*).[14] In CASSCF three different sets of orbitals are identified: closed-shell (i, j, k and l), active (t, u, v, w, x, y and z) and virtual (a, b, c and d). One may furthermore define 2 more sets of orbitals and one subset: the internal space (m and n), which is the union of the closed-shell and active; the set of all orbitals, defined as the union of all 3 sets (p, q, r and s); the set of core orbitals, a subset of the closed-shell. Each closed-shell orbital is doubly occupied in every configuration. Virtual orbitals are always vacant in CASSCF configurations. Active orbitals have an overall net occupation as a set, leaving the occupation number of each active orbital free. This is thus a number between 0 and 2, the average of all occupation numbers in the reference configurations with the CI coefficients acting as weights (*45,48*). Typical occupation numbers for active orbitals lay between 0.02 and 1.98 (*63*). Finally, core orbitals are the innermost orbitals in a system, from lower shells, and correspond in essence to free-atom orbitals in a molecule (*46*). These usually have extremely low energies and are well separated from the rest of the closed-shell orbitals. Core orbitals are thus usually not correlated (*45*) and will be omitted from here on. To build the active space one unites a small subset of external HF orbitals with a small subset of it's occupied ones. A suitable active space contains all orbitals changing significantly along the coordinates of a transformation, and choosing those orbitals should provide a balanced wavefunction. Unbalanced solutions overestimate the bi-radical character of the system. A special case of active spaces is the full valence active space, which considers all valence orbitals in this orbital set. Since molecular systems usually dissociate to valence states of the constituent atoms, then the full valence active space ensures an appropriate description for practically all molecular processes. Having selected an active space, one may describe the Complete Active Space (CAS) reference with CAS[N, M] (*6, 10*), where N is the number of active electrons and M the number of active orbitals.

The CASSCF wavefunction is built as an FCI expansion of the active space, correlating only these orbitals (*48, 51, 303–307*). It includes thus the complete set of CSFs built by arranging the active electrons amongst the active orbitals in viable ways consistent with both the spin and the space symmetries (*58*). The problem of selecting the most relevant configurations is relegated to the selection of the active orbitals. Even if the ansatz becomes wasteful by including less relevant configurations, the FCI nature of CASSCF enables the use of efficient techniques. This renders in the end an easier and less cumbersome calculation than smaller and more general MCSCF calculations with the same

[14]The first version for this model was first proposed by Ruedenberg as Full Optimized Reaction Space (FORS) (*51, 52*).

internal orbital space (*45*). On the other hand, even small CAS spaces may easily become unmanageable. To overcome this liability and increase the number of active orbitals treated in the MCSCF, simplifications like Restricted Active Space Self-Consistent Field (RASSCF) have been proposed (*308*). This method consists in a restriction to CASSCF in which the active space is further partitioned into three Restricted Active Spaces (RASs): RAS1; RAS2; RAS3. The FCI expansion is only done to RAS2. In both other RAS spaces the structure of the configurations is restricted such that orbitals in RAS1 act as electron donors in substitutions, while orbitals in RAS3 act as electron acceptors (*6, 63*).

Seeing the MCSCF as another truncated version of CI allows to succinctly describe its general procedure. The energy has to be made stationary with respect to changes in the coefficients of the wavefunction (c^R) and the orbitals. The full optimization is performed by diagonalizing the electronic Hamiltonian over the MCSCF wavefunction basis set (3.41), *i.e.*, minimizing the expression

$$E_{\mathrm{MCSCF}} = \langle \Psi_{\mathrm{MCSCF}} | \hat{H} | \Psi_{\mathrm{MCSCF}} \rangle = \sum_{mn} h_{mn} D^{(1)}_{mn} + \frac{1}{2} \sum_{mn} \sum_{m'n'} (mn|m'n') D^{(2)}_{mn,m'n'} \quad (3.43)$$

The first- and second-order density matrices are defined by contracting expansion coefficients with coupling coefficients,

$$\begin{aligned} D^{(1)}_{mn} &= \langle \Psi_{\mathrm{MCSCF}} | \hat{E}_{mn} | \Psi_{\mathrm{MCSCF}} \rangle = \langle 0 | \hat{E}_{mn} | 0 \rangle = \sum_{RR'} c_R c_{R'} \langle R | \hat{E}_{mn} | R' \rangle \\ D^{(2)}_{mn,m'n'} &= \langle 0 | \hat{E}_{mn,m'n'} | 0 \rangle = \sum_{RR'} c_R c_{R'} \langle R | \hat{E}_{mn,m'n'} | R' \rangle \end{aligned} \quad (3.44)$$

Eq. 3.43 is valid under the restriction that both the MCSCF wavefunction and the orbital basis are orthonormal, *i.e.*

$$\langle \Psi_{\mathrm{MCSCF}} | \Psi_{\mathrm{MCSCF}} \rangle = \sum_R |c_R|^2 = 1 \quad (3.45)$$

$$\langle \phi_m | \phi_n \rangle = \langle m | n \rangle = \delta_{mn} \quad (3.46)$$

To minimize the energy (3.43) under the constraint 3.45 one builds the Lagrangian

$$\mathcal{L} = \sum_{R,R'} c_R \langle \Phi_R | \hat{H} | \Phi_{R'} \rangle c_{R'} - \epsilon \sum_R \left(|c_R|^2 - 1 \right) = 0 \quad (3.47)$$

and zeroes its differential with respect to the coefficients c_R,

$$\frac{\partial}{\partial c_R} L = \sum_{R'} \langle \Phi_R | \hat{H} | \Phi_{R'} \rangle c_{R'} - 2\epsilon c_R = 0 \quad (3.48)$$

These are the usual eigenvalue equations for regular CI theory (*45*).

The optimization of MOs follows a parameterization by orthogonal rotations among these, where the rotations are defined by a unitary transformation. Older MCSCF programs truncated the orbital rotations to second-order expressions in terms of the rotation. Using these programs, for most cases, *ca.* 10 iterations are required to optimize a wavefunction, with a relatively high computational cost for each iteration. This is because both the gradient and the Hessian matrix must be built for each set of MOs. The radius of convergence is rather reduced, as the periodicity of orbitals cannot be described. Such liability may be improved by direct inclusion of higher orders of energy derivatives, which then makes the method more expensive as well (*45*).

More recent implementations offer an alternative, which is able to express orbitals in infinite order with respect to the orbital rotations, thus keeping the orbitals periodic (*43, 309*). The algorithm becomes more robust and convergence is also improved. This Lagrange coupled MCSCF program works in two steps, the macro- and microiterations. Simply put, the macroiterations consist in the (re)calculation of the Coulomb and exchange integrals, as well as a variational energy. The microiterations consist in the iterative calculation of the orbitals and CI vector for fixed integrals obtained in the macroiterations. When a minimum is found, the orbitals are transformed. Of course this method has the additional complication arising from the non-linearity of the equations in the microiterations, but this is usually overcome by the use convergence accelerators like Direct Inversion of the Iterative Subspace (DIIS).[15] The number of macroiterations is usually very low, about 3, which is a result of the method's almost cubic convergence. Additionally, the radius of convergence is significantly larger than purely second-order methods, making it more suitable for general application (*45*).

MCSCF is now routinely used to obtain wavefunctions for GSs and ESs. A general treatment of the later requires multiroot capability to retrieve the coefficients for the wavefunction of the desired state, and in principle a set of orbitals is obtained for each calculated electronic state. However, this procedure yields ill-defined MCSCF wavefunctions (*44*), since one set of orbitals is only suitable for one state. Alternatively, a single set of state-averaged orbitals can be calculated in the MCSCF procedure (*52, 309, 312*). This brings many advantages, namely stabilized convergence and prevention of root-flipping problems, which can occur for close-lying electronic states (*313*). Furthermore, using a

[15]DIIS is an extrapolation procedure, which both forces convergence and reduces the number of iterations. For each iteration, it finds the point with the lowest error by minimizing an error function subject to the normalization constraint. This minimization is then used to generate an extrapolated Fock matrix for each iteration (*6, 310, 311*).

single set of orbitals for several states eases the calculation of properties like transition moments (*314*). The differences between state-averaged and single-state MCSCF is basically in the calculated orbitals and in the respective density matrices. The latter become the average of the respective densities for the x states included in the calculation, $D_x^{(1)}$, using as such the weight of each state w_x. *E.g.*, the state-averaged first-order density $D_{SA}^{(1)}$ is given by

$$\left(D_{SA}^{(1)}\right)_{mn} = \sum_x w_x \left(D_x^{(1)}\right)_{mn} \tag{3.49}$$

3.6 Local Methods

Local methods aim to reduce CI expansions both at the configuration and orbital levels by using a suitable orbital basis. The use of local orbitals allows the exploration of the locality of correlation effects, meaning that correlation effects between two electrons far enough are minor if not even negligible (*132*). Furthermore, local orbitals offer an interpretation resembling chemical intuition (*132*), similar to the concepts of Lewis' structures. The changes in orbitals in these methods occur at two levels: i) the occupied space is localized, generating Localized Molecular Orbitals (LMOs); ii) the virtual space is expressed in a local basis. A local/localized orbital is a probability density function which takes the value of zero outside a (significantly) restricted spatial region of a molecular system (*132*). The difference between local and localized orbital is however at the mathematical level: localized orbitals are obtained by minimizing/maximizing a functional; a local orbital requires changing to a local basis. While the localization is a non-singular unitary transformation (*134*) that introduces no approximation at the SCF level (*132, 134*), a transformation matrix to a local basis yields a different orbital space with different properties, which might even have different dimensions.

The localization of occupied spaces to generate LMOs is possible whenever these sets of MOs are invariant to unitary rotations. This is the case of both HF and MCSCF orbitals.[16] The success of these techniques depends on the general structure of the functional used to determine the orbitals, especially the presence of strong and isolated minima (*157*). However, the localization scheme itself does rarely play a relevant role for the efficiency and accuracy of the local method (*283*). There are several possible localization schemes available, of which the most widely used are the method of Boys (*169–171*) and the one of Pipek and Mezey (*172*). Common to all localization methods is that the Fock matrix

[16]For the case of MCSCF the closed-shell and active spaces can be localized separately.

is no longer diagonal (*132*) and that the diagonal elements of the Fock matrix are not orbital energies with physical meaning. However, orbital orthogonality is usually kept. All these methods yield a set of MOs with coefficients $L_{\mu i}$, which are gathered in a coefficient matrix $\mathbf{L}$.

$$|\phi_i\rangle = |i\rangle = \sum_{\mu} |\chi_\mu\rangle L_{\mu i} = \sum_{\mu} |\mu\rangle L_{\mu i} \tag{3.50}$$

In the method of Boys the spatial extension of MOs is minimized. This is accomplished by minimizing the functional

$$B = \sum_{i=1}^{m} \langle \phi_i \phi_i | \left(|\mathbf{r}_1 - \mathbf{r}_2| \right)^2 | \phi_i \phi_i \rangle \tag{3.51}$$

Although rather inexpensive (*132*), LMOs built from this procedure usually mix σ-π orbitals. This leads to asymmetric solutions, which might not even be unique (*147*).

A similar approach is the one of Edmiston and Ruedenberg (*315*), where localized orbitals are obtained by maximizing the intraorbital Coulomb repulsion (*6, 132*).

$$ER = \sum_{i=1}^{m} \langle \phi_i \phi_i | \left(\frac{1}{|\mathbf{r}_1 - \mathbf{r}_2|} \right) | \phi_i \phi_i \rangle \tag{3.52}$$

This naturally requires the availability of Coulomb integrals, which have a computational high cost. Therefore, the method of Edmiston and Ruedenberg is not commonly used. Nevertheless, this method improves over Boys localization as it allows for a clear separation of σ and π orbitals.

In a completely different approach, the Pipek-Mezey method (*172*) maximizes Mulliken atomic charges, meaning that for each LMO i the functional

$$PM = \sum_{A}^{atoms} \left(\sum_{\alpha \in A}^{AO} \sum_{\beta}^{AO} q_{\alpha i} S_{\alpha \beta} q_{\beta i} \right)^2 \tag{3.53}$$

is maximized. This method produces a set of orbitals with clear σ-π separation as well (*132, 173, 316*), but unphysically tied to the basis set.

An improvement over the latter came recently with the introduction of Intrinsic Bond Orbitals (IBOs) (*173*), based on free-atom AOs (*317–319*). With IBOs an intrinsic minimal basis is defined in a first instance, in order to exactly describe the occupied MOs of a wavefunction. This minimal basis is then orthonormalized, dividing one-particle spaces into many atomic contributions, Intrinsic Atomic Orbitals (IAOs). IBOs are built from orthogonalized IAOs by rotating these in order to maximize the number of electrons in each LMO.

$$IBO = \sum_{A}^{atoms} \sum_{i}^{occ} \left(2 \sum_{\mu \in A} \langle i|\mu\rangle\langle\mu|i\rangle \right)^n \tag{3.54}$$

In the expression above, μ runs over the IAOs of atom A and the exponent n takes the values of 4 or 2. IBOs are very similar to the orbitals resulting from the Pipek-Mezey method. They keep a clear distinction between σ and π orbitals (*173*) and allow for the analysis and chemical interpretation of wavefunctions. However, IBOs are insensitive to basis set variations and do not suffer from artifacts of diffuse basis sets.

Having localized the internal molecular spaces, gains in computational efficiency can be obtained if the virtual space is changed to a local basis (*132*). There are many possible choices of virtual orbitals, the most popular being Projected Atomic Orbitals (PAOs), Pair Natural Orbitals (PNOs) and Orbital Specific Virtuals (OSVs). No matter which choice is taken, the substitution spaces are always reduced, becoming only subsets (domains) of the full virtual space (*66, 136*). This sacrifices however orbital invariance. The cuts are not random and follow specific criteria, which depends on the choice of virtuals. Their purpose is to ensure minimal loss in accuracy according to the thresholds used.

The domain approximation can be easily pictured in a physical or spatial way (*132*): the farther orbitals are apart from each other, the harder it should be for the electronic substitution to take place, having thus a smaller weight in the global wavefunction. This restriction is not just intuitive, it has a mathematical basis (*132, 148*). The correlation energy of an electron pair mn is in PT proportional to $\sum_{ab}\left(K_{ab}^{mn}\right)^2$. The magnitude of the integrals K_{ab}^{mn} depends on the value of the differential spatial overlaps ρ_{am} and ρ_{bn}.

$$K_{ab}^{mn} = \int_{\mathbb{R}^3} \rho_{am}(\mathbf{r}_1)\frac{1}{\mathbf{r}_{12}}\rho_{bn}\left(\mathbf{r}_2\right) d_{\mathbf{r}_1} d_{\mathbf{r}_2} \tag{3.55}$$

$$\rho_{am}(\mathbf{r}) = \phi_a(\mathbf{r})\phi_m(\mathbf{r}) \tag{3.56}$$

If m (n) is a LMO with charge center in $\mathbf{R}_m$ ($\mathbf{R}_n$) and if a (b) is a local virtual near m (n), then ρ_{am} (ρ_{bn}) is local and is centered around $\mathbf{R}_m$ ($\mathbf{R}_n$). By expanding the orbitals m and a as Gaussian functions, then the integrals K_{ab}^{mn} will be a combination of functions which decay exponentially with the distance $R_{am} = |\mathbf{R}_m - \mathbf{R}_a|$ (*148*). As such, if the internal orbitals and the respective substitution space do not span the same spatial region, then the energy contribution of that respective substitution is in practice negligible.

With the domains for each LMO m, $[m]$, domains for pairs are assembled by uniting the domains of two orbitals m and n, *i.e.*, $[mn] = [m] \cup [n]$ (*136*) (for the case of PAOs and OSVs) or by finding a common domain with a specific procedure (PNOs). Since the internal space is localized and the virtual space is local, domain sizes are (significantly) smaller than the full canonical virtual space. In the case of PAOs, for each LMO m the substitution space contains one to two shells of neighbouring atoms (*148*). This typically

corresponds to local virtuals centered on two to eight atoms (*147*). There are thus three main consequences from using domain approximations: i) transformation matrices to local basis are rectangular, with more rows than columns (*149*);[17] ii) the dimensions of amplitude and residual tensors are reduced, leading to a speed up of the calculation; iii) the domain sizes become independent of the molecular size, given that the molecules are large enough (*2, 68, 134, 136, 216*). Thus, domain approximations ensure that the correlation space for each orbital pair does not increase unphysically with the molecular size (*68, 132*).

To select a domain for an LMO m many criteria may be used:

➢ Spatial or distance - A local virtual belongs to m's domain if it is within a certain radius from the atomic centers of m (PAO).

➢ Energy - All virtuals in the vicinity of m belong to its domain until at least $x\%$ of the correlation energy is recovered (PNO,OSV,PAO).

➢ Occupation number - Densities are built for an orbital m or pair mn and then diagonalized. The eigenvalues define occupation numbers for each local virtual. All virtuals with an "occupation number" larger than a threshold belong to the domain of m (or mn) (PNO,OSV).

Domain approximations reduce drastically the number of excited configurations built for each orbital pair. However, these do not affect the number of pairs, which without introducing further approximations, still scale quadratically with the system's size. Orbital pairs can thus be sorted according to specific criteria that allows treating different pair classes at different levels (*2, 66, 136*). This differential treatment is known as pair approximations. These different pair classes can be determined using: the minimum distance R between any atoms in the domains of i and j (*2, 3, 150*); atomic connectivity (*3, 150*); MP2 energy contributions (*1, 136*). The connectivity scheme keeps the definition of pair classes independent of bond lengths and atomic sizes, and it is equivalent for any molecule. However, some atoms might be spatially close, even though they are separated by many bonds. Such pairs might have strong contributions to correlation but are nevertheless wrongly classified according to bond criteria. Mixed schemes are also possible, for which distance criteria determines distant and very distant pairs, while the other classes are determined by bond criteria.

Pair approximations are made possible from the definition of the exchange integrals as well, *c.f.* eq. 3.55. In the conditions above specified, for local ρ_{am} and ρ_{bn}, the larger the

[17] Because only square matrices are invertible, the transformation to a local virtual basis is unidirectional: from canonical to local in the residuals and reversed for amplitudes.

distance between m and n, then the larger is the distance between ρ_{am} and ρ_{bn} (*148*). This means that the exchange integrals take smaller values and the contribution of a specific substitution to the correlation energy has but a minor weight. If the summed contribution of an orbital pair is barely noticeable in the total correlation energy, then this pair can either be completely neglected or treated at a different (lower) level of theory.

Pair and domain approximations come without much loss in accuracy (when incorrectly applied, pair approximations may cause errors up to 10 $kcal/mol$ in energy differences (*265*)). Typically 0.5% or even less is lost of the total correlation for a triple-ζ quality basis set (*133*). However, domain and pair approximations are responsible for the major improvements in the computational costs and are essential for the success of local methods. Without pair and domain approximations, linear scaling electron correlation methods would not have been possible (*2, 3, 133, 215–219, 228, 231, 234, 236–240*). Last, but not least, local approximations typically reduce the effect of undesired errors, like basis set superposition errors (*8, 132*).

In summary, since amplitude matrices are usually organized by orbital pair, pair approximations reduce the number of amplitude matrices required in a calculation (*148*). Domain approximations reduce the dimensions of each amplitude matrix.

3.6.1 Transformation to Local Virtual Orbitals

Although many choices of virtuals are available, the transformation from canonical to local virtuals follows a common procedure (*148, 149*). In this section such general procedure is given for general transformation matrices $\mathbf{Q}^{ij}$ and general local virtual orbitals α^{ij} in the domain $[ij]$. In other sections, specific transformation matrices are detailed for each different choice of local virtuals. The transformation matrices $\mathbf{Q}^{ij}$ for each pair ij transform canonical orbitals into general local virtuals in the domain ij, α^{ij}.

$$\left|\alpha^{ij}\right\rangle = \sum_{a} |a\rangle Q_{a\alpha}^{ij} \tag{3.57}$$

Since local virtuals are not *a priori* orthogonal, overlap matrices are defined as well,

$$\left(\mathbf{S}_{[ij,kl]}\right)_{\alpha\beta} = \left\langle \alpha^{ij} | \beta^{kl} \right\rangle = \sum_{ab} Q_{a\alpha}^{ij} \langle a|b\rangle Q_{b\beta}^{kl} = \left(\mathbf{Q}^{ij\dagger}\mathbf{Q}^{kl}\right)_{\alpha\beta} \tag{3.58}$$

Because pair functions are transformation invariant, it follows that

$$\sum_{ab} |ab\rangle c_{ab}^{ij} = \sum_{\alpha\beta} \left|\alpha^{ij}\beta^{ij}\right\rangle c_{\alpha\beta}^{ij} \tag{3.59}$$

Inserting eq. 3.57 in 3.59 results in the following transformation for amplitudes

$$c_{ab}^{ij} = \sum_{\alpha\beta} Q_{a\alpha}^{ij} c_{\alpha\beta}^{ij} Q_{b\beta}^{ij} \tag{3.60}$$

A similar expression transforms singles amplitudes as well. The difference is that these only depend on one virtual index. Since there is a dependence on one closed-shell index, one either uses the domain for the orbital i (PAO) or for the pair ii (PNO).

$$c_a^i = \sum_{\alpha} Q_{a\alpha}^{i} c_{\alpha}^{i} \tag{3.61}$$

The residual equations on the other hand are transformed from the canonical to the local basis,

$$R_{\alpha\beta}^{ij} = \sum_{ab} Q_{a\alpha}^{ij} R_{ab}^{ij} Q_{b\beta}^{ij} \tag{3.62}$$

Again, the residuals for singles transform analogously. The transformed residuals contain all the integrals in the local basis, subject to domain restrictions.

3.6.2 Local Density Fitting

Imposing a particular structure to tensors is an efficient way of reducing the computational effort required for the calculation of a particular quantity (*131*). This can be achieved, *e.g.*, by factorizations over auxiliary indices. Typical methods are the Cholesky decomposition[18] or Density Fitting (DF). DF consists on approximating the charge distributions $\rho_{ai} = \phi_a \phi_i$ using an auxiliary basis of functions $\{A\}$ (*137, 148, 226, 227, 320, 321*).

$$\rho_{ai} \simeq \sum_{A} \chi_A d_{ai}^A = \tilde{\rho}_{ai} \tag{3.63}$$

By minimization of the self-interaction of the error e_{SI} (*322*)

$$e_{SI} = \langle (\rho_{ai} - \tilde{\rho}_{ai}) | \, \frac{1}{r_{12}} \, | (\rho_{bj} - \tilde{\rho}_{bj}) \rangle \tag{3.64}$$

the following approximation to two-electron integrals is obtained:

$$(ai|bj) \simeq \sum_{AB} (ai|A) \, J_{AB}^{-1} \, (bj|B) = \sum_{A} (ai|A) \, d_{bj}^A \tag{3.65}$$

with

$$J_{AB} = (A|B) = \int \chi_A (\mathbf{r}_1) \, \frac{1}{\mathbf{r}_{12}} \chi_B (\mathbf{r}_2) \, d\mathbf{r}_1 d\mathbf{r}_2 \tag{3.66}$$

[18] Factorization of a matrix $\mathbf{A}$ into the product of a lower triangular matrix $\mathbf{V}$ by its conjugate transpose, $\mathbf{A} = \mathbf{V}\mathbf{V}^*$.

$$(B|ai) = \int \phi_a(\mathbf{r}_1)\,\phi_i(\mathbf{r}_1)\,\frac{1}{\mathbf{r}_{12}}\chi_B(\mathbf{r}_2)\,d\mathbf{r}_1 d\mathbf{r}_2 \tag{3.67}$$

$$d_{ai}^A = \sum_B J_{AB}^{-1}(B|ai) \tag{3.68}$$

Because the integrals are fitted with the aid of the auxiliary basis, the efficiency of this procedure significantly improves by increasing the size of the auxiliary basis, as the fitting becomes more flexible (*322*). There are in the literature many DF bases available. The optimization of the two DF bases used in this work can be found in (*322, 323*).

The calculation of two-electron integrals using DF starts with the calculation of the two- (eq. 3.66) and three-center (eq. 3.67) integrals, which are significantly less in number than the full set of four-center integrals (*148*). The three-center integrals are calculated in the AO basis, and then they are converted to the MO basis by contraction with the MO coefficient matrices $\mathbf{C}$ (in the canonical basis).

$$(B|ai) = \sum_{\mu\nu} (B|\mu\nu)\, C_{\mu a} C_{\nu i} \tag{3.69}$$

To calculate integrals as just the contraction of two quantities, the J_{AB}^{-1} term is split in two symmetric parts using Cholesky decomposition. This yields lower triangular matrices $\mathbf{V}$ such that $J_{AB}^{-1} = \mathbf{V}\mathbf{V}^* = \mathbf{V}\mathbf{V}^\dagger$. These matrices $\mathbf{V}$ rotate the integrals over the auxiliary basis to yield the quantities $\left(\bar{A}|ai\right)$. Building these rotated integrals has the great advantage of considerably reducing the data that needs to be stored (*324*).

$$\left(\bar{A}|ai\right) = \sum_B V_{\bar{A}B}\,(B|ai) \tag{3.70}$$

These $\left(\bar{A}|ai\right)$ integrals are then contracted with themselves to approximate the $(ai|bj)$ integrals, similarly to 3.65.

$$(ai|bj) = \sum_{\bar{A}} \left(\bar{A}|ai\right)\left(\bar{A}|bj\right) \tag{3.71}$$

The expression 3.71 can be evaluated in any orbital basis for the internal, virtual and auxiliary spaces. However it is advantageous to evaluate the integrals in a local basis, which can use local approximations to reduce the computational effort. This gives rise to local variants of DF (*3, 148, 228–235*). In these conditions, eq. 3.69 is rewritten using the coefficient matrices for LMOs and PAOs, respectively $\mathbf{L}$ and $\mathbf{P}$, to yield

$$(B|\tilde{r}i) = \sum_{\mu\nu} (B|\mu\nu)\, P_{\mu\tilde{r}} L_{\nu i} \tag{3.72}$$

where i refers to an LMO in 3.72. When calculating the integrals $(\tilde{r}i|\tilde{s}j)$ using local approximations the indices $\tilde{r}$ and $\tilde{s}$ are restricted to the domains of i and j. Additionally, domain approximations can also be applied to the auxiliary basis functions given that also these are local (*3*). Since with the domain approximation the number of $\tilde{r}$ and A in each domain is independent of the molecular size, then i) the number of integrals required in the summations in eqs. 3.71 and 3.70, and ii) the number of integrals required to calculate are significantly reduced. However, transforming the integrals $(B|\mu\nu)$ to $(B|\mu i) = \sum_{\nu} (B|\mu\nu) L_{\nu i}$ scales quadratically with the molecular size. To achieve linear scaling the sparsity of LMO coefficient matrices must be also employed. Directly neglecting smaller $L_{\mu m}$ matrix elements leads to sizeable errors. Instead, a parameter l_m can be defined to control which elements in the LMO coefficient matrices are set to zero. l_m is built by contracting the coefficient matrices over the AO dimension

$$l_m = \sum_{\mu \in C} L_{\mu m} L_{\mu m} \tag{3.73}$$

This sum goes over all orbitals located at an atomic center C. If l_m is smaller than a given threshold T_{LMO}, then all the coefficients $L_{\mu m}$ are zeroed. The approximate LMOs obtained by neglecting smaller $L_{\mu m}$ elements are then fit to the original LMOs using the least squares technique. The same can be applied to PAO coefficient matrices but with a smaller influence in efficiency (*148*).

DF is now-a-days widely used in all methods of quantum chemistry, making them significantly faster (*3*). The errors introduced by DF are typically negligible and systematic. Therefore, the errors introduced will tend to cancel out for energy differences (*3*).

3.6.3 Multipole Approximation

Another important approximation used to significantly reduce the cost of computational resources in electron correlation treatments is the Multipole Approximation (MPA) (*137, 214, 325*). A two-electron integral $(am|bn)$ can be expressed in terms of the product of charge distributions ρ_{am} and ρ_{bn} over the $\mathbf{r}_{12}$ operator. This is given in eqs. 3.55 and 3.56. For the following analysis, we assume that we are dealing with localized and local orbitals. Canonical orbitals are delocalized through the whole system and the multipole expansion becomes divergent (*325*). PAOs were originally used in the work of Hetzer *et al.* (*214, 325*). OSVs have also been successfully used (*137, 148*).

To build the integrals $(am|bn)$ in a multipole expansion one starts by expressing the Coulomb operator $(\mathbf{r}_{12})^{-1}$ in terms of the electron coordinates with respect to their orbital

charge centers ($\bar{\mathbf{r}}$). For electrons 1 and 2 (respectively) in orbitals m and n,

$$\mathbf{r}_{12} = |\mathbf{r}_2 - \mathbf{r}_1| = |\bar{\mathbf{r}}_2 - \bar{\mathbf{r}}_1 + \mathbf{R}_n - \mathbf{R}_m| = |\bar{\mathbf{r}}_2 - \bar{\mathbf{r}}_1 + \mathbf{R}| \tag{3.74}$$

The Coulomb operator comes thus as (quantities not in bold are the norms of the tensor in bold)

$$\begin{aligned} \frac{1}{\mathbf{r}_{12}} = \frac{1}{(\mathbf{r}_{12}^2)^{\frac{1}{2}}} &= \left[R^2 + \bar{r}_1^2 + \bar{r}_2^2 + 2\mathbf{R}.\bar{\mathbf{r}}_1 + 2\mathbf{R}.\bar{\mathbf{r}}_2 - 2\bar{\mathbf{r}}_1.\bar{\mathbf{r}}_2\right]^{-\frac{1}{2}} \\ &= \frac{1}{R}\left[1 + \frac{1}{R^2}\left(\bar{r}_1^2 + \bar{r}_2^2 + 2\mathbf{R}.\bar{\mathbf{r}}_1 + 2\mathbf{R}.\bar{\mathbf{r}}_2 - 2\bar{\mathbf{r}}_1.\bar{\mathbf{r}}_2\right)\right]^{-\frac{1}{2}} \\ &= \frac{1}{R}(1+x)^{-\frac{1}{2}} \end{aligned} \tag{3.75}$$

$$x = \bar{r}_1^2 + \bar{r}_2^2 + 2\mathbf{R}.\bar{\mathbf{r}}_1 + 2\mathbf{R}.\bar{\mathbf{r}}_2 - 2\bar{\mathbf{r}}_1.\bar{\mathbf{r}}_2 \tag{3.76}$$

Expanding then the function $(1+x)^{-\frac{1}{2}}$ in its Maclaurin series we get

$$\begin{aligned} \frac{1}{\mathbf{r}_{12}} = \frac{1}{R}\sum_k^\infty a_k x^k &= \frac{1}{R}\sum_k^\infty \left[\frac{1}{k!}\left(\frac{d^k}{dx^k}(1+x)^{-\frac{1}{2}}\right)_{x=0}\right]x^k \\ &= \frac{1}{R}\sum_k^\infty \frac{(-1)^k(2k)!}{2^{2k}}(k!)^2 x^k \end{aligned} \tag{3.77}$$

For $x < 1$ (or sufficiently large R) the above series is convergent. Inserting then 3.76 in 3.77 we obtain

$$\frac{1}{\mathbf{r}_{12}} = \sum_{n=0}^\infty \frac{1}{R^{n+1}} \sum_{m=0}^n V_{m,n-m}\left(\bar{\mathbf{r}}_1, \bar{\mathbf{r}}_2, \tilde{\mathbf{R}}\right) \tag{3.78}$$

where $\tilde{\mathbf{R}} = \frac{\mathbf{R}}{R}$. Using the series 3.78 in the definition of the exchange integrals (eq. 3.55) and truncating the series 3.78 at a given order $p = n+1$ we can approximate the integrals $(am|bn)$ as:

$$(am|bn)^{(p)} = \sum_{n=2}^{p+1} \frac{1}{R^{n+1}} \sum_{m=1}^{n-1} \int\int \rho_{am}(\mathbf{r}_1)\, V_{m,n-m}\left(\mathbf{r}_1, \mathbf{r}_2, \tilde{\mathbf{R}}\right) \rho_{bn}(\mathbf{r}_2)\, d\mathbf{r}_1 d\mathbf{r}_2 \tag{3.79}$$

Eq. 3.79 is a finite sum of integrals of $V_{m,n-m}$ over the spatial overlaps ρ_{am} and ρ_{bn}. Note that there are no contributions from the orders $n = 0$ nor $n = 1$, because the overlaps ρ_{am} cannot carry any charge. The first non-vanishing term is with $n = 2$. p is thus the highest order of multipole operators used in the approximation. For $p = 1$ one only uses the first-moment vectors, consisting this in the dipole-dipole approximation to the

MPA. $p = 2$ includes up to second-moment terms, introducing additionally the dipole-quadrupole interaction, $p = 3$ introduces the quadrupole-quadrupole and dipole-octopole interactions, *etc.*. For the first-moment approximation ($p = 1$, $m = 1$)

$$V_{1,1}\left(\mathbf{r}_1, \mathbf{r}_2, \tilde{\mathbf{R}}\right) = -2a_1\bar{\mathbf{r}}_1.\bar{\mathbf{r}}_2 - 8a_2(\tilde{\mathbf{R}}.\bar{\mathbf{r}}_1)(\tilde{\mathbf{R}}.\bar{\mathbf{r}}_2) = \bar{\mathbf{r}}_1.\bar{\mathbf{r}}_2 - 3(\tilde{\mathbf{R}}.\bar{\mathbf{r}}_1)(\tilde{\mathbf{R}}.\bar{\mathbf{r}}_2) \tag{3.80}$$

and

$$(am|bn)^{(1)} = \frac{1}{R^3}\left[\langle a|\mathbf{r}|m\rangle\,.\,\langle b|\mathbf{r}|n\rangle - 3\left(\tilde{\mathbf{R}}.\,\langle a|\mathbf{r}|m\rangle\right)\left(\tilde{\mathbf{R}}.\,\langle b|\mathbf{r}|n\rangle\right)\right] \tag{3.81}$$

where $\langle a|\mathbf{r}|m\rangle$ are dipole moment vectors evaluated over the orbitals a and m. This is the exact expression for the dipole approximation in the MPA. Another simplified approximation to eq. 3.81 is however proposed and used in most calculations (*137, 148*),

$$(am|bn) \simeq \frac{\sqrt{2}}{(R)^3}[\langle a|\mathbf{r}|m\rangle.\langle b|\mathbf{r}|n\rangle] \tag{3.82}$$

When inserted in MP2's pair energy expression, eq. 3.82 gives a dependence on $(R)^{-6}$. The resulting pair energy, E_{mn}^{DIP}, decays thus with the 6^{th} power of the distance between the internal orbitals m and n. Note that the decay for contributions with $p > 1$ is even faster. These estimated pair energies can then be used to select distant pairs and to approximate long-range correlation effects. Whenever the pair energy E_{mn}^{DIP} is below a threshold *thrdist*, the respective exchange integral matrix for that pair is approximated using the MPA. Since the calculation of the exchange integrals using this approximation is inexpensive, large savings of the computational resources can be achieved. The MPA can be used as a pre-screening of the integrals required to explicitly be computed.

In the work of Hetzer (*214*), it was showed that higher-order multipole contributions play a non-negligible role in estimating the integrals for long-range pairs. Ideally, this expansion is truncated by the multipole order of $p = 3$. Approximating the multipole series by its dipole-dipole term underestimates energies by up to 30%. Including higher-order terms improves accuracy but reduces convergence given small enough values for R. There is furthermore a limit to the accuracy and convergence of the multipole expansion. This is determined by the lowest order of the expansion used but also by the conditions initially assumed. Other factors influencing convergence and accuracy are the locality of the charges and the distance between them: the higher the locality and the distance, the better the results are. The requirement for high locality and high separation of charges has repercussions in restricting even further domain approximations. Since the charges ρ_{am} and ρ_{bn} require good localization and good separation, the domains for orbitals m and n are not merged to form an united domain. Instead, domains are kept asymmetric.

This means that when calculating the integrals $(am|bn)$, the domain restrictions are respectively $a \in [m]$ and $b \in [n]$, not $a, b \in [m, n]$: only terms like $(a^m m|b^n n)$ are included in the MPA, but not crossed exchange terms like $(a^n m|b^m n)$.

3.6.4 Projected Atomic Orbitals

In the Projected Atomic Orbital (PAO) method the virtual space is expressed with AOs, which were previously projected onto the virtual orbitals. By definition, AOs are local (*132*) and they do not constitute an orthonormal basis of orbitals (*326*). Nevertheless, due to their projective nature onto the virtual space, PAOs retain orthogonality towards LMOs (*65*). They are furthermore built independently of any occupied orbital, created to provide a full substitution space for any LMO (*155*). The transformation to the PAO basis is defined as

$$\tilde{Q}_{a\tilde{r}} = \left\langle a|\chi^{\mathrm{AO}}_{\tilde{r}}\right\rangle = \left(\mathbf{C}^{v\dagger}\mathbf{S}\mathbf{C}^{\mathrm{AO}}\right)_{a\tilde{r}} = \left(\mathbf{C}^{v\dagger}\mathbf{S}^{\mathrm{AO}}\right)_{a\tilde{r}} \tag{3.83}$$

where $\mathbf{S}$ is the overlap matrix for the basis used to expand both the canonical virtuals and the AOs (*2, 3, 216*) and $\mathbf{S}^{\mathrm{AO}}$ the AO overlap matrix. Because AOs are contracted Gaussian type orbitals, the coefficient matrix $\mathbf{C}^{\mathrm{AO}}$ that expresses AOs in terms of contracted Gaussians has to be considered in eq. 3.83. For correlation consistent or atomic natural orbitals the matrix $\mathbf{C}^{\mathrm{AO}}$ is simply the identity matrix (*3*), since the basis set is composed by atomic core and valence orbitals or by correlation functions. Alternatively, canonical HF AOs can be used, for which $\mathbf{C}^{\mathrm{AO}}$ is a block diagonal matrix. Normalization of the PAOs transforms $\mathbf{C}^{\mathrm{AO}}$ into a diagonal matrix containing the normalization factors. This means that PAOs are associated with Gaussian type orbitals.

It is also possible to define a PAO coefficient matrix $\mathbf{P}$ as

$$\mathbf{P} = \mathbf{C}^{v}\tilde{\mathbf{Q}} = \mathbf{C}^{v}\mathbf{C}^{v\dagger}\mathbf{S}\mathbf{C}^{\mathrm{AO}} = \mathbf{C}^{v}\mathbf{C}^{v\dagger}\mathbf{S}^{\mathrm{AO}} \tag{3.84}$$

and an overlap matrix for the PAOs given by

$$\mathbf{S}^{\mathrm{PAO}} = \tilde{\mathbf{Q}}^{\dagger}\tilde{\mathbf{Q}} \tag{3.85}$$

Building orbital domains associated to an orbital i is not automatic in the PAO method. This can be achieved by the Boughton-Pulay method (*327*), generating the transformation to the PAO space of m, $\tilde{\mathbf{Q}}^m$. The method assigns a subset of the PAOs to each m and this subset contains all the PAOs located at the same atoms, in which the LMO m is located. This allows the truncation of the wavefunction expansion in a

physically reasonable way (*65*). The selection of atoms belonging to a certain domain is determined by the atoms contributing most to the Mulliken orbital charges, until the value of 1.8 is surpassed. Those atomic centers are used to build an approximate orbital $\phi_m^{'}$. $\phi_m^{'}$ is then fitted to ϕ_m using least squares. The approximate orbital is represented by the orbital domain of m and is defined by the elements of the matrix $\mathbf{L}^{'}$.

$$\phi_m^{'} = \sum_{\rho \in [m]} |\chi_\rho\rangle \, L_{\rho m}^{'} \tag{3.86}$$

The matrix $\mathbf{L}^{'}$ corresponds to the matrix of coefficients of the atomic orbitals in the orbital $\phi_m^{'}$. This matrix is determined by comparison with the equivalent quantity from the actual orbital m,

$$\sum_{\nu \in [m]} S_{\mu\nu}^{\mathrm{AO}} L_{\nu m}^{'} = \sum_{\rho} S_{\mu\rho}^{\mathrm{AO}} L_{\rho m} \tag{3.87}$$

yielding the least squares functional

$$f\left(\mathbf{L}^{'}\right) = min\left[\int \left(\phi_m - \phi_m^{'}\right)^2\right] = 1 - \sum_{\nu \in [m]} \sum_{\rho} L_{\nu m}^{'} S_{\mu\rho}^{\mathrm{AO}} L_{\rho m} \tag{3.88}$$

This procedure is applied until $f\left(\mathbf{L}^{'}\right)$ is smaller than a given threshold. More basis functions are added until that criterion is satisfied. Adding neighboring centers improves even more the accuracy but at a higher computational cost: typical domains recover usually 98-99% of the correlation energy, while extended domains can recover up to 99.8-99.9% (*229, 328*). However, this selection of domains is *ad hoc*. In other methods domains are selected according to wavefunction or energy criteria. In the PAO method selection takes place with distance or connectivity criteria, not involving information on the virtual space. This may cause unbalanced results in energy differences. This procedure is furthermore strongly dependent on the basis set (*3*).

Alternatively one may use the Mata-Werner domain selection (*329*) based on natural population analysis (*330*). This procedure is more stable towards basis sets, but since no simple localization functional is employed, this method cannot be used in analytic gradient calculations (*210, 215*). In our work we are going to use IBO charges to build PAO domains, which is going to be discussed later.

Since the domain for mn is the union of the domains of m with n (*132*), the transformation matrix to the PAO space for the pair mn is given as

$$\tilde{\mathbf{Q}}^{mn} = \left(\tilde{\mathbf{Q}}^{m} | \tilde{\mathbf{Q}}^{n}\right) \tag{3.89}$$

Note that since the domains of m and n may overlap eq. 3.89 is not a product of two matrices. Eq. 3.89 represents thus the union of domains.

Convergence may be improved by using an orthonormal set of PAOs for each domain individually. But before orthogonalization (*3, 147*), it is recommended to eliminate PAOs with norm smaller than a certain threshold. These are usually inner-shell core orbitals. Afterwards, the remaining virtual orbitals are renormalized for convergence reasons. The new set of orthogonal PAOs can be found by diagonalization of the PAO overlap matrices $\left(\mathbf{S}_{[mn,mn]}\right)_{rs}$, followed by removal of the eigenvectors associated to eigenvalues smaller than a certain threshold value. $\bar{\mathbf{V}}^{mn}$ is the matrix mapping non-orthogonal PAOs to orthogonal and domain-specific PAOs. The transformation from canonical to orthogonal and domain specific PAOs can thus be defined as

$$\bar{\mathbf{Q}}^{mn} = \tilde{\mathbf{Q}}\bar{\mathbf{V}}^{mn} \tag{3.90}$$

and the new set of orbitals come as

$$|\bar{r}^{mn}\rangle = \sum_{\tilde{s}} |\tilde{s}\rangle \, \bar{V}^{mn}_{\tilde{s}\bar{r}} = \sum_{b} |b\rangle \, \bar{Q}^{mn}_{b\bar{r}} \tag{3.91}$$

Note that since the orthonormalization of PAOs is domain-specific, it is also pair-specific, and the resulting set of PAOs becomes also pair-specific. This is advantageous when solving the residual equations using the perturbative update of amplitudes.

Finally, a set of non-redundant SemiCanonical PAOs (PAO(SC)s) can ensure these also diagonalize the virtual block of the Fock matrix (*327, 331*). Semicanonicalization of PAOs does not affect the final result, it only improves convergence (this is a rotation of the previous PAO transformation matrix). A more detailed description on how to obtain these orbitals is presented in the section 3.6.5.

3.6.5 Pair Natural Orbitals

Pair Natural Orbitals (PNOs) are a set of approximate Natural Orbitals for each pair mn. While PAOs restrict significantly the domain for each orbital pair, PNOs offer the most compact description of pair domains (*3, 149, 155*), and therefore also improved convergence for dynamic correlation energies (*148, 149*). By construction, PNOs are localized in the same spatial region as the internal orbitals they are built from, meaning that the locality of PNOs is determined by the orbitals they stem from: for canonical orbitals PNOs are not local.

The transformation mapping canonical orbitals to PNOs is given by the eigenvectors of MP2 pair density matrices $\mathbf{D}^{mn}$. These are built from the respective amplitude matrices

$\mathbf{c}^{mn}$, as expressed in eq. 3.92.

$$D_{ab}^{mn} = \frac{1}{1+\delta_{mn}} \left(\tilde{\mathbf{c}}^{mn\dagger} \mathbf{c}^{mn} + \tilde{\mathbf{c}}^{mn} \mathbf{c}^{mn\dagger} \right)_{ab} \tag{3.92}$$

$$\tilde{c}_{ab}^{mn} = 2c_{ab}^{mn} - c_{ab}^{nm} \tag{3.93}$$

Alternatively, for singlet-triplet configurations,

$$D_{ab}^{mnp} = \left(\mathbf{c}^{mnp\dagger} \mathbf{c}^{mnp} \right)_{ab} \tag{3.94}$$

$$c_{ab}^{mnp} = \frac{1}{2}(c_{ab}^{mn} + p c_{ba}^{mn}), \quad p = \pm 1 \tag{3.95}$$

Since the eigenvalues of the pair densities $\mathbf{D}^{mn}$ correspond to natural occupation numbers a threshold may be used to select just the most relevant eigenvectors. This cut to the PNO transformation matrices allows the minimization of the number of virtuals for each domain. Furthermore, since PNOs are obtained from a diagonalization process specific to each pair, these form by construction an orthonormal set for each pair (*148, 153*). But such orthogonality does not apply for PNOs in different domains.

Typically, a few PNOs per pair are sufficient for a good approximation of the amplitude tensors. Consequently, amplitude and residual tensors are very compact, wavefunction expansions are shorter and lesser integrals are required. Substitution spaces in the PNO basis can be up to 100 times more compact than their PAOs relatives, allowing for great savings in data size, I/O, thus also in CPU timings (*153*). These properties come as a consequence of the rotation-like character of the transformation, instead of a projective nature like PAOs (*2, 3, 216*). PNOs are optimal with respect to convergence of the correlation energy: in the single reference case, 50 PNOs recover approximately 99.8% of the correlation energy (*131, 153, 155*). Furthermore, they permit control of the domain size and of the accuracy of the energy with a single parameter, the PNOs' natural occupation number (*4, 137, 139, 148, 153*). This is particularly advantageous for energy differences, for which the errors from the domain approximation can be kept at minimum values. This same parameter is applied to all pairs. For larger distances between the orbitals m and n (distant pairs) the respective pair occupation numbers decrease. As such, pair domains for distant orbital pairs are smaller (when compared to non-distant pairs) (*153*).

On the other, the price to pay for having such a compact description is that PNOs have to be built for each pair specifically. The direct consequence is also that for each pair a set of integrals must be built from the respective canonical quantities. Secondly, for large enough molecules the total number of PNOs for all pairs may become quite unmanageable (*149*), easily surpassing the total number of PAOs for the same system

(*2, 3, 216*). This brings complications not only because of all the sets of integrals that have to be built and transformed, but also because of all the overlap matrices that must be constructed. The problem of the integral transformation for very large spaces was only recently overcome with the LDF approach (*137, 139, 229*) together with building PNOs from PAOs (*c.f.* chapter 4.7). Finally, the criteria used to truncate the PNO expansion is not independent of the molecular geometry, which creates microscopical artifacts, *e.g.*, in PES (*132*).

Semicanonical PNOs

Having a set of PNO transformation matrices, nothing guarantees *a priori* that these diagonalize the virtual block of the Fock matrix.

$$\tilde{\mathbf{F}}^{mn}_{\mathrm{PNO}} = \tilde{\mathbf{W}}^{mn\dagger}\mathbf{F}\tilde{\mathbf{W}}^{mn} \tag{3.96}$$

This means that the transformed Fock matrix $\left(\tilde{\mathbf{F}}^{mn}_{\mathrm{PNO}}\right)_{\tilde{a}\tilde{b}}$ does not have necessarily the structure $\left(\tilde{\mathbf{F}}^{mn}_{\mathrm{PNO}}\right)_{\tilde{a}\tilde{b}} = \varepsilon^{mn}_{\tilde{a}}\delta_{\tilde{a}\tilde{b}}$.

Since the full eigenvector matrix of each $\tilde{\mathbf{F}}^{mn}_{\mathrm{PNO}}$ is a unitary matrix, it can be multiplied to the respective PNO transformation matrix, creating a set of SemiCanonical PNOs (PNO(SC)s). The whole process consists in a rotation of the PNO space, not affecting the final result. In this new PNO basis, $\tilde{\mathbf{F}}^{mn}_{\mathrm{PNO}}$ is diagonal. Therefore, the diagonal elements of $\tilde{\mathbf{F}}^{mn}_{\mathrm{PNO}}$, the elements ε^{mn}_{a}, are orbital energies. The energy denominators used in the perturbative update of amplitudes are thus more accurate, which results in improved convergence. Being $\mathbf{U}^{mn}$ the eigenvector matrix for $\tilde{\mathbf{F}}^{mn}_{\mathrm{PNO}}$,

$$\left(\mathbf{U}^{mn\dagger}\tilde{\mathbf{F}}^{mn}_{\mathrm{PNO}}\mathbf{U}^{mn}\right)_{ab} = \varepsilon^{mn}_{a}\delta_{ab}, \quad a, b \in [mn] \tag{3.97}$$

The PNO(SC)s can be defined by

$$\mathbf{W}^{mn} = \tilde{\mathbf{W}}^{mn}\mathbf{U}^{mn} \tag{3.98}$$

Semicanonical sets of PAOs may be similarly defined for each orbital or pair domain. If PAO(SC)s are not orthogonalized within each pair domain, the right side of eq. 3.97 must be further multiplied by the elements of the matrix contraction $\mathbf{U}^{mn\dagger}\mathbf{S}^{mn}_{\mathrm{PAO}}\mathbf{U}^{mn}$.

4. Local CASPT2 Theory

The first stage of the PNO-PAO Local Complete Active Space 2nd-order Perturbation Theory (LCASPT2) is the optimization of the reference wavefunction. The reference is an optimized CAS$[N, M]$ wavefunction as defined in eq. 3.41. Its energy is calculated as in eq. 3.43. The orbital spaces emerging from the CASSCF calculation were described before in the section 3.5.1: we will find n_{closed} closed-shell orbitals; n_{active} active orbitals; $n_{virtual}$ virtual orbitals (n_{pao} for PAOs). Core orbitals can be distinguished from within the closed-shell space. These are however not correlated and can be completely omitted from the CASPT2 formalism. Thus n_{closed} excludes the core orbitals. The MOs are assumed to be orthogonal and expanded by a set of non-orthogonal AOs $|\chi_\mu(\mathbf{r})\rangle \equiv |\mu\rangle$.

$$|\phi_r(\mathbf{r})\rangle \equiv |r\rangle = \sum_\mu |\mu\rangle \mathbf{C}_{\mu r} \tag{4.1}$$

with $\mathbf{C}^\dagger \mathbf{S}^{\mathrm{AO}} \mathbf{C} = \mathbf{1}$. $\mathbf{S}^{\mathrm{AO}}$ is the overlap matrix for the AO basis. The optimization of the orbitals can be either state-specific or state-averaged, if these are optimized to simultaneously suit only one or more than one electronic state, respectively. However, the theory herein developed is state specific, thus any state specifications are omitted.

The first part of the Theory section addresses the CASPT2 theory. Then, the two main expansions for the first-order wavefunction and the possible mixtures of these are analyzed. We then focus on the transformation to the local virtual space. Finally we present the wavefunction's ansatz as well as the residual and energy equations.

4.1 Complete Active Space 2nd-Order Perturbation Theory

MP2's biggest limitation is the restriction to single configuration GSs (*30, 32–34, 37, 38*). To overcome the limitations of MP2, strong correlation effects must be introduced. This can be achieved by using a multi-configurational reference (*15*). Complete Active Space 2nd-order Perturbation Theory (CASPT2) is one possible formulation of 2nd-order MRPT, which results in a MR generalization of MP2.

The first difference between MP2 and CASPT2 is the fact that in the latter the reference is a linear combination of CSFs from a preceding MCSCF calculation, as given in eq. 3.41. This significantly changes the spectrum of configurations in the first-order

wavefunction. Although the starting equations for the energy and residuals remain the same (eqs. 3.34 and 3.35), including an active space requires the definition of a new $\hat{H}^{(0)}$ for MRPT, thus also the final form of the residual and energy equations. The final equations are therefore significantly more complex.

Table 4.1: Comparison between different MRPT methods. $\Psi^{(1)}$ is the first-order wavefunction, C.S.S. stands for configuration subspaces and $\hat{H}^{(0)}$ is the zeroth-order Hamiltonian. This Table contains information about GMP, Murphy and Messmer's MRPT, MR-MP, Kozlowski and Davidson's MRPT and NEVPT.

METHOD	$\Psi^{(1)}$	**C.S.S.**	$\hat{H}^{(0)}$	**Comments**
GMP (*13, 57*)	ICCs	pairs, singles, internals	non-diagonal built with non-diagonal Fock	2 Configuration Wavefunction
Murphy, Messmer (*41, 42*)	Substitution operators applied to each reference	—	non-diagonal built with non-diagonal Fock	—
MR-MP (*9, 40, 44*)	CSFs	pairs, singles, internals	diagonal built with diagonal Fock	natural orbitals, not iterative
Kozlowski, Davidson (*12, 23, 73*)	CSFs	—	diagonal built with diagonal Fock	not iterative
NEVPT (*69–72*)	ICCs	pairs, singles, internals	Dyall Hamiltonian	covers limitations of CASPT2

There are several successful choices for $\hat{H}^{(0)}$ available in the literature. A few of these choices and the resulting MRPT methods are listed in Table 4.1. In a first classification one has one- and two-electron zeroth-order Hamiltonians. $\hat{H}^{(0)}$s with two-electron terms yield size consistent wavefunctions and energies. These are used in NEVPT. One-electron $\hat{H}^{(0)}$s are simpler and most widely used. However, wavefunctions and energies calculated with these one-electron $\hat{H}^{(0)}$s are not size consistent. Nevertheless, these errors are usually small (*332*). In the second level of classification one separates $\hat{H}^{(0)}$s according to their diagonality in the full configuration space. Diagonal $\hat{H}^{(0)}$s are not orbital invariant, but the resulting equations do not have to be solved using iterative procedures. Non-diagonal

choices for $\hat{H}^{(0)}$ are particularly attractive (*14*): the resulting methods are orbital invariant for CAS references; these can be brought to sparse block diagonal forms with improved convergence. And even though the linear PT equations must be solved iteratively, the relative computational cost of each iteration is relatively low.

In a true generalization of MP, the CASSCF wavefunction should be an eigenfunction of the zeroth-order Hamiltonian. However, the orbitals obtained from MCSCF calculations (thus also the wavefunctions) are not eigenfunctions of a single $\hat{F}$.

$$\hat{F}|0\rangle = \sum_{rs} f_{rs}\hat{E}_{rs}|0\rangle \tag{4.2}$$

Using projectors to the reference space ($\hat{P} = |0\rangle\langle 0|$) and to its orthogonal complementary ($\hat{Q} = 1 - \hat{P}$)[1] on both sides of $\hat{F}$ is possible to define an operator $\hat{H}^{(0)}$, which has $\Psi^{(0)}$ as eigenfunction with eigenvalue $E^{(0)}$ (*14*). This choice for $\hat{H}^{(0)}$ is the one used in Complete Active Space Perturbation Theory (CASPT).

$$\hat{H}^{(0)} = \hat{P}\hat{F}\hat{P} + \hat{Q}\hat{F}\hat{Q} \tag{4.3}$$

$$\hat{H}^{(0)}|0\rangle = |0\rangle\langle 0|\hat{F}|0\rangle\langle 0|0\rangle = \left(2\sum_{i} f_{ii} + \sum_{tu} f_{tu}D^{(1)}_{tu}\right)|0\rangle = E^{(0)}|0\rangle \tag{4.4}$$

It follows directly from eq. 4.4 that if there are no active orbitals, MP theory is recovered. As defined in eq. 4.3, $\hat{H}^{(0)}$ is block diagonal for the $\hat{P}$ and $\hat{Q}$ spaces. It is furthermore invariant to orbital rotations among the active or closed-shell spaces (*39*). In contrast to $\hat{H}^{(0)}$, the perturbation term remains equivalent to what was previously defined for MP. In CASPT2 this term is still defined as $\hat{V} = \hat{H} - \hat{H}^{(0)}$, and it is thus still associated to two-electron terms of the Hamiltonian (*10*).

The first-order wavefunction, $\Psi^{(1)}$, is built by considering all linearly independent configurations occurring in the Hamiltonian when acting on the reference (*58*). $\Psi^{(1)}$ is expanded with configurations orthogonal to the reference, remaining thus also itself orthogonal to the latter. Once more, because $\hat{H}$ is a rank two operator, $\Psi^{(1)}$ is spanned only by singly or doubly excited configurations (in the sense of eqs. 3.5 and 3.6). However, because active orbitals are not occupied in all the reference configurations, substitutions from the inactive to the active space must also be considered. This allows the definition of three different configuration spaces (*58, 109*): the space of pairs or externals (P; Φ^{ab}_{P}), in which 2 electrons are excited to the virtual space; the singles or semi-internals (S; Φ^{a}_{S}), in which an electron is excited to the virtual space and another to an active orbital; the

[1] $\hat{Q}$ projects to the wavefunction's orthogonal complementary space.

internals (I; Φ_I), in which 2 electrons are excited to the active space. The internal and semi-internal excited configurations have significant contributions which are important to consider for correlation corrections to the first-order density matrix (*46*) and to account for the open-shell character of the systems (*58*). Since electrons in the excited configurations may come either from the closed-shell or from the active space, the configuration spaces can be further divided into three different subspaces. As proposed by Celani and Werner, a subscript indicates the number of closed-shell holes in each subspace (*15*): 0 if no electron comes from the closed-shell space; 1 if one electron comes from the closed-shell space; 2 if both electrons come from the closed-shell space. The full spectrum of configuration subspaces can thus be summarized in the following scheme:

$$\begin{aligned}\left\{P^{ab}\right\} = \{P\} &= \{P_0\} \cup \{P_1\} \cup \{P_2\} \\ \{S^a\} = \{S\} &= \{S_0\} \cup \{S_1\} \cup \{S_2\} \\ \{I\} &= \{I_0\} \cup \{I_1\} \cup \{I_2\}\end{aligned}$$

A similar partitioning of the configuration subspaces was proposed also by Andersson *et al.*, but with a different nomenclature and specifically applied to the case of internal contraction (*39, 64*).

With this definition of doubly excited configurations, pure singles in the sense of eq. 3.5 become redundant with semi-internals and internals: in the configuration spaces S and I internal-to-external substitutions may be coupled with active-to-active substitutions (spectator substitutions) (*129*). Explicit consideration of singles Φ_i^a is then redundant for a CASPT2 wavefunction.[2]

Using these configuration spaces and eq. 3.35 it is possible to write down the CASPT2 residuals, which once more should zero at convergence.

$$\begin{aligned}R_{ab}^P &= \left\langle P^{ab}\right| \left(\hat{H}^{(0)} - E^{(0)}\right) \left|\Psi^{(1)}\right\rangle + \left\langle P^{ab}\right| \hat{H} \left|0\right\rangle \\ R_a^S &= \left\langle S^a\right| \left(\hat{H}^{(0)} - E^{(0)}\right) \left|\Psi^{(1)}\right\rangle + \left\langle S^a\right| \hat{H} \left|0\right\rangle \\ R^I &= \left\langle I\right| \left(\hat{H}^{(0)} - E^{(0)}\right) \left|\Psi^{(1)}\right\rangle + \left\langle I\right| \hat{H} \left|0\right\rangle\end{aligned} \tag{4.5}$$

Defining any general excited configurations by Φ_i and Φ_j we can build: a vector $\mathbf{R}$ containing all the residuals R^i; a matrix $\mathbf{H}^{(0)}$ with all the quantities $\left\langle \Phi_i\right| \hat{H}^{(0)} \left|\Phi_j\right\rangle$; a vector $\mathbf{c}$

[2] Assuming a doubly excited configuration with an internal active substitution given by substitution operators applied to the reference, two forms are possible for these, but with similar results:

$\sum_t \hat{E}_{am}\hat{E}_{tt} \left|0\right\rangle = \hat{E}_{am} \sum_t \sum_R c^R \hat{E}_{tt} \left|R\right\rangle = \hat{E}_{am} \sum_R c^R \left|R\right\rangle \sum_t n_t^R = N_{act}\hat{E}_{am} \left|0\right\rangle$

$\hat{E}_{au,tm}|0\rangle = \hat{E}_{au}\hat{E}_{tm}|0\rangle - \delta_{tu}\hat{E}_{am}|0\rangle$

n_t^R is the occupation number of the active orbital t in the reference configuration R, and N_{act} is the number of active electrons.

with all the amplitudes; a matrix $\mathbf{S}$ containing the overlaps $\langle\Phi_i|\Phi_j\rangle$; a vector $\mathbf{K}$ containing the quantities $\langle\Phi_i|\,\hat{H}\,|0\rangle$. This allows one to write the whole set of residuals in a single matrix equation (*333*).

$$\mathbf{R} = \mathbf{H}^{(0)}\mathbf{c} - E^{(0)}\mathbf{S}\mathbf{c} + \mathbf{K} \tag{4.6}$$

Due to the orthogonality of orbitals, all these nine different configuration spaces are mutually orthogonal. This allows each subspace to be independently considered. Furthermore, they all contribute to $\Psi^{(1)}$. But if the reference is a CASSCF wavefunction, then there is no Φ_{tu}^{vw} configuration which is not in the reference, meaning that the I_0 space is empty. For any other reference, I_0 must also be considered. Including I_0 in the first-order interacting space gives CASPT2 enough theoretical flexibility to accommodate references other than CAS (*63*), *e.g.*, from a RASSCF calculation.

Given that the correct active space is selected, CASPT2 improves over MP2. Just like its SR parent, CASPT2 does not have the computational costs of (MR)CI or (MR)CC. In the general case, if the CASSCF calculation is feasible, so is the CASPT2 (*65*). CASPT2 is thus one of the best choices for a relatively low cost electron correlation method that is still accurate, effective and robust (*63*). However, CASPT2 is not strictly size extensive (*332*). Furthermore, like any other MR method, CASPT2 requires a non-black-box method: the CASSCF. Knowing how to build an active space is key for success, as it greatly influences the results. This requires not only experience but also intuition and deep understanding of electronic structure (*63*). Finally, CASPT2 suffers from one other fault, the problem of intruder states. Intruder states occur whenever the reference becomes quasi-degenerate with configurations from its orthogonal space (*57, 89*). Consequently, a singularity in $\hat{H}^{(0)} - E_0$ occurs and the energy diverges (*63*). This problem can be solved either by including level-shifts in the residuals and energy (*c.f.* section 4.11.1) or by increasing the size of the active space (*63, 91, 334*).[3]

CASPT2's greatest impact is surely on excited states (*81–85*), as it can *a priori* treat any system (*63*) without strong mixing with other (Rydberg) states (*89*). There are also some successful examples in the studies of PES, in which CASPT2 closely models the behavior of FCI or equivalent benchmarking methods (*10, 64, 86*). However, prudence is recommended for PES studies, since whenever avoided crossings are present CASPT2 typically fails (*14, 41, 65, 90*). This problem can be overcome by using multi-state variants of CASPT2 (*74, 89, 92*).

[3]Note that the latter solution may introduce other intruder states.

4.2 Configuration State Functions

A convenient way of spanning the first order wavefunction uses an uncontracted basis with all the possible spin-adapted Configuration State Functions (CSFs) (*10, 108, 109*). A CSF is a linear combination of degenerate SDs[4] built to be an eigenfunction of the total spin, $\hat{S}^2$, while still being an eigenfunction of the spin component z, $\hat{S}_z$. By construction, CSFs form an orthonormal and linearly independent basis of configurations. This basis can be used to span any kind of wavefunction containing excited SDs from a reference. This includes both CASSCF and correlated wavefunctions. Some of the methods in which CSFs are used are MRCI (*112–114, 118–120*) and in Nakano's Multi-Configuration Quasi-Degenerate Perturbation Theory (*335, 336*), similar to MS-CASPT2.

The general procedure to construct this basis requires (*10*): i) the number of electrons (N); ii) the possible electronic distributions among M free orbitals until full occupation is reached; iii) to populate the M orbitals with N electrons, building orbital configurations;[5] iv) to assign pure and explicit spin eigenfunctions to each singly occupied orbital (spins α or β). For a singlet system with 7 orbitals and 8 electrons the steps i)-iv) are schematically represented by

$$|\rangle \rightarrow |2210021\rangle \left(|22\alpha002\beta\rangle\,, |22\beta002\alpha\rangle\right); |2201120\rangle \left(|220\alpha\beta20\rangle\,, |220\beta\alpha20\rangle\right); ... \qquad (4.7)$$

Orbital configurations are specified by the number of unpaired electrons they have (*10*). Since SDs are eigenfunctions of $\hat{S}_z$, it results that so are orbital configurations. The respective eigenvalues are given by $M_S = \frac{1}{2}(N_\alpha - N_\beta)$ (*108*). N_α is the number of α spins, and N_β the number of β spins. The resulting quantities after iv) are however not eigenfunctions of $\hat{S}^2$. Ones needs to combine determinants from each orbital configuration to satisfy the eigenvalue equation for $\hat{S}^2$, while still keeping the built functions eigenvectors of $\hat{S}_z$. This is achieved by successive application of standard angular momentum coupling theory (for more detailed information refer to (*108*) and references therein).

The process described in i)-iv) is the basis for the more systematic genealogical coupling scheme (*10, 108*). The genealogical coupling scheme is a sequence of N steps, in which each electron is coupled with other electrons already present in an orbital configuration. This means that to build an N-electron CSF the whole set of intermediary $(N-1)$-electron CSFs are required. The construction is recursive and in the end the N electrons are distributed over a set of M orbitals from scratch. Accordingly, the first

[4] Degenerate in occupation number.

[5] A set of (SDs) degenerate in the occupation number operator.

set of CSFs built describes doublets. Adding an electron yields singlet and triplet configurations, and so on. Since only singly occupied orbitals change the spin multiplicity of the CSF, only these are considered in the scheme. Due to its structure, the scheme defines furthermore the coefficients of each SD in the CSF. Because all unique combinations of SDs are taken, the set of CSFs arising from the genealogical coupling scheme is orthonormal, complete and more compact than the full set of SDs.

Having a set of CSFs describing the reference wavefunction we can build the configuration subspaces for the correlated wavefunction by substitution of one and two electrons from each and every reference configuration (*15*). Due to the strong coupling of CSFs, a process to simultaneously excite $N > 1$ electrons does not exist. One starts by creating all unique two- and (then) one-hole CSFs.[6] It is then when two or one electrons are added to the active or virtual spaces. With this procedure one avoids building multiple times the same excited configuration, as the removal of one or two electrons from different reference configurations may actually yield the same hole structure.

$$|2202\rangle \rightarrow |2200\rangle \qquad |2220\rangle \rightarrow |2200\rangle \tag{4.8}$$

Afterwards, all the possible unique combinations of excited CSFs suitable to span the correlated wavefunction are obtained. This includes by construction all the possible spin couplings of open-shell electrons.

The main advantage of using CSFs lies on the fact that these force approximate wavefunctions to the adequate spin symmetry of the system, ensuring thus the correct spin multiplicity for the solution (*10*). Because CSFs are spin eigenfunctions, the wavefunction expansion may be significantly reduced while still remaining flexible. This is due to the fact that functions without the correct spin symmetry may be neglected without any loss of accuracy (*10*). The calculation of Hamiltonian elements is relatively simple, due to the sparsity of the matrix **H** in the CSF basis. Furthermore, efficient techniques are now already available in the literature for the calculation of these matrix elements, (*15, 337*) and references therein. Since we make the CSFs by changing orbital occupations, a disadvantage is that the size of this basis[7] grows quite quickly with the size of the reference space (*15, 93*). As the number of reference configurations increases, the calculations get so expensive that they might become unfeasible. The use of CSFs is restricted thus to small reference spaces. But this brings up an advantage as well in multistate-theories (*110*): the same CSF basis can be used for many excited states. This simplifies solving the secular

[6] One-hole CSFs are built by addition of one electron to the internal space of two-hole CSFs.

[7] As well as the number of associated parameters, like amplitudes.

equation for many electronic states at the same time. Another disadvantage of CSFs is that this basis spans a space larger than the first order interacting space of the reference. The non-interacting configurations still remain in the wavefunction since the zeroth-order Hamiltonian is non-diagonal in this basis (*15*).

CSFs provide the most accurate ansatz for a correlated wavefunction: For MRCI it yields a very accurate variational solution, when compared to FCI (*111*). However, this ansatz is also extremely expensive due to the very high number of CSFs required.

4.3 Internally Contracted Configurations

Another possibility is to span the first order wavefunction in terms of Internally-Contracted Configurations (ICCs), obtained by applying N-particle substitution operators to the reference as a whole (*15, 43, 65, 107, 108, 338, 339*). Using spin summed excitation operators (fully spin-adapted formalism) we build ICCs as

$$\Phi_{mn}^{rs} = \hat{E}_{rm,sn}\Phi_0 \tag{4.9}$$

Proposed by both Meyer (*338*) and Siegbahn (*339*), ICCs were detailed and first used by Werner and Reinsch in their Internally Contracted Multireference Configuration Interaction (ICMRCI) method (*107*). This expansion is also used in PT, namely in Wolinski's and Pulay's GMP (*13, 57*), Roos' CASPT2 (*39, 58, 64, 340*), MS-CASPT2 (*89*) and NEVPT (*69–71*). The Internally Contracted Multireference Coupled-Cluster (ICMRCC) method was firstly studied by both Banerjee and Simmons (*121*) and was later revived by both Gauss and Evagelista (*122, 123*), and also by Köhn and Hanauer (*124–126*). ICCs are furthermore used in the extension to explicitly correlated ICMRCC, ICMRCCSD(F12*) (*127*), and to linear response theory (*128*). Of special reference is the use of the sequential orthogonalization technique in the ICMRCC methods of Köhn and Hanauer. This technique yields only linear combinations of operators with identical rank, thus, orthogonalizing sequentially an N^{th}-order substitution from all $M < N$ substitutions (*126*). Finally, ICCs are also used in Canonical Transformation Theory (*341–348*).

Since the reference is treated as whole, its coefficients are always held constant. The result is a wavefunction independent on the number of reference configurations but less flexible than a CSF expansion. ICCs offer a natural partitioning of correlation spaces into n^{th}-order interacting spaces without introducing limitations on configuration spaces (*13, 57*). Including all the ICC-spanned excited configurations Φ_i for which $\left\langle \Phi_i|\hat{H}|0 \right\rangle \neq 0$ guarantees that only the dominant configurations are captured in a balanced way (*15, 111,*

124). This makes sure i) that the number of expansion coefficients is kept to a minimum without much loss in accuracy and ii) that no linear combination of excited configurations zeroes the respective Hamiltonian matrix elements with the reference for any basis set or geometry (*15*).

$$a \langle \Phi_i | \hat{H} | 0 \rangle + b \langle \Phi_i | \hat{H} | 0 \rangle \neq 0, \quad \forall a, b \in \mathbb{R} \tag{4.10}$$

In ICC expansions the number of amplitudes depends only on the sizes of the internal and external spaces (*15, 65, 111*). Furthermore, because substitution operators are spin conservative, then an ICC basis conserves the spin of the reference (*13*).

Although the compactness of ICCs is very attractive, since each electronic state has its own reference, a set of ICCs can only be used for one electronic state (*99, 110*). ICCs are thus state-specific. Futhermore, ICCs belonging to the same configuration subspace lack orthogonality. This may be remedied by orthogonalization of the configuration subspaces, and indeed linear independent ICC spaces keep some of the attractiveness of the parent non-orthogonal spaces (*13, 14, 58, 107, 338*). However, the orthogonalization of some ICC spaces for larger active spaces can become expensive from the computational point of view (*15, 43, 111*). This depends naturally on the size of the active space.

The overlap matrices for these spaces can also be quite complex, depending on higher order reduced density matrices (*43*). This complexity is also transferred to Hamiltonian terms, which depend on even higher order density matrices. These terms are sometimes harder to evaluate than matrix elements between CSFs (*15, 43, 111*). Evaluating matrix terms involving ICCs requires evaluating the effect of strings of annihilation and creation operators over the reference. Using Wick's theorem or the anticommutation relations (eqs. 3.7, 3.8 and 3.9), these can however be simplified to lower order N^{th}-order substitution operators (*10*). The virtual orbitals end up being grouped in delta Kronecker terms, and the substitution operators involve only internal indices. As an example we take the overlap function for P_1 configurations,

$$\left\langle \Phi_{it}^{ab} | \Phi_{ju}^{cd} \right\rangle = \langle 0 | \hat{E}_{ia,tb} \hat{E}_{cj,du} | 0 \rangle = \delta_{ac} \delta_{bd} \langle 0 | \hat{E}_{tu,ij} | 0 \rangle + \delta_{bc} \delta_{ad} \langle 0 | \hat{E}_{tj,iu} | 0 \rangle \tag{4.11}$$

The density matrices can also be simplified using the anti-commutation rules. Taking as an example the 2$^{\text{nd}}$-order density it comes:

$$\langle 0 | \hat{E}_{pq,rs} | 0 \rangle = \langle 0 | \hat{E}_{pq} \hat{E}_{rs} | 0 \rangle - \langle 0 | \delta_{rq} \hat{E}_{ps} | 0 \rangle \tag{4.12}$$

Using the orthogonality of orbitals and the symmetry of single-electron substitution operators the N^{th}-order density matrix of internal orbitals is reduced to the M^{th}-order density

matrix of the active orbitals.

$$\begin{aligned}\hat{E}_{ri}\left|0\right\rangle &= \hat{E}_{ir}\left|0\right\rangle = 2\delta_{ir}\left|0\right\rangle \\ \hat{E}_{ar}\left|0\right\rangle &= \hat{E}_{ar}\left|0\right\rangle = 0\end{aligned} \tag{4.13}$$

Note that no simplification is possible for an element involving two active orbitals ($\hat{E}_{tu}\left|0\right\rangle$), the only case not contemplated in 4.13. This is due to the variable occupation of active orbitals in the reference space. Unlike closed-shells, for which the orbital indices and the reference configurations must match in the coupling coefficients $\left\langle R\right|\hat{E}_{ij}\left|R^{'}\right\rangle = 2\delta_{ij}\delta_{RR'}$, for active orbitals it can happen that $\hat{E}_{tu}\left|R^{'}\right\rangle = \left|R\right\rangle$. Consequently the reference configurations R and $R^{'}$ and active indices do not have necessarily to match (*115*).

For some configuration subspaces this reduction of order might still generate overlaps involving 3$^{\text{rd}}$-order densities, *e.g.*, S_0 or I_1. For Hamiltonian terms of CASPT2's residuals this means that the 4$^{\text{th}}$-order density of the active space is involved. This term appears in a double index contraction with the active block of the Fock matrix. The direct calculation of this contraction requires obtaining the 4$^{\text{th}}$-order density matrix and then contract it with the Fock matrix. Unfortunately, the direct calculation of the 4$^{\text{th}}$-order density is significantly expensive and would restrict the use of ICCs to even smaller active spaces (*15,43,111*).[8] However, it is possible to calculate this term and still avoid building the 4$^{\text{th}}$-order density. For that, the four-particle substitution operator is partitioned to

$$\hat{E}_{tu,vw,xz,yz'} = \hat{E}_{tu,vw,xz}\hat{E}_{yz'} - \delta_{uy}\hat{E}_{tz',vw,xz} - \delta_{wy}\hat{E}_{tu,vz',xz} - \delta_{zy}\hat{E}_{tu,vw,xz'} \tag{4.14}$$

This is then inserted in the double index contraction with the active block of the Fock matrix. Because the first term on the right side of the equality involves a product of substitution operators, the resolution of the identity $\hat{1} = \sum_R \left|R\right\rangle\left\langle R\right|$ is used, leading to

$$\begin{aligned}\sum_{yz'} f_{yz'} D^{(4)}_{tu,vw,xz,yz'} &= \sum_R \left\langle 0\right|\hat{E}_{tu,vw,xz}\left|R\right\rangle \sum_{yz'} f_{yz'}\left\langle R\right|\hat{E}_{yz'}\left|0\right\rangle \\ &- \sum_y D^{(3)}_{vw,xz,ty} f_{yu} - \sum_y D^{(3)}_{tu,xz,vy} f_{yw} - \sum_y D^{(3)}_{tu,vw,xy} f_{yz}\end{aligned} \tag{4.15}$$

Note that the actual resolution of the identity should also include projectors for all excited configurations. But since we use it to break a substitution operator dealing only with active orbitals only reference configurations need to be considered. As we calculate directly a quantity with the dimensions of the 3$^{\text{rd}}$-order density of the active space, this leads to a significant reduction of the computational costs.

[8] For an active space of dimension 4, this matrix has dimensions $\left(4^4\right)^2 = 65536$.

Table 4.2 summarizes the relative computational cost in terms of the maximal order of the active density matrix needed using ICCs (the larger the highest-order needed, the larger the computational effort). The highest order needed can be easily obtained by counting the number of active indices in the matrix element to calculate. Table 4.2 compares the effort required for overlaps, CASPT2 and for MRCI terms.

Although less flexible than CSF expansions, benchmark calculations show that ICCs raise the CSF energy only slightly: ICCs underestimate correlation energy by 2-3% (*349*). This error is below the intrinsic error of a method (*e.g.* MRCI with respect to FCI), thus both expansions have essentially the same accuracy (*63*). The advantage of ICCs towards CSFs is the significant reduction of both the computational effort and of storage requirements (*14*). ICC-MR methods are built to resemble and exhibit scalings of computational effort comparable to SR methods (*43, 124*). However, ICC expansions break down near the crossing points in sharp avoided crossings, as dynamical correlation reverts the energy order of the two states (*13*).

Table 4.2: Maximal order of active density matrix needed with ICCs for overlap, CASPT2, and MRCI terms.

Space	Holes (Closed-Shell)	Electrons (Virtual)	Order Active Density Matrix		
			Overlap	CASPT2	MRCI
P_2	2	2	0	1	2
P_1	1	2	1	2	3
P_0	0	2	2	3	4
S_2	2	1	1	2	3
S_1	1	1	2	3	4
S_0	0	1	3	4	5
I_2	2	0	2	3	4
I_1	1	0	3	4	5
I_0	0	0	4	5	6

4.3.1 Contravariant Configurations

The direct application of substitution operators to a reference wavefunction gives rise to covariant configurations. Due to the structure of their overlap functions, the internal product of covariant configurations with a correlated wavefunction is a combination of

different amplitudes. This linear combination of amplitudes may eventually be contracted with the active density matrix. Taking as an example the case of P_1 configurations,

$$\begin{aligned}\left\langle \Phi_{it}^{ab}|\Psi^{(1)}\right\rangle &= \sum_{ju}\sum_{cd}\left\langle \Phi_{it}^{ab}|\Phi_{ju}^{cd}\right\rangle c_{cd}^{ju} = \sum_{ju}\sum_{cd}\left[\delta_{ac}\delta_{bd}D_{tu,ij}^{(2)} + \delta_{bc}\delta_{ad}D_{tj,iu}^{(2)}\right] c_{cd}^{ju} \\ &= \sum_{ju}\delta_{ij}\sum_{cd}\left[2\delta_{ac}\delta_{bd}D_{tu}^{(1)} - \delta_{bc}\delta_{ad}D_{tu}^{(1)}\right] c_{cd}^{ju} = \sum_{u}\left[2c_{ab}^{iu} - c_{ba}^{iu}\right] D_{tu}^{(1)}\end{aligned} \tag{4.16}$$

An alternative way of dealing with ICCs is with the use of contravariant configurations (*65, 350, 351*). For the SR case contravariant configurations $\tilde{\Phi}_X$ are built in such a way that when we calculate their internal product with the correlated wavefunction only one amplitude is obtained, *i.e.*,

$$\left\langle \tilde{\Phi}_X|\Psi^{(1)}\right\rangle = \sum_Y \left\langle \tilde{\Phi}_X|\Phi_Y\right\rangle c^Y = \sum_Y \delta_{XY}c^Y = c^X, \quad \left|\Psi^{(1)}\right\rangle = \sum_Y |\Phi_Y\rangle c^Y \tag{4.17}$$

For the MR case contravariant configurations are defined such that their overlap with $\Psi^{(1)}$ only contains amplitudes with one possible combination of closed-shell and virtual indices. This definition excludes linear combinations of amplitudes with different active orbitals because active indices are affected by the orthogonalization of ICC spaces. Taking as an example contravariant P_1 configurations, we start by defining these as a linear combination of covariant configurations

$$\tilde{\Phi}_{it}^{ab} = x\Phi_{it}^{ab} + y\Phi_{it}^{ba} \tag{4.18}$$

We then calculate the overlap function defined in 4.17 to get

$$\left\langle \tilde{\Phi}_{it}^{ab}|\Psi^{(1)}\right\rangle = \sum_u \left[(2x-y)c_{ab}^{iu} + (2y-x)c_{ba}^{iu}\right] D_{tu}^{(1)} \tag{4.19}$$

Contravariant P_1 configurations are obtained by ensuring that the terms with c_{ba}^{iu} vanish. As such, making $2y - x = 0$ and $2x - y = 1$ leads to $x = \frac{2}{3}$ and $y = \frac{1}{3}$ or

$$\tilde{\Phi}_{it}^{ab} = \frac{2}{3}\Phi_{it}^{ab} + \frac{1}{3}\Phi_{it}^{ba} \tag{4.20}$$

Assuming that contravariant amplitudes are a linear combination of covariant amplitudes (eq. 4.21) and using the condition that the correlated wavefunction is independent of transformations used (eq. 4.22) yields eq. 4.23.

$$\tilde{c}_{ab}^{it} = wc_{ab}^{it} + zc_{ba}^{it} \tag{4.21}$$

$$\sum_{it}\sum_{ab}\left(\Phi_{it}^{ab}c_{ab}^{it} - \tilde{\Phi}_{it}^{ab}\tilde{c}_{ab}^{it}\right) = 0 \Leftrightarrow \tag{4.22}$$

$$\sum_{it}\sum_{ab}\left(\Phi_{it}^{ab}c_{ab}^{it}-\frac{2}{3}\Phi_{it}^{ab}\tilde{c}_{ab}^{it}-\frac{1}{3}\Phi_{it}^{ba}\tilde{c}_{ab}^{it}\right)=0 \tag{4.23}$$

which by insertion of 4.21 yields the solution

$$\tilde{c}_{ab}^{it}=2c_{ab}^{it}-c_{ba}^{it} \tag{4.24}$$

Similarly contravariant formulations for other configuration subspaces may be defined, as long as the overlap 4.17 can be factorized as a product of amplitudes with density matrices. Due to this restriction, the generalization is only possible for the P_2, P_1 and S_2 subspaces. These can be built either before or after the orthogonalization of the respective subspaces, remaining the final result unchanged. For all other configuration subspaces, contravariant configurations as defined in this section are not possible.

Besides simplifying the overlap of an excited configuration with $\Psi^{(1)}$, contravariant configurations also simplify Hamiltonian terms with the reference: the linear combination of exchange integrals is similarly reduced to just one element. For the case of P_1 configurations it follows that

$$\left\langle\tilde{\Phi}_{it}^{ab}|\hat{H}|0\right\rangle=\sum_{u}K_{ab}^{iu}D_{tu}^{(1)} \tag{4.25}$$

Similar simplifications occur in other terms in the residual equations, given that the same configuration subspace is involved. For the case of CCSD, contravariant configurations offer inclusively the most compact description of the residuals (*350–352*).

4.3.2 Singlet-Triplet Configurations

Whenever applying substitution operators to a reference wavefunction, the two external (or internal) electrons may be coupled to form singlet and triplet configurations. The total spin quantum number of the configurations is not affected, as this coupling only concerns the pairs of electrons. The advantage of using Singlet-Triplet configurations is that overlap and Hamiltonian matrices become block diagonal (*58*) since the singlet and the triplet configurations are orthogonal to each other. Singlet-Triplet ICCs can be built as a balanced combination of 2 configurations (*65, 109*)

$$\Phi_{mnp}^{rs}=\frac{1}{2}(\Phi_{mn}^{rs}+p\Phi_{mn}^{sr}),\quad p=1(singlet),-1(triplet) \tag{4.26}$$

These functions are not naturally normalized and thus normalization is required (*43, 65, 353*). To establish a relation between singlet-triplet and covariant amplitudes, we assume the former are a linear combination of the latter, but affected by the parameter p.

$$c_{rs}^{mnp}=xc_{rs}^{mn}+ypc_{sr}^{mn} \tag{4.27}$$

Taking once more a condition like 4.22,

$$\sum_{rs}\sum_{mn}\left(\Phi^{rs}_{mn}c^{mn}_{rs} - \Phi^{rs}_{mnp}c^{mnp}_{rs}\right) = 0 \tag{4.28}$$

by insertion of 4.27 in 4.28 we get that $x + y = 1$. Assuming that the amplitudes are balanced like the configurations ($x = y$), this yields the expression

$$c^{mnp}_{rs} = \frac{1}{2}\left(c^{mn}_{rs} + pc^{mn}_{sr}\right) \tag{4.29}$$

From their definition it follows that (*15*)

$$\Phi^{rs}_{mnp} = p\Phi^{sr}_{mnp} = p\Phi^{rs}_{nmp} \quad c^{mnp}_{rs} = pc^{mnp}_{sr} = pc^{nmp}_{rs} \tag{4.30}$$

4.4 Expanding First-Order Wavefunction

There are two options to expand the first-order wavefunction: ICCs and CSFs. ICCs belonging to different configuration subspaces are orthogonal. Thus, in an ICC basis all configuration subspaces are mutually orthogonal (*15, 58*). Furhtermore, CSFs form by definition an orthogonal basis of functions. Some configuration subspaces can be spanned with ICCs, using then CSFs for the remaining subspaces, leading to the concept of mixed ansätze. Mixed ansätze try to bring a compromise between advantages and drawbacks of each expansion, using either ICCs or CSFs whenever it is most advantageous (*93*).

According to the analysis in section 4.3, it is most advantageous to use ICCs for subspaces containing less active and more closed-shell orbitals (*15, 93, 354*). On the other hand, the number of CSFs required to describe a configuration subspace depends on the number of reference configurations and on the number of correlated orbitals. CSFs are thus more advantageous for subspaces with smaller closed-shell spaces. The use of ICCs and CSFs is thus somehow complementary.

The first mixed expansion for MR wavefunctions was the Werner-Knowles (WK) ansatz (*14, 43, 108*). It was successfully used on MRCI (*43, 108–110*), MRCI-F12 (*98*), multi-state MRCI-F12 (*99*), CASPT2 (*14*), CASPT3 (*14*), CASPT2-F12 (*97*) and on XMS-CASPT2 (*74, 92*). In this ansatz no configuration subspaces are distinguished and the spaces are thus treated as a whole: pairs are expanded by ICCs; singles and internals are both uncontracted. Since no subspaces are distinguished, the internal orbitals are also not partitioned (closed-shell orbitals are not distinguished from the active). Full density matrices of internal orbitals are thus required. The highest rank of density matrices needed remains unchanged, and the most demanding terms involving ICCs requires

the second-order density in the overlap and third order density in the CASPT2 residuals (*c.f.* Table 4.2). In the WK ansatz the number of uncontracted singles is still heavily influenced by the amount of reference configurations and correlated orbitals. This easily leads to bottlenecks in the calculations (*14, 15*).

Later on, Celani and Werner (*15*) improved the WK ansatz by partitioning the configuration spaces according to the number of closed-shell holes. With this partitioning they derived explicit expressions for the overlap functions of each configuration subspace. It was showed that only for a few subspaces the overlap depended on the third- or fourth-order density matrix of the active space. In the Celani-Werner (CW) ansatz, all subspaces with overlap depending at most on the second-order density were expressed by ICCs, leaving the other subspaces uncontracted. This extended the internal contraction to subspaces in the singles and internals, namely to S_2, S_1 and I_2. S_0, I_1 and eventually I_0 are spanned by CSFs. Of the latter subspaces, only I_1 depends linearly on the closed-shell space. I_0 depends only on active orbitals and S_0 depends on the external space. Since inactive orbitals are explicitly treated in spaces spanned by ICCs, all density matrices depend solely on active orbitals. All these conditions together built an ansatz, which allowed arbitrarily larger inactive spaces to be handled than other ansätze (*15,111*): The CW scheme maximized efficiency and decreased computational costs without much change in accuracy (*93,111*). The first use of the CW scheme was in CASPT2 (*15*). This was later extended to MRCI (*111*) and Configuration Interaction Perturbation Theory 2 (CIPT2) (*116*). The main liability of both mixed ansätze is the additional requirement of ICC-CSF coupling coefficients (*93*). Although not particularly complicated, these require the use of special techniques and machinery (*43*).

Since we explicitly require our method to use CAS references, I_0 is empty and can therefore be completely neglected from any further discussion. As the CW ansatz showed, it is most advantageous to expand with ICCs the P_2, P_1, P_0, S_2, S_1 and I_2 spaces. The question remains solely with S_0 and I_1. As these require the orthogonalization of larger overlap matrices, the use of ICCs may result in bottlenecks in the calculation whenever the active space becomes too large. But our goal is to derive a local CASPT2 method for systems with relatively small and local active spaces. Additionally, with the current technology, the diagonalization of third-order densities is no longer as limiting as it once was. Indeed we verified with our code that the diagonalization of the overlap matrices for S_0 and I_1 takes in average 22 s for 14 active orbitals and 0.17 s for 8 active orbitals. Choosing a CSF expansion on the other hand, requires both calculating and storing ICC-

CSF coupling coefficients with all the other subspaces.[9] ICCs require terms involving the fourth-order density, but these quantities can be easily calculated without a significant increase in the computational cost. As such, i) to explore the compactness that only ICCs can offer (minimize the number of configurations), ii) to minimize memory requirements and iii) to avoid the spin coupling between different types of configurations we chose to expand our first-order wavefunction in a fully internally contracted fashion.

Before presenting our ansatz of the first-order wavefunction in the canonical external basis, a few more details are required. ICCs require orthogonalization, and the orthogonal ICC spaces are obtained from the respective non-orthogonal spaces. It is thus necessary to define first how to express the non-orthogonal subspaces. The indices dealing with orthogonal ICC spaces are defined in this section but the conversion between non-orthogonal and orthogonal subspaces is presented and discussed in section 4.5.

We chose a formalism based on normal ordered operators acting on a CAS reference as a Fermi vacuum. The first-order wavefunction in LCASPT2 is built from excited configurations obtained when applying the Hamiltonian operator to the reference (*58*). This means that any non-orthogonal doubly excited configuration considered is constructed using two particle substitution operators, as defined in eq. 4.9. Covariant configurations for each subspace are defined in 4.31, 4.32 and 4.33.

$$\begin{aligned}
P_2 &: \left|\Phi_{ij}^{ab}\right\rangle = \hat{E}_{ai}\hat{E}_{bj}|0\rangle = \hat{E}_{bj}\hat{E}_{ai}|0\rangle = \underline{\hat{E}_{ai,bj}|0\rangle} \\
P_1 &: \left|\Phi_{it}^{ab}\right\rangle = \hat{E}_{ai}\hat{E}_{bt}|0\rangle = \hat{E}_{bt}\hat{E}_{ai}|0\rangle = \underline{\hat{E}_{ai,bt}|0\rangle} \\
P_0 &: \left|\Phi_{tu}^{ab}\right\rangle = \hat{E}_{at}\hat{E}_{bu}|0\rangle = \hat{E}_{bu}\hat{E}_{at}|0\rangle = \underline{\hat{E}_{at,bu}|0\rangle}
\end{aligned} \tag{4.31}$$

$$S_2 : \left|\Phi_{ij}^{at}\right\rangle = \hat{E}_{ai}\hat{E}_{tj}|0\rangle = \hat{E}_{tj}\hat{E}_{ai}|0\rangle = \underline{\hat{E}_{ai,tj}|0\rangle}$$

$$S_1 : \begin{cases}
|\Phi_{iu}^{at}\rangle = \hat{E}_{ai}\hat{E}_{tu}|0\rangle = \hat{E}_{tu}\hat{E}_{ai} = \underline{\hat{E}_{ai,tu}|0\rangle} \\
|\Phi_{ui}^{at}\rangle = \hat{E}_{au}\hat{E}_{ti}|0\rangle = \delta_{tu}\hat{E}_{ai}|0\rangle + \hat{E}_{au,ti}|0\rangle \\
|\Phi_{ui}^{at}\rangle = \hat{E}_{ti}\hat{E}_{au}|0\rangle = \underline{\hat{E}_{au,ti}|0\rangle}
\end{cases} \tag{4.32}$$

$$S_0 : \begin{cases}
|\Phi_{tu}^{av}\rangle = \hat{E}_{at}\hat{E}_{vu}|0\rangle = \delta_{tv}\hat{E}_{au}|0\rangle + \hat{E}_{at,vu}|0\rangle \\
|\Phi_{tu}^{av}\rangle = \hat{E}_{vu}\hat{E}_{at}|0\rangle = \underline{\hat{E}_{at,vu}|0\rangle}
\end{cases}$$

$$I_2 : \left|\Phi_{ij}^{tu}\right\rangle = \hat{E}_{ti}\hat{E}_{uj}|0\rangle = \hat{E}_{uj}\hat{E}_{ti}|0\rangle = \underline{\hat{E}_{ti,uj}|0\rangle}$$

$$I_1 : \begin{cases}
|\Phi_{iv}^{tu}\rangle = \hat{E}_{uv}\hat{E}_{ti}|0\rangle = \delta_{tv}\hat{E}_{ui}|0\rangle + \hat{E}_{ti,ui}|0\rangle \\
|\Phi_{iv}^{tu}\rangle = \hat{E}_{ti}\hat{E}_{vu}|0\rangle = \underline{\hat{E}_{ti,vu}|0\rangle}
\end{cases} \tag{4.33}$$

[9] Because I_1 and S_0 do not interact in the CASPT2 residuals, CSF-CSF terms need not to be calculated.

The underlined expressions are the ones used to uniquely define each subspace. For most cases, two-particle substitution operators are equivalent to the successive application of two one-particle substitution operators. Exceptions occur whenever active indices appear simultaneously in the annihilator of the leftmost one-particle substitution operator and in the creator of the rightmost one-particle substitution operator, namely for I_1, S_0 and in one type of S_1 configurations. For those three cases, the difference is the explicit inclusion of pure singles. But single substitutions are implicit when applying the respective two-particle substitutions. Pure singles were explicitly implemented for S_1 by considering separately the configurations $\hat{E}_{ai}\left|0\right\rangle$. In all the test cases used, including the pure singles influenced the number of non-orthogonal S_1 configurations, thus also the orthogonalization matrix. However, the number of orthogonal S_1 configurations always matched the case without pure singles and the energy remained unchanged. Therefore, explicitly including the pure singles is redundant and just brings complexity to the equations. Even though we left the explicit singles still implemented, these are by default off. From these results we assumed that also the pure singles of I_1 and S_0 are redundant. Although we derived expressions with the explicit inclusion of these I_1 and S_0 pure singles, due to the extra complexity they brought to the equations, we decided to completely leave these out, of both the formalism and implementation.

Table 4.3 summarizes the configuration subspaces for which special types of configurations were built, namely contravariant or singlet-triplet.

Table 4.3: Configuration subspaces expressed with special non-orthogonal configurations.

Space	Type	Configuration	Amplitude
P_2	Contravariant	$\left\|\tilde{\Phi}_{ij}^{ab}\right\rangle = \frac{1}{6}\left(2\left\|\Phi_{ij}^{ab}\right\rangle + \left\|\Phi_{ij}^{ba}\right\rangle\right)$ $= \frac{1}{6}\left(2\hat{E}_{ai,bj} + \hat{E}_{bi,aj}\right)\left\|0\right\rangle$	$\tilde{c}_{ab}^{ij} = 2c_{ab}^{ij} - c_{ba}^{ij}$
P_1	Contravariant	$\left\|\tilde{\Phi}_{it}^{ab}\right\rangle = \frac{1}{3}\left(2\left\|\Phi_{it}^{ab}\right\rangle + \left\|\Phi_{it}^{ba}\right\rangle\right)$ $= \frac{1}{3}\left(2\hat{E}_{ai,bt} + \hat{E}_{bi,at}\right)\left\|0\right\rangle$	$\tilde{c}_{ab}^{it} = 2c_{ab}^{it} - c_{ba}^{it}$
P_0	Singlet-Triplet	$\left\|\Phi_{tup}^{ab}\right\rangle = \frac{1}{2}\left(\left\|\Phi_{tu}^{ab}\right\rangle + p\left\|\Phi_{tu}^{ba}\right\rangle\right)$ $= \frac{1}{2}\left(\hat{E}_{at,bu} + p\hat{E}_{bt,au}\right)\left\|0\right\rangle$	$c_{ab}^{tup} = c_{ab}^{tu} + pc_{ba}^{tu}$ $pc_{ab}^{tup} = c_{ba}^{tup} = c_{ab}^{utp}$
S_2	Contravariant	$\left\|\tilde{\Phi}_{ij}^{at}\right\rangle = \frac{1}{3}\left(2\left\|\Phi_{ij}^{at}\right\rangle + \left\|\Phi_{ji}^{at}\right\rangle\right)$ $= \frac{1}{3}\left(2\hat{E}_{ai,tj} + \hat{E}_{ti,aj}\right)\left\|0\right\rangle$	$\tilde{c}_{at}^{ij} = 2c_{at}^{ij} - c_{at}^{ji}$
I_2	Singlet-Triplet	$\left\|\Phi_{ijp}^{tu}\right\rangle = \frac{1}{2}\left(\left\|\Phi_{tu}^{ij}\right\rangle + p\left\|\Phi_{ut}^{ij}\right\rangle\right)$ $= \frac{1}{2}\left(\hat{E}_{ti,uj} + p\hat{E}_{ui,tj}\right)\left\|0\right\rangle$	$c_{tu}^{ijp} = c_{tu}^{ij} + pc_{tu}^{ij}$ $pc_{tu}^{ijp} = c_{ut}^{ijp} = c_{tu}^{jip}$

For P_2, P_1 and S_2 we built contravariant configurations as described in section 4.3.1. Singlet-triplet configurations would have also been possible, but we verified that the residuals for all these spaces were simpler when using contravariant configurations. Appendix 8.1 presents both types of P_2 residuals for comparison. The main advantage of contravariant configurations for P_2 comes with the fact they simplify the delta Kronecker terms for both the closed-shell and external spaces. For P_1 the simplification comes only with the delta Kronecker terms involving external orbitals and for S_2 only with the delta Kronecker terms involving the closed-shell orbitals. This is reflected in the factors of the contravariant configurations, as Table 4.3 shows.

The P_0 overlap depends on the second-order density and no combination of two configurations factorizes out the delta Kronecker terms in the sense of contravariant configurations. These are therefore not possible to formulate for P_0.

$$\begin{aligned} \left\langle \tilde{\Phi}^{ab}_{tu} | \Phi^{cd}_{vw} \right\rangle &= x \left\langle \Phi^{ab}_{tu} | \Phi^{cd}_{vw} \right\rangle + y \left\langle \Phi^{ba}_{tu} | \Phi^{cd}_{vw} \right\rangle \\ &= \delta_{ac}\delta_{bd} \left(x D^{(2)}_{tv,uw} + y D^{(2)}_{tw,uv} \right) + \delta_{bc}\delta_{ad} \left(x D^{(2)}_{tw,uv} + y D^{(2)}_{tv,uw} \right) \end{aligned} \tag{4.34}$$

On the other hand, singlet-triplet P_0 configurations are possible and can make both the overlap and the zeroth-order Hamiltonian sparse block: one block for singlet configurations (symmetric), another for triplet configurations (anti-symmetric). Using covariant P_0 configurations on the other hand ends up mixing the symmetric and anti-symmetric configurations when diagonalizing the zeroth-order Hamiltonian terms: the symmetric and anti-symmetric parts are mixed back and the eigenvalues come out pairwise degenerate. Such mixture does not allow the clear orthogonalization required for a local PNO MR method. Finally, with singlet-triplet configurations both integral and amplitude matrices are stored in lower triangular forms due to their symmetries. Similarly to P_0, for I_2 it is also not possible to build contravariant configurations and thus singlet-triplet configurations were also built.

For S_1, two different non-mutually orthogonal types of configurations can be defined (inclusively with different overlap functions). These differ by the exchange of two indices. Therefore, neither contravariant nor singlet-triplet configurations can be defined and this space is left covariant, as a linear combination of the two types of configurations. Finally there is still the cases of S_0 and I_1. Again, contravariant configurations cannot be built and singlet-triplet configurations render over-complicated equations, without providing any kind of advantage. These spaces are also left covariant.

Having defined how non-orthogonal configurations are going to be built and the indices for orthogonal configurations, the wavefunction ansätze using the canonical external basis

and both the non-orthogonal and the orthogonal configuration bases are given by

$$\begin{aligned}\Psi^{(1)} = &\frac{1}{2}\sum_{ij}\sum_{ab}\Phi^{ab}_{ij}c^{ij}_{ab} + \sum_{it}\sum_{ab}\Phi^{ab}_{ti}c^{ti}_{ab} + \sum_{p}\sum_{tu}\sum_{ab}\Phi^{ab}_{tup}c^{tup}_{ab} \\ &+ \sum_{ij}\sum_{ta}\Phi^{at}_{ij}c^{ij}_{at} + \sum_{ia}\left(\Phi^{a}_{i}c^{i}_{a} + \sum_{tu}\left[\Phi^{au}_{it}c^{it}_{au} + \Phi^{au}_{ti}c^{ti}_{au}\right]\right) + \sum_{tu}\sum_{va}\Phi^{av}_{tu}c^{tu}_{av} \\ &+ \sum_{p}\sum_{ij}\sum_{tu}\Phi^{tu}_{ijp}c^{ijp}_{tu} + \sum_{iv}\sum_{tu}\Phi^{tu}_{iv}c^{iv}_{tu}\end{aligned} \tag{4.35}$$

$$\begin{aligned}= &\frac{1}{2}\sum_{ij}\sum_{ab}\Phi^{ab}_{ij}c^{ij}_{ab} + \sum_{iD_1}\sum_{ab}\Phi^{ab}_{D_1 i}c^{D_1 i}_{ab} + \sum_{p}\sum_{D_0}\sum_{ab}\Phi^{ab}_{D_0 p}c^{D_0 p}_{ab} \\ &+ \sum_{ij}\sum_{S_2 a}\Phi^{aS_2}_{ij}c^{ij}_{aS_2} + \sum_{iS_1}\sum_{a}\Phi^{a}_{iS_1}c^{iS_1}_{a} + \sum_{S_0}\sum_{a}\Phi^{a}_{S_0}c^{S_0}_{a} \\ &+ \sum_{p}\sum_{ij}\sum_{I_2}\Phi^{I_2}_{ijp}c^{ijp}_{I_2} + \sum_{i}\sum_{I_1}\Phi_{iI_1}c^{iI_1}\end{aligned} \tag{4.36}$$

Note that the two expressions are perfectly equivalent, meaning that different configuration subspaces may be expressed in the orthogonal or in the non-orthogonal basis.

4.5 Orthogonalization of ICC Spaces

Unlike CSFs, configuration subspaces spanned by ICCs are not in general orthonormal. This lack of orthogonality arises from the fact that a general N^{th}-order active density matrix cannot be simplified to a linear combination of products of delta Kronecker functions, like it happens with the closed-shell density matrix.[10] This can already be seen for the 1^{st}-order density, which is diagonal only if natural orbitals are used.[11] For any other order of the density matrix there is no orbital basis diagonalizing it.

This lack of orthogonality is furthermore transmitted to the residuals (*14, 93*). In the non-orthogonal configuration basis, residuals depend on the overlap functions of each configuration subspace. These overlap functions are contracted with the amplitudes, meaning that in the non-orthogonal basis the overlap-amplitude contraction must be calculated in every iteration. For orthogonal subspaces on the other hand, the orthogonalization matrix

[10] This result follows directly after using the anticommutation relations and the orthogonality of MOs. For the 2^{nd}-order density, *e.g.*, $\left\langle 0|\hat{E}_{ij,kl}|0\right\rangle = 4\delta_{ij}\delta_{kl} - 2\delta_{ik}\delta_{jl}$.

[11] Natural orbitals is the set of MOs diagonalizing the 1^{st}-order density matrix and yield the most rapidly convergent CI expansion. Natural orbitals correspond thus to the eigenvectors of the first-order density. The respective eigenvalues are occupation numbers (*6, 292*).

transforms the overlap matrices into the identity matrix and such contractions vanish from the calculation. Furthermore, only orthogonal configuration subspaces allow the perturbative update of amplitudes, which improves greatly computational costs and timings. In each iteration the amplitudes are calculated by adding a correction to the amplitudes from the previous iteration (*111*). For an orthogonal P_1 configuration $\Phi_{iD_1}^{ab}$, the perturbative amplitude update is given by

$$\Delta c_{ab}^{iD_1} = -\frac{R_{ab}^{iD_1}}{\left\langle \tilde{\Phi}_{iD_1}^{ab} \middle| \left(\hat{H}^{(0)} - E\right) \middle| \Phi_{iD_1}^{ab} \right\rangle} \tag{4.37}$$

$$c_{ab}^{iD_1}(new) = c_{ab}^{iD_1}(old) + \Delta c_{ab}^{iD_1} \tag{4.38}$$

where $\Delta c_{ab}^{iD_1}$ is the amplitude update in the orthogonal basis and $R_{ab}^{iD_1}$ the residual for the configuration $\Phi_{iD_1}^{ab}$. Similarly, amplitude updates for any other configuration subspace can be defined. The perturbative update of amplitudes requires a unique set of excited configurations to be selected and used. For instance, non-orthogonal configurations are linear combinations of orthogonal configurations and cannot be used in the amplitude update. Furthermore, building PNOs for non-orthogonal configurations would end up mixing the PNOs for different pairs upon the orthogonalization step to perform the amplitude update. Consequently, the LCASPT2 equations must be assembled and solved in the orthogonal configuration basis.

However, the orthogonalization of these configuration subspaces can become quite expensive. For instance, the orthogonalization of S_0 and I_1 are $\mathcal{O}\left(M^9\right)$ processes. Fortunately, the prefactors in diagonalizing the respective overlap functions are rather small, and for a CAS as large as CAS[14, 14], both S_0 and I_1 can be orthogonalized within 20 s each. Methods to orthogonalize configuration subspaces are algebraic methods used to orthogonalize vector spaces. In principle, the full overlap matrix for all configuration subspaces should be diagonalized, generating a full orthogonalization tensor. However, the configuration subspaces are mutually orthogonal, meaning that the full overlap matrix is block diagonal. This allows the separation of the orthogonalization tensors for each configuration subspace. By diagonalizing the overlap matrices we construct orthogonalization matrices $\mathbf{T}$ for each configuration subspace. Since the spectrum of eigenvalues for overlap matrices may be wide, the ones smaller than a given threshold are zeroed (the default value is 10^{-7}). The respective eigenvectors are therefore neglected and the matrices $\mathbf{T}$ become rectangular, projecting out linear dependencies (*126*). Consequently, the $\mathbf{T}$ matrices map non-orthogonal to orthogonal spaces, but not the other way around (*111*).

We chose the orthogonalization method for symmetric matrices $\mathbf{S}$ as proposed by Siegbahn (*339, 355, 356*),[12] which changes the original basis as little as possible (*355, 356*). Since all overlap matrices $\mathbf{S}$ symmetric, they are also diagonalizable, meaning that there is a matrix $\mathbf{V}$ and a diagonal matrix $\mathbf{d}$ holding the eigenvectors and eigenvalues of $\mathbf{S}$.

$$\mathbf{V}^{\dagger}\mathbf{S}\mathbf{V} = \mathbf{d} \tag{4.39}$$

Having the eigenvectors and eigenvalues, we build the orthogonalization matrices from the eigenvectors and eigenvalues as

$$\mathbf{T} = \mathbf{V}\mathbf{d}^{-\frac{1}{2}} \tag{4.40}$$

Since $\mathbf{S}$ is by definition symmetric, its eigenvectors form an orthogonal basis. It follows then immediately that $\mathbf{T}$ orthogonalizes the matrix $\mathbf{S}$.

Having defined how to obtain orthogonalization matrices, we require the overlap functions for each configuration subspace. These can be obtained using the definition of each subspace (*c.f.* section 4.4) and then applying the anticommutation relations 3.7, 3.8, 3.9, and the simplification of the Nth-order internal density matrix (4.12 and 4.13). The structure of the overlaps is always a product of three terms[13]: a string of delta Kronecker functions with virtual indices - virtual overlap; a product of delta Kronecker functions with closed-shell indices - closed-shell overlap; an active orbital term depending on (possibly) many orders of the active density matrix - active overlap. Because delta Kronecker terms only take the values of 0 and 1 both the closed-shell and virtual overlaps vanish if the respective indices do not match in some fashion. On the other hand, the active overlap is not necessarily zero if the active indices are not matching. Consequently, both closed-shell and virtual indices are dummy to the transformation matrices above defined, and the matrices $\mathbf{T}$ depend only on active indices. They diagonalize the active overlaps $\mathbf{S}^X$ for each full configuration subspace overlap $\langle\Phi_X|\Phi_{X'}\rangle$. Because the active overlaps may depend on more than just two active indices, these can be grouped together to form compound active indices for both left and right configurations.

We note here that due to the complex structure of S_1 configurations this subspace involves many different active overlap matrices. These should not be orthogonalized separately or the full orthogonality of S_1 configurations is not ensured. Instead, a super overlap matrix is built, which is diagonalized, allowing one to retrieve from the diagonal-

[12] This method is also known as symmetric or canonical orthogonalization.

[13] Or a linear combination of these.

ization procedure the three different orthogonalization tensors: T_{tu,S_1}, T'_{tu,S_1} and T_{S_1}.

$$\begin{bmatrix} 2S_A^{S_1} & -S_A^{S_1} & 2S^{S_1} \\ -S_A^{S_1} & S_B^{S_1} & -S^{S_1} \\ 2S^{S_1} & -S^{S_1} & 2 \end{bmatrix}, \quad \begin{bmatrix} T_{tu,S_1} \\ T'_{tu,S_1} \\ T_{S_1} \end{bmatrix} \tag{4.41}$$

This super structure of S_1's active overlap is transmitted to other quantities, like for instance the γ^{S_1} terms. We should furthermore mention that the most compact formulation of I_2's overlap was obtained using hole-particle density matrices, *i.e.*, the normal order of the final strings of annihilators and creators is reversed: in the particle-hole formulation all creators are written first, then all annihilators; in the hole-particle formulation annihilators are written first, then the creators. For each of these formulations we define the general pair overlaps $S^{(p)}_{tu,vw}$ and $\bar{S}^{(p)}_{tu,vw}$ in analogy

$$S^{(p)}_{tu,vw} = D^{(2)}_{tv,uw} + pD^{(2)}_{tw,uv} \tag{4.42}$$

$$\begin{aligned} \bar{S}^{(p)}_{tu,vw} = \bar{D}^{(2)}_{tv,uw} + p\bar{D}^{(2)}_{tw,uv} = S^{(p)}_{tu,vw} + 2\,(2-p)\,(\delta_{tv}\delta_{uw} + p\delta_{tw}\delta_{uv}) \\ + (-1)\,(2-p)\left(\delta_{tv}D^{(1)}_{uw} + p\delta_{tw}D^{(1)}_{uv} + \delta_{uw}D^{(1)}_{tv} + p\delta_{uv}D^{(1)}_{tw}\right) \end{aligned} \tag{4.43}$$

Tables 4.4, 4.5 and 4.6 resume the overlap functions for each configuration subspace.

Table 4.4: Overlap functions for the singles configuration subspaces.

Singles Subspace	Overlap
S_2	$\left\langle \tilde{\Phi}^{at}_{ij} \middle\| \Phi^{bu}_{kl} \right\rangle = \delta_{ab}\delta_{ik}\delta_{jl}\left(\mathbf{S}^{S_2}\right)_{tu}$
	$\left(\mathbf{S}^{S_2}\right)_{tu} = 2\delta_{tu} - D^{(1)}_{tu}$
S_1	$\left\langle \Phi^{a}_{i} \middle\| \Phi^{b}_{j} \right\rangle = 2\delta_{ab}\delta_{ij}$
	$\left\langle \Phi^{au}_{it} \middle\| \Phi^{bw}_{jv} \right\rangle = 2\delta_{ab}\delta_{ij}\left(\mathbf{S}^{S_1}_{A}\right)_{tu,vw}$
	$\left\langle \Phi^{au}_{ti} \middle\| \Phi^{bw}_{jv} \right\rangle = -\delta_{ab}\delta_{ij}\left(\mathbf{S}^{S_1}_{A}\right)_{tu,vw}$
	$\left\langle \Phi^{au}_{ti} \middle\| \Phi^{bw}_{vj} \right\rangle = \delta_{ab}\delta_{ij}\left(\mathbf{S}^{S_1}_{B}\right)_{tu,vw}$
	$\left\langle \Phi^{au}_{it} \middle\| \Phi^{b}_{j} \right\rangle = 2\delta_{ab}\delta_{ij}\left(\mathbf{S}^{S_1}\right)_{tu}$
	$\left\langle \Phi^{au}_{ti} \middle\| \Phi^{b}_{j} \right\rangle = -\delta_{ab}\delta_{ij}\left(\mathbf{S}^{S_1}\right)_{tu}$
	$\left(\mathbf{S}^{S_1}_{A}\right)_{tu,vw} = \delta_{uw}D^{(1)}_{tv} + D^{(2)}_{tu,wv}$
	$\left(\mathbf{S}^{S_1}_{B}\right)_{tu,vw} = 2\delta_{uw}D^{(1)}_{tv} - D^{(2)}_{tv,wu}$
	$\left(\mathbf{S}^{S_1}\right)_{tu} = D^{(1)}_{tu}$
S_0	$\left\langle \Phi^{av}_{tu} \middle\| \Phi^{bz}_{wx} \right\rangle = \delta_{ab}\left(\mathbf{S}^{S_0}\right)_{tuv,wxz}$
	$\left(\mathbf{S}^{S_0}\right)_{tuv,wxz} = \delta_{vz}D^{(2)}_{tw,ux} + D^{(3)}_{tw,uv,zx}$

Table 4.5: Overlap functions for pairs.

Pair Subspace	Overlap
P_2	$\left\langle \tilde{\Phi}^{ab}_{ij} \middle\| \Phi^{cd}_{kl} \right\rangle = \delta_{ac}\delta_{bd}\delta_{ik}\delta_{jl} + \delta_{bc}\delta_{ad}\delta_{jk}\delta_{il}$
P_1	$\left\langle \tilde{\Phi}^{ab}_{it} \middle\| \Phi^{cd}_{ju} \right\rangle = \delta_{ij}\delta_{ac}\delta_{bd}\left(\mathbf{S}^{D_1}\right)_{tu}$ $\left(\mathbf{S}^{D_1}\right)_{tu} = D^{(1)}_{tu}$
P_0	$\left\langle \Phi^{ab}_{tup} \middle\| \Phi^{cd}_{vwq} \right\rangle = \frac{1}{2}\delta_{pq}\left(\delta_{ac}\delta_{bd} + p\delta_{bc}\delta_{ad}\right)\left(\mathbf{S}^{D_0 p}\right)_{tu,vw}$ $\left(\mathbf{S}^{D_0 p}\right)_{tu,vw} = S^{(p)}_{tu,vw}$

Table 4.6: Overlap functions for internal configuration subspaces.

Internal Subspace	Overlap
I_2	$\left\langle \Phi^{tu}_{ijp} \middle\| \Phi^{vw}_{klp} \right\rangle = \frac{1}{2}\delta_{pq}\left(\delta_{ik}\delta_{jl} + p\delta_{jk}\delta_{il}\right)\left(\mathbf{S}^{I_2 p}\right)_{tu,vw}$ $\left(\mathbf{S}^{I_2 p}\right)_{tu,vw} = \bar{S}^{(p)}_{tu,vw}$
I_1	$\left\langle \Phi^{tu}_{iv} \middle\| \Phi^{wx}_{jz} \right\rangle = \delta_{ij}\left(\mathbf{S}^{I_1}\right)_{tuv,wxz}$ $\left(\mathbf{S}^{I_1}\right)_{tuv,wxz} = 2\delta_{tw}\delta_{ux}D^{(1)}_{vz} - \delta_{tx}\delta_{uw}D^{(1)}_{vz} + 2\delta_{tw}D^{(2)}_{vu,xz}$ $- \delta_{uw}D^{(2)}_{vt,xz} - \delta_{tx}D^{(2)}_{vu,wz} - \delta_{ux}D^{(2)}_{wt,vz} - D^{(3)}_{wt,vu,xz}$

Because the transformations $\mathbf{T}$ are unidirectional, they are used differently with configurations (residuals) and with amplitudes. We use orthogonalization tensors to bring non-orthogonal configurations to the orthogonal configuration basis. Thus, by definition, orthogonal configurations (residuals) are linear combinations of the respective non-orthogonal quantities. Because correlated wavefunctions are invariant to transformations like the orthogonalization of configuration subspaces, non-orthogonal amplitudes are linear combinations of the orthogonal ones (*93*). Taking as an example the case of P_1,

$$\begin{aligned} &Definition: \quad \tilde{\Phi}^{ab}_{iD_1} = \sum_t \tilde{\Phi}^{ab}_{it} T_{tD_1} \\ &\sum_{it}\sum_{ab} \tilde{\Phi}^{ab}_{it}\tilde{c}^{it}_{ab} = \sum_{iD_1}\sum_{ab} \tilde{\Phi}^{ab}_{iD_1}\tilde{c}^{iD_1}_{ab} = \sum_{iD_1}\sum_{ab}\sum_t \tilde{\Phi}^{ab}_{it} T_{tD_1}\tilde{c}^{iD_1}_{ab} \Rightarrow \tilde{c}^{it}_{ab} = \sum_t \tilde{c}^{iD_1}_{ab} T_{tD_1} \end{aligned} \tag{4.44}$$

Table 4.7 provides the respective conversions for both configurations and amplitudes for all the configuration subspaces.

Table 4.7: Conversion between non-orthogonal and orthogonal configurations and amplitudes.

Space	Configuration	Residuals	Amplitude
P_2	Orthogonal	Orthogonal	Orthogonal
P_1	$\Phi^{ab}_{iD_1} = \sum_t \Phi^{ab}_{it} T_{tD_1}$	$R^{ab}_{iD_1} = \sum_t R^{ab}_{it} T_{tD_1}$	$c^{ab}_{it} = \sum_{D_1} c^{iD_1}_{ab} T_{tD_1}$
P_0	$\Phi^{ab}_{D_0p} = \sum_{tu} \Phi^{ab}_{tup} T^{(p)}_{tu,D_0}$	$R^{ab}_{D_0p} = \sum_{tu} R^{ab}_{tup} T^{(p)}_{tu,D_0}$	$c^{ab}_{tup} = \sum_{D_0} c^{D_0p}_{ab} T^{(p)}_{tu,D_0}$
S_2	$\Phi^{aS_2}_{ij} = \sum_t \Phi^{at}_{ij} T_{tS_2}$	$R^{aS_2}_{ij} = \sum_t R^{at}_{ij} T_{tS_2}$	$c^{at}_{ij} = \sum_{S_2} c^{ij}_{aS_2} T_{tS_2}$
S_1	$\Phi^{a}_{iS_1} = \sum_{tu} \Phi^{au}_{it} T_{tu,S_1}$ $+ \sum_{tu} \Phi^{ua}_{it} T_{tu,S_1}$ $+ \sum_{tu} \Phi^{a}_{i} T_{S_1}$	$R^{a}_{iS_1} = \sum_{tu} R^{au}_{it} T_{tu,S_1}$ $+ \sum_{tu} R^{ua}_{it} T_{tu,S_1}$ $+ \sum_{tu} R^{a}_{i} T_{S_1}$	$c^{it}_{au} = \sum_{S_1} c^{iS_1}_{a} T_{tu,S_1}$, $c^{it}_{ua} = \sum_{S_1} c^{iS_1}_{a} T'_{tu,S_1}$, $c^{i}_{a} = \sum_{S_1} c^{iS_1}_{a} T_{S_1}$
S_0	$\Phi^{S_0}_{a} = \sum_{tuv} \Phi^{av}_{tu} T_{tuv,S_0}$	$R^{S_0}_{a} = \sum_{tuv} R^{av}_{tu} T_{tuv,S_0}$	$c^{tu}_{av} = \sum_{S_0} c^{S_0}_{a} T_{tuv,S_0}$
I_2	$\Phi^{I_2}_{ijp} = \sum_{tu} \Phi^{tu}_{ijp} T^{(p)}_{tu,I_2}$	$R^{I_2}_{ijp} = \sum_{tu} R^{tu}_{ijp} T^{(p)}_{tu,I_2}$	$c^{ijp}_{tu} = \sum_{I_2} c^{ijp}_{I_2} T^{(p)}_{tu,I_2}$
I_1	$\Phi_{iI_1} = \sum_{tu} \Phi^{tu}_{iv} T_{tuv,I_1}$	$R_{iI_1} = \sum_{tu} R^{tu}_{iv} T_{tuv,I_1}$	$c^{iv}_{tu} = \sum_{I_1} c^{iI_1} T_{tuv,I_1}$

4.5.1 Diagonalization of Zeroth-Order Hamiltonian Terms

In the perturbative update of the amplitudes we require the calculation of energy denominators given by

$$\varepsilon^X = \langle \Phi_X | \left(\hat{H}^{(0)} - E \right) | \Phi_X \rangle \tag{4.45}$$

with Φ_X orthogonal configurations for the configuration subspace X. These ε^X quantities depend on sums of diagonal elements of the virtual and closed-shell blocks of the Fock matrix,[14] as well as one- and two index contractions between the active block of the Fock matrix and the many orders of the density matrix. Of the latter, we distinguished two terms: A zeroth-order active energy given by $E^{(0)}_{act} = \sum_{tu} f_{tu} D^{(1)}_{tu}$; all other contractions specific for each configuration subspace X collected in matrices $\gamma^X(X, X')$. Tables 4.10, 4.8 and 4.9 present for each configuration subspace the γ^X matrices and the respective energy denominators ε^X. The energy denominators are presented for a generic virtual basis, for which the virtual block of the Fock matrix is not necessarily diagonal. We note here that for canonical virtuals and for semicanonical virtuals the virtual block of the Fock

[14] *e.g.*, for a P_1 configuration $\Phi^{ab}_{iD_1}$ these Fock matrix terms are f_{aa}, f_{bb}, and f_{ii}.

matrix is diagonal, meaning that $f_{ab} = \epsilon_a \delta_{ab}$. Any other basis can be used however, which only requires the respective changes of indices. Note that the P_2 energy denominators have the same structure as in MP theory. For all the other configuration subspaces the external or closed-shell Fock matrix elements are replaced by contractions of the active block of the Fock matrix with the many orders of the density matrix.

Table 4.8: γ and energy denominators for Singles.

Space	γ^S;ε^S
S_2	$\left(\gamma^{S_2}\right)_{tu} = E^{(0)}_{act} D^{(1)}_{tu} + D^f_{tu} + \sum_v \left[\left(\mathbf{S}^{S_2}\right)_{tv} f_{vu} - f_{tv} D^{(1)}_{vu}\right]$
	$\gamma\left(S_2, T_2\right) = \sum_{tu} T_{t,S_2} \left(\gamma^{S_2}\right)_{tu} T_{u,T_2}$
	$\varepsilon^{ij}_{aS_2} = f_{aa} + \gamma\left(S_2, S_2\right) - f_{ii} - f_{jj}$
S_1	$\gamma\left(S_1, T_1\right) = \sum_{i,j=1}^{3} \gamma_{ij}\left(S_1, T_1\right)$
	$\gamma_{11}\left(S_1, T_1\right) = 2 \sum_{tu} \sum_{vw} T_{tu,S_1} \left(\gamma^{S_1}_A\right)_{tu,vw} T_{vw,T_1}$
	$\gamma_{12}\left(S_1, T_1\right) = -\sum_{tu} \sum_{vw} T_{tu,S_1} \left(\gamma^{S_1}_A\right)_{tu,vw} T'_{vw,T_1}$
	$\gamma_{21}\left(S_1, T_1\right) = \gamma_{12}\left(S_1, T_1\right)$
	$\gamma_{22}\left(S_1, T_1\right) = \sum_{tu} \sum_{vw} T'_{tu,S_1} \left(\gamma^{S_1}_B\right)_{tu,vw} T'_{vw,T_1}$
	$\gamma_{13}\left(S_1, T_1\right) = 2 \sum_{tu} T_{tu,S_1} \left(\gamma^{S_1}_C\right)_{tu} T_{T_1}$
	$\gamma_{31}\left(S_1, T_1\right) = \gamma_{13}\left(S_1, T_1\right)$
	$\gamma_{23}\left(S_1, T_1\right) = -\sum_{tu} T'_{tu,S_1} \left(\gamma^{S_1}_C\right)_{tu} T_{T_1}$
	$\gamma_{32}\left(S_1, T_1\right) = \gamma_{23}\left(S_1, T_1\right)$
	$\gamma_{33}\left(S_1, T_1\right) = 2 T_{S_1} E^{(0)}_{act} T_{T_1}$
	$\left(\gamma^{S_1}_A\right)_{tu,vw} = D^f_{tv} \delta_{uw} + D^{(1)}_{tv} f_{uw} + D^f_{tu,wv}$
	$+ \sum_x f_{wx} D^{(2)}_{tu,xv} + \sum_x D^{(2)}_{tx,wv} f_{xu}$
	$\left(\gamma^{S_1}_B\right)_{tu,vw} = 2 D^f_{tv} \delta_{uw} + 2 D^{(1)}_{tv} f_{uw} - D^f_{tv,wu}$
	$- \sum_x f_{wx} D^{(2)}_{tv,xu} - \sum_x D^{(2)}_{tv,wx} f_{xu}$
	$\left(\gamma^{S_1}_C\right)_{tu} = D^f_{tu} + \sum_v D^{(1)}_{tv} f_{vu}$
	$\varepsilon^{iS_1}_a = f_{aa} + \gamma\left(S_1, S_1\right) - E^{(0)}_{act} - f_{ii}$
S_0	$\left(\gamma^{S_0}\right)_{tuv,wxz} = D^f_{tw,uv,xz} + f_{vx} D^{(2)}_{tw,zu}$
	$+ \sum_y D^{(3)}_{tw,xz,uy} f_{yv} + \sum_y f_{xy} D^{(3)}_{yz,tw,uv} + \delta_{vx} D^f_{tw,uz}$
	$\gamma\left(S_0, T_0\right) = \sum_{tuv} \sum_{wxz} T_{tuv,S_0} \left(\gamma^{S_0}\right)_{tuv,wxz} T_{wxz,T_0}$
	$\varepsilon^{S_0}_a = f_{aa} + \gamma\left(S_0, S_0\right) - E^{(0)}_{act}$

Here we have

$$D^f_{tu} = \sum_{vw} D^{(2)}_{tu,vw} f_{vw} \tag{4.46}$$

$$D^f_{tu,vw} = \sum_{xz} D^{(3)}_{tu,vw,xz} f_{xz} \tag{4.47}$$

$$D^f_{tu,vw,xz} = \sum_{yz'} D^{(4)}_{tu,vw,xz,yz'} f_{yz'} \tag{4.48}$$

Table 4.9: γ and energy denominators for Pairs.

Space	γ^P;ε^P
P_2	$\varepsilon^{ij}_{ab} = f_{aa} + f_{bb} - f_{ii} - f_{jj}$
P_1	$\left(\gamma^{P_1}\right)_{tu} = D^f_{tu}$ $\gamma\left(D_1, E_1\right) = \sum_{tu} T_{tD_1} \left(\gamma^{P_1}\right)_{tu} T_{uE_1}$ $\varepsilon^{iD_1}_{ab} = f_{aa} + f_{bb} + \gamma\left(D_1, D_1\right) - E^{(0)}_{act} - f_{ii}$
P_0	$\left(\gamma^{P_0(p)}\right)_{tu,vw} = D^f_{tv,uw} + pD^f_{tw,uv}$ $\gamma^{(p)}\left(D_0, E_0\right) = \frac{1}{4} \sum_{tu} \sum_{vw} T^{(p)}_{tu,D_0} \left(\gamma^{P_0(p)}\right)_{tu,vw} T^{(p)}_{vw,E_0}$ $\varepsilon^{D_0 p}_{ab} = f_{aa} + f_{bb} + \gamma^{(p)}\left(D_0, D_0\right) - E^{(0)}_{act}$

Table 4.10: γ and energy denominators for Internals.

Space	γ^I;ε^I
I_2	$\left(\gamma^{I_2(p)}\right)_{tu,vw} = 2\left(2-p\right) E^{(0)}_{act} \delta_{tv} \delta_{uw} - 2\left(2-p\right) f_{tv} D^{(1)}_{uw}$ $+ 4\left(2-p\right) f_{tv} \delta_{uw} - 2\left(2-p\right) \delta_{uw} \sum_x f_{tx} D^{(1)}_{xv}$ $- 2\left(2-p\right) \delta_{uw} \sum_x D^{(1)}_{tx} f_{xv} - 2\left(2-p\right) \delta_{uw} D^f_{tv} - 2D^f_{tv,uw}$ $+ \sum_x f_{vx} \left(\mathbf{S}^{(p)}\right)_{tu,xw} + \sum_x f_{tx} \left(\mathbf{S}^{(p)}\right)_{vw,xu}$ $\gamma^{(p)}\left(I_2, J_2\right) = \frac{1}{4} \sum_{tu} \sum_{vw} T^{(p)}_{tu,I_2} \left(\gamma^{I_2(p)}\right)_{tu,vw} T^{(p)}_{vw,J_2}$ $\varepsilon^{ijp}_{I_2} = 2\gamma^{(p)}\left(I_2, I_2\right) - E^{(0)}_{act} - f_{ii} - f_{jj}$
I_1	$\left(\gamma^{I_1}\right)_{tuv,wxz} = \left(2\delta_{tw}\delta_{ux} - \delta_{tx}\delta_{uw}\right) D^f_{vz} - D^f_{wt,vu,xz}$ $- \sum_y D^{(3)}_{vu,xz,wy} f_{yt} - \sum_y D^{(3)}_{wt,xz,vy} f_{yu} - \sum_y f_{wy} D^{(3)}_{yt,vu,xz}$ $- \sum_y f_{xy} D^{(3)}_{yz,vu,wt} + 2f_{tw} D^{(2)}_{vu,xz} - f_{ux} D^{(2)}_{wt,vz}$ $- f_{tx} D^{(2)}_{vu,wz} - f_{uw} D^{(2)}_{vt,xz}$ $+2\delta_{tw} \left[D^{(1)}_{vz} f_{ux} + D^f_{vu,xz} + \sum_y D^{(2)}_{xz,vy} f_{yu} + \sum_y f_{xy} D^{(2)}_{yz,vu}\right]$ $+\delta_{ux} \left[2D^{(1)}_{vz} f_{tw} - D^f_{wt,vz} - \sum_y D^{(2)}_{vz,wy} f_{yt} - \sum_y f_{wy} D^{(2)}_{yt,vz}\right]$ $-\delta_{tx} \left[D^{(1)}_{vz} f_{uw} + D^f_{vu,wz} + \sum_y D^{(2)}_{wz,vy} f_{yu} + \sum_y f_{wy} D^{(2)}_{yz,vu}\right]$ $- \delta_{uw} \left[D^{(1)}_{vz} f_{tx} + D^f_{vt,xz} + \sum_y D^{(2)}_{xz,vy} f_{yt} + \sum_y f_{xy} D^{(2)}_{yz,vt}\right]$ $\gamma\left(I_1, J_1\right) = \sum_{tuv} \sum_{wxz} T_{tuv,I_1} T_{wxz,J_1}$ $\varepsilon^{iI_1} = \gamma\left(I_1, I_1\right) - E^{(0)}_{act} - f_{ii}$

The terms of each γ^X always involve multiple summations over the active space. The number of active indices in these summations is twice the number of active orbitals in each configuration subspace (*e.g.*, S_2 configurations depend on one active index; the summation runs over two active indices). On the other hand, the energy denominators just involve the indices for the configuration subspace X. This means that only the diagonal elements of the Fock and of the orthogonal γ^X matrices contribute to the energy denominator. But since the latter are by definition symmetric and only depend on quantities available from the beginning of the calculation, these can be both pre-computed and diagonalized (*14*). Finding an orthogonalization matrix for a configuration subspace that also (block) diagonalizes the respective γ^X matrices requires a rotation of the orthogonalization tensors using the eigenvectors $\mathbf{\Lambda}^X$ of each orthogonal γ^X matrix. Because such rotation matrices exist, there is no unique set of orthogonal ICCs: many sets are possible. But since the CASPT2 energy is invariant to rotations of the orthogonalization matrices, we can choose to uniquely build the orthogonalization tensors so that the γ^X matrices are diagonal. This is convenient in building PNOs since it guarantees that a unique set of configurations is used for each subspace. Furthermore, using diagonal γ^X matrices reduces the computational cost for solving the equations and speeds up convergence significantly (*14*).

To get diagonal $\gamma^X(X, X')$ matrices, we require the matrix of eigenvectors $\mathbf{\Lambda}^X$ for each γ^X to rotate the respective orthogonalization matrix $\mathbf{T}^X$. This is achieved by direct contraction with the respective $\mathbf{\Lambda}^X$.

$$\tilde{\mathbf{T}}^X = \mathbf{T}^X \mathbf{\Lambda}^X \tag{4.49}$$

4.6 Pair Approximations

In local SR theories several categories of pairs are distinguished: strong pairs; close pairs; weak pairs; distant pairs; very distant pairs. This partitioning allows different classes of pairs to be treated at different levels of theory. In pair theories only the strong pairs are treated at the highest level of theory, which usually is CCSD. This distinguishes strong pairs from all other classes. Both close and weak pairs are usually not distinguished in pair theories and are treated at a lower level of theory, which typically corresponds to MP2. The MR equivalent to MP2 is CASPT2, and it is thus the lowest level of theory possible to apply. As such, no distinction is made between strong, close or weak pairs, and all pairs are treated at the same level of theory. However, we differentiate distant and very distant pairs from the former.

In the MR case, unlike SR theories, three orbital sets are distinguished. With the current level of technology there is a maximum of about fourteen active orbitals possible to treat in MR calculations. Therefore the number of active orbitals is independent of the molecular size. Of the two sets of internal orbitals, only the closed-shell space scales linearly with the system's size. Furthermore, after domain approximations, the substitution spaces are in any configuration subspace always independent of the molecular size. Since the P_0 configurations are independent of closed-shell orbitals, the number of pairs in P_0 is independent of the molecular size. The same is true for S_0. In the P_1 case, there is a dependence on one active, a closed-shell orbital and two virtuals. The number of P_1 configurations scales thus linearly with the molecular size. Similarly, both S_1 and I_1 show the same linear scaling. For the cases of P_2, S_2 and I_2 there is a dependence on two closed-shell indices, meaning that the number of these configurations scales quadratically with the molecular size.

The first type of approximation we apply to P_2's pair list concerns very distant pairs. Distance criteria determines the minimal distance between the atomic centers of orbitals i and j, $DISTij$. If $DISTij$ is larger than a given threshold $RVDIST$, the respective pair is omitted from the pair list and ignored in the subsequent calculation. By default this option is off. If desired, a value of 25 *bohr* is recommended. A vicinity parameter can also be used for the very distant pair approximation, which is also by default off. By setting $IVDIST$ to an integer, all the orbitals j centered in atoms beyond the $IVDIST$ neighboring shells of the atom A, in which i is centered, are removed from the pair list (*2, 3, 133*). The number of very distant pairs scales quadratically with the molecular size (*68, 132, 136*) (the other pair classes scale linearly (*2, 133*)), and these dominate asymptotically the computational effort in canonical methods. Neglecting very distant pairs is essential to reduce to linearity the scaling of a method with the number of closed-shell orbitals (*2, 3, 65, 148, 149, 216, 231, 329, 331, 357*).

After removing the very distant pairs, approximate exchange integrals for the remaining P_2 pairs are calculated using the MPA (*214, 325*). These are used to estimate a pair energy, and if the estimated pair energy lies below a given threshold *thrdist*, the pair is classified as distant and the respective exchange integrals are approximated using the MPA. For all other pairs the two-electron integrals are explicitly calculated. This significantly reduces the computational effort for assembling the integrals for this class of pairs. By default, $thrdist = 10^{-6}\ E_h$ as recommended in the literature (*148, 149, 214, 325*). This is an energy criterion.

As above mentioned, also the S_2 and I_2 configuration subspaces exhibit a quadratic

scaling on closed-shell orbitals. In a first approximation, we reuse the P_2 list to build the S_2 and I_2 lists. This ensures consistency in applying pair approximations to all configuration subspaces. Furthermore, integrals like K_{at}^{ji}, K_{at}^{ui} or K_{tu}^{ij} decay exponentially with the distance between closed-shell and active orbitals, $DISTit$. This allowed the introduction of another distant pair criterion to neglect exchange integrals related to the P_1, S_2, S_1, I_2 and I_1 subspaces, $RDIST$. If $DISTit > RDIST$, the respective exchange integrals for P_1, S_2, S_1, I_2 and I_1 are neglected. By default we have $RDIST = 15$ *bohr*, and for consistency and invariance, $DISTit$ is defined as the minimal distance between the closed-shell orbital i and any of the active orbitals.

In the following, pair approximations are specified by curly brackets. The specification $\{ij\}$ means that orbitals i and j are in the vicinity of each other. $\{i\}_{\mathbf{t}}$ refers to a subset of the closed-shell space that is in the spatial vicinity of any active orbital and $\{ij\}_{\mathbf{t}}$ means that not only orbitals i and j are restricted to the vicinity of each other, but also that these orbitals should be close enough to any active orbital.

4.7 Building PAOs and PNOs

PNOs and their generation depend on the properties of the orbital spaces in which pair densities are built. *E.g.*, if the set of internal orbitals is not local, neither are the resulting PNOs. PNOs are generated as local orbitals when the internal orbitals they aim correlating are also local(ized). Furthermore, the scaling of algorithms to generate PNOs depends on the nature of the virtual space and the approximations used.

Without any approximation, both the diagonalization of pair densities and the construction of two-electron integrals required to build PNOs scale with the 5^{th} power of the molecular size (*148, 149, 266*): the diagonalization of pair densities depends cubically on the virtual space and quadratically on the number of internal orbitals; constructing two-electron integrals depends quadratically on the number of internal orbitals, quadratically on the number of virtuals and linearly on the DF basis. However, since the transformation of integrals has a small prefactor, the main bottleneck in generating PNOs is the diagonalization of the pair densities. Pair approximations reduce by one the exponent of the dependence on the molecular size of these algorithms. Use of domain approximations makes the substitution and DF spaces associated to each orbital pair independent of the molecular size. Therefore, the simultaneous use of both pair and domain approximations reduces drastically the scaling of the algorithms that generate PNOs to (near) linear scaling (if local DF is also used). In order to be able to use both pair and domain

approximations in building PNOs one must use previously a local basis of virtual orbitals, *e.g.* PAOs (*72, 137, 148, 149, 235, 264–266*) or OSVs (*149, 266, 273, 358*). Because PNOs are built only after applying pair and domain approximations to intermediate amplitudes, the global effect of building PNOs from local virtuals is the reduction of the number of PNO transformation matrices and of integrals (*148*). Matrices become very compact, allowing all quantities to be kept in high-speed memory (*235*). Two additional intermediate steps have also been reported by building first PAOs, then OSVs (*148, 149*), which leads to computational savings by yet another order of magnitude.

The way we generate PNOs resembles the techniques employed in PNO-MP2 (*148,235*) and PNO-CCSD (*137, 149, 265*). In our implementation, the first step for near linear scaling PNO generating algorithms starts by building IBOs. Although any other set of localized orbitals are suitable, IBOs yield stable orbital partial charges, an important feature when assigning PAO domains.

We construct then PAOs, and PAO domains are assigned for each closed-shell orbital i. Building orbital domains for closed-shell orbitals takes place just like in the SR case. For active orbitals however, further considerations must be taken. We solve the residuals in the orthogonal configuration basis and this requires amplitudes to be also in this basis. We build PNOs from unique orthogonal pair amplitudes. The orthogonalization of configuration subspaces creates orthogonal "active" indices, which differ for each configuration subspace. The transformation may even affect more than just one active index. As seen in section 4.5, these orthogonal configuration indices have no direct correspondence to the (non-orthogonal) active orbital indices. Building single orbital domains for the active space is then pointless, as with the orthogonalization procedure any single orbital domain we can build loses its validity. Furthermore, because PNOs are built from orthogonal configuration subspaces, invariance to unitary transformations within the active space is mandatory. This invariance can only be achieved with a single domain for the whole active space, $\mathbf{t}$. This single domain is built from the union of the domains of all single active orbitals, and it is thus an extension of the concept used to build pair domains from single orbital domains. Even though the orthogonalization of configuration subspaces does not allow us to fully explore the locality of active orbitals, localization of the active space is required to obtain stable active PAO domains.

Because of the inherent efficiency of PNOs, the accuracy of LCASPT2 is often limited by the PAO domains. These are thus of utmost relevance in determining the quality of calculations. The PAO domains must be as large as possible so that their accuracy is virtually the same as with canonical virtuals. For every LMO, all atoms with partial charge

larger than $thresLMO$ are included in the orbital's domain. By default we established $thresLMO = 0.2\ e$ (atomic units of electronic charge), which typically leads to domains relatively stable with respect to geometry changes (*148*). Because partial charges smaller than the default value lack physical meaningfulness and might be randomly scattered throughout molecules, these primary domains are extended by adding neighboring atom shells. The number of shells can be controlled by $iext$, which by default we set to 2 (neighboring shells). An atom B is considered to be in a neighboring shell of atom A if the distance d_{AB} is at most 20% larger than the sum of the atomic radii of A and B. A distance criterion $rext$ can also be used, which by default is set to $2 \times iext + 1$ $bohr$. $rext$ is more advantageous in cases for which bonds are stretched. Nevertheless, our program uses by default both parameters simultaneously to complement each other: either $d_{AB} \leq rext$ or B is within the $iext$ neighboring shells of A.

Having PAO domains for each closed-shell orbital and for the active space, we build pair domains by union of orbital domains. We build domains for pairs ij (P_2) and for pairs $i\mathbf{t}$ (P_1). Note that for P_0 pairs we do not have to build any special pair domain, due to the singular domain for active orbitals. We orthogonalize the PAOs in each domain and make them semicanonical. At the end of this step we build the conversion between canonical virtuals, b, and PAO(SC)s, $\bar{r}^{ij}$.

$$|\bar{r}^{mn}\rangle = \sum_{\tilde{s}} |\tilde{s}\rangle\, \bar{V}^{mn}_{\tilde{s}\bar{r}} = \sum_{b} |b\rangle\, \bar{Q}^{mn}_{b\bar{r}} \tag{4.50}$$

From the last equation, $\bar{\mathbf{Q}}^{mn} = \tilde{\mathbf{Q}}\bar{\mathbf{V}}^{mn}$ transforms canonical orbitals into the orthogonal PAO(SC)s. The matrix $\tilde{\mathbf{Q}}$ transforms canonical virtuals into PAOs, $\tilde{r}$, while $\bar{\mathbf{V}}^{mn}$ simultaneously orthogonalizes and semicanonicalizes PAOs for each pair mn.

From orthogonal PAO(SC)s zeroth-iteration pair amplitudes are calculated in the orthogonal configuration and orthogonal PAO(SC) bases. These are obtained from the expressions of the perturbative update of amplitudes. The resulting expression for the amplitudes has for pairs the general structure of an exchange integral divided by the respective energy denominators as given in Table 4.9. The expressions for the zeroth iteration amplitudes are given below. For the sake of simplicity, PAO domains are omitted, since the PAOs below used are always associated to a specific orbital pair.

$$c^{ij}_{\bar{r}\bar{s}} = -\frac{K^{ij}_{\bar{r}\bar{s}}}{\varepsilon^{ij}_{\bar{r}\bar{s}}} \tag{4.51}$$

$$c^{iD_1}_{\bar{r}\bar{s}} = -\frac{\sum_{tu} K^{it}_{\bar{r}\bar{s}} \left(\mathbf{S}^{D_1}\right)_{tu} T_{uD_1}}{\varepsilon^{iD_1}_{\bar{r}\bar{s}}} \tag{4.52}$$

$$c_{\bar{r}\bar{s}}^{D_0p} = -\frac{1}{2}\frac{\sum_{tu}\sum_{vw} K_{\bar{r}\bar{s}}^{tu}\left(\mathbf{S}^{D_0p}\right)_{tu,vw} T_{vw,D_0}^{(p)}}{\varepsilon_{\bar{r}\bar{s}}^{D_0p}} \tag{4.53}$$

These amplitudes are then used to calculate pair densities as given in eqs. 3.92 and 3.94. Note that even though in eq. 3.94 there is a compound pair mnp this is equivalent to a D_0p pair. For P_1, eq. 3.92 is used because of the contravariant configurations. With the pair densities, PNOs are built, which we also semicanonicalize. With these two steps the transformation matrices to the PNO basis are generated, allowing the transformation from canonical virtuals or PAOs to PNOs, $\tilde{a}^{mn}$, or to PNO(SC)s, a^{mn}.

$$|\tilde{a}^{mn}\rangle = \sum_{\bar{r}} |\bar{r}^{mn}\rangle\, \tilde{W}_{\bar{r}\tilde{a}}^{mn} = \sum_{b} |b\rangle \bar{W}_{b\tilde{a}}^{mn} \tag{4.54}$$

$$\begin{aligned} |a^{mn}\rangle &= \sum_{\tilde{b}} \left|\tilde{b}^{mn}\right\rangle U_{\tilde{b}a}^{mn} = \sum_{\tilde{b}}\sum_{\bar{r}} |\bar{r}^{mn}\rangle\, \tilde{W}_{\bar{r}\tilde{b}}^{mn} U_{\tilde{b}a}^{mn} = \sum_{\tilde{b}}\sum_{\bar{s}}\sum_{\tilde{r}} |\tilde{r}\rangle\, \bar{V}_{\tilde{r}\bar{s}}^{mn} \tilde{W}_{\bar{s}\tilde{b}}^{mn} U_{\tilde{b}a}^{mn} \\ &= \sum_{\tilde{r}} |\tilde{r}\rangle\, W_{\tilde{r}a}^{mn} = \sum_{b}\sum_{\tilde{b}} |b\rangle\, \bar{W}_{b\tilde{b}}^{mn} U_{\tilde{b}a}^{mn} = \sum_{b}\sum_{\tilde{r}} |b\rangle\, \tilde{Q}_{b\tilde{r}} W_{\tilde{r}a}^{mn} \end{aligned} \tag{4.55}$$

PNO domains can be easily determined using thresholds on the eigenvalues of the pair densities, *thrpno_occ*. For more distant pairs, this occupation criterion yields too small or even empty domains, underestimating long range dispersion energies (*148*). An energy completion threshold balances the percentage of correlation recovered for all pairs, independently of their class, guaranteeing that domains are sufficiently large and accurate for short- and long-range pairs. In the energy completeness criterion, PNOs are considered in the domain of a pair P until an estimated pair energy in the PNO basis, E_{PNO}^P, is at least $100\times thrpno\%$ of the same energy in the PAO basis, E_{PAO}^P (or canonical virtual basis, E^P).[15] Accessing PNO energies requires having two-electron integrals and amplitudes in the PNO basis, which is done using full transformation matrices. By default we combine both strategies to build PNO domains and demand both conditions to be simultaneously fulfilled. This means that all PNOs corresponding to eigenvalues larger than *thrpno_occ* are included in the domain of pair P and if $\frac{E_{\mathrm{PNO}}^P}{E_{\mathrm{PAO}}^P} \leq thrpno$ then more PNOs are added until this condition is also verified. For consistency, further PNOs are added with decreasing occupation number. By default $thrpno\_occ = 10^{-8}$ and $thrpno = 0.997$.

PNOs are thus built for all pairs in the orthogonal configuration basis. This means we have PNOs for all pairs ij, iD_1 and D_0p. Alike the SR case, PNOs cannot be built specifically for singles. However, PNOs can be reused from pairs in singles. The difference is that only one external index must be transformed in the case of singles. The first case

[15] PNO and PAO pair energies are given or can be adapted from the energy expressions given in section 4.11.

to consider is S_2, in which we have configurations of the form $\Phi_{ij}^{aS_2}$. Since an electron pair originating the substitution is always identifiable, the pair ij, we may relate each S_2 configuration to one and only one P_2 configuration. It is thus possible to assign for each S_2 configuration a unique set of P_2's PNOs. The second case to take in consideration is S_1. Here there are configurations of the form $\Phi_{iS_1}^{a}$. Since the orthogonalization of S_1 configurations is unrelated to the orthogonalization of P_1 configurations, there is no possible connection between the indices S_1 and P_1. It is thus not possible to reuse P_1's PNOs for S_1. The other possibilities are either keeping PAOs for S_1 or using P_2's OSVs (intrapair PNOs). We verified that the latter causes greater losses in the correlation energy, as well as convergence problems. This was also verified by others (*72*). In the final version of our equations we used thus PAOs for S_1. Finally we have the S_0 space, with configurations of the form $\Phi_{S_0}^{a}$. Because there is no connection between the indices S_0 and D_0p, neither singlet nor triplet, no set of PNOs can be assigned to any of S_0's configurations. S_0 configurations were also left in the PAOs basis.

For the case of internals, because no external indices are involved, there is no transformation to local virtual bases.

4.8 Transformation of Integrals

The two-electron integrals used in the LCASPT2 implementation have one of two possible sources. The first possibility is to read the integrals from a file of the previous CASSCF calculation, which are loaded in the canonical MO basis. This is how the program worked in the initial stages. Later on, the program was changed to calculate the integrals in the AO basis using LDF and to directly transform these to the LMO and PAO bases subject to pair and domain approximations. Transforming the integrals from one virtual basis to another consists solely on a matrix multiplication over virtual indices. These operations take place using the respective transformation matrices for all virtual indices. The transformation of two- and one-external exchange integrals from canonical virtuals to the PAO basis is given by

$$K_{\tilde{r}\tilde{s}}^{mn} = \sum_{ab} \tilde{Q}_{a\tilde{r}} K_{ab}^{mn} \tilde{Q}_{b\tilde{s}} \tag{4.56}$$

$$K_{\tilde{r}t}^{mn} = \sum_{a} \tilde{Q}_{a\tilde{r}} K_{at}^{mn} \tag{4.57}$$

Note that the all internal integrals K_{tu}^{mn} have no external index and therefore require no transformation. Alternatively, integrals can be directly transformed to the orthogonal

pair specific PAO(SC) basis. This requires simply exchanging the transformation matrices $\tilde{\mathbf{Q}}$ by the matrices $\bar{\mathbf{Q}}^{mn}$. The resulting integrals are, respectively, $K^{mn}_{\bar{r}\bar{s}}$ and $K^{mn}_{\bar{r}t}$.

In a similar fashion the integrals in the PAO basis can be transformed to the PNO basis. The transformations are equivalent to the transformations to the PAO basis. However, PNO domains are built for orthogonal pairs, meaning that only for the cases of P_2 and S_2 these expressions hold as they were presented. Note that for S_2 the orthogonal configuration index does not influence the PNO domains. For P_1 and P_0 the exchange integrals are transformed to the PNO basis after performing the necessary contractions to get quantities depending on orthogonal configuration indices only. These transformations will be presented later. Taking as an example the integrals $K^{tu}_{\tilde{r}\tilde{s}}$ for P_0's residuals, the direct transformation to the PNO basis yields a tensor dependent on the indices a, b, t, u and D_0p. If on the other hand we first contract the indices t and u to D_0p and then transform $K^{D_0p}_{\tilde{r}\tilde{s}}$ to the PNO basis, we only need to keep track of the indices a, b and D_0p. This same principle holds also for P_1. Transforming exchange integrals to the PNO basis can be performed by the following transformations:

$$K^{ij}_{ab} = K^{ij}_{a^{ij}b^{ij}} = \sum_{\tilde{r}\tilde{s}} W^{ij}_{\tilde{r}a} K^{ij}_{\tilde{r}\tilde{s}} W^{ij}_{\tilde{s}b} \tag{4.58}$$

$$K^{ij}_{aS_2} = K^{ij}_{a^{ij}S_2} = \sum_{\tilde{r}} W^{ij}_{\tilde{r}a} K^{ij}_{\tilde{r}S_2} \tag{4.59}$$

$$K^{iD_1}_{ab} = K^{iD_1}_{a^{iD_1}b^{iD_1}} = \sum_{\tilde{r}\tilde{s}} W^{iD_1}_{\tilde{r}a} K^{iD_1}_{\tilde{r}\tilde{s}} W^{iD_1}_{\tilde{s}b} \tag{4.60}$$

$$K^{D_0p}_{ab} = K^{D_0p}_{a^{D_0p}b^{D_0p}} = \sum_{\tilde{r}\tilde{s}} W^{D_0p}_{\tilde{r}a} K^{D_0p}_{\tilde{r}\tilde{s}} W^{D_0p}_{\tilde{s}b} \tag{4.61}$$

Similarly, blocks of the Fock matrix involving external indices can be equally transformed to the PAO or PNO bases. These blocks are specifically the virtual block, f_{ab}, or the virtual:internal block, f_{am}. Due to the structure of the elements in the Fock matrix, these integrals can be directly transformed to any local virtual basis.

4.9 Wavefunction Ansatz in Local Basis

Having defined how the external substitution spaces are expressed for each configuration subspace we can define the wavefunction ansatz given in eq. 4.35 in the local basis.

The local ansatz for the wavefunction we used is given by

$$\Psi^{(1)} = \frac{1}{2}\sum_{ij\in\{ij\}}\sum_{ab\in[ij]_{\mathrm{PNO}}} c_{ab}^{ij}\Phi_{ij}^{ab} + \sum_{iD_1\in\{i\}_{\mathbf{t}}}\sum_{ab\in[iD_1]_{\mathrm{PNO}}} c_{ab}^{iD_1}\Phi_{iD_1}^{ab} + \sum_{p}\sum_{D_0}\sum_{ab\in[D_0p]_{\mathrm{PNO}}} c_{ab}^{D_0p}\Phi_{D_0p}^{ab}$$
$$+\sum_{S_2}\sum_{ij\in\{ij\}_{\mathbf{t}}}\sum_{a\in[ij]_{\mathrm{PNO}}} c_{aS_2}^{ij}\Phi_{ij}^{aS_2} + \sum_{S_1}\sum_{i\in\{i\}_{\mathbf{t}}}\sum_{\bar{r}\in[i,\mathbf{t}]_{\mathrm{PAO}}} c_{\bar{r}}^{iS_1}\Phi_{iS_1}^{\bar{r}} + \sum_{S_0}\sum_{\bar{r}\in[\mathbf{t}]_{\mathrm{PAO}}} c_{\bar{r}}^{S_0}\Phi_{S_0}^{\bar{r}}$$
$$+\sum_{ij\in\{ij\}_{\mathbf{t}}}\sum_{I_2} c_{I_2}^{ijp}\Phi_{ijp}^{I_2} + \sum_{i\in\{i\}_{\mathbf{t}}}\sum_{I_1} c^{iI_1}\Phi_{iI_1} \tag{4.62}$$

In the wavefunction's ansatz, square brackets refer to orbital domains, just as previously defined. Different indices are used for PNOs and PAOs. Subscripts on square brackets specifically identify which local orbitals are used for each case and to which domain they belong to. As such, *e.g.*, in the P_1 term, the PNOs a and b run over the domain of the pair iD_1; in the S_0 term, PAOs $\bar{r}$ run over the domain for the active space. In the configuration subspaces spanned by PAOs the restriction $\mathbf{t}$ refers to the united PAO domain for active orbitals. We remind the reader that curly brackets affecting closed-shell indices refer to pair approximations.

4.10 Residual Equations

In canonical MR methods the residual equations are derived and implemented in the non-orthogonal configuration basis. Changing to the orthogonal configuration basis is a side step used in the update of amplitudes that removes linear dependencies and improves convergence. Afterwards, amplitudes are back-transformed to the non-orthogonal configuration basis and the new amplitudes are used to calculate new residuals in the next iteration. The procedure is repeated until all the residuals are zero within a certain accuracy. There is then this pattern of residuals being calculated in the non-orthogonal configuration basis and then transformed to the orthogonal configuration basis. The amplitudes follow the opposite path, they are first obtained in the orthogonal configuration basis and then transformed to the non-orthogonal configuration basis. In the LCASPT2 method, the residuals must be both built and solved in the orthogonal configuration basis. Likewise amplitudes are always in the orthogonal configuration basis, at least for the configuration subspaces spanned in the PNO basis. For P_2, P_1, P_0 and S_2 the program only deals with residuals and amplitudes in the orthogonal configuration basis. For S_1, S_0, I_2 and I_1 this is however not a must. This is a significant difference towards other MR implementations, since it is required for some quantities to be always in the orthogonal

configuration basis.

The residual equations can be directly derived in the orthogonal configuration and local bases. However, working out the expressions for all terms in the residuals is a lengthy and demanding task, prone to error. We therefore opted for a three step derivation: expressing non-orthogonal operator expressions as tensor contractions; change to orthogonal configuration basis; change to local bases. The following explanation of the many steps used to assemble the final residual equations in the orthogonal configuration and local bases is complemented with a suitable example. This example is the P_1-P_0 term contributing to P_1's residuals. All equations were first derived by hand in the non-orthogonal basis. This required the anticommutation relations 3.7, 3.8 and 3.9, as well as eqs. 4.12, and 4.13. All these relations allowed us to work out products of substitution operators and to go from operator expressions [16] to tensor-formulated expressions. The latter depended exclusively on the many orders of the density matrix, on integrals like the Fock or exchange matrices and eventually also on amplitudes (the terms $\langle\Phi_i|\,\hat{H}\,|0\rangle$ do not depend on amplitudes). The resulting expressions were afterwards confirmed using Dr. D. Kats' Quantwo software (*359*). Quantwo is a C++ program that takes an operator expression written in LaTeX format and evaluates it to a sum of tensor contractions. The evaluation is based on simple creation and annihilation operators along with Wick's theorem. The resulting expressions are spin-summed to yield spin-free expressions, and transformed back to LaTeX form.

In the example, the quantity needed to be calculated in the non-orthogonal basis is

$$\begin{aligned}
&\sum_{p}\sum_{uv}\sum_{cd}\left\langle\tilde{\Phi}^{ab}_{it}|\hat{F}|\Phi^{cd}_{uvp}\right\rangle c^{uvp}_{cd} = \\
=&\frac{1}{6}\sum_{p}\sum_{uv}\sum_{cd}\sum_{rs} f_{rs}c^{uvp}_{cd}\Big[2\langle 0|\,\hat{E}_{ai,bt}\hat{E}_{rs}\hat{E}_{cu,dv}\,|0\rangle + \langle 0|\,\hat{E}_{at,bi}\hat{E}_{rs}\hat{E}_{cu,dv}\,|0\rangle\Big] \\
+&\frac{1}{6}p\sum_{p}\sum_{uv}\sum_{cd}\sum_{rs} f_{rs}c^{uvp}_{cd}\Big[2\langle 0|\,\hat{E}_{ai,bt}\hat{E}_{rs}\hat{E}_{cv,du}\,|0\rangle + \langle 0|\,\hat{E}_{at,bi}\hat{E}_{rs}\hat{E}_{cv,du}\,|0\rangle\Big]
\end{aligned} \tag{4.63}$$

Using eqs. 3.7, 3.8, 3.9, 4.12 and 4.13 to evaluate all terms inside brackets yields

$$\sum_{p}\sum_{uv}\sum_{cd}\left\langle\tilde{\Phi}^{ab}_{it}|\hat{F}|\Phi^{cd}_{uvp}\right\rangle c^{uvp}_{cd} = -\frac{1}{6}\sum_{p}(2+p)\sum_{w} f_{iw}S^{(p)}_{tw,vu}c^{vup}_{ab} \tag{4.64}$$

All quantities were then transformed to the orthogonal configuration basis using the relations in Table 4.7. The end result of both transformations (residuals and amplitudes) is that quantities in the non-orthogonal configuration basis ended up being expressed in

[16] For excited configurations i and j, terms like $\langle\Phi_i|\,\hat{F}\,|\Phi_j\rangle$ or $\langle\Phi_i|\,\hat{H}\,|0\rangle$.

terms of orthogonal configuration indices. All the terms depending on internal orbitals were furthermore separated from terms depending on virtual orbitals and conveniently collected and rearranged as intermediates. With this step, most terms in the residual equations could be built as the contraction of three tensors: an orthogonal amplitude; a term depending on a specific block of the Fock matrix; a coupling term depending on many orders of the density matrix contracted with orthogonalization tensors. Whenever possible, the Fock matrix terms were contracted with the coupling term, creating one single intermediate. This contraction depended on the block of the Fock matrix required. The exceptions to these rules were terms which did not depend on amplitudes. These involved either exchange integrals or some mixed block of the Fock matrix[17] contracted with many orders of the density matrix and orthogonalization tensors.

All these rearrangements allowed us to store just the essential quantities. The latter depended on the least possible number of parameters, allowing the minimization of memory requirements. Furthermore, only terms depending on amplitudes would require update in each iteration and all other quantities were calculated just once in the beginning of each calculation. In the case of the selected example, the term we wished to calculate in the orthogonal basis is

$$\begin{aligned}\sum_{D_0p}\sum_{cd}\left\langle\tilde{\Phi}^{ab}_{iD_1}|\hat{F}|\Phi^{cd}_{D_0p}\right\rangle c^{D_0p}_{cd} &= \sum_{D_0p}\sum_{cd}\sum_{tuv} T_{tD_1}\left\langle\tilde{\Phi}^{ab}_{it}|\hat{F}|\Phi^{cd}_{uvp}\right\rangle T^{(p)}_{uv,D_0} c^{D_0p}_{cd} \\ &= -\frac{1}{3}\sum_{p}(2+p)\sum_{D_0p} c^{D_0p}_{ab} f_{iD_1,D_0p}\end{aligned} \tag{4.65}$$

with

$$f_{iD_1,D_0p} = \sum_t f_{it}\alpha^{(p)}_{t,D_1,D_0} \qquad \alpha^{(p)}_{w,D_1,D_0} = \frac{1}{2}\sum_{tuv} T^{(p)}_{tu,D_0} S^{(p)}_{tu,vw} T_{vD_1} \tag{4.66}$$

In this specific example, the closed-shell:active block of the Fock matrix contracts with the coupling term α. As a result, in the beginning of the calculation we calculate f_{iD_1,D_0p} as a matrix with the dimensions of the full P_1 space times the full P_0 singlet or triplet spaces. This tensor is loaded and contracted with the amplitudes $c^{D_0p}_{ab}$ in every iteration.

We distinguished four types of coupling coefficients according to the block of the Fock matrix appearing in that same term: α terms are associated to the closed-shell:active block of the Fock matrix, coupling different subspaces within a space of excited configurations (*e.g.*, P_1 with P_0); β coefficients are associated with the active:virtual block of the Fock matrix, coupling different subspaces with the same subscript (*e.g.*, P_1 with S_1);

[17] As mixed blocks of the Fock matrix we understand the closed-shell:active, closed-shell:virtual, or active:virtual blocks.

γ coefficients appear in terms involving the active block of the Fock matrix, coupling one subspace with itself; σ coefficients appear along with the closed-shell:virtual block of the Fock matrix, and are present in the remaining couplings.

In the final step we transformed both the residuals and amplitudes to the local bases by using eqs. 3.60 for the amplitudes and 3.62 for the residuals. Despite these last two expressions being given only for P_2 configurations, these can be used for both amplitudes and residuals of other configuration subspaces. This means that each canonical virtual index was contracted with the transformation matrix to either the PNO or PAO bases. These transformation matrices contracted then either with integrals, yielding the integrals in the respective local basis, or with each other, yielding overlap matrices for local bases. These overlap matrices occur in the residual equations because of the general non-orthogonality of orbitals in these local virtual bases. For general orbital/pair domains P, Q, the PNO ($\mathbf{S}^{\mathrm{PNO}}_{[P,Q]}$), PAO ($\mathbf{S}^{\mathrm{PAO}}$, for non-orthogonal PAOs; $\mathbf{S}^{\mathrm{PAO}}_{[P,Q]}$ for orthogonal semicanonical PAOs), and PNO-PAO ($\mathbf{S}^{\mathrm{PAO-PNO}}_{[P,Q]}$) overlap matrices are defined as

$$\begin{aligned}\left(\mathbf{S}^{\mathrm{PNO}}_{[P,Q]}\right)_{a^P b^Q} &= \sum_{cd}\sum_{\tilde{r}\tilde{s}} \tilde{Q}_{c\tilde{r}} W^P_{\tilde{r}a^P}\langle c|d\rangle \tilde{Q}_{d\tilde{s}} W^Q_{\tilde{s}b^Q} \\ = \sum_{c}\sum_{\tilde{r}\tilde{s}} W^P_{\tilde{r}a^P}\tilde{Q}_{c\tilde{r}}\tilde{Q}_{c\tilde{s}} W^Q_{\tilde{s}b^Q} &= \sum_{c}\sum_{\tilde{r}\tilde{s}} W^P_{\tilde{r}a^P}\mathbf{S}^{\mathrm{PAO}} W^Q_{\tilde{s}b^Q}\end{aligned} \tag{4.67}$$

$$\left(\mathbf{S}^{\mathrm{PAO}}_{[P,Q]}\right)_{\bar{r}\bar{s}} = \sum_{ab} \bar{Q}^P_{a\bar{r}}\langle a|b\rangle \bar{Q}^{b\bar{s}}_Q = \sum_a \bar{Q}^P_{a\bar{r}}\bar{Q}^Q_{a\bar{s}} \tag{4.68}$$

$$\left(\mathbf{S}^{\mathrm{PAO-PNO}}_{[P,Q]}\right)_{\bar{r}a^Q} = \sum_{cd}\sum_{\tilde{s}} \bar{Q}^P_{c\bar{r}}\langle c|d\rangle \tilde{Q}_{d\tilde{s}} W^Q_{\tilde{s}a^Q} = \sum_{c}\sum_{\tilde{s}} \bar{Q}^P_{c\bar{r}}\tilde{Q}_{c\tilde{s}} W^Q_{\tilde{s}a^Q} \tag{4.69}$$

Note that the domains are inherited from the corresponding pairs. Thus, transforming the a and b canonical indices from the residuals R^P_{ab} or from the amplitudes c^P_{ab} generates local orbitals in the domain of pair P. Note as well that all PNOs in the same domain are orthogonal. As such, $\left(\mathbf{S}^{\mathrm{PNO}}_{[P,P]}\right) = \mathbf{I}$. The same is valid for the orthogonal pair specific PAO(SC)s. The differences between local and canonical residuals is that integrals must be in the local virtual bases and all virtual indices of amplitude matrices are not contracted with integrals. Instead they contract with overlap matrices of the local bases.

Regarding the selected example, applying the above mentioned changes to the last equality in 4.65 gives the term in the PNO basis:

$$-\frac{1}{3}\sum_p (2+p)\sum_{D_0} f_{iD_1,D_0p}\left(\mathbf{S}^{\mathrm{PNO}}_{[iD_1,D_0p]}\mathbf{c}^{D_0p}\mathbf{S}^{\mathrm{PNO}}_{[D_0p,iD_1]}\right)_{ab} \tag{4.70}$$

In a first stage, all the residuals were derived and implemented in the orthogonal configuration and local bases. For S_0 and I_1 this meant however that we had to build terms,

which had scalings up to $\mathcal{O}\left(n_{active}^{9}\right)$. Building the residuals in the non-orthogonal configuration basis and orthogonalizing them at a later stage changes the maximum scaling to $\mathcal{O}\left(n_{active}^{6} \times n_{pao}\right)$ for S_0 and to $\mathcal{O}\left(n_{active}^{6} \times n_{closed}\right)$ for I_1. The relative speed of these procedures depends naturally on the ratios $\frac{n_{active}^{3}}{n_{pao}}$ and $\frac{n_{active}^{3}}{n_{closed}}$. Because building all intermediates in the orthogonal basis is significantly worse for larger active spaces, we found suitable to build the residuals for S_0 and I_1 first in the non-orthogonal configuration basis and then contract the resulting tensors with the respective orthogonalization matrices for each subspace. Due to the presence of non-orthogonal configuration subspaces we had to introduce an extra class of coupling terms, which we named ρ. ρ terms depend only on one orthogonal configuration index.

We present now the residuals for LCASPT2. The α, β, σ, and ρ coupling terms are presented in the Appendix 8.2. The γ terms were presented in Tables 4.8, 4.9 and 4.10 in section 4.5.1. All residuals have the same basic structure. We identified i) Hamiltonian terms depending on exchange integrals and eventually also on a mixed block of the Fock matrix; ii) external contraction terms contracting amplitudes with the virtual block of the Fock matrix ($\mathbf{F}^{v}$); iii) internal contraction terms contracting amplitudes with the closed-shell block of the Fock matrix, with γ terms and with $E_{act}^{(0)}$; iv) G terms with all interactions of a specific subspace with all others. There are simplifications to the residuals, which are not showed here, but instead in reference (*242*). An example are the terms involving the virtual block of the Fock matrix, a diagonal matrix in the semicanonical PNO basis. The elements f_{ab} are in this basis written as orbital energies ϵ_a.

$$\begin{aligned}\tilde{R}_{ab}^{ij} &= K_{ab}^{ij} + \left(\mathbf{F}^{v}\mathbf{c}^{ij}\right)_{ab} + \left(\mathbf{c}^{ij}\mathbf{F}^{v}\right)_{ab} + G_{ab}^{ij} + G_{ba}^{ji} \\ &- \sum_{k} f_{ik}\left(\mathbf{S}_{[ij,kj]}\mathbf{c}^{kj}\mathbf{S}_{[kj,ij]}\right)_{ab} - \sum_{k}\left(\mathbf{S}_{[ij,ik]}\mathbf{c}^{ik}\mathbf{S}_{[ik,ij]}\right)_{ab} f_{kj}\end{aligned} \tag{4.71}$$

$$\begin{aligned}G_{ab}^{ij} &= -\frac{1}{2}\sum_{D_1}\left(\mathbf{S}_{[ij,iD_1]}^{\mathrm{PNO}}\mathbf{c}^{iD_1}\mathbf{S}_{[iD_1,ij]}^{\mathrm{PNO}}\right)_{ab} f_{jD_1} \\ &+ \frac{1}{2}\sum_{S_2} c_{aS_2}^{ij} f_{S_2 b} + f_{ai}\sum_{S_1}\left(\mathbf{c}^{jS_1}\mathbf{S}_{[j\mathbf{t},ij]}^{\mathrm{PAO-PNO}}\right)_{b}\sigma\left(S_1\right)\end{aligned} \tag{4.72}$$

$$f_{iD_1} = \sum_{tu} f_{it} D_{tu}^{(1)} T_{uD_1} \tag{4.73}$$

$$f_{S_2 b} = \sum_{tu} T_{uS_2}\left(\mathbf{S}^{S_2}\right)_{ut} f_{tb} \tag{4.74}$$

$$\begin{aligned}\tilde{R}_{ab}^{iD_1} &= K_{ab}^{iD_1} + \left[\gamma\left(D_1, D_1\right) - E_{act}^{(0)}\right] c_{ab}^{iD_1} + G_{ab}^{iD_1} \\ &- \sum_{j} f_{ij}\left(\mathbf{S}_{[iD_1,jD_1]}^{\mathrm{PNO}}\mathbf{c}^{jD_1}\mathbf{S}_{[jD_1,iD_1]}^{\mathrm{PNO}}\right)_{ab} + \left(\mathbf{F}^{v}\mathbf{c}^{iD_1} + \mathbf{c}^{iD_1}\mathbf{F}^{v}\right)_{ab}\end{aligned} \tag{4.75}$$

$$K_{ab}^{iD_1} = \sum_{tu} K_{ab}^{it} \left(\mathbf{S}^{P_1}\right)_{tu} T_{uD_1} \tag{4.76}$$

$$\begin{aligned} G_{ab}^{iD_1} = &- \sum_{j} \left(\mathbf{S}_{[iD_1,ij]}^{\mathrm{PNO}} \mathbf{c}^{ij} \mathbf{S}_{[ij,iD_1]}^{\mathrm{PNO}}\right)_{ab} f_{jD_1} + f_{ai} \sum_{tuv} \left(\mathbf{S}_{[iD_1,\mathbf{t}]}^{\mathrm{PNO-PAO}} \mathbf{c}^{vt}\right)_{bu} \rho_{tvu}\left(D_1\right) \\ &- \frac{1}{3} \sum_{p} \left(2+p\right) \sum_{D_0} f_{iD_1,D_0p} \left(\mathbf{S}_{[iD_1,D_0p]}^{\mathrm{PNO}} \mathbf{c}^{D_0p} \mathbf{S}_{[D_0p,iD_1]}^{\mathrm{PNO}}\right)_{ab} \\ &+ \sum_{S_1} \left[f_{a,D_1,S_1}^{A} \left(\mathbf{c}^{iS_1} \mathbf{S}_{[i\mathbf{t},iD_1]}^{\mathrm{PAO-PNO}}\right)_{b} + \left(\mathbf{c}^{iS_1} \mathbf{S}_{[i\mathbf{t},iD_1]}^{\mathrm{PAO-PNO}}\right)_{a} f_{S_1,D_1,b}^{B} \right] \end{aligned} \tag{4.77}$$

$$f_{iD_1,D_0p} = \sum_{t} f_{it} \alpha_t^{(p)}\left(D_1, D_0\right) \tag{4.78}$$

$$f_{S_1,D_1,a}^{B} = \sum_{t} f_{at} \beta_t^{B}\left(D_1, S_1\right) \tag{4.79}$$

$$f_{a,D_1,S_1}^{A} = \sum_{t} f_{at} \beta_t^{A}\left(D_1, S_1\right) \tag{4.80}$$

$$\begin{aligned} R_{ab}^{D_0p} = &K_{ab}^{D_0p} + \left[\gamma^{(p)}\left(D_0, D_0\right) - E_{act}^{(0)}\right] c_{ab}^{D_0p} \\ &+ \left(\mathbf{c}^{D_0p} \mathbf{F}^{v} + \mathbf{F}^{v} \mathbf{c}^{D_0p}\right)_{ab} + \frac{1}{2} G_{ab}^{D_0p} + \frac{1}{2} p G_{ba}^{D_0p} \end{aligned} \tag{4.81}$$

$$K_{ab}^{D_0p} = \frac{1}{4} \sum_{tu} \sum_{vw} K_{ab}^{vw} \left(\mathbf{S}^{D_0p}\right)_{tu,vw} T_{tu,D_0}^{(p)} \tag{4.82}$$

$$\begin{aligned} G_{ab}^{D_0p} = &\sum_{w} f_{aw} \sum_{vxz} \left(\mathbf{S}_{[D_0p,\mathbf{t}]}^{\mathrm{PNO-PAO}} \mathbf{c}^{vx}\right)_{bz} \rho_{wvxz}^{(p)}\left(D_0\right) \\ &- \sum_{D_1} \sum_{i} \left(\mathbf{S}_{[D_0p,iD_1]}^{\mathrm{PNO}} \mathbf{c}^{iD_1} \mathbf{S}_{[iD_1,D_0p]}^{\mathrm{PNO}}\right)_{ab} f_{iD_1,D_0p} \end{aligned} \tag{4.83}$$

$$\begin{aligned} \tilde{R}_{aS_2}^{ij} = &K_{aS_2}^{ij} - \sum_{k} \left[f_{ik} \left(\mathbf{S}_{[ij,kj]}^{\mathrm{PNO}} \mathbf{c}^{kj}\right)_{aS_2} + \left(\mathbf{S}_{[ij,ik]}^{\mathrm{PNO}} \mathbf{c}^{ik}\right)_{aS_2} f_{kj} \right] \\ &+ \left(\mathbf{F}^{v} \mathbf{c}^{ij} + \gamma\left(S_2, S_2\right) \mathbf{c}^{ij}\right)_{aS_2} + G_{aS_2}^{ij} \end{aligned} \tag{4.84}$$

$$K_{aS_2}^{ij} = \sum_{tu} K_{at}^{ij} \left(\mathbf{S}^{S_2}\right)_{tu} T_{uS_2} \tag{4.85}$$

$$\begin{aligned} G_{aS_2}^{ij} = &\sum_{b} c_{ab}^{ij} f_{S_2b} + \sum_{S_1} \left[\left(\mathbf{c}^{iS_1} \mathbf{S}_{[i\mathbf{t},ij]}^{\mathrm{PAO-PNO}}\right)_{a} f_{S_1,S_2,j}^{A} + \left(\mathbf{c}^{jS_1} \mathbf{S}_{[j\mathbf{t},ij]}^{\mathrm{PAO-PNO}}\right)_{a} f_{S_1,S_2,i}^{B} \right] \\ &+ f_{ai} \sum_{tuv} c_{tu}^{jv} \rho_{tuv}\left(S_2\right) + \sum_{p} \frac{\left(2+p\right)}{3} \sum_{I_2} f_{a,S_2,I_2}^{(p)} c_{I_2}^{ijp} \end{aligned} \tag{4.86}$$

$$f_{a,S_2,I_2}^{(p)} = \sum_{t} f_{at} \beta_t^{(p)}\left(S_2, I_2\right) \tag{4.87}$$

$$f_{S_1,S_2,i}^{A} = \sum_{t} f_{it} \alpha_t^{A}\left(S_2, S_1\right) \tag{4.88}$$

$$f^{B}_{S_1,S_2,i} = \sum_t f_{it}\alpha^{B}_{t}\left(S_2,S_1\right) \tag{4.89}$$

$$\begin{aligned} R^{iS_1}_{\bar{r}} = 2f^{clos}_{\bar{r}i}\sigma\left(S_1\right) + K^{iS_1}_{\bar{r}} + \left(\mathbf{F}^{v}\mathbf{c}^{iS_1}\right)_{\bar{r}} - \sum_j f_{ij}\left(\mathbf{S}^{\mathrm{PAO}}_{[i\mathbf{t},j\mathbf{t}]}\mathbf{c}^{jS_1}\right)_{\bar{r}} \\ + \left(\mathbf{S}^{\mathrm{PAO}}_{[i\mathbf{t},i\mathbf{t}]}\mathbf{c}^{iS_1}\right)_{\bar{r}}\left[\gamma\left(S_1,S_1\right) - E^{(0)}_{act}\right] + G^{iS_1}_{\bar{r}} \end{aligned} \tag{4.90}$$

$$f^{clos}_{rs} = h_{rs} + \sum_i \left[2(rs|ii) - (ri|is)\right] \tag{4.91}$$

$$\begin{aligned} G^{iS_1}_{\bar{r}} &= 2\sum_j \left(\mathbf{S}^{\mathrm{PAO-PNO}}_{[i\mathbf{t},ij]}\left[2\mathbf{c}^{ij} - \mathbf{c}^{ji}\right]\mathbf{F}^{vc}_{[ij]}\right)_{\bar{r}j}\sigma\left(S_1\right) \\ &- \sum_{tuv}\left(\mathbf{S}^{\mathrm{PAO}}_{[i\mathbf{t},\mathbf{t}]}\mathbf{c}^{tu}\right)_{\bar{r}v}\sum_w f_{iw}\rho_{utwv}\left(S_1\right) \\ &+ \sum_{S_2}\sum_j\left[\left(\mathbf{S}^{\mathrm{PAO-PNO}}_{[i\mathbf{t},ij]}\mathbf{c}^{ij}\right)_{\bar{r}S_2} f^{C}_{j,S_2,S_1} - f^{D}_{S_1,S_2,j}\left(\mathbf{S}^{\mathrm{PAO-PNO}}_{[i\mathbf{t},ij]}\mathbf{c}^{ji}\right)_{\bar{r}S_2}\right] \\ &+ \sum_{D_1}\sum_a\left[\left(\mathbf{S}^{\mathrm{PAO-PNO}}_{[i\mathbf{t},iD_1]}\mathbf{c}^{iD_1}\right)_{\bar{r}a} f^{C}_{a,D_1,S_1} + f^{D}_{S_1,D_1,a}\left(\mathbf{c}^{iD_1}\mathbf{S}^{\mathrm{PNO-PAO}}_{[iD_1,i\mathbf{t}]}\right)_{a\bar{r}}\right] \\ &+ \sum_w f_{\bar{r}w}\sum_{tu}\left[c^{it}_{wu}(\mathbf{U}_{S_1})_{tu,S_1} - c^{it}_{uw}(\mathbf{V}_{S_1})_{tu,S_1} - \sum_v c^{iv}_{tu}\rho_{utwv}\left(S_1\right)\right] \end{aligned} \tag{4.92}$$

$$\begin{aligned} K^{iS_1}_{\bar{r}} = \sum_{tu} T_{tu,S_1}\sum_{vw}\left(S^{S_1}_{A}\right)_{tu,vw}\left(2K^{iv}_{aw} - K^{vi}_{aw}\right) \\ + \sum_{tu} T^{'}_{tu,S_1}\sum_{vw}\left[\left(S^{S_1}_{B}\right)_{tu,vw}K^{vi}_{aw} - \left(S^{S_1}_{A}\right)_{tu,vw}K^{iv}_{aw}\right] \end{aligned} \tag{4.93}$$

$$\begin{aligned} (\mathbf{U}_{S_1})_{tu,S_1} =& 2T_{S_1}D^{(1)}_{tu} + \sum_v D^{(1)}_{tv}\left(2T_{vu,S_1} - T^{'}_{vu,S_1}\right) \\ &+ \sum_{vw} D^{(2)}_{tu,wv}\left(2T_{vw,S_1} - T^{'}_{vw,S_1}\right) \end{aligned} \tag{4.94}$$

$$\begin{aligned} (\mathbf{V}_{S_1})_{tu,S_1} = T_{S_1}D^{(1)}_{tu} - \sum_v D^{(1)}_{tv}\left(2T^{'}_{vu,S_1} - T_{vu,S_1}\right) \\ + \sum_{vw} D^{(2)}_{tu,wv}T_{vw,S_1} + \sum_{vw} D^{(2)}_{tv,wu}T^{'}_{vw,S_1} \end{aligned} \tag{4.95}$$

$$f^{C}_{j,S_2,S_1} = \sum_t f_{jt}\alpha^{C}_{t}\left(S_1,S_2\right) \tag{4.96}$$

$$f^{D}_{S_1,S_2,j} = \sum_t f_{jt}\alpha^{D}_{t}\left(S_1,S_2\right) \tag{4.97}$$

$$f^{C}_{a,D_1,S_1} = \sum_t f_{at}\beta^{C}_{t}\left(S_1,D_1\right) \tag{4.98}$$

$$f^{D}_{S_1,D_1,a} = \sum_t f_{at}\beta^{D}_{t}\left(S_1,D_1\right) \tag{4.99}$$

$$R^{tu}_{\bar{r}v} = \left(\mathbf{K}^{tu}_{S_0}\right)_{\bar{r}v} + \sum_w D^{(2)}_{uv,tw} f^{clos}_{w\bar{r}} + \sum_{wxz} \left(\gamma^{S_0}\right)_{tuv,wxz} \left(\mathbf{S}^{\mathrm{PAO}}_{[\mathbf{t},\mathbf{t}]} \mathbf{c}^{wx}\right)_{\bar{r}z} + G^{tu}_{\bar{r}v} + \sum_{wxz} \left(\mathbf{F}^{v} \mathbf{c}^{wx}\right)_{\bar{r}z} \left(\mathbf{S}^{S_0}\right)_{tuv,wxz} - E^{(0)}_{act} \sum_{wxz} \left(\mathbf{S}^{S_0}\right)_{tuv,wxz} \left(\mathbf{S}^{\mathrm{PAO}}_{[\mathbf{t},\mathbf{t}]} \mathbf{c}^{wx}\right)_{\bar{r}z} \tag{4.100}$$

$$\left(\mathbf{K}^{tu}_{S_0}\right)_{\bar{r}v} = \sum_{wxz} K^{wz}_{\bar{r}x} \left(\mathbf{S}^{S_0}\right)_{tuv,wzx} \tag{4.101}$$

$$\begin{aligned} G^{tu}_{\bar{r}v} = & \sum_{D_1} \sum_i \left(\mathbf{F}^{cv}_{[iD_1]} \left[2\mathbf{c}^{iD_1} - \mathbf{c}^{iD_1 \dagger} \right] \mathbf{S}^{\mathrm{PNO-PAO}}_{[iD_1,\mathbf{t}]} \right)_{i\bar{r}} \rho_{uvt}\left(D_1\right) \\ & - \sum_{S_1} \sum_i \left(\mathbf{S}^{\mathrm{PAO}}_{[\mathbf{t},i\mathbf{t}]} \mathbf{c}^{iS_1} \right)_{\bar{r}} \sum_w f_{iw} \rho_{tuwv}\left(S_1\right) \\ & + \sum_p \sum_{D_0} \sum_w \left(\mathbf{F}^{av}_{[D_0 p]} \mathbf{c}^{D_0 p} \mathbf{S}^{\mathrm{PNO-PAO}}_{[D_0 p,\mathbf{t}]} \right)_{w\bar{r}} \rho^{(p)}_{wutv}\left(D_0\right) \end{aligned} \tag{4.102}$$

$$\begin{aligned} R^{ijp}_{I_2} = & K^{ij(p)}_{I_2} - \sum_k f_{ik} c^{kjp}_{I_2} - \sum_k c^{ikp}_{I_2} f_{kj} \\ & + \frac{1}{2} G^{ij(p)}_{I_2} + \frac{1}{2} p G^{ji(p)}_{I_2} + \left[2\gamma^{(p)}\left(I_2, I_2\right) - E^{(0)}_{act} \right] c^{ijp}_{I_2} \end{aligned} \tag{4.103}$$

$$K^{ij(p)}_{I_2} = \frac{1}{4} \sum_{tu} \sum_{vw} K^{ij}_{vw} \left(\mathbf{S}^{I_2(p)}\right)_{tu,vw} T^{(p)}_{tu,I_2} \tag{4.104}$$

$$G^{ij(p)}_{I_2} = \sum_{S_2} \sum_a c^{ij}_{aS_2} f^{(p)}_{a,S_2,I_2} + \sum_w f_{jw} \sum_{tuv} c^{iv}_{tu} \rho^{(p)}_{tuvw}\left(I_2\right) \tag{4.105}$$

$$\begin{aligned} R^{iv}_{tu} = & 2 f^{clos}_{it} D^{(1)}_{uv} - f^{clos}_{iu} D^{(1)}_{tv} - \sum_w f^{clos}_{iw} D^{(2)}_{uv,tw} + \left(\mathbf{K}^{iv}_{I_1}\right)_{tu} + \sum_{wxz} \left(\gamma^{I_1}\right)_{tuv,wxz} c^{iz}_{wx} \\ & - \sum_j f_{ij} \sum_{wxz} \left(\mathbf{S}^{I_1}\right)_{tuv,wxz} c^{jz}_{wx} - E^{(0)}_{act} \sum_{wxz} \left(\mathbf{S}^{I_1}\right)_{tuv,wxz} c^{iz}_{wx} + G^{iv}_{tu} \end{aligned} \tag{4.106}$$

$$\left(\mathbf{K}^{iv}_{I_1}\right)_{tu} = \sum_{wxz} K^{iz}_{wx} \left(\mathbf{S}^{I_1}\right)_{tuv,wxz} \tag{4.107}$$

$$\begin{aligned} G^{iv}_{tu} = & \sum_{S_2} \sum_j \left(\mathbf{F}^{cv}_{[ij]} \left[2\mathbf{c}^{ji} - \mathbf{c}^{ij} \right] \right)_{jS_2} \rho_{tuv}\left(S_2\right) + \sum_{S_1} \left(\mathbf{c}^{iS_1} \mathbf{F}^{va}_{[i,\mathbf{t}]} \right)_t \left(\mathbf{U}_{S_1}\right)_{vu,S_1} \\ & + \sum_p \sum_{I_2} \sum_j c^{ijp}_{I_2} \sum_w f_{jw} \rho^{(p)}_{tuvw}\left(I_2\right) - \sum_{S_1} \left(\mathbf{c}^{iS_1} \mathbf{F}^{va}_{[i,\mathbf{t}]} \right)_u \left(\mathbf{V}_{S_1}\right)_{vt,S_1} \\ & - \sum_{S_1} \sum_w \left(\mathbf{c}^{iS_1 va}_{[i,\mathbf{t}]} \right)_w \rho_{vwtu}\left(S_1\right) \end{aligned} \tag{4.108}$$

4.11 Energy and the Hylleraas Functional

The Hylleraas functional (*360*) offers a functional construction of the second-order energy, which allows the variational optimization of the first-order wavefunction. With the Hylleraas functional one gets thus an upper-bound of the energy for second-order

perturbation theory (and not of the exact energy). The objective is to minimize the energy expression

$$E^{(2)} = 2\left\langle \Psi^{(1)} \right| \hat{H} \left| 0 \right\rangle + \left\langle \Psi^{(1)} \right| \left(\hat{H}^{(0)} - E^{(0)} \right) \left| \Psi^{(1)} \right\rangle \tag{4.109}$$

with respect to the amplitudes (*93*). The expression 4.109 for the energy $E^{(2)}$ is rather general. Due to the additivity of the energy, $E^{(2)}$ can be further partitioned in the Hylleraas energy for each configuration subspace by partitioning the wavefunction in the contribution of each configuration subspace. This yields

$$E^{(2)} = E^{(2)}_{P_2} + E^{(2)}_{P_1} + E^{(2)}_{P_0} + E^{(2)}_{S_2} + E^{(2)}_{S_1} + E^{(2)}_{S_0} + E^{(2)}_{I_2} + E^{(2)}_{I_1} \tag{4.110}$$

Note that the minimization takes place for the total energy and not for individual energies. This means that any properties herein derived apply only to the sum of energies. We can thus define the Hylleraas energy for each configuration subspace as

$$\begin{aligned} E^{(2)}_X &= 2\sum_{x\in X} c^x \langle \Phi_x | \hat{H} | 0 \rangle + \sum_{x\in X} c^x \langle \Phi_x | \left(\hat{H}^{(0)} - E^{(0)} \right) \left| \Psi^{(1)} \right\rangle \\ &= \sum_{x\in X} c^x \langle \Phi_x | \hat{H} | 0 \rangle + \sum_{x\in X} c^x R^x \end{aligned} \tag{4.111}$$

Since there is a formal dependence on the residuals, which at convergence are zero, the Hylleraas energy functional converges to second-order PT's energy (*8*). Because the procedure is variational, convergence takes place from above (ceiling). But only at convergence is the correct correlation energy reached.

For the calculation of the energy for each configuration subspace using Hylleraas' functional one only requires the evaluation of the terms $\langle \Phi_x | \hat{H} | 0 \rangle$. From the evaluation of all terms in the residual equations we know that these correspond to the exchange integral and Fock matrix terms. The Hylleraas energies for each configuration subspace are thus given by

$$E^{(2)}_{P_2} = \sum_{ij}\sum_{ab} \tilde{c}^{ij}_{ab}\left(K^{ij}_{ab} + \tilde{R}^{ij}_{ab} \right) \tag{4.112}$$

$$E^{(2)}_{P_1} = \sum_{iD_1}\sum_{ab} \tilde{c}^{iD_1}_{ab}\left(K^{iD_1}_{ab} + \tilde{R}^{iD_1}_{ab} \right) \tag{4.113}$$

$$E^{(2)}_{P_0 p} = \sum_{D_0 p}\sum_{ab} c^{D_0 p}_{ab}\left(K^{D_0 p}_{ab} + R^{D_0 p}_{ab} \right) \tag{4.114}$$

$$E^{(2)}_{S_2} = \sum_{ij}\sum_{aS_2} \tilde{c}^{ij}_{aS_2}\left(K^{ij}_{aS_2} + \tilde{R}^{ij}_{aS_2} \right) \tag{4.115}$$

$$E^{(2)}_{S_1} = \sum_{iS_1}\sum_{\bar{r}} c^{iS_1}_{\bar{r}}\left[K^{iS_1}_{\bar{r}} + 2f^{clos}_{\bar{r}i}(X_{S_1} + T_{S_1}) + R^{iS_1}_{\bar{r}}\right] \tag{4.116}$$

$$E^{(2)}_{S_0} = \sum_{S_0}\sum_{\bar{r}} c^{S_0}_{\bar{r}} \sum_{tuv}\left[\left(\mathbf{K}^{tu}_{S_0}\right)_{\bar{r}v} + \sum_{w} D^{(2)}_{tw,uv} f^{clos}_{w\bar{r}} + R^{tu}_{\bar{r}v}\right] T_{tuv,S_0} \tag{4.117}$$

$$E^{(2)}_{I_2p} = \sum_{ij}\sum_{I_2p} c^{ijp}_{I_2}\left(\frac{1}{2}K^{ij(p)}_{I_2} + R^{ijp}_{I_2}\right) \tag{4.118}$$

$$E^{(2)}_{I_1} = \sum_{iI_1} c^{iI_1} \sum_{tuv}\left[2f^{clos}_{it}D^{(1)}_{uv} - f^{clos}_{iu}D^{(1)}_{tv} - \sum_{w} f^{clos}_{iw}D^{(2)}_{uv,tw} + \left(\mathbf{K}^{iv}_{I_1}\right)_{tu} + R^{iv}_{tu}\right] T_{tuv,I_1} \tag{4.119}$$

The amplitudes used in these expressions must correspond to the amplitudes used in the residual calculation. Although the Hylleraas energy is only equal to the actual energy upon convergence, this functional offers two significant advantages: the errors are quadratic with respect to the errors in the amplitudes; variational optimization of the wavefunction with respect to the amplitudes.

4.11.1 Level-Shifts

Intruder states can cause serious convergence problems in CASPT2 calculations (*62*). Although more often when involving excited states, this problem can also occur for calculations involving GSs (*83, 86, 91, 361*).

To remove the divergence caused by intruder states from LCASPT2 calculations a level-shift ϵ is added to $\hat{H}^{(0)}$ as described by Roos and coworkers (*91*). With this change, an equivalent set of level-shifted residuals is built, this affecting also the first-order wavefunction ($\tilde{\Psi}^{(1)}$) and the 2$^{\text{nd}}$-order energy ($\tilde{E}^{(2)}$). The energy functional to minimize is then given in eq. 4.120 instead of eq. 4.109.

$$\tilde{E}^{(2)} = 2\left\langle\Psi^{(1)}\right|\hat{H}\left|0\right\rangle + \left\langle\Psi^{(1)}\right|\left(\hat{H}^{(0)} - E^{(0)} + \epsilon\right)\left|\Psi^{(1)}\right\rangle \tag{4.120}$$

Because the level-shift is added to $\hat{H}^{(0)}$, the difference between $\tilde{\Psi}^{(1)}$ and $\Psi^{(1)}$ is just in the amplitudes, which are different with and without the level-shift.

To remove the level-shift effect from the energy a correction term is used, the latter depending on ϵ affected by the weight of $\tilde{\Psi}^{(1)}$ to $\tilde{E}^{(2)}$:

$$E^{(2)} = \tilde{E}^{(2)} - \epsilon\left\langle\Psi^{(1)}|\Psi^{(1)}\right\rangle \tag{4.121}$$

This back transformation is not exact though. Even though the effects of level-shifts are negligible (*91*), these are not zero. Level-shifts should thus only be used if there is an eminent problem with intruder states.

5. Implementation

The LCASPT2 method described above was implemented in MOLPRO 's development version (*284, 362*). To test the accuracy of LCASPT2 we have also implemented the respective canonical Fully Internally-Contracted CASPT2 (ic-CASPT2) method. This code was written by adapting the local code to the canonical case. The ic-CASPT2 method required simplified drivers, simplified routines and different algorithm files. In all the cases, changes amount to differences in the orbital spaces, overlap matrices for local virtuals are no longer required and the fact that integrals are no longer transformed to the local virtual bases. Therefore, the structure of the ic-CASPT2 program resembles in everything the structure of the LCASPT2 program. The ic-CASPT2 code was not optimized in itself. Any improvements from a first implementation came from the parent local implementation. The discussion on the implementation focus thus only on LCASPT2.

The LCASPT2 program was implemented at two levels: i) a FORTRAN part to initialize the program and prepare all the quantities required; ii) an ITF part (*111, 284–286*), where the actual LCASPT2 calculation takes place. The ITF part of our code uses the ITF extension to treat local approximations, LITF (*286, 287*), extended during the course of this work by Dr. D. Kats. ITF provides a very efficient machinery to solve residual equations, and this determined our choice. Because of its resemblance with actual mathematical formulas, ITF's algorithms simplified the implementation and debugging of the code. However, ITF is less effective in calculating quantities like integrals. On the other hand, MOLPRO contains efficient FORTRAN subroutines for the calculation of integrals and other quantities, like PAOs or PNOs. Apart from reusing these routines, new code was written to build the densities, contractions of densities with the Fock matrix and to orthogonalize configuration subspaces. Prof. Dr. H.-J. Werner adapted the code to calculate density matrices and wrote the latest version of the code to calculate the contractions of the Fock matrix with the reduced density matrices. Prof. Dr. H.-J. Werner also adapted to the case of LCASPT2 the code to calculate integrals and the codes to build PAOs, PAO(SC)s and PNO(SC)s; he wrote the latest versions of the code for the symmetric orthogonalization and orthogonalization of pairs; he wrote the code to calculate the integrals associated to pairs expressed in terms of orthogonal configuration indices. Besides the LITF extension, Dr. D. Kats wrote most of the interface between FORTRAN and ITF and the calling of LCASPT2 within ITF. Dr. D. Kats also wrote and developed Quantwo, a program that took a significant part in deriving the equations.

The following chapter is divided in four sections. First the simulation of the LCASPT2 program is discussed. This simulation allowed us to understand how to implement the final method, providing information on accuracy, potential efficiency and in showing eventual faults and strengths. The next two sections deal solely with the implementation at FORTRAN and ITF levels. In both sections the written code is described and in the end a sketch of the algorithm is presented. The algorithms are divided into the many tasks the program undertakes, and all these tasks are numbered. The numbers on tasks have a correspondence with the numbers placed in the text describing the program. The last section explains how to call and use the LCASPT2 program in `MOLPRO` .

5.1 Simulation of PNO-CASPT2

The full implementation of a quantum chemistry method is a cumbersome and lengthy task, which is prone to errors. Therefore, the first stage of this work consisted in simulating a PNO-LCASPT2 method using an already implemented CASPT2 program in `MOLPRO` (*284, 362*). Our objectives were: i) to understand how to build PNOs so that accuracy is maximized; ii) to test how well PNOs work for the CASPT2 method. At this stage no tests on PAOs were performed. Our simulation was based on the CASPT2 method implemented by Celani and Werner, CW-CASPT2 (RS2C) (*15, 62*). Differences between the CW ansatz for the wavefunction and our full ICC implementations are: S_0 and I_1 are spanned by CSFs; P_2, P_1 and S_2 configurations are spanned using singlet-triplet ICCs.

This simulation consisted in projecting both the CASPT2 residual equations and the wavefunction's amplitudes into the PNO space. The program started by building in the first iteration pair densities from pair amplitudes in the orthogonal configuration basis (eq. 3.92). After diagonalizing the pair densities, PNO transformation matrices were retrieved from the eigenvector matrices. These were subject to cuts on the number of columns according to the magnitude of the respective eigenvalues. Such cuts were determined by the threshold *thrpno_occ* and allowed us to test the accuracy as a variable of Average PNO Domain Size (avg(PNO)). At this stage the direct study of how *thrpno_occ* influenced timings of calculations was not possible. *thrpno_occ* influences domain sizes, and the larger the domain, the longer a calculation takes. Convergence is also affected, providing insight on the efficiency.

Because RS2C does not handle pairs with variable dimensions for the substitution spaces, projection matrices were used to simulate the PNO-LCASPT2 method. These matrices were built by multiplying PNO transformation matrices by their transposes, eq.

5.1, and these used to project both amplitudes and residuals onto the PNO basis.

$$\mathbf{P}^{mn} = \bar{\mathbf{W}}^{mn}\bar{\mathbf{W}}^{mn\dagger} \tag{5.1}$$

This projection was tested for many possible combinations of configuration subspaces. Because RS2C uses singlet-triplet pairs, PNOs were built for all singlet and triplet pairs separately (S,T). PNOs for singlet-triplet pairs together (ST) were also built by adding the respective pair densities before diagonalizing them. Although not relevant for the final implementation, this played an important role in the simulation, since the method's accuracy can be affected. Because singlet and triplet pairs have different normalization factors, to make the results comparable for ST and S,T PNOs, we switched off the normalization step. PNOs built from zero-iteration amplitudes (IniPNOs) and PNOs built from converged amplitudes (EndPNOs) were also tested. Finally, although the PNO-LCASPT2 simulation was tried on a significantly wider variety of examples, only two representative cases are presented here. This data is summarized in Figs. 5.1 and 5.2. Tables 8.1 and 8.2 (in Appendix 8.3) complement these results.

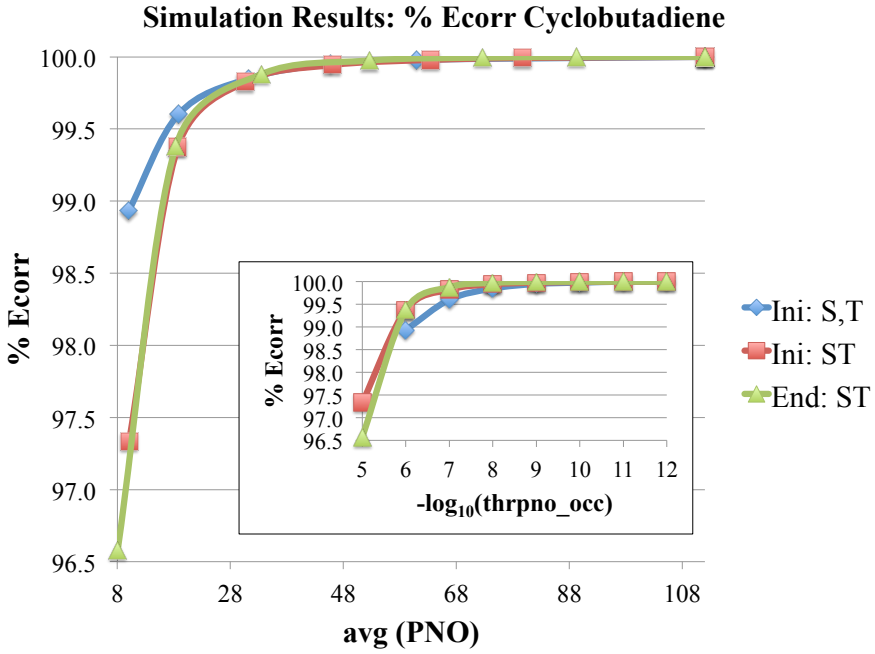

Figure 5.1: %Ecorr against avg(PNO) for the cases of zeroth-iteration S,T PNOs, Ini: S,T, zeroth-iteration ST PNOs, Ini: ST and converged ST PNOs, End: ST. The interior plot represents the exact same data but against $-log_{10}(thrpno\_occ)$. Representative example of cyclobutadiene.

In order to maximize efficiency and accuracy, our goal with the simulation was to

maximize the percentage of correlation energy being recovered, %Ecorr, while minimizing avg(PNO). Using ST IniPNO and $thrpno\_occ = 10^{-8}$ (about 50-60 PNOs) the simulated PNO-LCASPT2 recovered in average 99.95% of Ecorr. As Fig. 5.1 shows, using $thrpno\_occ < 10^{-8}$ S,T PNOs yield higher accuracy. However, for those cases, S,T PNOs require $thrpno\_occ$ to be 10 times smaller than the respective $thrpno\_occ$ for ST PNOs. For $thrpno\_occ > 10^{-8}$ both types of PNOs are equivalent. Therefore, for the same value of $thrpno\_occ$, ST PNOs yielded better results than using S,T PNOs. The results for excitation energies (ΔE, Fig. 5.2) showed that using $thrpno\_occ = 10^{-7}$ or about 40-50 PNOs is enough for accuracies within the meV with respect to the canonical RS2C results. Absolute values for the errors in excitation energies are actually smaller for $thrpno\_occ = 10^{-7}$ than they are for $thrpno\_occ = 10^{-8}$ because of differences in the curves %Ecorr Vs. avg(PNO) for the GS and the ES. Globally speaking, an average reduction of substitution spaces to 20-30% of the canonical values for these small molecules is observed.

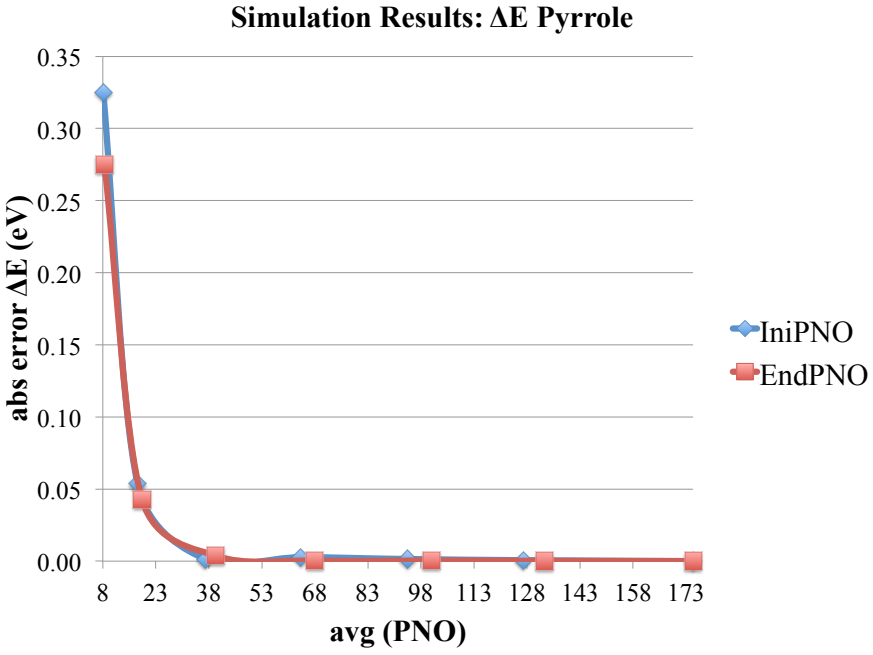

Figure 5.2: Absolute error in eV for the excitation energy of Pyrrole, ΔE, against avg(PNO). Comparison between converged EndPNO and zeroth-iteration (IniPNO) using ST PNOs.

The simulation results demonstrate that zero-iteration PNOs can be used without much loss in accuracy. We also verified that whenever using PNOs to describe substitution

spaces for S_1 configurations, not only there was a more pronounced loss in accuracy, but also a deterioration of convergence. This drove us to use PAOs to express the substitution spaces of S_1 configurations.

5.2 FORTRAN

The FORTRAN part of LCASPT2 is divided in many modules. The person responsible for the latest version of each module is indicated in the end of each bullet: W - Prof. Dr. H.-J. Werner; K - Dr. D. Kats; M - the author of this Thesis. The main LCASPT2 module (driver) controls the calculation by using the modules:

➢ Density module - set of subroutines to build the first three orders of the density matrix and to calculate contractions of the density matrix with the active block of the Fock matrix (W).

➢ ITF interface module - set of subroutines that organize and write tensors and their dimensions to a file to be later read by ITF (K).

➢ PAO domain module - contains subroutines to build the PAO domains (W).

➢ PNO generation module - contains subroutines to build transformation matrices to the PNO basis from zeroth-iteration PAO amplitudes (and to respectively transform incoming amplitudes and integrals); to solve the CASPT2 equations just for pairs, in the PNO basis (W).

➢ Integral module - set of subroutines to build two-electron integrals or to read these from a file; to get the Fock matrix (in PAO basis); to build PAOs (*get_paos*); to extract non-orthogonal PAO domains from the full transformation matrix from canonical to non-orthogonal PAO basis (W).

➢ Pair module - contains subroutines to build the pair list; to apply pair approximations; to orthogonalize pairs; to diagonalize the γ's for pairs in the orthogonal configuration basis; to calculate energy denominators for pairs (W).

➢ Singles module - subroutines to build lists for singles from the pair list; to orthogonalize singles; to diagonalize the γ's for singles in the orthogonal configuration basis; to transform one-external two-electron integrals into the orthogonal configuration basis of singles; to read, sort and put in the PAO basis one-external two-electron integrals (M).

➢ Internals module - contains subroutines to orthogonalize the internals; to diagonalize the γ's for internals in the orthogonal configuration basis; to transform zero-external two-electron integrals to the orthogonal configuration basis of internals; to read and sort zero-external two-electron integrals (M).

➢ Utils module - contains subroutines to apply symmetric orthogonalization to a given (symmetric) matrix (W).

➢ Variables module - contains the declaration of all global variables.

The LCASPT2 driver starts by (1:) setting the environment for the quantum chemical calculation. This includes reading from the input file relevant options and defining some system variables. Parameters set from the input file specify the ITF code later to be used, whether to diagonalize the γ matrices in the orthogonal configuration basis (on/off), whether PAOs and/or PNOs are used (on/off), whether integrals are read from a file or calculated, and thresholds. The latter define both the domains of local orbitals and the orthogonalization of configuration subspaces. All the on/off options above mentioned are by default on. Integrals are by default calculated and domain thresholds for local orbitals are going to be the subject of discussion in the chapter of results. The threshold to neglect small eigenvalues in the orthogonalization of configuration subspaces is by default 10^{-7}. The system variables set in the beginning of the calculation are the dimensions of each orbital space (which are only dependent on each system) and the total number of PAOs.

The first computation task performed by the LCASPT2 driver is (2:) building PAOs. The routine *get_paos* starts by reading in the AO overlap matrix and the MO coefficient matrix. These matrices are used to build the transformation to the PAO basis $\tilde{\mathbf{Q}}$ (eq. 3.83 in section 3.6.4) and the PAO coefficient matrix $\mathbf{P}$ (eq. 3.84). The overlap matrix for PAOs (eq. 3.85) is also computed, although all PAOs with norm below a given threshold (default 10^{-7}) are removed.

After getting the PAOs the next step is (3:) getting the Fock matrix, which is read from a file. This is either from the reference CI calculation or from a previous MCSCF calculation. Then (4:) density matrices are calculated up to the third order ($D^{(1)}$, $D^{(2)}$ and $D^{(3)}$), together with the double contractions of the active block of the Fock matrix with the many orders of the density matrix ($E^{(0)}_{act}$ and D^f_*, where the $*$ as subscript indicates that these tensors may arise from $D^{(2)}$, $D^{(3)}$ or $D^{(4)}$). The program starts by building the transition densities $A_{R,tu} = \langle R|\, \hat{E}_{tu}\, |0\rangle$, which are kept in memory. These are going to be used in the calculation of all quantities. Getting $D^{(1)}$ is immediate and requires only a matrix-vector inner product, $D^{(1)}_{tu} = \left(\mathbf{A}^\dagger \mathbf{c}\right)_{tu}$, where $\mathbf{c}$ is the MCSCF amplitude vector. Looping over t and v, for a fixed tv pair, transition densities $B^{(tv)}_{uw,R} = \langle 0|\, \hat{E}_{tu,vw}\, |R\rangle$ are calculated on the fly for each u and w. Direct contraction of $B^{(tv)}_{uw,R}$ with $\mathbf{c}$ yields the elements $D^{(2)}_{tu,vw} = \left(\mathbf{B}^{(tv)}\mathbf{c}\right)_{uw}$, which are positioned in the tensor $D^{(2)}$. The leading term in the third-order density is obtained from the matrix-matrix product of $B^{(tv)}_{uw,R}$ with $A_{R,xz}$. The other terms, products of $D^{(2)}$ with the respective delta Kronecker terms, are then

subtracted.

$$D^{(3)}_{tu,vw,xz} = \sum_R B^{(tv)}_{uw,R} A_{R,xz} - \delta_{ux} D^{(2)}_{tz,vw} - \delta_{wx} D^{(2)}_{tu,vz} \tag{5.2}$$

The calculation of the transition densities $A_{R,tu}$ and $B^{(tv)}_{uw,R}$ uses a simplification of the symmetric group technique described in (*108*) and the code is parallelized over the indices tu. In a similar fashion the double contraction of the Fock matrix with the fourth-order density is calculated, using eq. 4.15. The first step is the contraction of $A_{R,tu}$ with the active block of the Fock matrix. The result is used as modified reference coefficients, which are contracted with the respective transition densities to get the two index contractions of the Fock matrix with all densities. The calculation of all the quantities is immediate, except for the contraction with the 4^{th}-order density matrix. This requires the calculation of the transition density $\langle 0| \hat{E}_{tu,vw,xz} |R\rangle$, which is obtained similarly to how the 3^{rd}-order density is calculated. As for efficiency, using a CAS[10, 10] (more than 19000 CSFs) or a CAS[12, 12] (more than 250000 CSFs) and using 4 computing nodes, all these quantities were obtained within 1 and 40 seconds, respectively. Even though the scaling is factorial, the calculation of all these densities and intermediates poses no bottleneck in any calculation, at least for the cases for which the MCSCF is also possible.

Subsequently (5: a)) comes the determination of the basis functions associated to each atom (subroutine *basis_centers*) and (5: b)) obtaining the PAO and PAO(SC) domains for the closed-shell orbitals (subroutine *pao_domains_drv*). These steps are important to apply before building the pair list so that pair approximations can be explored. The subroutine *pao_domains_drv* starts by reading the IBO charges (note that IBOs are built prior to the call to the LCASPT2 driver). The PAO domains built are center and charge based. Thus, with the IBOs, the centers contributing most to rebuild the charge of each IBO are determined. This allows us to associate to each IBO a certain number of atomic centers (a set $\{A\}_i$ for each IBO i), which have a charge larger than a given threshold (0.2 e, atomic units of electronic charge). The primary PAO domain for each IBO is given by the union of all PAOs belonging to the centers in $\{A\}_i$. The secondary domains are built by adding atoms in the vicinity of the primary domains. These are either the *iext* neighboring shells or the atoms within the *rext* radius of the primary domains. The driver for orbital domains determines both which PAOs and which DF basis functions belong to the orbital domain of a given closed-shell orbital. If no PAOs are used, the orbital domains are full of canonical virtuals instead. In a previous step a full transformation matrix to the PAO basis is calculated. When orbital domains are built, a list containing the columns from the full transformation matrix associated to each closed-shell i is also

constructed. This allows to specifically transform from canonical virtuals into the PAOs in the domain of i. Calculation of domains for pairs ij consist in the merging of those lists for orbitals i and j. As previously mentioned, pair domains are generated for both P_2 and P_1 pairs. For P_0 pairs, the single orbital domain for active orbitals is used. Finally, in *pao_pairdom* all PAOs within a pair domain are orthogonalized and semicanonicalized.

(6:) Afterwards the pair list is created. The subroutine *make_pairlist* starts by building a list of very distant pairs for the case distance criteria to neglect pairs is on. This list is a matrix with rows and columns representing orbitals. For pairs considered to be very distant, the respective matrix element is non-zero. The routine *make_pairlist* loops then over the possible orbital pairs (individually) skipping orbital pairs in the very distant pair matrix. With the pair list available, (7:) the program checks whether to apply the MPA to distant pairs. It is possible to go to orders higher than the dipole-dipole term in the multipole expansion. This brings more accuracy and was indeed used in the past (*214, 325*). In this work however, only the dipole-dipole approximation of the multipole expansion of exchange integrals is actually used. The program reads in *thrdist*, which by default is 10^{-6}. If the MPA is on ($thrdist > 0$), the subroutine *pao_dip* is called, acting like a driver for the MPA. Internally this routine calls *pao_pairen_dip*. The latter reads in dipole moment vectors, calculates pair energies using the dipole approximation and determines the number of distant pairs (n_{dist}), to which the MPA is applied. In the end, *pao_dip* removes distant pairs from the pair list. Note that alike very distant pairs, the MPA is only applied to P_2 pairs. Distance criteria to neglect exchange integrals related to P_1, S_2, S_1, I_2 and I_1 was implemented, thus reducing the respective lists. This was previously discussed in section 4.6, for which we refer the reader to. In this case, all integrals related to any of the above mentioned configurations can be neglected, whenever the respective R_{it} is larger than a predefined threshold R_{dist}, $R_{it} > R_{dist}$. By default $R_{dist} = 15\ bohr$. Besides this restriction, the lists for S_2 and I_2 are furthermore restricted to P_2's list. These are the last steps before distributing pairs over processors.

The first step executed parallel is (8:) the orthogonalization of all configuration subspaces. This is performed by a set of configuration subspace specific subroutines named *ovl_X*, where X represents a specific configuration subspace. All these routines share a common structure, in which the overlap function for the configuration subspace X is built and immediately diagonalized. The out-coming eigenvector matrices are then used to build the orthogonalization matrices. Even though the overlap functions are always built inside the subroutines *ovl_X*, the diagonalization of overlaps and the building of the orthogonalization matrices are performed by the subroutine *sym_orthog* in *pno_cas_utils*.

Then (9:) PAO and PAO(SC)s domains are built using once again *pao_domains_drv*. At this stage the domains for the active space are obtained and (10:) the two-electron exchange integrals (**K**) are calculated/read. The subroutine calculating the integrals is *pao_integrals_drv* and is based on what was previously described for PNO-LMP2 (*148, 235*). Here, two main subroutine calls are performed: $define\_block\_basis$; *block_trans_drv*. In the first subroutine the DF basis, $(B|\mu\nu)$, is read and transformed to the LMO and PAO bases. Prior to the projection, the DF basis is blocked according to atomic centers. The subroutine *block_trans_drv* calculates then the **K** integrals, which are afterwards sorted once they return to *pao_integrals_drv*. In CASPT2 three types of integrals are required: two-external integrals, K_{ab}^{mn}; one-external (or one-active), K_{at}^{mn} and K_{at}^{nm}; the zero-external (or two active) integrals, K_{tu}^{mn}. Instead of having a subroutine for each type of integral required to calculate, all integrals are calculated in the same routine. For each pair mn the program writes the integrals in an array with dimensions $(n_{pao} + n_{active})^2$. The full matrix $\mathbf{K}^{mn}$ is obtained as

$$\mathbf{K}^{mn} = \begin{bmatrix} K_{\tilde{r}\tilde{s}}^{mn} & K_{\tilde{r}u}^{mn} \\ K_{t\tilde{s}}^{mn} & K_{tu}^{mn} \end{bmatrix} \tag{5.3}$$

If the integrals are read, they only require the transformation to the PAO or PAO(SC) basis, if that case applies.

After obtaining the rest of all the required integrals (11: a)) the γ matrices are diagonalized and (11: b)) the **K**'s are transformed to the orthogonal configuration basis using eqs. 4.76, 4.82, 4.85, 4.93, 4.101, 4.104 and 4.107. The transformation of integrals is done blockwise. The two-external integrals are stored as matrices for each pair, the one-external stored as vectors with virtual indices and the zero-external stored either as matrices (K_{tu}^{ij}) or vectors ($K_{tuv}^{i} = K_{tu}^{iv}$). Because a CAS reference is used, the all active integrals are only needed for the calculation of the reference energy. This is by default taken from a previous CASSCF calculation. At this point in the calculation, both PAO and PAO(SC) are accessible. Integrals which are later transformed to the PNO basis are previously transformed to the PAO(SC) basis. However, the one-external integrals for S_1 and S_0 are left in the non-orthogonal PAO basis to avoid overloading the memory. The last quantities required are PNOs and the respective transformation matrices. The first step towards building PNOs is (12:) the calculation of energy denominators so that zeroth-iteration amplitudes can be estimated. Energy denominators are calculated in the orthogonal configuration basis for each pair.

The last three steps before termination of the FORTRAN code are (13:) building the

coupling coefficients for the interactions between pairs (not needed in ITF though), (14:) building PNOs and (15:) transforming the integrals associated to S_2 to the PNO(SC) basis. PNOs are built in *pno_cas_generate*, which starts by getting from the input file the PNO related thresholds (*thrpno* and *thrpno_occ*). PAO amplitudes are built (eqs. 4.51, 4.52, 4.53), which are used to build the respective pair densities. We note that if level-shifts are given in the input file the PAO amplitudes are affected by these, thus also the PNOs. After diagonalization of pair densities to get PNOs, the respective domains are selected using the subroutine *pno_cas_select*. In *pno_cas_select* the program starts by transforming both the **K** integrals and PAO amplitudes to the full PNO basis, making pair energies available in the PNO basis. PNOs are then added to each pair domain until the occupation number is below *thrpno_occ* and the pair energy is consistent with *thrpno*.

Algorithm 1 pno-caspt2 (FORTRAN)

1: set environment (parameters and variables);
2: make PAOs;
3: get all blocks Fock matrix;
4: get densities ($D^{(1)}$, $D^{(2)}$, $D^{(3)}$), and double contractions Fock-densities ($E^{(0)}_{act}$, D^{f}_{*});
5: a) determine basis functions for atomic centers; b) build PAO and PAO(SC)s domains for closed-shell orbitals;
6: make pair list;
7: pair approximations;
8: build orthogonalization matrices: pairs; singles; internals;
9: build full PAO domains and PAO(SC)s;
10: get **K** matrices in PAO or PAO(SC) basis;
11: a) orthogonalize γ's; b) build orthogonal **K** matrices: pairs; singles; internals;
12: calculate energy denominators: pairs;
13: calculate coupling coefficients for pairs;
14: make PNO(SC)s;
15: transform $\mathbf{K}S_2$ to PNO(SC) basis;
16: termination:
    a) send data to ITF and go to ITF;
    b) solve LCASPT2 just for pairs (in FORTRAN);

Both the integral transformation and the generation of the PNOs were implemented parallel using the Global Array Software (*363*). Dynamic parallelization is used as de-

scribed in (*148, 235*). All pairs are distributed over processors to keep an arrangement as balanced and even as possible. To avoid any sort of communication between processors in tasks like the orthogonalization of configuration subspaces, pairs are distributed over closed-shell indices. This means that different pairs ij might be in different processors. However, all pairs it with the same i are in the same processor, the same with all pairs tu. Each processor performs its own tasks independently of any other processor so that the scaling is well behaved even for more than one node.

Finally, if an ITF method is used, all data is sent to ITF. This step is controlled by the subroutine $itf\_interface$, which writes arrays and their dimensions to specific records.

5.3 Integrated Tensor Framework

As its name implies, the Integrated Tensor Framework (ITF) (*284, 285*) is a tensor framework integrated in the `MOLPRO` quantum chemical's program package. This is a C++ program able to read and execute algorithm files. The latter are human-readable formula files containing sequences of binary tensor contractions written in an equation-like format. A quantum chemical's full set of equations can thus be written as a set of inter-dependent binary contractions of n-dimensional tensors (*285*), which is not only significantly easier to implement but also to read (by the programmer).

For an efficient implementation of LCASPT2 we have used the Local ITF (LITF). As previously mentioned, this is an extension of ITF for the treatment of local approximations. Up to now, LITF was able to handle SR cases. Extending LITF to MR systems was performed by Dr. D. Kats during the course of this work. These extensions allowed LITF to handle transformations of tensors using active orbitals (like density matrices and orthogonalization tensors), as well as to define PAO and PNO spaces involving active orbitals and to manage non-triangular pair lists (like for instance the case of P_1).

The ITF part of the LCASPT2 implementation is composed by two parts: an algorithm file containing algorithms to calculate all quantities required, written in a human-readable format (*.itfaa* file); a set of C++ files (*.cpp*) able to interpret the former algorithms and use them to perform quantum chemical calculations. There is still an *.itfca* file bridging the human-readable algorithms in machine-readable codes.

The algorithm file can be further subdivided in two parts, a declaration section (of index spaces and tensors) and the codes for the algorithms. In the LCASPT2 case the declaration of index spaces includes both orbital and (orthogonal) configuration spaces.

The declaration of any of these index spaces follows the structure

$$\text{index}-\text{space}: \quad indices, \quad name \quad of \quad space, \quad index \quad type$$

$index-space$ is used to declare indices and $indices$ are the indices used for the space in declaration, given without commas. Multiple letter indices like $S0$ can be declared inside {}, like $\{S0\}$. $name \quad of \quad space$ is the name chosen to identify the index space. For the case of LCASPT2 there are, Closed(-shell), Active, PAO, PNO and orthogonal configuration indices. $index \quad type$ refers to a letter used to identify index spaces. This reference index can be used to simplify input-output actions of tensors in ITF. As a title of example, a general active space may be defined as follows:

$$\text{index}-\text{space}: \quad tuvwxyz, \quad Active, \quad a$$

After declaring the index spaces comes the declaration of tensors required to write the algorithms. This includes final quantities stored on disk, like amplitudes, residuals or coupling coefficients, but also intermediates used for the calculation of the final tensors, which may or may not require storing on disk. The declaration of these tensors determines their use, their storage and their structure. One starts by defining the name of each tensor and their respective indices inside square brackets. The index order is selected by the programmer, and the leftmost index is the one running faster. For instance, the P_2 residuals in the PNO basis can be represented by tensors $R[pqij]$, where p and q are PNOs and i and j closed-shell orbitals. Because in the declaration only index spaces should be specified, $R[ppii]$ can equivalently be used. In this particular case, PNO indices run faster than closed-shell indices. In ITF two tensors may have the same name as long as they do not have the same index structure. This means that all residuals can be named R, just like all exchange integrals can be named K.

The second part of the declaration of tensors is determined inside the statement $!Create$. Here, type, cuts and symmetry properties of tensors are defined. The type can be, *e.g.*, *disk*, if the tensor is stored on disk, *plain*, if not stored on disk, or *scalar*. *disk* tensors can be loaded, stored, allocated and dropped, *plain* tensors can only be allocated and dropped. *scalar* tensors are like *disk* tensors but have no dependence on any index. In LCASPT2 we have as *disk* tensors, *e.g.*, density matrices, residuals and amplitudes, both energies and energy shifts are defined as *scalar*, and all intermediates used in the calculation of *disk* tensors are declared as being *plain*.

Defining cuts is where orbital domains and pair approximations can be detailed. This is accomplished using the position number for each index, starting from zero, from left

to right. In the case of P_2's residuals we can specify $cut : 0/23, 1/23, 23$, meaning that the indices in positions 0 and 1 (the first two indices) are restricted to the pair domain of the last two indices. Since the indices in 0 and 1 are in the same pair domain, this cut command can be simplified to $cut : 01/23, 23$. The final 23 after the comma specifies the pair list. For PAO domains for the active space $cut : 0/A$ can be used to specify that the orbitals in the first position are in the domain of the active space. Some indices serve just the purpose of defining domains. These phantom indices are not present in the tensor, thus summations cannot go over these indices. They serve the purpose of addressing, allowing to easily address a specific tensor or a specific block inside a larger tensor. These can be identified by adding after the cut an f followed by the respective index numbers. For instance, to declare the indices i and j as phantom in the P_2 residuals $cut : 01/23, 23, f23$ can be used. Although not useful for quantities like residuals or amplitudes, this definition is important when declaring, *e.g.*, PNO overlap matrices. Another type of cuts are the ones in (pair) lists loaded from the FORTRAN part of the code. Examples are pair approximations for closed-shell orbitals, which must be in the proximity of active orbitals. Specifying $cut : A1$ in I_1's residuals tensor $R[\{I1\}i]$ specifies that the closed-shell orbital i (position 1) should be in the spatial vicinity of an active orbital. Finally, symmetry properties are defined using $sym :$. For instance, P_2 amplitudes have the index exchange symmetry $c_{ab}^{ij} = c_{ba}^{ji}$, which can be specified using $sym : 23/01$. For the case of singlet-triplet configurations the index exchange symmetries are specified with $sym : +12$ (singlet) or $sym : -12$ (triplet).

The algorithm codes use the previously defined tensors to ultimately calculate the energy of a quantum chemical system. Algorithms are abstract high-level instructions that adequately and consecutively use tensors to calculate other tensors. Tensors can be allocated, loaded, stored and/or dropped according to their type. When allocated, tensors are also automatically zeroed. When loaded, they assume the values of the previous store action. Most importantly, tensors can be contracted or linearly combined. Any two tensors can be contracted in ITF, as long as they have matching indices. LITF requires furthermore the cuts to be compatible. A dot in the beginning of a statement indicates that a tensor contraction takes place. After the dot the tensor being calculated in the current step is specified, and on the other side of the equality the two tensors being contracted. The contraction takes place automatically and is solely defined by the indices involved in the expression. ITF interprets two indices within an index contraction as an implicit sum over the full space spanned by the index. Pairs of indices occurring on the right side of the statement which do not occur on the left side are contracted. However,

these pairs of indices must belong to each of the tensors contracted. Contractions take place over as many pairs of indices as required, as long as all pairs of indices are different. Furthermore, the sign on the contraction can be defined with $+=$ or $-=$. This means that summations are affected by the respective sign. Taking as an example the calculation of the term

$$D^f_{tu} = \sum_{vw} f_{vw} D^{(2)}_{vw,tu} \tag{5.4}$$

in ITF's algorithm code can be written as

$$.\text{trFaDM2}[tu] += \text{f}[vw]\text{DM}[vwtu]$$

where trFaDM2$[tu]$ represents D^f_{tu}, f$[vw]$ is f_{vw} and DM$[vwtu]$ betakes $D^{(2)}_{vw,tu}$. Alternatively one tensor can be used on the right side of the equality, meaning that a tensor is added to the tensor on the left side of the equality. Finally, tensor contractions can be performed along with the multiplication by a real number. If, *e.g.*, we wished to define D^f_{tu} as half of the active block of the Fock matrix, we could simply make

$$D^f_{tu} = 0.5 \times f_{tu} \longrightarrow .\text{trFaDM2}[tu] += 0.5 * \text{f}[tu]$$

Using these tensor operations, algorithms were written for: all coupling coefficients and the required intermediates; contractions of the Fock matrix with the density matrix or coupling coefficients; initialization of the residual tensors; calculation of the residual tensors; amplitude update; calculation of PNO, PAO and PAO-PNO overlap matrices; transformation of the Fock matrix from PAO to PNO basis; calculation of the reference energy; calculation of the energy for each configuration subspace. Even though some quantities were already calculated at the FORTRAN level, only the strictly necessary tensors are imported. This minimizes as much as possible the time spent in writing and reading of tensors. All these codes had the same internal structure: i) an input section, in which all tensors are loaded and allocated; ii) a contraction section, in which all tensors are contracted; iii) an output section, in which tensors are stored and dropped. This structure is however not fix, since inside the contraction section tensors may be sporadically loaded, allocated, stored or dropped. Furthermore, like previously mentioned, residuals are built and solved in the orthogonal configuration basis. The exceptions were the cases of S_0 and I_1, for which the residuals are built in the non-orthogonal basis. Since the orthogonalization of the residuals is performed immediately after building them, only residual tensors in the orthogonal configuration basis are stored.

For the codes performing the update of amplitudes a function that scales residual tensors by the denominators was utilized, allowing the direct application of the perturbative

update of amplitudes. This function is $denom - scale$, and contrary to tensor contractions it allows the repetition of an index inside one tensor (like for instance the addition of diagonal elements from the closed-shell block of the Fock matrix).

All these codes were partitioned according to configuration (sub)spaces and according to which basis the residual tensors are built. The calculation of coupling coefficients and intermediates was partitioned into general intermediates (like general contractions of the density matrix with other tensors) and the coupling coefficients specific for each configuration subspace. Because they are not memory demanding, the calculation of coupling coefficients for the pairs are all grouped in the same algorithm. All the algorithms dealing with residuals and amplitudes are separated into three different codes: one for the pairs; one for S_2, S_1 and I_2; one for S_0 and I_1. The calculation of energies is separated according to configuration spaces: pairs; singles; internals. Other codes calculate overlap matrices for local virtuals and transform the Fock matrix to the PNO basis.

The C++ part required a new driver routine equipped with functions to read and execute the algorithms written in the $.itfca$ file. The latter is built from the $.itfaa$ file. After initializing and defining internal variables, (1:) the new quantum chemical method is initialized by setting, among other variables, the reference energy and the algorithm file name. After initialization of the quantum chemical method, (2:) relevant quantities are imported to ITF. This includes logical options relevant for the execution of the algorithm, just like all the tensors previously calculated or prepared to export to ITF: integrals; PAO and PNO transformation matrices; density matrices; *etc.*. It is after the importing section that the execution of algorithms using the C++ function $AlgoSet.Execute$ starts. (3:) PNO, PAO and PAO-PNO overlap matrices are calculated and followed by (4:) the transformation of the Fock matrix to the PNO basis. Then (5:, 6:) all coupling coefficients are calculated and written to disk. We note that all these quantities were written and defined in order to remain unchanged throughout the whole calculation. This is a significant change with respect to other variants of CASPT2 implemented in `MOLPRO` , like RS2C, in which coupling coefficients are recalculated in each iteration.

After setting the whole environment with all tensors and options required, the actual execution of LCASPT2 begins. This is done by (7:) initializing the residual tensors to the respective exchange integral tensor elements (all amplitudes are taken to be zero) and by performing the (8:) first perturbative update of amplitudes. All zeroth-iteration amplitudes are thus defined similarly to what pair amplitudes are defined in eqs. 4.51, 4.52 and 4.53. (9:) The zeroth-iteration energies are calculated without using the Hylleraas functional (by zeroing the residuals in eqs. 4.112-4.119) and the actual (10:) iterative

solving of the residual equations begins. Like in any other iterative procedure this is done by setting thresholds for energies and for variances, as well as the maximum number of iterations, timers for the iterations and a boolean (logical) convergence variable.

The next steps consist in consecutive calls for the algorithms to (11:) calculate the residuals, to (12:) calculate the Hylleraas energies and to (13:) update the amplitudes until convergence or the maximum number of iterations is reached. The end of each iteration is marked by the printing of the iteration number, the current correlation energy, the energy change towards the previous iteration, the variance and the CPU time.

If convergence is reached, (15:) all the results are printed, namely the energy of the reference, the correlation energy, the second-order corrected energy (LCASPT2 energy) and the individual energies for each configuration subspace. Timings and memory usage are sent back to FORTRAN, so that the program can be terminated. The whole ITF procedure can be schematized in the following algorithm:

Algorithm 2 pno-caspt2 (ITF)

1: set environment; initialize method;
2: import integrals, orthogonalization matrices, densities, transformations for PAOs, and PNOs;
3: Build PNO, and PAO-PNO overlaps;
4: transform Fock matrix into PNO basis;
5: calculate general intermediates;
6: calculate coupling coefficients: pairs; S_2; S_1; S_0; I_2; I_1;
7: initialize residuals to $\langle \Phi^* | \hat{H} | 0 \rangle$: pairs; $S_2 + S_1 + I_2$; $S_0 + I_1$;
8: initialize amplitudes: pairs; $S_2 + S_1 + I_2$; $S_0 + I_1$; ▷ using update algorithm
9: calculate (zeroth-iteration) energies: pairs; singles; internals;
10: **while** ((not converged) or ($n_{iter} \leq max_{iter}$)) **do**
11: evaluate residuals: pairs; $S_2 + S_1 + I_2$; $S_0 + I_1$;
12: calculate Hylleraas energies: pairs; singles; internals;
13: update amplitudes: pairs; S_2; S_1; S_0; I_2; I_1;
14: **end while**
15: termination and printing of energies, timings, and memory usage.

Even though the FORTRAN code is already fully parallel, the ITF code is only moderately parallel, and a fully parallel implementation will take place in a near future.

5.4 Using LCASPT2 and ic-CASPT2

Both the drivers for LCASPT2 and ic-CASPT2 are called within the RS2C directive in MOLPRO . All options for RS2C are thus also valid for LCASPT2 and ic-CASPT2. To call LCASPT2, the MOLPRO directive *pno-caspt2* should be used. An independent directive for ic-CASPT2 was not introduced and calling this program is done with $df\text{-}rs2c, fc$, where fc stands for fully-contracted. By default, the LCASPT2 and ic-CASPT2 programs use DF integrals. Also by default, the ITF's *cpp_prog* is defined by calling each program and the user does not need to select any algorithm. Using the non-DF variant of LCASPT2 needs the calculation of the reference CI, which makes the calculation slower. The basic calls for LCASPT2 and for ic-CASPT2 are then respectively $\{pno{-}caspt2\}$ and $\{df{-}rs2c, fc\}$. These calls require a previous MCSCF or CASSCF calculation to obtain the reference. Furthermore, by default, LCASPT2 uses IBOs. For ic-CASPT2, no localization is used.

With the default options, Fock matrices and CI vectors are taken from the previous MCSCF calculation. Two-electron integrals are however calculated with specific routines written for LCASPT2. A CI record and orbitals are by default taken from the previous CASSCF calculation and must be saved in the *multi* directive

$$\{df{-}multi; save, cirec{=}5150.2, orb{=}2150.2; ...\}$$

and this same record must be read in LCASPT2

$$\{pno{-}caspt2, cirec{=}5150.2; orbital, 2150.2; ...\}$$

On the orbital directives in *multi*, electronic states might be given, building state specific (and not state-averaged) $\hat{H}_0$ operators and state specific densities.

$$\{df{-}multi; save, cirec{=}5150.2, orb{=}2150.2; state, 2; natorb, state{=}1.1; natorb, state{=}2.1\}$$

If nothing is specified, state-averaged densities are used allover.

Alternatively, the reference CI can be calculated in the beginning of the LCASPT2 calculation. In this situation, all integrals and quantities are read from a file. This variant of LCASPT2 can be called using the options $\{pno\text{-}caspt2, blocking{=}.false., addact{=}0\}$ (the defaults for *blocking* and *addact* are respectively *.true.*, and 1). Since the reference CI is performed, no special commands or options are needed in the preceding *multi* calculation.

The default DF basis used to assemble integrals is $mp2fit$ (*323*). It is also possible to switch off the diagonalization of zeroth-order Hamiltonian terms, *i.e.*, not to force the γ

matrices to be diagonal in the orthogonal configuration basis. This is done by setting to false the option $diag\_denf$. It is also possible to turn on the use of pure singles within the S_1 subspace by making true the option $use\_singles$. We remind the reader that these are completely redundant in CASPT2 and no changes in the energy nor timings are observed. This option is by default off.

Both level- and denominator-shifts can be employed just like in the RS2C program. The variable $diisspace$ chooses which configuration subspaces use DIIS to improve convergence. By default $diisspace = p2p1p0s2s1s0i2i1$, meaning that all spaces use the DIIS convergence accelerator.

PNOs are by default used for P_2, P_1, P_0 and S_2. For the remaining singles (S_1, and S_0) PAOs are used. It is however possible to switch off both the use of PNOs and PAOs. Setting $use\_pno=.false.$ turns off the transformation to the PNO basis and setting $use\_pao=.false.$ turns off the transformation to the PAO basis. Setting the domain sizes for PAOs can be done using the options $iext$ or $rext$. While $iext$ is a vicinity parameter (neighboring shells), $rext$ is a distance criterion. Both these options were previously detailed in section 4.7, for which we refer the reader to. There is furthermore the option $reduce\_act$, which makes for active orbitals $iext = reduce\_act$. By default $reduce\_act = iext$. The domain sizes for PNOs can be determined using the energy criterion $thrpno$ or the occupancy criterion $thrpno\_occ$. Once more, both these options were detailed in the section 4.7. The MPA can be switched off by setting $thrdist = 0$. The value of 10^{-6} (E_h) is however recommended. The very distant pair approximation can be switched on by giving values to either $rvdist$ (distance criterion) or $ivdist$ (vicinity parameter). The truncation of P_1, S_2, S_1, I_2 and I_1 pairs can be controlled using $distp1$. By default this takes the value of 2, and can be switched off by setting $distp1 = 0$. The default distance criterion in $distp1$ is the same as $rvdist$.

Variables to save domain sizes were also implemented, which can be used either for printing or for comparison purposes. These are saved in the arrays $avdom\_pao(x)$ and $avdom\_pno(x)$. In the first position, $x = 1$, the average PAO/PNO domain size is saved. For $x = 2$, the average domain size for P_2; for $x = 3$, the average domain size for P_1; for $x = 4$ and $x = 5$, the average domain size for P_0 singlet and triplet, respectively.

6. Results and Discussion

In this section benchmark calculations on LCASPT2 and some applications are presented. We will present: i) comparison between CW and full ICC ansätze for the wavefunction - section 6.1; ii) effect of orbital domains - section 6.2; iii) benchmarking the accuracy of LCASPT2 for medium-sized molecules for a larger set of molecules - section 6.3; iv) comparison of excitation energies with experimental values - section 6.3.1; v) calculation of reaction energies - section 6.3.2; vi) basis set effects - section 6.4; vii) effect of pair approximations - section 6.5; viii) scaling of the computational costs with the molecular size - section 6.6; vii) PESs - section 6.7.

Due to the wide spectrum of studies used to benchmark LCASPT2, each subsection works with specific groups of molecules. Unless otherwise stated, structures were optimized using MP2 with Dunning's correlation consistent augmented double-ζ basis set (aug-cc-pVDZ) (*364, 365*). Even though symmetry might have been used in the first HF calculation to separate π orbitals from the σ, all calculations were ultimately performed without symmetry. All optimized geometries, just like all the energies of the calculations performed are in the supplementary material.

Finding a suitable active space for the description of a (photo)chemical process can be a very difficult task. It is usual for the MOs to rotate during optimization of the CAS reference, yielding thus an incorrect active space. Any active space can in principle be found by rotating initial guess orbitals (HF for instance) in and out of the active space in the CASSCF calculation. This procedure works well for π and $n + \pi$ active spaces, which are relatively stable and for which the intervening orbitals are easily identified. However, when searching for active spaces with σ bonds or even d orbitals, this procedure is not robust and most probably the desired active space will not be found due to rotations among different orbital spaces. For such cases, IBOs are generated after a HF calculation. Using a local MP2 calculation, regions are defined from domains and the IBOs located exclusively on some user selected atoms are isolated. These IBOs are then used to select the desired active space. However, this procedure does not provide any help in selecting the HF virtual orbitals we wish to include into the active space. Nevertheless, as long as the virtual orbitals contain the correct antibonding character, the desired active space is usually obtained. Still, for some larger molecules, the virtual space was far too large to avoid a tedious and error prone search for orbitals with a specific antibonding character. One can for such cases start with a small basis set to conduct an initial orbital search.

After confirming that the CASSCF has the correct active space, the size of the basis set can be increased. For cases in which the closed-shell HF orbitals were highly mixed, the latter procedure could be combined with the IBO procedure, facilitating the task of finding active spaces.

The default basis set was aug-cc-pVDZ (*364–369*). For second-row atoms, like sulfur or phosphorous, *d* orbitals were added to the augmented basis sets (aug-cc-pV(X+d)Z or aug-cc-pVDZ+d). cc-pVDZ, cc-pVTZ, aug-cc-pVTZ, aug-cc-pVQZ, aug-cc-pV5Z and Ahlrichs triple-ζ basis sets with polarization (def2-tzvp) (*370*) were also utilized. In all calculations DF approximations were used for the calculation of integrals. This includes LCASPT2 (*242*), CASSCF (*96, 371, 372*), HF (*232, 373*), RS2C (for comparison of different wavefunctions in the canonical basis) (*15, 62, 96*), LMP2 (for getting IBOs and the atomic regions to build active spaces) (*229*) and LUCCSD(T) (to compare some energy differences) (*239, 240, 374–376*). Both HF and CASSCF used the corresponding JKFIT auxiliary bases of Weigend (*322*). By default the non-augmented variants of these basis sets were used, although for some particular cases augmented bases were employed. We verified that the difference between using augmented and non-augmented DF bases is negligible. By default the "old" implementation of DF-HF was used (*232*). For larger molecules however, the most recent implementation of the linear scaling DF-HF was chosen (*373*). Since the default is not the recent linear scaling DF-HF program, we will mention for which cases we applied this method. Two state-averaged CASSCF references are also by default optimized, calculated using the 2^{nd}-order MCSCF program as described in (*371, 372*). This means that by default all orbital spaces are simultaneously optimized. For larger molecules this procedure becomes too expensive and we end up having very large MCSCF times. This is a consequence of the fact that all integrals involving up to two external indices must be calculated, without any form of pair or domain approximation. For those cases the active orbitals were optimized, and a few orbitals of some atoms in the neighboring shells of the active space are also eventually relaxed. For the rest of the closed-shell skeleton the IBOs computed previously are used. Alternatively, HF orbitals for the closed-shell skeleton could be directly used. IBOs offer however the advantage of a clear σ-π separation. This facilitates the determination and isolation of all orbital spaces: the closed-shell skeleton; the orbitals to relax; the active orbitals. This procedure does not introduce large errors, especially in the calculation of energy differences. However, the energy differences can slightly increase because the IBOs are optimized for GSs. More details can be found in (*242*). For LCASPT2, RS2C, LRMP2 and LUCCSD(T) the two-electron integrals are calculated using the MP2FIT auxiliary

basis of the corresponding non-augmented variant of the basis set (*323*). For most cases, the minimal AO basis required for building IBOs was the default for `MOLPRO` .

From the CASSCF calculations the Fock operator, the orbitals, the reference energy and the reference itself (coefficients) are saved. This allowed to skip the calculation of the reference CI in the beginning of the CASPT2 calculation. The effective Fock operator used in the zeroth-order Hamiltonian was thus computed using the JKFIT auxiliary basis. We note here that the exchange integrals required in CASPT2 are calculated inside the LCASPT2 driver using MP2FIT. The calculation of quantities taken from the previous CASSCF are not considered in timings presented. Furthermore, all calculations are run in serial (parallel calculations are presented in reference (*242*)).

The calculations on pure organic molecules were performed by default with an energy convergence threshold of 10^{-7} E_h. For organometallic compounds however, this threshold was relaxed to 10^{-6} E_h. In all cases a threshold for the orthogonalization of singles ($thrdls$) of 10^{-8} was used. This is because the default threshold of 10^{-7} leads to different sizes for S_1 for the CW and the fully-contracted wavefunctions, not making the methods directly comparable. Finally, a level-shift of 0.3 was considered by default for all LCASPT2 calculations which involved previously a state-averaged CASSCF calculation. This shift of 0.3 was used for GS and ES(s). Furthermore, by default, LCASPT2 calculations use $iext = 2$, $rext = 5$, $thrpno\_occ = 10^{-8}$ and $thrpno = 0.997$. The MPA is by default off, and the neglecting of pairs, $distp1$, is by default on, using $rvdist = 15$ $bohr$. For most molecules here studied this parameter has no effect and no pair is skipped.

Excitation energies were computed by applying (L)CASPT2 on top of state-averaged references for each state isolated. Unless otherwise stated, we always refer to vertical excitation energies. Whenever dealing with adiabatic excitation energies or with both types of excitations, each type of excitation is specified.

Benchmarks for LCASPT2 are based on eight different families of molecules. These families are presented in Figs. 6.1-6.6 and described afterwards.

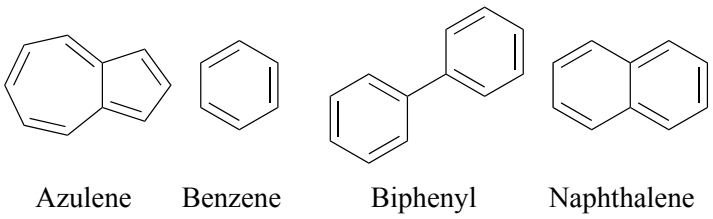

Figure 6.1: Family of aromatic molecules used to benchmark LCASPT2.

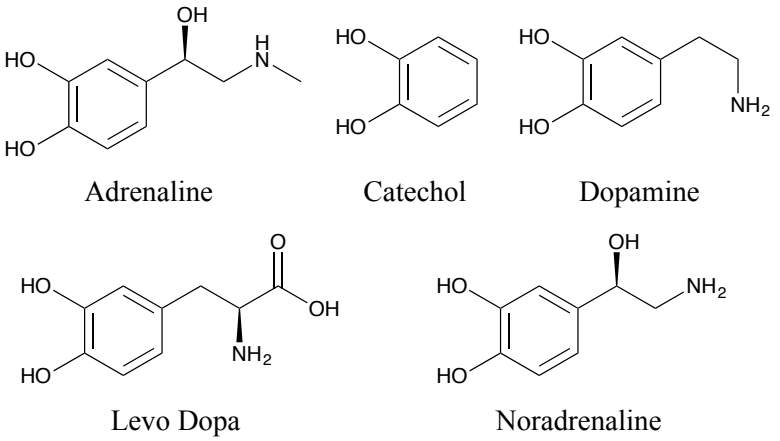

Figure 6.2: Family of catechols used to benchmark LCASPT2.

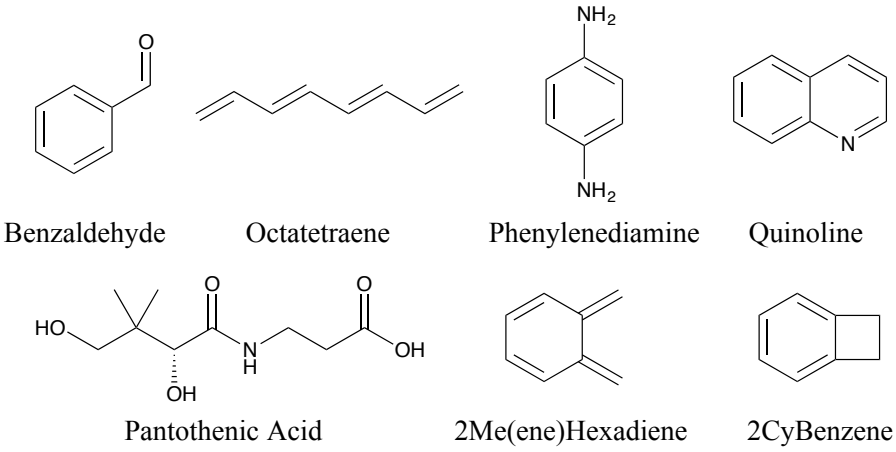

Figure 6.3: Family of "other" molecules used to benchmark LCASPT2.

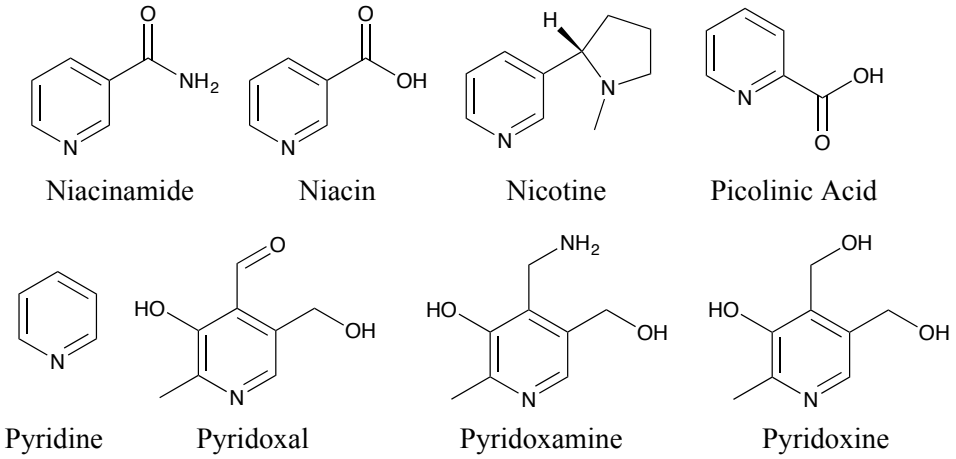

Figure 6.4: Family of pyridines used to benchmark LCASPT2.

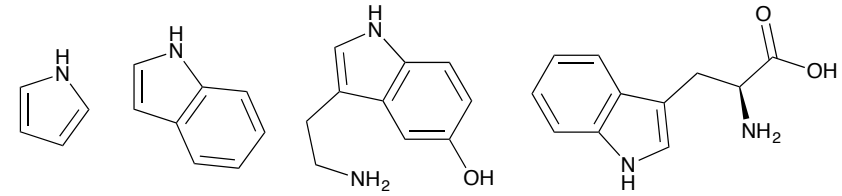

Figure 6.5: Family of pyrrole-indoles used to benchmark LCASPT2.

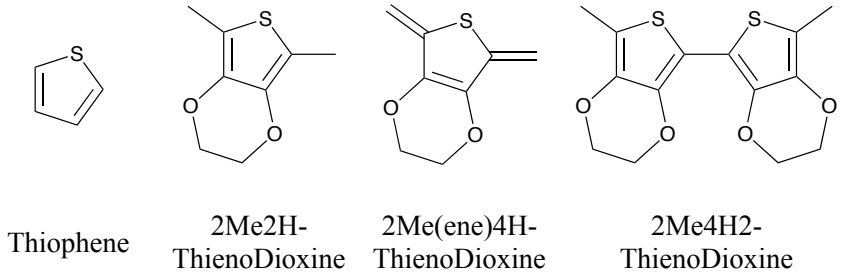

Figure 6.6: Family of thiophenes used to benchmark LCASPT2.

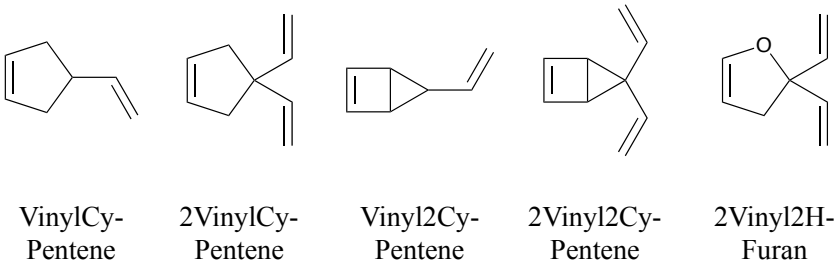

Figure 6.7: Family of "reaction" molecules used to benchmark LCASPT2.

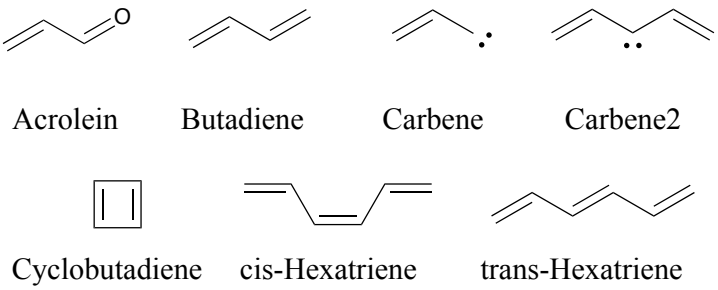

Figure 6.8: Family of small molecules used to benchmark LCASPT2.

The family of aromatics is composed by azulene, benzene, biphenyl and naphthalene. The active spaces used for these molecules corresponds to π systems in conjugation. These

are: benzene - CAS[6, 6]; azulene and naphthalene - CAS[10, 10]; biphenyl - CAS[12, 12]. Schematic representations of the active spaces used for this and other families of molecules are presented in Appendix 8.4. Both the default aug-cc-pVDZ basis set and aug-cc-pVTZ were used for this family of molecules.

The family of catechols includes adrenaline (hormone and drug with an important role in fight-or-flight responses), catechol, dopamine (neurotransmitter involved in the reward-motivation system), levo-dopa (LDopa, a biological precursor to dopamine also sold as a drug in the treatment of Parkinson) and noradrenaline (neurotransmitter and hormone also with an important role in fight-or-flight responses). The active spaces chosen for these molecules included the extended π systems in conjugation. This means that for all molecules in this family all π and $\pi*$ orbitals were included, as well as two non-bonding pairs of electrons, one from each oxygen. The wavefunction corresponds thus to a CAS[10, 8]. Except for LDopa, calculations on these molecules were performed using both aug-cc-pVDZ and aug-cc-pVTZ.

The inhomogeneous group of molecules "other" contains benzaldehyde, octatetraene, phenylenediamine, quinoline, pantothenic acid (PanthAcid, vitamin B_5), 5,6-dimethylene-cyclohexa-1,3-diene (2Me(ene)Hexadiene) and bicyclo[4.2.0]octa-1,3,5-triene (2CyBenzene). The TS structure for the electrocyclic ring closure transforming 2Me(ene)Hexadiene into 2CyBenzene was also optimized. For benzaldehye, octatetraene, phenylenediamine and quinoline the extended π systems in conjugation were used as active spaces. This means: benzaldehyde and octatetraene - CAS[8, 8]; phenylenediamine - CAS[10, 8]; quinoline - CAS[10, 10]. For quinoline a CAS[12, 11] was also used, in which the non-bonding pair of the nitrogen atom orthogonal to the π system was included. Note that for benzaldehyde the non-bonding orbitals from the oxygen atom were not included in the active space. For PanthAcid two different CAS[4, 3] wavefunctions were used. The first (PanthAcid1) describes the amide functionality, while the second (PanthAcid2) describes the carboxylic acid group. Finally, for 2Me(ene)Hexadiene and 2CyBenzene a CAS[8, 8] consistent with the electrocyclic ring closure from 2Me(ene)Hexadiene to 2CyBenzene was optimized, *i.e.*, the π system for 2Me(ene)Hexadiene and the π system with two σ orbitals (bonding and anti-bonding) describing the bond between the two sp^3 carbons for 2CyBenzene. An equivalent CAS was used for the TS. For PanthAcid only the default basis set was used. For the electrocyclic ring closure reaction both aug-cc-pVDZ and aug-cc-pVTZ were used. For the other systems aug-cc-pVDZ and def2-tzvp were employed.

The family of pyridines considers niacinamide, niacin (vitamin B_3), nicotine, picolinic acid (Pico), pyridine, pyridoxal (one form of vitamin B_6), pyridoxamine (another form of

vitamin B_6) and pyridoxine (yet another form of vitamin B_6). Once more the extended π systems in conjugation were considered for the active spaces. This means that besides the π orbitals from the conserved pyridine rings the orbitals from amide, carboxylic acid, aldehyde and alcohol groups directly attached to the pyridine rings were included: nicotine and pyridine - CAS[6, 6]; pyridoxamine and pyridoxine - CAS[8, 7]; niacinamide, niacin, Pico and pyridoxal - CAS[10, 9]. For niacin, nicotine, pyridoxal and pyridoxamine the active spaces were extended to include the non-bonding orbital from the N-pyridine atom, orthogonal to the π system: nicotine - CAS[8, 7]; pyridoxamine - CAS[10, 8]; niacin and pyridoxal - CAS[12, 10]. The suffix 1 is used for these larger active spaces. For the active spaces without the non-bonding electron pair from the pyridine-nitrogen the suffix 2 was used. The calculation of excitation energies using the larger active space served to confirm the stability of the calculated excitation energies. We also wanted to have access to higher ESs, but the second, third and fourth states are quasi-degenerate for the optimized GS geometries of some molecules with the active space 1. We had thus to optimize five-state state-averaged references. Of the pyridines, only on niacin2, niacinamide2, Pico and pyridine we performed calculations using also the aug-cc-pVTZ basis set. For Pico also aug-cc-pVQZ and aug-cc-pV5Z were tested.

The family of pyrrole-indoles incorporates pyrrole, indole, serotonin (neurotransmitter associated with the feeling of happiness) and tryptophan (aminoacid). For this family of molecules we optimized the following references: pyrrole - CAS[6, 5]; indole and tryptophan - CAS[10, 9]; serotonin - CAS[12, 10]. For pyrrole a four state state-averaged CAS reference was optimized. For tryptophan aug-cc-pVTZ and aug-cc-pVQZ were also used.

The family of thiophenes is composed by thiophene, 5,7-dimethyl-2,3-dihydrothieno [3,4-b] [1,4] dioxine (2Me2HSDiox), 5,7-dimethylene-2,3,5,7-tetrahydrothieno [3, 4-b] [1,4] dioxine (2Me4HSDiox) and 7,7'-dimethyl-2,2',3,3'-tetrahydro-5,5'-bithieno [3,4-b] [1,4] dioxine (2Me4H2SDiox). The last three structures were taken from the structure of poly(3,4-ethylenedioxythiophene):polystyrene sulfonate (PEDOT:PSS), a widely used mixture of two ionomers in the manufacture of Organic Light-Emitting Diodes (OLEDs) due to their high ductility and conductivity (*377–381*). The active spaces were built from extended π systems in conjugation. These include not only the thiophene moieties, but also the oxygen atoms directly attached to the former: thiophene - CAS[6, 5]; 2Me2HSDiox - CAS[10, 7]; 2Me4HSDiox - CAS[12, 9]; 2Me4H2SDiox - CAS[20, 14].

The family of small molecules comprises acrolein, butadiene, two conjugated carbenes, cyclobutadiene, (Z)-hexa-1,3,5-triene (cis-hexatriene) and (E)-hexa-1,3,5-triene (trans-hexatriene). For the cases of cis- and trans-hexatriene both the GS and first ES structures

were optimized. These geometries were optimized at the CASSCF level using a CAS[6, 6] and aug-cc-pVDZ. This CAS was used in all other calculations in this system. A similar CAS was previously used by Olivucci *et al.* for the same system (*382*). The absolute minimum in the S1 PES was also optimized, just like the Conical Intersection (C.I.) between S0 and S1 and the TSs from cis-hexatriene (S1) and trans-hexatriene (S1) to the C.I.. All the structures involving the hexatriene system compose the main points in the S0 and S1 PESs describing the cis-trans isomerization of hexatriene. Under this context we performed calculations on those 8 structures (S0 cis, S1 cis, S0 trans, S1 trans, minimum S1, C.I., both TSs) using aug-cc-pVQZ. Besides the hexatriene system, reaction energies were also calculated for the addition of the two carbenes to acrolein, butadiene or cyclobutadiene. The active spaces used in these cases correspond once more to the conjugated π systems. For the cases of the carbenes both unpaired electrons were also considered. As such, the active spaces used are: acrolein, butadiene, carbene and cyclobutadiene - CAS[4, 4]; carbene2 - CAS[6, 6]. More details on these calculations can be found in the next paragraph. Only aug-cc-pVDZ was used in these calculations.

The family of "reaction" molecules includes idealized molecules obtained from the addition of carbene and carbene2 to butadiene, cyclobutadiene and acrolein: 4-vinylcyclopent-1-ene (VinylCyPentene), 4,4-divinylcyclopent-1-ene (2VinylCyPentene), 5-vinylbicyclo [2.1.0] pent-2-ene (Vinyl2CyPentene), 5,5-divinylbicyclo [2.1.0] pent-2-ene (2Vinyl-2CyPentene) and 2,2-divinyl-2,3-dihydrofuran (2Vinyl2HFuran). All these reactions are hypothetical, mostly because it is very hard to obtain consistent active spaces for both reagents and products, which allows both species to be treated on equal foot. Because of the way these molecules were built, the active spaces had to be consistent with the respective reactions. Besides π orbitals, the respective σ orbitals were added to the active space. These included the following references: VinylCyPentene and Vinyl2CyPentene - CAS[8, 8]; 2VinylCyPentene, 2Vinyl2CyPentene and 2Vinyl2HFuran - CAS[10, 10]. The optimized orbitals are presented in Appendix 8.5. The calculation of reaction energies was performed using one geometry file for the reagents. The molecules were placed at a minimal distance of at least 23 Å (arbitrary large value). For the reaction to form 2Vinyl2HFuran an intermediate with diradical structure was also considered. We searched for other intermediates and for TSs, but no other structure was yet found. For the excitation energies of reaction molecules the same active space was used but a larger level-shift was required (0.5). Two possible additions of carbene to cinnamaldehyde (the molecule responsible for the cinnamon flavor) were also studied. The structures of cinnamaldehyde and the addition products are presented later in subsection 6.3.2. For this case, carbene

and cinnamaldehyde were optimized together. The separation between the molecules is about 2.2 Å in the optimized geometry. The active spaces considered in these reactions were built just alike the active spaces for all the reactions above discussed, meaning a CAS[14, 14]. No ES was considered in these two reactions, meaning that single-state references were optimized.

LCASPT2 was applied to a nickel complex with a di-imine and a Cyclopentadienyl (CP) ligand. The structure, *c.f.* Fig. 6.9, was determined by X-Ray Crystallography by Dr. M. Ringenberg, who provided us the geometry of the complex. The optimized active space contained the π system of the di-imine ligand and the d_{Ni} orbitals in interaction with this π system. This CAS[8, 6] had no contribution from the CP ligand. No Effective Core Potential (ECP) was used in these calculations, except for the definition of nickel's minimal AO basis (to build the IBOs). For this complex both the cc-pVDZ and cc-pVTZ bases were used. By default, the corresponding JKFIT and MP2FIT auxiliary bases were used, except for the metal center, for which def2-tzvpp was used.

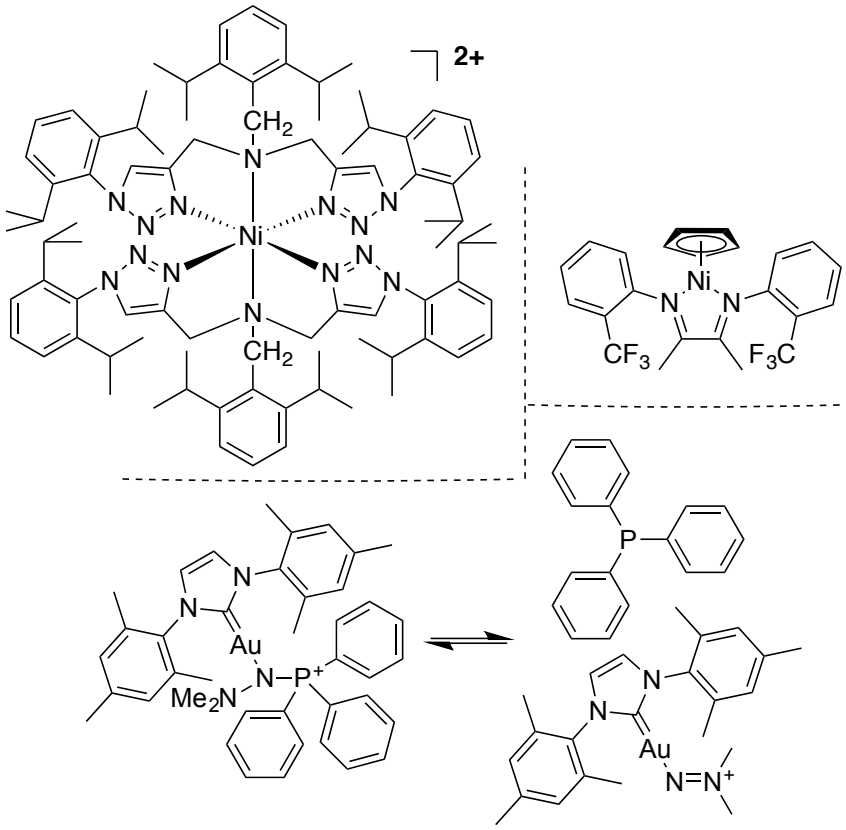

Figure 6.9: Organometallic complexes used for benchmarking LCASPT2.

LCASPT2 was also applied gold complexes, which are involved in a simple elimination

reaction. The gold structures were taken from reference (*148*) (this is a reoptimization of the structures from (*383*)). For both cases single-state CAS references consistent with the reaction were optimized after a linear scaling DF-HF calculation. The reaction involving the gold complexes involves breaking a N-P bond. This is the first process in a many step reaction. Even though other steps of the whole process would be more suitable to be studied using MR methods, this step in particular was chosen due to the size of the molecules involved. The active space chosen for the reagent included the σ_{NP}, σ^*_{NP}, the lone pair from the nitrogen not bonded to the phosphorous (n_N) and a d_{Au} orbital suitable to interact with the changing π system. For the product the active space is composed by the orbitals π_{NN}, π^*_{NN}, n_P and the equivalent d_{Au} orbital. For both cases the CAS[6, 4] reference was obtained by first optimizing the active space (with IBOs as closed-shell) and then optimizing the closed-shell space while freezing the active orbitals. The results of a fully optimized CAS reference are mentioned for comparison reasons. The basis set used for this system was cc-pVDZ with aug-cc-pVDZ+d for the phosphorous and cc-pVDZ-pp for the gold atom. Gold's inner-shell 60 electrons were treated with a pseudo-potential (ECP60MDF). For the DF auxiliary bases JKFIT and MP2FIT we used def2-tzvpp.

Last but not least we calculated the singlet-triplet splitting of a nickel complex with 231 atoms. This is up to the moment the largest molecule treated at the LCASPT2 level of theory. The structure of this complex was taken from (*72*), and a similar active space comprising the d orbitals of the metal atom was isolated. However, contrary to what is presented in (*72*), we did not fully optimize the CAS reference. Instead we calculated the GS IBOs (triplet state) and we used these to isolate the desired active space for the triplet and singlet states. We then optimized the active orbitals of a CAS[8, 5] reference, using for the closed-shell space the IBOs of the triplet state. This means that for both electronic states we optimized the respective active orbitals and also for both states the IBOs of the triplet GS are used to describe the closed-shell space. Since only one state for each spin symmetry is used, the references consist on single state CASs. For this system we used the basis set def2-tzvpp.

Besides the hexatriene system already described, PES studies were performed on ethylene. The distance between carbon atoms was increased by 0.025 Å, ranging from 0.919 to 3.269 Å. All geometries were optimized at the single-state MCSCF level using a full valence active space. In all these cases all parameters were optimized, except for the distance between the carbon atoms, which was fixed. After geometry optimizations, the CAS reference was recalculated for the singlet GS and for the first triplet state. LCASPT2 calculations were performed on top of each reference with single-state orbitals. All options

were used with their default values, except for the PAO domains, which were full. This allowed us to study the effects of PNO domain sizes isolated. The basis set used in all these calculations was aug-cc-pVTZ.

The calculations to show the scaling of the computational costs with the molecular size were performed on alkyl substituted benzenes (alkyl benzenes) and on the dications of bithiophenes connected by an alkyl chain (bithiophene chains), Fig. 6.10. These conserved always the same structure, but with an increasing alkyl chain. For the alkyl benzenes the alkyl chain goes from size 0 (benzene) up to 15 (n-pentadecylbenzene). The active space consisted in all cases in the π system (CAS[6, 6]), so that the only variable in the systems is the size of the closed-shell space. All these geometries were optimized using Becke's 3-parameter, Lee-Yang-Parr Functional (B3LYP) with the aug-cc-pVDZ basis set. Even though two-state references were optimized, these calculations were performed only on one electronic state, which made unnecessary the use of level-shifts. The bithiophene chains were taken from reference (*72*), and the structures range from $n = 10$ to $n = 50$, increasing the alkyl chain by 10 carbon atoms. After performing the HF calculation and getting the IBOs for these systems, the active orbitals were optimized for these molecules in a 5 state state-averaged CAS[10, 10] reference. For the results here shown, we only used the first electronic state. The basis set used for these bithiophene chains was def2-tzvp.

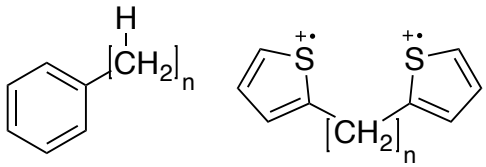

Figure 6.10: General structure for the alkyl benzenes and for the bithiophene chains used in the scaling calculations. The alkyl chain for the benzenes goes from 0 (H) to 15 (n-pentadecyl) increasing the number of carbons by a unit. The chain in the bithiophenes goes from 10 to 50, increasing the chain by 10 carbons.

6.1 CW Vs. full ICC Ansatz

In the present subsection the ic-CASPT2 and RS2C wavefunction ansätze are compared for a selected group of representative molecules. These are catechol, indole, noradrenaline, serotonin, LDopa and tryptophan. The comparison between total energies for the respective GSs and ESs is given in Table 6.1. Excitation energies using both ansätze are presented in Table 6.2. This Table also contains information about the dimensions of

the closed-shell and active spaces.

The ICC ansatz constitutes a less flexible wavefunction. It is then to expect that total energies calculated with ic-CASPT2 are slightly higher than total energies calculated using RS2C. This is observed for all the cases here investigated. The highest difference between these energies lies at 0.3 mE_h for GS energies and 0.9 mE_h for the ESs. The average difference is of 0.2 mE_h for GS and 0.4 mE_h for ES energies. We can thus corroborate that the differences between the two ansätze are indeed negligible (*43*).

Table 6.1: Comparison of total energies for GS and ES structures using RS2C and ic-CASPT2. For GSs there is a maximum difference of 0.3 mE_h, an average difference of 0.2 mE_h and a minimum difference of 0.1 mE_h. For ESs there is a maximum difference of 0.9 mE_h, an average difference of 0.5 mE_h and a minimum difference of 0.1 mE_h.

	CASSCF		RS2C		ic-CASPT2	
Molecule	E_{GS} (E_h)	E_{ES} (E_h)	E_{GS} (E_h)	E_{ES} (E_h)	E_{GS} (E_h)	E_{ES} (E_h)
Catechol	-380.54148	-380.36544	-381.67039	-381.50978	-381.67034	-381.50963
Indole	-361.60118	-361.43027	-362.74863	-362.59421	-362.74839	-362.59345
Noradrenaline	-588.52324	-588.34860	-590.32654	-590.16806	-590.32648	-590.16791
Serotonin	-569.58393	-569.41850	-571.40343	-571.26067	-571.40314	-571.25979
Ldopa	-701.28750	-701.11263	-703.40984	-703.25164	-703.40979	-703.25150
Tryptophan	-682.36146	-682.19126	-684.49864	-684.34575	-684.49839	-684.34493

Table 6.2: Comparison between excitation energies using RS2C and ic-CASPT2. Maximum difference of 16 meV, average difference of 9 meV and minimum difference of 2.5 meV. C stands for n_{closed}, and A for n_{active}.

			ΔE (eV)			
Molecule	C	A	CASSCF	RS2C	ic-CASPT2	Exp
Catechol	16	8	4.790	4.370	4.373	4.43 (*384*)
Indole	17	9	4.651	4.202	4.216	4.36 (*385*)
Noradrenaline	28	8	4.752	4.312	4.315	4.28 (*386*)
Serotonin	28	10	4.501	3.884	3.901	4.04 (*387*)
Ldopa	33	8	4.758	4.305	4.307	4.13 (*388*)
Tryptophan	34	9	4.631	4.160	4.176	4.43 (*389*)

Similarly, differences between excitation energies calculated with both ansätze are

negligible. On average there is a difference of 9 meV, and the highest difference is of 16 meV. In both cases errors are below the intrinsic error of CASPT2. These relative errors are however not necessarily derogative for ic-CASPT2 since for almost all cases the excitation energies are predicted below the experimental values.

6.2 Orbital Domains

This next section investigates how the PAO domain size and *thrpno* (PNO completion threshold) affect the accuracy of LCASPT2. The PAO domain size is an important factor controlling the accuracy of LCASPT2 in the limit of very small *thrpno_occ*. *thrpno* is a parameter balancing the fraction of correlation energy recovered for all types of pairs. This study considered: $iext = 2$ *shells*, $rext = 5$ *bohr* $(I = 2)$;[1] $iext = 0$, $rext = 2$ $(I = 0)$; $iext = 1$, $rext = 3$ $(I = 1)$; $iext = 2$, $rext = 5$, $reduce\_act = 1$ $(I = 2, RA)$; $rext = 1000$ $(full)$; $thrpno = 0$ (off) while $iext = 2$ and $rext = 5$. The set of molecules used in these studies can be found in Fig. 6.12. In all cases, the Ecorr of LCASPT2 compares against the Ecorr of ic-CASPT2.

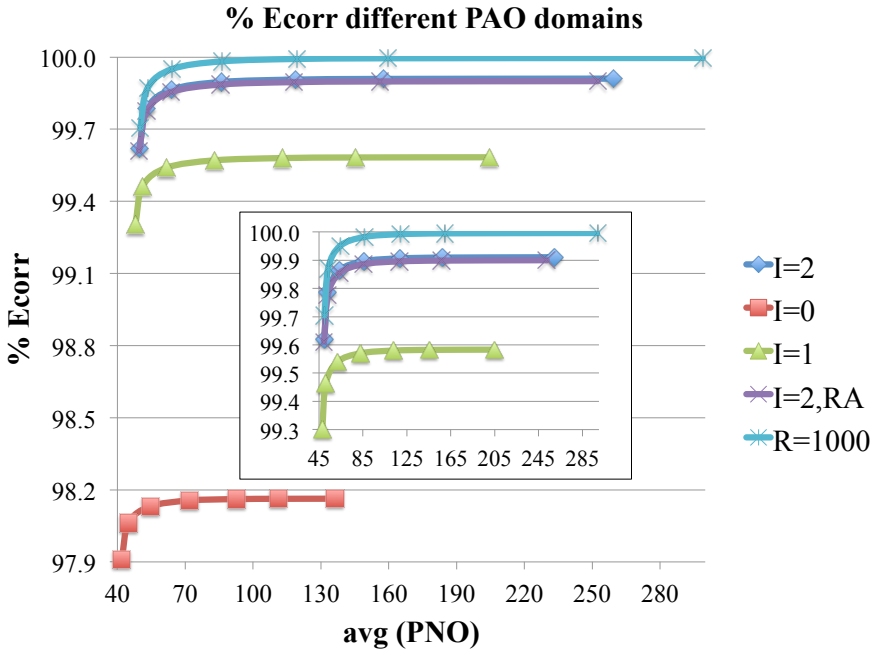

Figure 6.11: Average %Ecorr against avg(PNO) for different PAO domain sizes. *thrpno_occ* ranges from 10^{-6} to 10^{-12}. Data averaging the curves for GS and ES.

[1]From here on we omit the units in *iext* and *rext*.

Table 6.3: Average PAO domain size, the respective standard deviation (σ), coefficients of variation (c_v), minima and maxima for different PAO domain options ($iext = 2$,$rext = 5$,$reduce\_act = 1$); *thrpno* off; and ($rext = 1000$). Data averaging GS with ES.

	$I = 0$	$I = 1$	$I = 2, RA$	$I = 2$	$full$
avg	131	199	248	254	292
σ	21	22	33	37	62
c_v	0.16	0.11	0.13	0.14	0.21
min	97	144	158	158	159
MAX	185	252	293	300	395

Table 6.4: Average %Ecorr and the respective statistical data for $I = 2$ and $full$ PAO domains. σ multiplied by 100, c_v multiplied by 10^4.

		$I = 2$					$full$				
State	*thrpno_occ*	%Ecorr	σ	c_v	min	MAX	%Ecorr	σ	c_v	min	MAX
GS	10^{-6}	99.62	4.0	4.0	99.54	99.69	99.71	1.0	1.0	99.68	99.72
	10^{-7}	99.79	3.6	3.7	99.71	99.86	99.87	0.83	0.83	99.86	99.89
	10^{-8}	99.87	3.7	3.8	99.79	99.93	99.95	0.45	0.45	99.94	99.96
	10^{-9}	99.90	3.6	3.6	99.83	99.95	99.98	0.32	0.32	99.97	99.99
	10^{-10}	99.91	3.5	3.5	99.84	99.96	99.99	0.29	0.29	99.98	100.00
	10^{-11}	99.91	3.5	3.5	99.84	99.96	100.00	0.29	0.29	99.99	100.00
	10^{-12}	99.91	3.5	3.5	99.84	99.96	100.00	0.28	0.28	99.99	100.00
ES	10^{-6}	99.62	3.8	3.8	99.53	99.68	99.70	0.94	0.95	99.68	99.72
	10^{-7}	99.78	3.5	3.5	99.70	99.85	99.87	0.94	0.94	99.85	99.89
	10^{-8}	99.86	3.7	3.7	99.79	99.92	99.95	0.51	0.51	99.94	99.96
	10^{-9}	99.90	3.6	3.6	99.83	99.95	99.98	0.36	0.36	99.97	99.99
	10^{-10}	99.91	3.6	3.6	99.84	99.96	99.99	0.32	0.32	99.98	100.00
	10^{-11}	99.91	3.5	3.5	99.84	99.96	99.99	0.31	0.31	99.99	100.00
	10^{-12}	99.91	3.6	3.6	99.84	99.96	100.00	0.31	0.31	99.99	100.00

Fig. 6.11 presents the average %Ecorr recovered against avg(PNO) for different PAO domain sizes. Tables 6.4, 6.5, 8.3, 8.4, 8.5 and 8.6 provide the respective statistical data. Table 6.3 presents statistical information for the many PAO domain options. In this chapter only the Tables for $I = 2$ and $full$ PAO domains are presented. Other Tables can be found in the section 8.6.

Table 6.5: avg(PNO) and the respective statistical data for $I = 2$ and $full$ PAO domains.

		$I = 2$					$full$				
State	*thrpno_occ*	avg(PNO)	σ	c_v	min	MAX	avg(PNO)	σ	c_v	min	MAX
GS	10^{-6}	50	3	0.06	45	56	50	3	0.06	45	56
	10^{-7}	53	3	0.05	49	59	53	3	0.05	49	60
	10^{-8}	63	4	0.06	56	71	63	4	0.06	57	71
	10^{-9}	84	6	0.07	73	94	84	6	0.07	74	94
	10^{-10}	116	8	0.07	100	131	116	8	0.07	101	132
	10^{-11}	155	11	0.07	136	177	156	11	0.07	136	179
	10^{-12}	259	31	0.12	200	300	299	56	0.19	206	395
ES	10^{-6}	50	3	0.06	44	57	50	3	0.06	44	57
	10^{-7}	53	3	0.05	49	60	53	3	0.05	49	60
	10^{-8}	65	4	0.07	58	74	65	4	0.06	58	74
	10^{-9}	88	7	0.08	77	101	89	7	0.07	77	101
	10^{-10}	122	9	0.07	105	138	123	9	0.07	106	138
	10^{-11}	161	11	0.07	141	184	163	12	0.07	141	186
	10^{-12}	259	31	0.12	200	300	299	56	0.19	206	395

As expected, for each value of *thrpno_occ*, the larger the PAO domain size, the more correlation energy is recovered by LCASPT2. For full PAO domains, LCASPT2 recovers the canonical ic-CASPT2 energy given that *thrpno_occ* is sufficiently small: LCASPT2 converges thus numerically to the canonical result. Furthermore, for full recovery of the canonical energy the PNO domains do not require to be full: *thrpno_occ* $= 10^{-11}$ recovers already the canonical energy. However, full PNO domains can only be obtained with *thrpno_occ* $= 10^{-12}$ (for full PAO domains). Using full PAO domains is also the case for which LCASPT2 has less variability with respect to recovering Ecorr: the lowest σ (standard deviation) and c_v (coefficient of variation) are always obtained. The minima in %Ecorr have the largest values. This is even higher than the average for any other set of data, which shows the relative accuracy that can be reached by using full PAO domains.

By decreasing the average PAO domain size, LCASPT2 begins to recover smaller fractions of the canonical Ecorr and having more variability in %Ecorr. However, the evolution of such behavior is rather slow, and only significantly notorious for very small PAO domains. Using the default values for *iext* and *rext* causes a loss of about 0.09%

in accuracy when compared to the full PAO domain case.[2] We note furthermore that the loss in average correlation recovered is four times larger between $I = 2$ and $I = 1$ (0.32%) than it is between $full$ and $I = 2$. The difference in the accuracies between $I = 1$ and $I = 0$ grows even larger, to 1.42%. Furthermore, the difference in accuracy for these curves using different PAO domain sizes is a constant, which depends only on the PAO domain size. This means that given any two PAO domains, the difference between the respective %Ecorr is constant, as long as the same values of *thrpno_occ* are compared.

Regarding the PAO domains themselves, the behavior is as expected: for larger *iext* larger PAO domains are obtained. The set of data $full$ shows a larger variation because the PAO domains are dependent on the molecular size. For other data, the larger the PAO domain is, the larger is the variability between the domains of different molecules. This behavior is consistent with what was observed for the PNO domains. Since PAO domains are defined from distance criteria, the domain sizes are exactly the same for both GS and ES.

The effects of the option RA should still be analyzed. Reducing the domain size for the active space has barely any effect in the accuracy of LCASPT2. Differences amount in average to 0.01%. However setting $RA = 1$ increases the variability of Ecorr recovered by about 20% (σ). As for the effect on the PAO domains, using RA decreases just slightly the average domain size and the variability. Given these results, using RA may eventually just compensate when performing calculations on systems with larger active spaces.

Looking at the absolute errors of LCASPT2 using the different PAO domain options brings exactly the same conclusions regarding accuracy and variability. These results are therefore presented in the Appendix 8.6.

Next we will inspect the effect of PAO domains in calculating excitation energies. Fig. 6.12 shows the absolute errors in excitation energies using *thrpno_occ* $= 10^{-6}$, Fig. 6.13 gives the absolute errors for *thrpno_occ* $= 10^{-8}$ and Table 6.6 gives the respective statistical data. It is clear that comparative to other options, $I = 0$ gives the worst results. Nevertheless, its absolute error for both *thrpno_occ* $= 10^{-6}$ and *thrpno_occ* $= 10^{-8}$ is around 10 meV, which is still significantly below the intrinsic error of the canonical CASPT2 (about 3% of this error). For all other options, the absolute error in the excitation energies is below 5 meV, even for $I = 1$. These four sets of data are split in two groups when comparing the average absolute errors. On one side there is $I = 1$ and $I = 2, RA$ with similar accuracy and variance, on the other side there is $I = 2$ closer

[2] This value was calculated using $\%E_{corr}^{rext=1000} - \%E_{corr}^{iext=2,rext=5}$

to the *full* results. Even though $I = 2, RA$ resembles in average %Ecorr the behavior of $I = 2$, when it comes to calculating excitation energies it resembles the behavior of $I = 1$. Since the only difference is in the dimension of the domains for the active space, we verify the importance of keeping active domains as large as possible. The origin for the formation of these two sets of results is the main source of the errors. For $I = 2$ and *full* the errors from PNO domains are comparable to the errors from the PAO domains. For $I = 0$, $I = 1$ and $I = 2, RA$ errors are dominated by the PAO domain size.

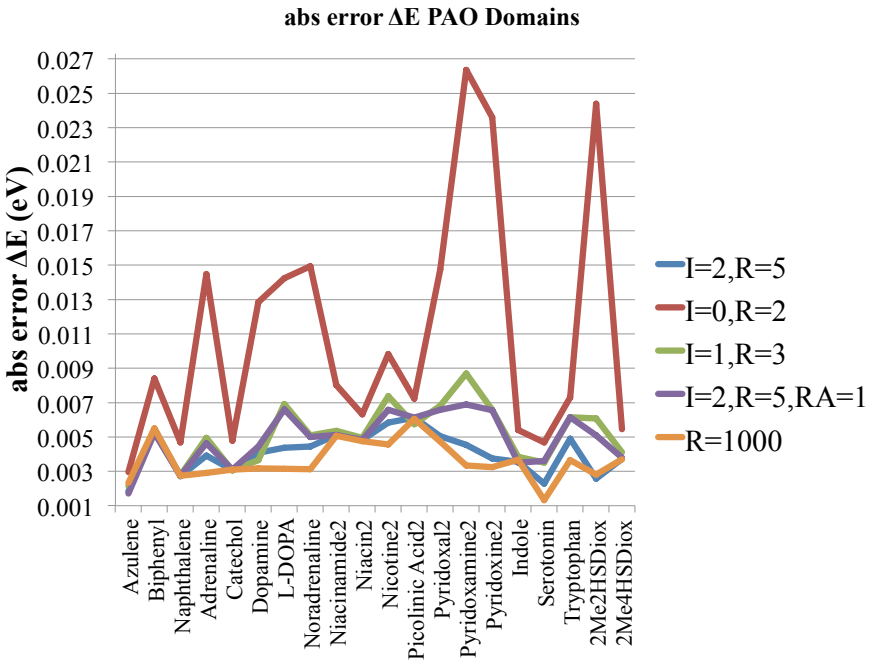

Figure 6.12: Absolute error on excitation energies (ΔE) in eV using $thrpno\_occ = 10^{-6}$. Comparison for different PAO domain sizes.

Although not stressed out in the way the data is represented, the differences between different PAO domain sizes increase with the molecular size. This can be seen elsewhere (*242*), where the molecules are organized differently, not according to their type but according to the sizes of the closed-shell and active spaces.

Due to the division of the results in two groups, using full domains does not improve significantly the excitation energies over the default PAO domain options, especially for $thrpno\_occ = 10^{-8}$. This stresses that with LCASPT2 the best compromise between accuracy and computational cost can be obtained using $iext = 2$, $rext = 5$ and $thrpno\_occ = 10^{-8}$.

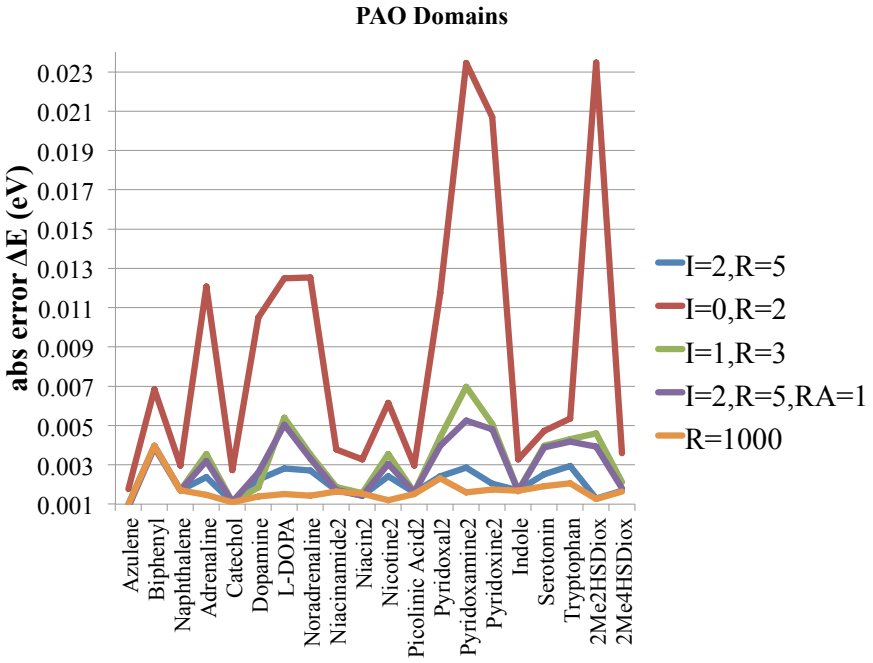

Figure 6.13: Absolute error on excitation energies (ΔE) in eV using $thrpno\_occ = 10^{-8}$. Comparison for different PAO domain sizes.

Table 6.6: Average error in excitation energies and the respective statistical data.

		$I=2$	$I=0$	$I=1$	$I=2, RA$	$full$
10^{-6}	avg	3.8	10.7	4.9	4.6	3.4
	σ	1.2	6.9	1.7	1.4	1.1
	c_v	0.3	0.6	0.3	0.3	0.3
	min	1.5	2.7	1.9	1.4	1.0
	MAX	5.8	26.1	8.4	6.6	5.8
10^{-8}	avg	2.1	8.7	3.2	3.0	1.7
	σ	0.7	6.8	1.6	1.4	0.6
	c_v	0.3	0.8	0.5	0.5	0.4
	min	1.0	1.8	0.9	0.9	1.0
	MAX	4.0	23.5	7.0	5.3	4.0

Fig. 6.14 evaluates the effects of the PNO energy completion threshold, *thrpno*, by comparing the results with and without this threshold. As it is shown, there is only an actual difference between having $thrpno = 0.997$ and having this threshold off ($thrpno = 0$) for $thrpno\_occ = 10^{-6}$ and $thrpno\_occ = 10^{-7}$. For $thrpno\_occ = 10^{-8}$ the difference is

negligible, both in %Ecorr and in avg(PNO). For even smaller *thrpno_occ* the difference vanishes, converging both cases to the same result. It is normal for *thrpno* to affect more %Ecorr for larger *thrpno_occ*, since this parameter ensures a minimum energy quality for the PNO domains built. Making $thrpno = 0.997$ is almost equivalent to decreasing *thrpno_occ* by an order of magnitude when using $thrpno = 0$. When $thrpno\_occ = 10^{-6}$ and $thrpno = 0.997$, the energy driven threshold dominates completely the building of the PNO domains, as previously proposed. Besides improving the accuracy of LCASPT2 and bringing balance to the correlation treatment of all pairs, *thrpno* brings uniformity to the calculation. Analysis of the absolute errors for $thrpno = 0.997$ and *thrpno* off simply reinforce the conclusions made above. This plot is also in Appendix 8.6.

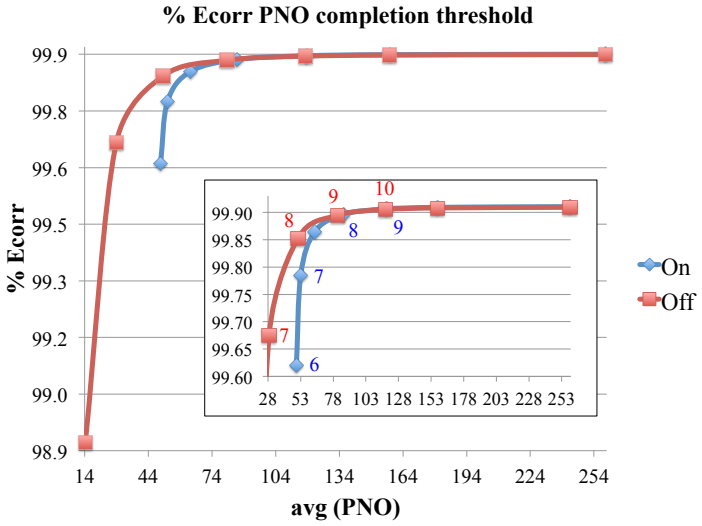

Figure 6.14: Average %Ecorr against avg(PNO) for $thrpno = 0.997$ and off. *thrpno_occ* ranges from 10^{-6} to 10^{-12}. Data was obtained by averaging the curves for GS, and ES.

Finally there is the effect of $thrpno = 0$ on excitation energies. Fig. 6.15 shows the rapid convergence of the excitation energies for different values of *thrpno_occ*. For $thrpno\_occ = 10^{-8}$ excitation energies are already converged, with an average absolute error of 2 meV. This is the same when using $thrpno = 0.997$. For $thrpno\_occ = 10^{-6}$ and $thrpno = 0$ the average absolute error is around 24 meV, which is 6 times higher than the average absolute error for the same conditions but with $thrpno = 0.997$. These are also the largest errors we have seen in excitation energies, which emphasize the dominance of the energy threshold in building the PNO domains for smaller *thrpno_occ*. While when $thrpno = 0.997$ one can afford to go to larger *thrpno_occ* without a significant loss in accuracy and increasing of the variability, whenever $thrpno = 0$ that is no longer possible.

To keep the average absolute error below 5 meV $thrpno\_occ = 10^{-8}$ is required, reinforcing our choice for the default value for this threshold. Due to the results here presented, from here on the energy completion threshold has always the default value of 0.997.

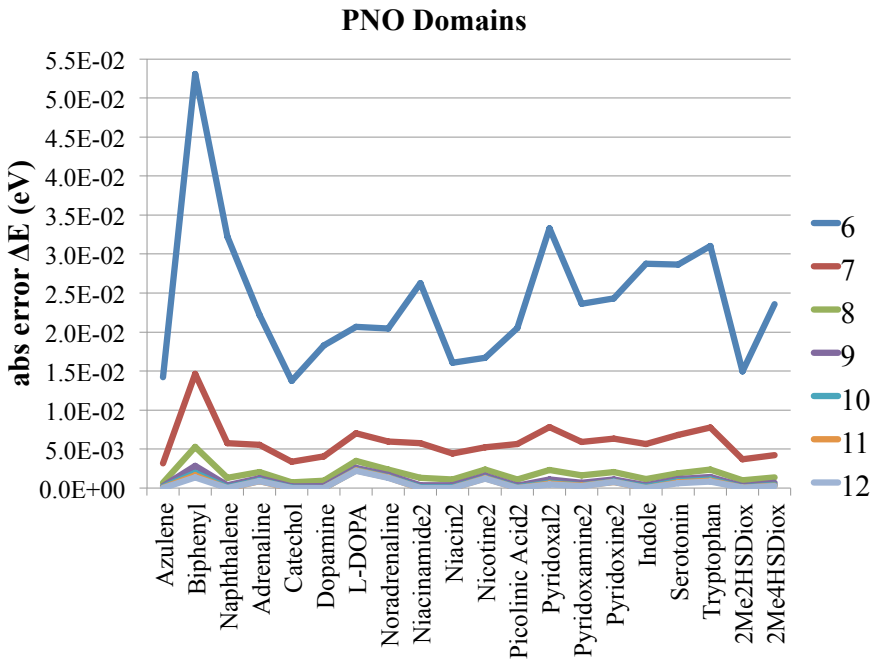

Figure 6.15: Absolute error on excitation energies (ΔE) in eV using $thrpno\_occ$ ranging from 10^{-6} to 10^{-12}.

6.3 Accuracy

To test the accuracy of LCASPT2, calculations on all systems presented in Figs. 6.1-6.7 were performed. This full test set was named "Medium Molecules". Fig. 6.16 presents the convergence of Ecorr with avg(PNO) for this sample of molecules, for both GSs and ESs. Note that we present curves for the average, minima and maxima of this sample. The respective data is presented in Tables 6.7 and 6.8. In these calculations $thrpno\_occ$ ranges from 10^{-6} to 10^{-12}. Domain sizes for PAOs were the default, *i.e.*, $iext = 2$ and $rext = 5$. The average size of PAO domains did not vary within a molecule.

As expected, as $thrpno\_occ$ decreases, both the %Ecorr and avg(PNO) increase. The error in Ecorr for LCASPT2 is with 115-120 PNOs converged (but not to zero). This corresponds to $thrpno\_occ = 10^{-10}$. However, using $thrpno\_occ = 10^{-8}$ introduces an error of $0.3 - 0.4\%$ in Ecorr, which is negligible. Using this threshold there are typically 60-65 PNOs per domain, a significant reduction of the canonical substitution spaces. We

also point out that the behavior of the average is closer to the behavior of the minima for avg(PNO) but closer to the behavior of the maxima when it comes to %Ecorr. This means that for most of the systems the accuracy is maximized and the domains are minimized.

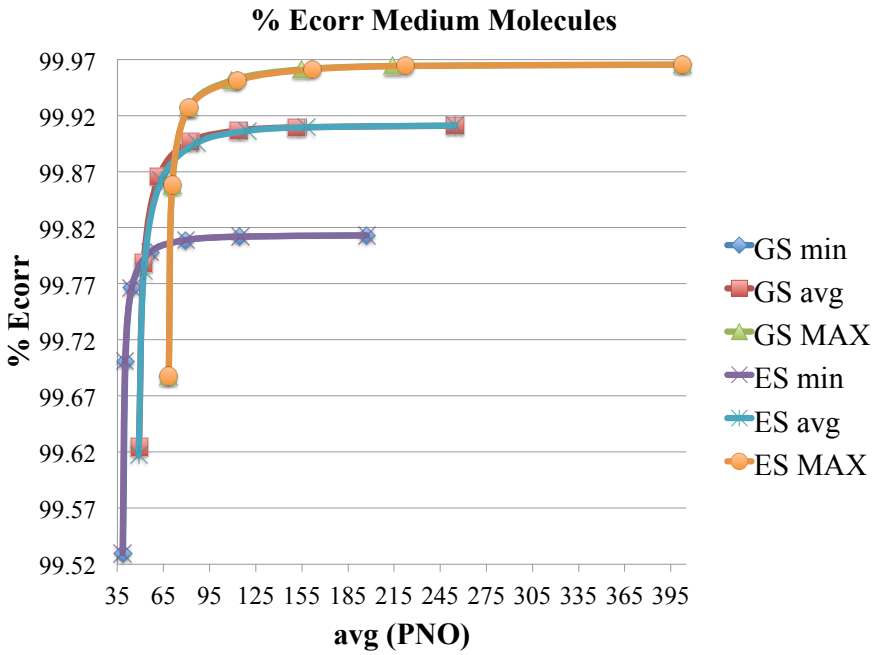

Figure 6.16: Average %Ecorr against avg(PNO) for medium molecules. *thrpno_occ* ranges from 10^{-6} to 10^{-12}.

Although both the curves for GSs and ESs are almost overlapping, the former has a slightly faster convergence. Therefore, excitation energies are all going to be predicted by excess. Fig. 6.17 shows the absolute error for $thrpno\_occ = 10^{-6}$ and $thrpno\_occ = 10^{-8}$ for both GSs and ESs of all systems, which stresses the difference in the Ecorr recovered for both GS and ES. This difference in Ecorr recovered is small and tends to decrease with *thrpno_occ*. For $thrpno\_occ = 10^{-8}$ the curves for the absolute errors in Ecorr for GSs and ESs are visually overlapping for almost all cases (not numerically though). For smaller *thrpno_occ* (10^{-6}) the domains and the recovery of Ecorr become larger and more consistent for all types of pairs, because the energy completion threshold dominates. This ensures that all pairs are somehow treated with more consistency. Only for $thrpno\_occ = 10^{-7}$ some closer pairs are better described than some more distant pairs. And of all, $thrpno\_occ = 10^{-7}$ shows larger discrepancies between the two curves, even though for a few molecules $thrpno\_occ = 10^{-8}$ can also be affected. We associate this unbalance with the origin for the difference in the amount of Ecorr recovered around $thrpno\_occ = 10^{-7}$

for different electronic states.

Table 6.7: Average %Ecorr, the respective standard deviation (σ), coefficients of variation (c_v; multiplied by 10^4), the minimum (min) and the maximum (MAX) for the medium molecules.

	GS					ES				
thrpno_occ	avg	σ	c_v	min	MAX	avg	σ	c_v	min	MAX
10^{-6}	99.62	0.05	4.9	99.53	99.69	99.62	0.05	4.7	99.53	99.69
10^{-7}	99.79	0.05	4.5	99.70	99.86	99.78	0.04	4.4	99.70	99.86
10^{-8}	99.87	0.05	4.5	99.77	99.93	99.86	0.04	4.5	99.77	99.93
10^{-9}	99.90	0.04	4.3	99.80	99.95	99.90	0.04	4.4	99.80	99.95
10^{-10}	99.91	0.04	4.2	99.81	99.96	99.91	0.04	4.3	99.81	99.96
10^{-11}	99.91	0.04	4.2	99.81	99.96	99.91	0.04	4.3	99.81	99.96
10^{-12}	99.91	0.04	4.2	99.81	99.97	99.91	0.04	4.3	99.81	99.97

Table 6.8: avg(PNO), the respective standard deviation (σ), coefficients of variation (c_v), the minimum (min) and the maximum (MAX) for the test set of medium molecules.

	GS					ES				
thrpno_occ	avg(PNO)	σ	c_v	min	MAX	avg	σ	c_v	min	MAX
10^{-6}	49	5	0.09	39	69	49	5	0.10	38	68
10^{-7}	52	5	0.09	40	71	52	5	0.09	40	71
10^{-8}	62	6	0.10	44	81	64	6	0.10	44	82
10^{-9}	82	9	0.10	56	110	87	10	0.11	56	113
10^{-10}	114	12	0.10	79	155	120	13	0.11	80	162
10^{-11}	152	16	0.11	114	214	158	17	0.11	115	222
10^{-12}	255	39	0.15	197	402	255	39	0.15	197	402

To analyze how scattered the data is we should look at the respective standard deviations (σ) and coefficients of variation (c_v). The σ's for %Ecorr barely change with *thrpno_occ*. Because %Ecorr increases then the c_v's have to decrease with *thrpno_occ*. However, such decrease of the c_v stagnates between *thrpno_occ* $= 10^{-9}$ and *thrpno_occ* $= 10^{-10}$, meaning that LCASPT2 reaches its limit in both accuracy and consistency (scatter of results). This point marks thus the numerical convergence of LCASPT2 with *thrpno_occ*. On the other hand, the c_v's tend to increase for avg(PNO). This means that

as avg(PNO) increases, so does the scattering of the domain sizes. This behavior is expected since larger PNO domains should become closer to full canonical virtual spaces, which differ greatly for all the cases studied. To keep the PNO domains as independent as possible from the molecular size larger values of *thrpno_occ* should be used. We should note that from $thrpno\_occ = 10^{-6}$ to $thrpno\_occ = 10^{-7}$ the σs for avg(PNO) have the tendency to decrease. This is again an effect of the completion threshold.

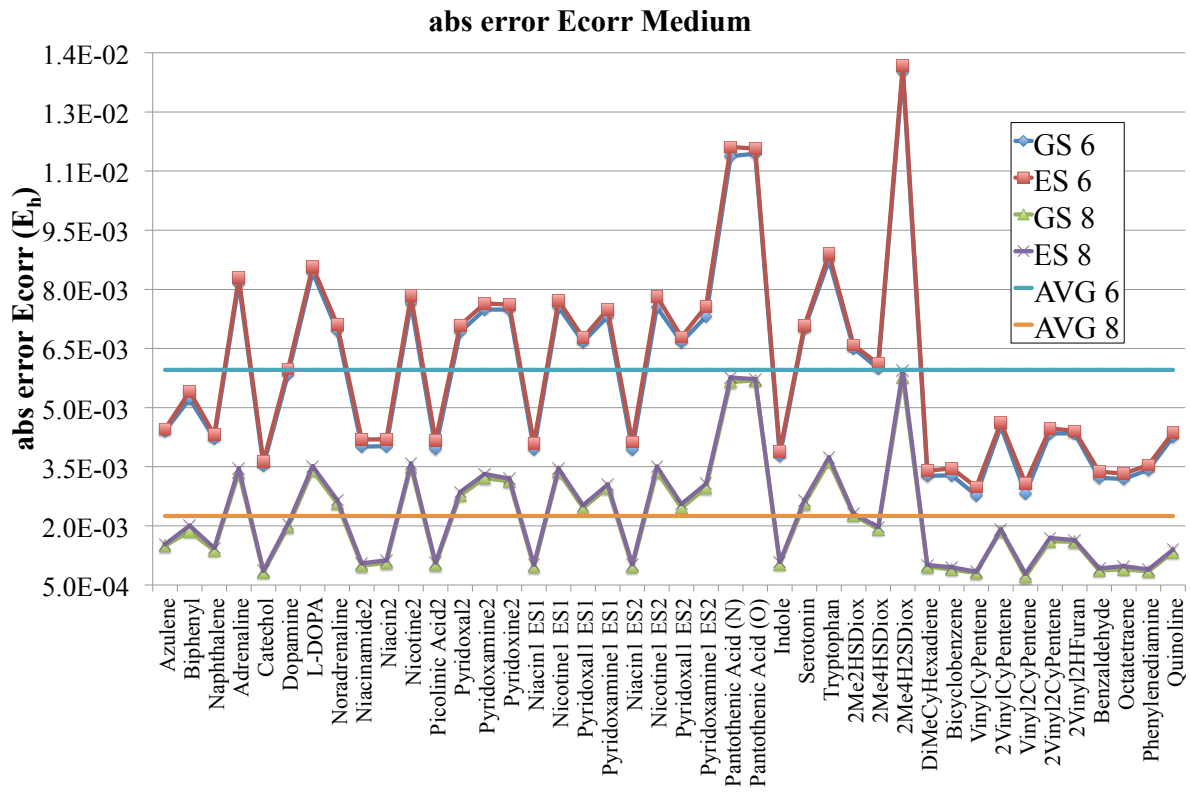

Figure 6.17: Absolute error on Ecorr in E_h on medium molecules for $thrpno\_occ = 10^{-6}$ (6) and $thrpno\_occ = 10^{-8}$ (8). The average absolute errors are 6.0 mE_h for $thrpno\_occ = 10^{-6}$ and 2.3 mE_h for $thrpno\_occ = 10^{-8}$.

Fig. 6.18 shows the absolute error in excitation energies (ΔE) in eV for $thrpno\_occ = 10^{-6}$ and $thrpno\_occ = 10^{-8}$.[3] On the average, $thrpno\_occ = 10^{-8}$ is more accurate than $thrpno\_occ = 10^{-6}$: the average absolute error for $thrpno\_occ = 10^{-8}$ is half of the average error for $thrpno\_occ = 10^{-6}$. The standard deviation also decreases with *thrpno_occ* but not as much as the average absolute error. It can be visually observed that the smaller the value of *thrpno_occ*, the more consistent are the calculated excitation

[3]In the next subsection the absolute values of excitation energies are analyzed.

energies and the less scattered the results are. Nevertheless, there are some cases for which $thrpno\_occ = 10^{-6}$ is more accurate than $thrpno\_occ = 10^{-8}$. These cases arise from fortuitous error compensation and from the fact that %Ecorr converges differently with avg(PNO) for GSs and ESs. We note furthermore that as expected, LCASPT2 ceils the canonical ic-CASPT2 excitation energies.

Finally the samples should be analyzed for outliers. Outliers are outside the range of the region between the first ($Q1$) and the third ($Q3$) quantiles.[4] We found three outliers for $thrpno\_occ = 10^{-6}$ (second ES of Nicotine1 and Pyridoxamine1 as well as Vinyl2CyPentene) and two outliers for $thrpno\_occ = 10^{-8}$ (Biphenyl and 2Me4H2SDiox). All outliers lay beyond $Q3$ and never below $Q1$. For the case of $thrpno\_occ = 10^{-8}$ these outliers are exactly the same molecules having larger differences in the absolute errors of the correlation energy for GS and ES (*c.f.* Fig. 6.17). Because of the sizes of the samples (42 molecules) and the reduced number of outliers (5% or less) the sample chosen is well balanced and consistent.

Table 6.9: Statistical data for excitation energies of medium molecules with $thrpno\_occ = 10^{-6}$ and $thrpno\_occ = 10^{-8}$. Data in meV, if applicable.

thrpno_occ	avg	σ	c_v	min	MAX
10^{-6}	4.2	1.4	0.3	1.5	7.9
10^{-8}	2.1	0.8	0.4	1.0	4.5

Even though the default $thrpno\_occ$ (10^{-8}) has a more consistent and accurate behavior, using $thrpno\_occ = 10^{-6}$ does not lead to a significant increase of the absolute errors (there is a difference below 5 meV between samples) nor to a significant decrease in the consistency and scattering of the results. Our results are consistent to the results of PNO-LMP2, for which 60 PNOs offer the best compromise between accuracy and CPU time (*148*). Even though we still recommend to use the default value of $thrpno\_occ = 10^{-8}$, for very large systems $thrpno\_occ = 10^{-6}$ can be safely used without much loss in accuracy or consistency.

[4]The median ($\bar{M}$) was determined just like the values of $Q1$ and $Q3$. From these $\bar{Q}1 = \bar{M} - Q1$ and $\bar{Q}3 = Q3 - \bar{M}$ were calculated. The interquantile range between $Q1$ and $Q3$ is given by the interval $\left[Q1 - 1.5\bar{Q}1, Q3 + 1.5\bar{Q}3\right]$. Outliers lay outside this interval.

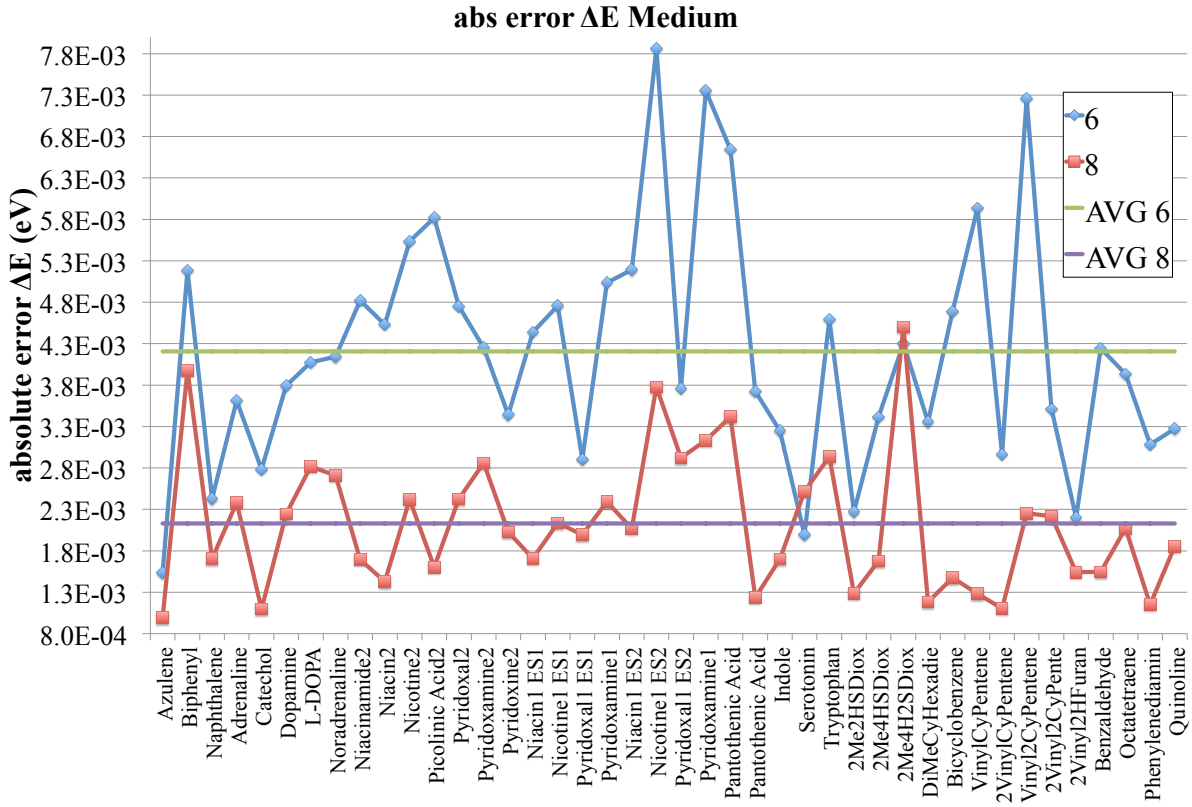

Figure 6.18: Absolute error of excitation energies (ΔE) in eV on medium molecules for $thrpno\_occ = 10^{-6}$ (6) and $thrpno\_occ = 10^{-8}$ (8).

6.3.1 Excitation Energies

As seen in the previous section, excitation energies calculated with LCASPT2 converge to the respective canonical results as *thrpno_occ* goes to zero and as the PAO domain sizes increase. In section 6.4 we will present a plot showing the convergence of the excitation energy of picolinic acid with *thrpno_occ* for many basis sets (Fig. 6.23). The convergence behavior we will see there is quite general and was observed for all molecules studied in section 6.3. But as important as verifying that errors tend to zero is to compare the calculated results with experimental values. A purely vertical excitation energy is never measured, since the transition occurs to the Franck-Condon structure. Nevertheless, we can assume that the Frank-Condon structure is almost the same as the minimum in the GS's PES. As such, we can compare the calculated (vertical) excitation energies with maxima in absorption spectra. This is the comparison made in this section.

Table 6.10: Comparison between experimental and calculated excitation energies for a sample of the medium molecules. Errors of LCASPT2 presented for $thrpno\_occ = 10^{-6}$ and $thrpno\_occ = 10^{-8}$.

	ΔE (eV)		Error LCASPT2 (meV)	
	Experimental	ic-CASPT2	10^{-6}	10^{-8}
Azulene	1.78 (*390*)	1.912	1.5	1.0
Benzene	4.86 (*391*)	4.595	4.6	0.6
Biphenyl	3.80 (*392*)	3.852	5.2	4.0
Naphthalene	3.97 (*393*)	3.791	2.4	1.7
Adrenaline	4.51 (*394*)	4.309	3.6	2.4
Catechol	4.43 (*384*)	4.373	2.8	1.1
Dopamine	4.43 (*395*)	4.306	3.8	2.2
LDOPA	4.13 (*388*)	4.307	4.1	2.8
Noradrenaline	4.28 (*386*)	4.315	4.1	2.7
Niacinamide	4.68 (*396*)	4.572	4.8	1.7
Niacin2	4.68 (*396*)	4.538	4.5	1.4
Niacin1	4.68 (*396*)	4.546	4.4	1.7
Nicotine2	4.77 (*397*)	4.604	5.5	2.4
Nicotine1	4.77 (*397*)	4.620	4.8	2.1
Picolinic Acid	4.68 (*398*)	4.554	5.8	1.6
Pyridine	4.86 (*399*)	4.688	4.7	0.8
Pyridoxal2	3.78 (*400*)	3.803	4.8	2.4
Pyridoxal1	3.78 (*400*)	3.774	2.9	2.0
Pyridoxamine2	4.84 (*401*)	4.351	4.2	2.9
Pyridoxamine1	4.84 (*401*)	4.390	5.0	2.4
Pyridoxine	3.96 (*402*)	4.305	3.4	2.0
Indole	4.36 (*385*)	4.216	3.2	1.7
Pyrrole	5.90 (*403*)	5.825	4.5	0.4
Serotonin	4.04 (*387*)	3.901	2.0	2.5
Tryptophan	4.43 (*389*)	4.176	4.6	2.9
Thiophene	5.17 (*404*)	5.193	4.0	0.1
2Me2HSDiox	1.55 to 1.13 (*405*)	4.801	2.3	1.3
2Me4HSDiox	1.55 to 1.13 (*405*)	4.570	3.4	1.7
2Me4H2SDiox	1.55 to 1.13 (*405*)	4.271	4.3	4.5

Table 6.10 presents the experimental excitation energies, the ones calculated using ic-CASPT2 and the magnitude of the errors introduced by the local treatment. Contrary to excitation energies, which are presented in eV, errors are presented in meV. For the cases of 2Me2HSDiox, 2Me4HSDiox and 2Me4H2SDiox we calculated the excitation energies of two monomers and a dimer. Experimental values are however only available for the polymer. As such, experimental and calculated excitation energies are not matching. For consistency, we give the values for the excitation energy of the polymer in Table 6.10.

As can be seen in Table 6.10, all calculated excitation energies are very close to experimental values. For LCASPT2 there is in average a difference of 160 meV for both $thrpno\_occ = 10^{-6}$ and $thrpno\_occ = 10^{-8}$ towards the experimental values. The maximum errors observed are of 490 meV for pyridoxamine and 350 meV for pyridoxine. these errors decrease slightly by increasing the size of the active spaces. The smallest error is curiously of 3 meV for pyridoxal. Considering the similarities between structures, it is doubtful that these differences in excitation energies arise from the (in)adequacy of the active spaces. It is more likely that the contrast between experimental and theoretical values comes from some other effect, which was not accounted for in the calculations. We remind the reader that the difference between the molecules is in the functional group *para* with respect to the nitrogen in the pyridine ring: pyridoxal has an aldehyde group; pyridoxine has an alcohol; pyridoxamine an amine group.

6.3.2 Reaction Energies

This section is dedicated to the convergence of reaction energies with *thrpno_occ*. Calculations were performed on the reactions in Fig. 6.19. We considered additions of carbenes to alkenes or aldehydes, which correspond to numbered reactions. An electrocyclization reaction is also presented.

Fig. 6.20 presents the convergence of errors in reaction energies with avg(PNO) for the reactions with carbenes. These errors are presented in $kcal.mol^{-1}$. For all these reactions, using $thrpno\_occ = 10^{-8}$ yields errors below 1 $kcal.mol^{-1}$ with respect to ic-CASPT2. The average error lies at 0.42 $kcal.mol^{-1} = 18\ meV$, which is 8-9 times larger than the errors in excitation energies. LCASPT2 introduces thus larger errors in the prediction of reaction energies than it does for excitation energies. These errors are still reducing for $thrpno\_occ < 10^{-8}$. For larger systems, like reactions 8 and 9 with cinnamaldehyde, the decrease in errors is however less significant. The difference between reaction and excitation energies is that there should not be any close relation between the convergence

behavior of reagents and products. As such, convergence curves of Ecorr with avg(PNO) for products and reagents may differ more than these curves for different electronic states. This justifies why $thrpno\_occ = 10^{-7}$ does not show in reaction energies a particularly bad result when compared to $thrpno\_occ = 10^{-6}$. We can observe for all cases, that even though close to, $thrpno\_occ = 10^{-7}$ improves over $thrpno\_occ = 10^{-6}$. Errors of individual reaction energies calculated with LCASPT2 do not go necessarily to zero when comparing with the canonical calculation. These differences should depend on the molecular size, and the larger the molecules, the larger the restrictive effect of the PAO domain sizes. But more importantly, all these reactions consist in additions: the reagents are calculated in the same geometry file and both molecules are separated by a large distance; products are always a single molecule. The PAO domain sizes for the reagents as an ensemble will not match the PAO domains for the products, unlike the case of excitation energies. Exceptions, *e.g.* reaction 8, can be accounted by error compensation.

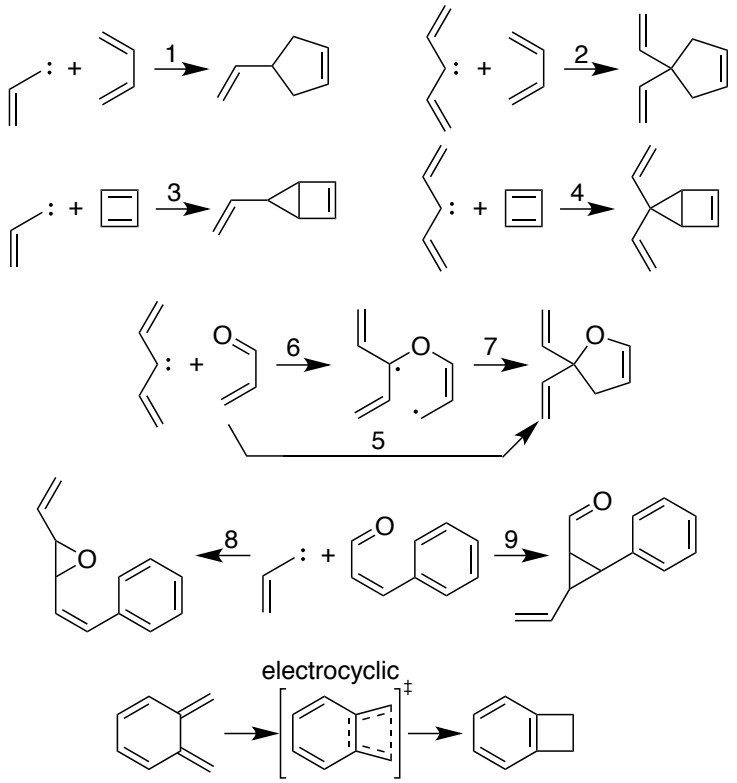

Figure 6.19: Schemes of the reactions studied using LCASPT2.

To verify the validity and pertinence of these CASPT2 calculations on the carbene reactions, the results are compared to local unrestricted SR methods. Table 6.11 presents the energies for the reactions with carbenes calculated using ic-CASPT2, LRMP2, LUCCSD

and LUCCSD(T0). All reaction energies are calculated using one geometry file for both reagents. For reactions 8 and 9 the reagents were optimized together, meaning that also the intermolecular distance was optimized. Contrary to other cases, the reagents for reactions 8 and 9 are only 2.2 Å apart. For reactions 1-6 the carbenes have a purely planar structure, with all atoms coplanar. In the cinnamaldehyde+carbene pair of reagents (reactions 8 and 9), the hydrogen atom bonded to the carbon with the carbene character is out-of-plane. However, all other atoms in the carbene are coplanar.

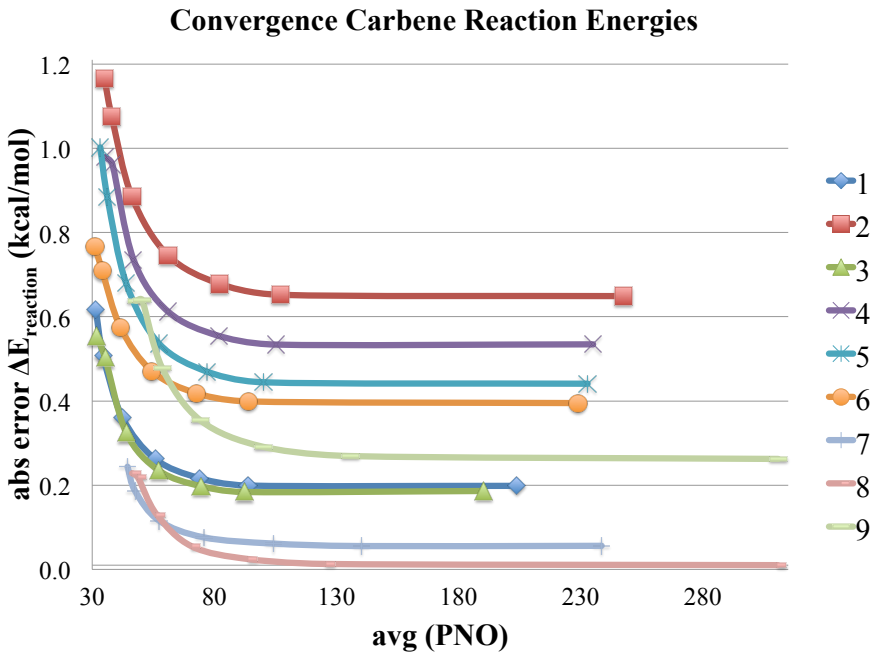

Figure 6.20: Convergence of carbene reaction energies with avg(PNO) for LCASPT2. Data in $kcal.mol^{-1}$.

SR theories cannot describe the MR character of these two simple carbenes. Only other MR methods can. But the active spaces found might not be adequate to describe these reactions. We also did not find experimental values to corroborate these results. However, the first triplet states of the carbenes have a dominant SR character. With balances of energies the reaction energies were calculated with the triplet carbene and then converted into singlet reaction energies. The conversion took place by adding the CASPT2 singlet-triplet splittings for the carbenes. The derivation of the expressions used to estimate the SR reaction energies is schematized in Appendix 8.7. The singlet-triplet splittings we calculated for the carbenes are 4.34 $kcal.mol^{-1}$ for carbene and 2.71 $kcal.mol^{-1}$ for carbene2.

Table 6.11: Energies for the carbene reactions for ic-CASPT2, LRMP2, LUCCSD and LUCCSD(T).

	ΔE ($kcal.mol^{-1}$)			
Reaction	ic-CASPT2	LRMP2	LUCCSD	LUCCSD(T0)
1	-117.79	-115.99	-106.33	-106.86
2	-105.97	-105.19	-96.43	-96.91
3	-124.06	-124.21	-112.42	-112.60
4	-113.41	-114.64	-106.15	-106.35
5	-92.22	-88.82	-82.84	-83.26
6	-29.95	—	—	—
7	-62.27	—	—	—
8	-70.73	-79.30	-69.80	-71.60
9	-85.01	-91.80	-83.36	-84.07

As Table 6.11 shows, the only two reaction energies for which the CASPT2 energies agree with the LUCC energies are the cinnamaldehyde reactions (8 and 9). For the first 5 reactions there are differences ranging from 7 to 11.5 $kcal.mol^{-1}$ between CASPT2 and LUCC, which is *ca.* 10% of the reaction energies. We could hypothesize the discrepancies arise from the active spaces. But since all these active spaces were built analogously and the reactions have the same character, it is not likely for that to be the dominant effect. We could also hypothesize the differences come from some MR character in the triplet carbenes, but the references for all carbenes have similar (SR) composition. Comparing the LCASPT2 reaction energies with the LRMP2 reaction energies we verify that the energies are in better agreement for the cases of reactions 1-5. The differences in these reaction energies should then arise from the different description that PT and CC provide for the correlation energy.

Finally, we would like to analyze the performance of LCASPT2 on a purely SR system. This is the electrocyclic ring closure of 2Me(ene)Hexadiene to 2CyBenzene. The results of our calculations are presented in Table 6.12. For this reaction LCASPT2 was used, which compares once more with LRMP2, LUCCSD and LUCCSD(T0). As can be seen, the LCASPT2 energies for this reaction are in very good agreement with the LUCC results. Differences amount to 0.2-2 $kcal.mol^{-1}$, where the largest differences are for the activation energy E_a. LCASPT2 and LRMP2 only agree in the activation energy. As for basis sets, both aug-cc-pVDZ and aug-cc-pVTZ yield very consistent reaction energies, which differ

by 1 $kcal.mol^{-1}$ (6%). Activation energies appear to be less consistent with a difference of 6.5 $kcal.mol^{-1}$. We note however that this energy has another order of magnitude, meaning that the differences are quite similar (8%). For the more interested reader, Appendix 8.7 presents an orbital diagram, which justifies why this particular electrocyclic reaction is forbidden in the GS, accounting for the magnitude of the activation energy.

Table 6.12: Reaction (ΔE_{rx}) and activation (E_a) energies calculated for the electrocyclic reaction using LCASPT2, LRMP2m LUCCSD and LUCCSD(T0) with aug-cc-pVTZ and aug-cc-pVDZ.

Basis Set	Method	avg(PNO)	E_a ($kcal.mol^{-1}$)	ΔE_{rx} ($kcal.mol^{-1}$)
aug-cc-pVTZ	LCASPT2 10^{-6}	90	111.73	-12.45
aug-cc-pVTZ	LCASPT2 10^{-8}	111	111.68	-12.56
aug-cc-pVDZ	LCASPT2 10^{-6}	47	105.05	-11.51
aug-cc-pVDZ	LCASPT2 10^{-8}	63	105.03	-11.56
aug-cc-pVDZ	LRMP2	—	102.88	-18.80
aug-cc-pVDZ	LUCCSD	—	108.17	-12.50
aug-cc-pVDZ	LUCCSD(T0)	—	103.19	-11.84

6.4 Basis Sets

This section studies the convergence of correlation and excitation energies of LCASPT2 for different basis sets. Using the default PAO domain option ($iext = 2$, $rext = 5$) *thrpno_occ* was varied from 10^{-6} to 10^{-12} for both aug-cc-pVDZ and aug-cc-pVTZ (*c.f.* Fig. 6.22 for the set of molecules used in this study). The convergence of Ecorr with avg(PNO) is given in Fig. 6.21. The respective statistical data is presented in Tables 8.7 and 8.8 in Appendix 8.8. As depicted in Fig. 6.21, the convergence curves for both basis sets are very similar, although for larger *thrpno_occ* the double-ζ basis set shows higher accuracy than the triple-ζ basis. But for *thrpno_occ* = 10^{-8} both bases become already equally accurate, meaning that all domain errors become similar. Furthermore, the PNO domain size relative to the full virtual space grows slower for aug-cc-pVTZ. Therefore, aug-cc-pVTZ shows a better convergence behavior, reaching earlier the maximum accuracy possible. This can be seen by plotting the reduced curves for each basis set (dividing each variable by the maximum value it takes, eg, $\frac{[avg(PNO)]^{thrpno\_occ=x}}{[avg(PNO)]^{thrpno\_occ=10^{-12}}}$).

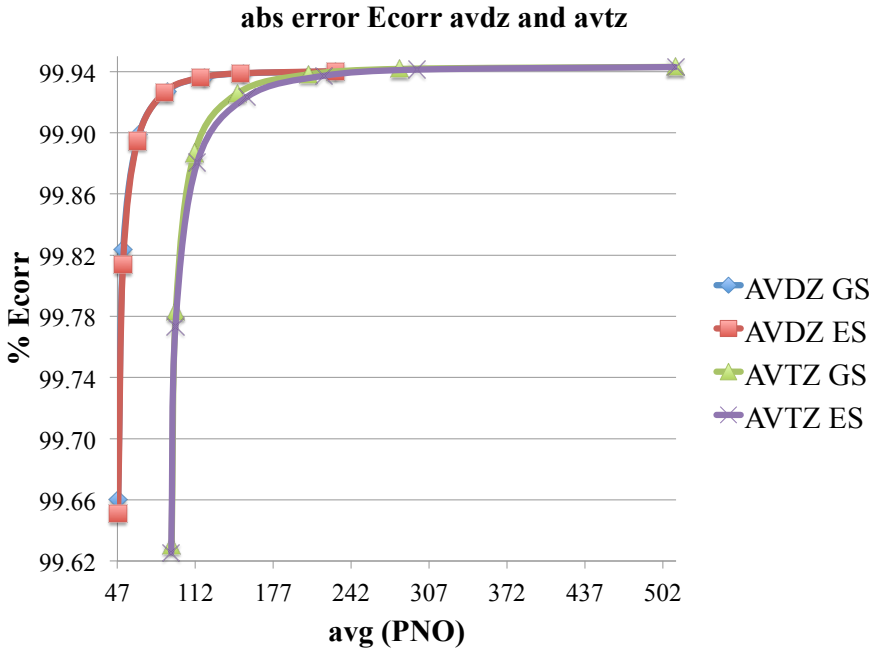

Figure 6.21: Average %Ecorr against avg(PNO) for aug-cc-pVDZ and aug-cc-pVTZ. *thrpno_occ* ranges from 10^{-6} to 10^{-12}.

The average %Ecorr recovered increases with decreasing *thrpno_occ* but the standard deviation remains practically unchanged. This agrees with previous results, for which for decreasing *thrpno_occ* LCASPT2 becomes more accurate, with less scattered results. avg(PNO) behaves also similarly to what was previously observed. We note furthermore that the scattering of the PNO domain sizes is independent of the basis set. For the recovered Ecorr on the other hand, the larger basis set shows less scattered results. aug-cc-pVTZ is thus more consistent for this test sample. We can therefore infer that LCASPT2 shows a better behavior in the convergence of Ecorr for larger basis sets. The analysis of absolute errors on Ecorr for the two basis sets simply reinforces the conclusions so far taken. Therefore, the comparison between absolute errors for this sample of molecules and for these basis sets is relegated to Appendix 8.8.

Finally, Fig. 6.22 presents the absolute errors in excitation energies for aug-cc-pVDZ and aug-cc-pVTZ. In both cases, the smaller *thrpno_occ*, the smaller the average absolute error in excitation energies. The improvement of excitation energies with *thrpno_occ* is more significant for aug-cc-pVDZ. For aug-cc-pVTZ the decrease in errors is softer.

The standard deviation for aug-cc-pVDZ also decreases with *thrpno_occ*, but the one for aug-cc-pVTZ increases. Even though biphenyl is an outlier in the aug-cc-pVTZ set, excluding these results does not improve the order of the σ for this basis set. Nevertheless,

the c_v's show similar values and trends for both aug-cc-pVDZ and aug-cc-pVTZ, results which are consistent with section 6.3. Therefore, we will not place much relevance in the behavior of the σ's for this particular case. From the average absolute errors and the respective standard deviations we infer it is better to use $thrpno\_occ = 10^{-8}$ when calculating excitation energies for the basis set aug-cc-pVDZ, consistent with our previous conclusions. For aug-cc-pVTZ the gain in decreasing *thrpno_occ* is not as significant. This may however be an artifact of the size of the sample here used.

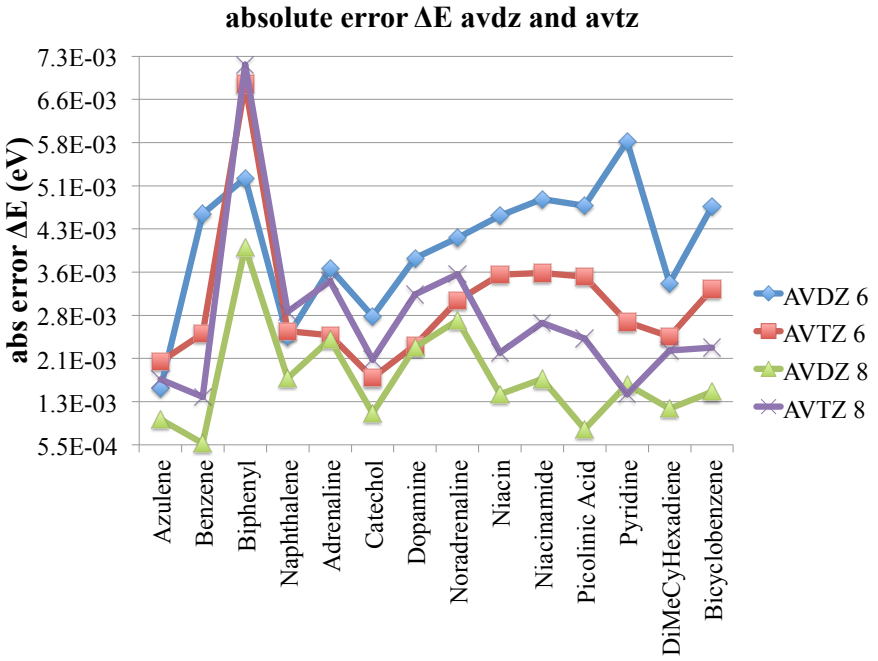

Figure 6.22: Absolute error on excitation energies (ΔE) in eV for $thrpno\_occ = 10^{-6}$ (6) and $thrpno\_occ = 10^{-8}$ (8). Comparison between aug-cc-pVDZ and aug-cc-pVTZ.

Table 6.13: Picolinic acid's excitation energies (eV) for ic-CASPT2 and CASSCF using aug-cc-pVDZ (2Z), aug-cc-pVTZ (3Z), aug-cc-pVQZ (4Z) and aug-cc-pV5Z (5Z).

	aug-cc-pVDZ	aug-cc-pVTZ	aug-cc-pVQZ	aug-cc-pV5Z
CASSCF	4.809	4.803	4.802	4.803
ic-CASPT2	4.554	4.491	4.484	4.484

To investigate further these effects, the basis set calculations were extended for the case of picolinic acid. Fig. 6.23 represents the convergence of the excitation energies for picolinic acid for four basis sets: aug-cc-pVDZ, aug-cc-pVTZ, aug-cc-pVQZ and aug-cc-pV5Z. The canonical ic-CASPT2 and the CASSCF excitation energies are presented in

Table 6.13. In reference (*242*) a similar analysis is undertaken on tryptophan. Part of these results (just the plots, no Table) are added to Appendix 8.8.

Table 6.14: Statistical data for excitation energies using *thrpno_occ* $= 10^{-6}$ and *thrpno_occ* $= 10^{-8}$. Data for aug-cc-pVDZ and aug-cc-pVTZ in *meV*, when applicable.

	aug-cc-pVDZ		aug-cc-pVTZ	
thrpno_occ	10^{-6}	10^{-8}	10^{-6}	10^{-8}
avg	4.0	1.7	3.0	2.7
σ	1.1	0.9	1.2	1.4
c_v	0.3	0.5	0.4	0.5
min	1.5	0.6	1.7	1.4
MAX	5.8	4.0	6.8	7.2

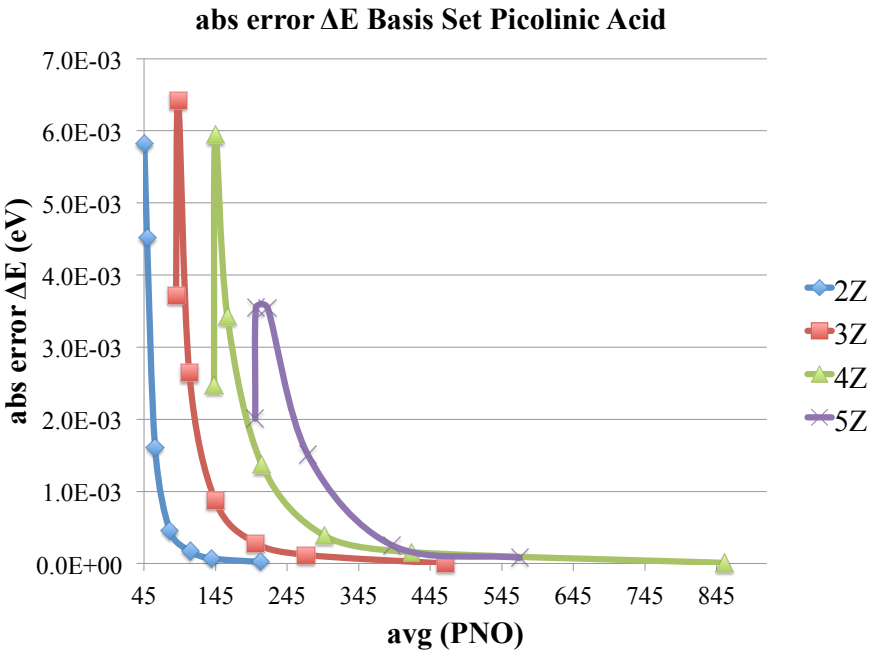

Figure 6.23: Convergence excitation energies for picolinic acid using aug-cc-pVDZ (2Z), aug-cc-pVTZ (3Z), aug-cc-pVQZ (4Z) and aug-cc-pV5Z (5Z) basis sets. *thrpno_occ* ranges from 10^{-6} to 10^{-12}. The exception is 5Z, for which the calculation with the smallest of *thrpno_occ* was not possible.

As Fig. 6.23 shows, if the size of the basis set increases, the relative accuracy of the calculation with *thrpno_occ* $= 10^{-6}$ approaches the accuracy of *thrpno_occ* $= 10^{-8}$. For

aug-cc-pVQZ and aug-cc-pV5Z, $thrpno\_occ = 10^{-6}$ shows smaller absolute errors in the excitation energy of picolinic acid than both $thrpno\_occ = 10^{-7}$ and $thrpno\_occ = 10^{-8}$. Because the total energy decreases with $thrpno\_occ$ for all basis sets,[5] the relative accuracy of $thrpno\_occ = 10^{-6}$ towards the relative accuracies of both $thrpno\_occ = 10^{-7}$ and $thrpno\_occ = 10^{-8}$ can be accounted by error compensation. This error compensation stems from differences in the convergence curves of Ecorr for different electronic states for intermediate values of $thrpno\_occ$, as previously observed. Ultimately, $thrpno\_occ = 10^{-7}$ is the worst value to use for $thrpno\_occ$ when calculating excitation energies: for larger basis sets, $thrpno\_occ = 10^{-7}$ has the largest error; for aug-cc-pVDZ this threshold is almost as accurate as the threshold $thrpno\_occ = 10^{-6}$. This same trend was also found for the case of tryptophan.

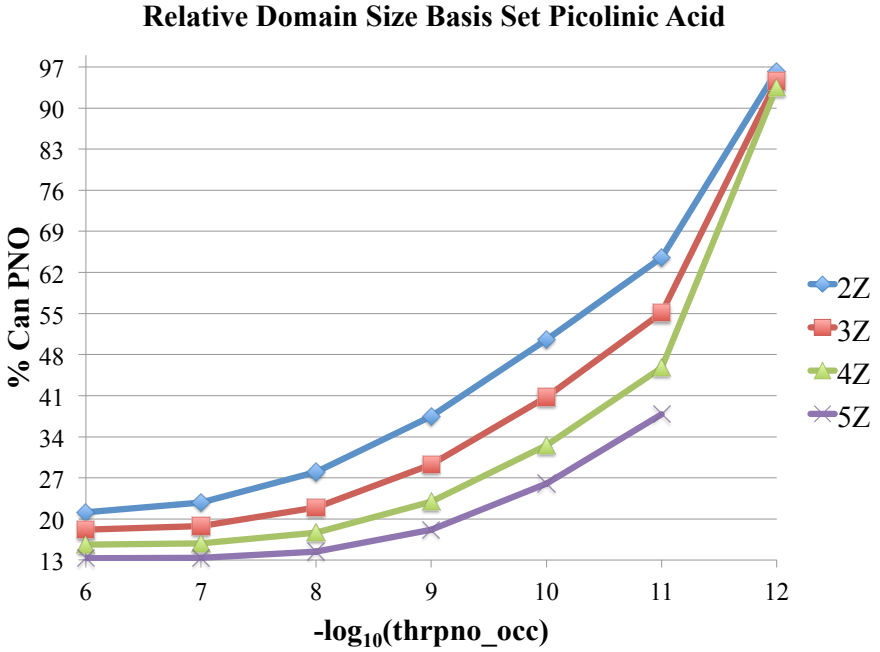

Figure 6.24: Relative PNO domain size against $-log_{10}(thrpno\_occ)$ for picolinic acid. Data for aug-cc-pVDZ (2Z), aug-cc-pVTZ (3Z), aug-cc-pVQZ (4Z) and aug-cc-pV5Z (5Z).

Next we would like to focus on how the relative domain size changes with the basis set size. Fig. 6.24 presents the ratio $\%CanPNO = \frac{avg(PNO)}{n_{virtual}}$ against the negative of the logarithm of $thrpno\_occ$. For the same value of $thrpno\_occ$, as the basis set size increases, $\%CanPNO$ decreases. For different basis sets, $\%CanPNO$ changes more for intermediate values of $thrpno\_occ$. The values for larger/smaller $thrpno\_occ$ tend to converge to

[5]The absolute values for total energies are presented in the supplementary material.

the same values for all basis sets. These are 0 (empty domains for very large *thrpno_occ*) and 1 (full domains). We would like furthermore to note that in all cases, when using $thrpno\_occ = 10^{-6}$, LCASPT2 builds PNO domains with about 15-20% of the dimension of the full canonical virtual space. These relative domain sizes are expected to decrease with the molecular size and by looking at the case of tryptophan that is indeed verified. The increase of the domain sizes for $thrpno\_occ = 10^{-6}$-10^{-8} is also relatively flat, especially for larger basis sets. For tryptophan, a larger molecule, that growth is even less accentuated. This means that for $thrpno\_occ = 10^{-8}$ the PNO domains do not increase significantly, and still the absolute error in Ecorr decreases by more than half. Since for $thrpno\_occ = 10^{-8}$ Ecorr is practically converged, then the gross of the correlation energy can be retrieved with PNO domains having about 60 PNOs.

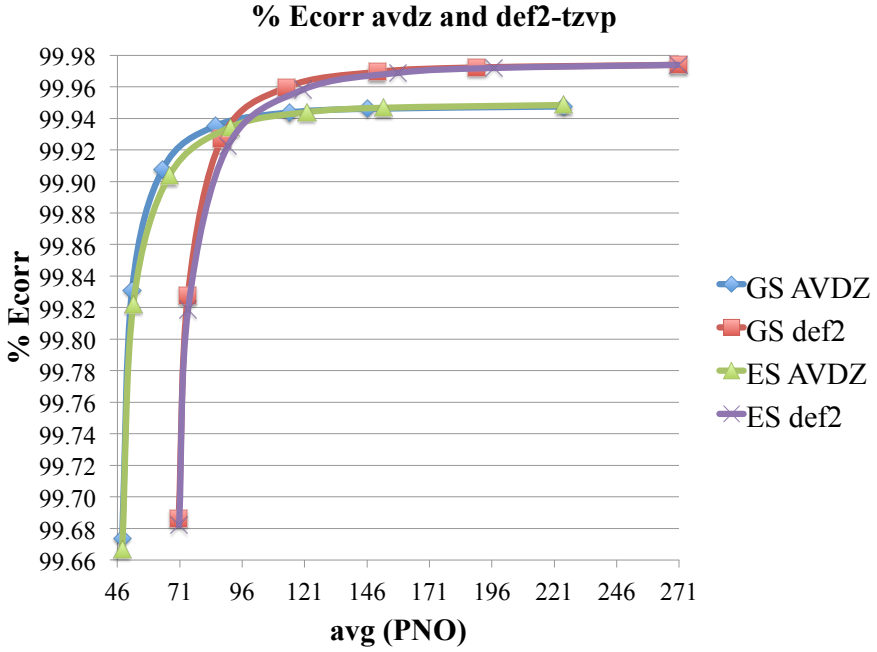

Figure 6.25: Average %Ecorr against avg(PNO) for aug-cc-pVDZ and def2-tzvp. *thrpno_occ* ranges from 10^{-6} to 10^{-12}.

Calculations were also performed to compare the basis sets aug-cc-pVDZ and def2-tzvp. The exact composition of the sample can be found in Fig. 6.26. Fig. 6.25 presents the convergence of %Ecorr with the PNO domain size. The respective data is presented in Tables 8.9 and 8.10, in Appendix 8.8. The results previously obtained when comparing aug-cc-pVDZ with aug-cc-pVTZ are transposable to the comparison aug-cc-pVDZ-def2-tzvp. Nevertheless, it should be pointed out that with the basis set def2-tzvp the Ecorr

converges closer to the canonical energy, differing just by 0.03% upon convergence. For def2-tzvp the PNO domains are also larger, as expected from a triple-ζ basis set. Other statistical data agrees well with previous analyses, even though for this particular study too much relevance to statistical parameters should not be given due to the extremely reduced size of the sample. Once more, the analysis of absolute errors brings no new information to this discussion. The respective plots can also be found in Appendix 8.8.

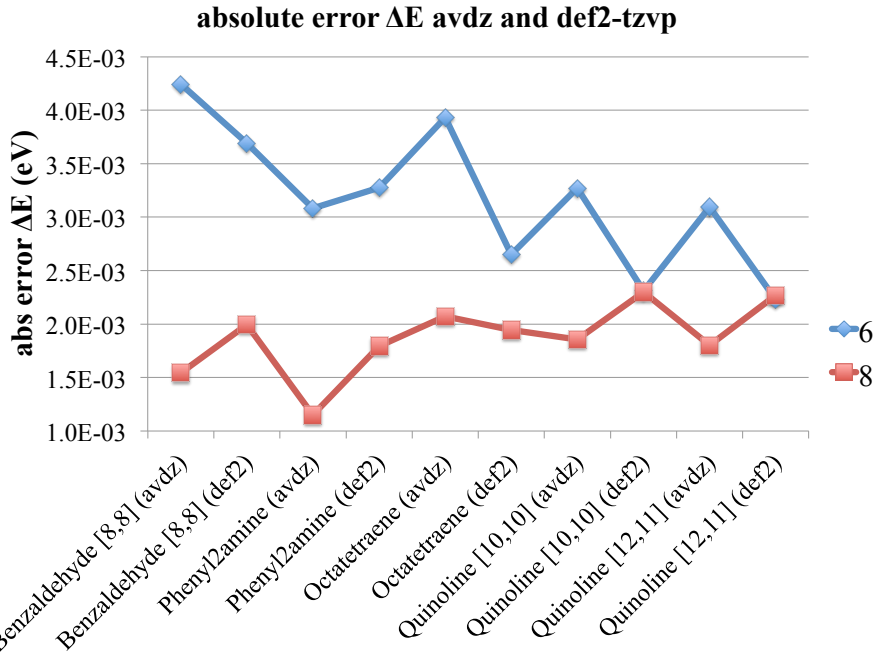

Figure 6.26: Absolute error on excitation energies (ΔE) in eV for $thrpno\_occ = 10^{-6}$ (6) and $thrpno\_occ = 10^{-8}$ (8). Comparison between basis setz aug-cc-pVDZ and def2-tzvp.

Finally, Fig. 6.26 presents the errors of these two basis sets in the calculation of excitation energies using $thrpno\_occ = 10^{-6}$ and $thrpno\_occ = 10^{-8}$. The respective statistical data is in Table 6.15. Even though for $thrpno\_occ = 10^{-6}$ def2-tzvp is more accurate than aug-cc-pVDZ, for $thrpno\_occ = 10^{-8}$ aug-cc-pVDZ becomes slightly more accurate with respect to its own canonical excitation energy. Differences amount however to the range of 0.5 meV, consistent with the comparison between aug-cc-pVDZ and aug-cc-pVTZ. In both cases, decreasing $thrpno\_occ$ leads to a decrease in the errors. This is also in good agreement with previous results, allowing us to conclude that the general behavior can be extrapolated for the increasing dimension of basis sets. For smaller basis sets (double-ζ), we recommend using the default $thrpno\_occ = 10^{-8}$, since this value offers clearly better results. $thrpno\_occ = 10^{-6}$ provides reasonable results without significant

loss in accuracy. For triple-ζ bases, $thrpno\_occ = 10^{-8}$ still offers a better accuracy, even though the advantages are not as pronounced as they are for the double-ζ case. For even larger basis sets there is no advantage in going beyond $thrpno\_occ = 10^{-6}$. Note that these conclusions are only valid for the case of excitation energies.

Table 6.15: Statistical data for excitation energies using $thrpno\_occ = 10^{-6}$ and $thrpno\_occ = 10^{-8}$. Data for aug-cc-pVDZ and def2-tzvp in meV, if applicable.

	aug-cc-pVDZ		def2-tzvp	
$thrpno\_occ$	10^{-6}	10^{-8}	10^{-6}	10^{-8}
avg	3.5	1.7	2.8	2.1
σ	0.5	0.3	0.6	0.2
c_v	0.1	0.2	0.2	0.1
min	3.1	1.2	2.2	1.8
max	4.3	2.1	3.7	2.3

6.5 Multipole Approximation and Larger Cases

Unlike other studies previously presented, the complete sample of molecules at our disposal is inappropriate to show the effects and consequences of using the Multipole Approximation (MPA). Using an energy threshold of 1 μE_h for the MPA in distant pairs is equivalent to consider these as being built from orbitals about 10-12 Å apart. For serotonin, using the MPA gives a difference of 60 μE_h in Ecorr towards the same calculation without the MPA. The difference in excitation energy is 20 μeV. For this case, 50 pairs are treated as distant, which correspond to 14% of the total pairs. For tryptophan, a molecule just slightly larger, differences of 1 mE_h in Ecorr and 2 meV in the excitation energy are observed. For tryptophan, 17% of the pairs are considered and treated as distant. We can thus conclude that the sample used in 6.3 is at the border line and no faithful conclusions can be made. In this section a different approach for the MPA is taken, using different systems. For these cases, the canonical ic-CASPT2 calculations were computationally too demanding. Furthermore, only energy differences are going to be analyzed, not total nor correlation energies. The very distant pair approximation will not be addressed here since its effects should be similar to the ones of the MPA.

The results for the elimination reaction of the gold complex presented in Fig. 6.9 are given in Table 6.16. The use of the MPA barely affects the final results: differences

between using the MPA and not using it amount to 0.2 $kcal.mol^{-1}$. For this case, differences between different *thrpno_occ* amount to a maximum of 0.1 $kcal.mol^{-1}$. In terms of computational savings, the MPA reduces by 35% the number of P_2 pairs for the reagent and by 58% for the product (without MPA there is a total of 7140 P_2 pairs). CPU times are reduced by factors of 2 to 4. One final remark is the size of the PNO domains, which range between 5% when the MPA is used and 3% when it is not. The fact that the average PNO domain size increases when the MPA is on can be understood by the fact that many distant pairs are no longer treated at the CASPT2 level. These pairs have typically smaller domains and contribute to the decrease of avg(PNO).

Table 6.16: avg(PNO), total energies and reaction energies for the gold system using IBOs from HF for the closed-shell space.

	thrpno_occ	avg(PNO)	$E_{Reagent}$ (E_h)	$E_{Product}$ (E_h)	ΔE ($kcal.mol^{-1}$)
CASSCF	—	748	-2272.118757	-2272.102876	9.97
$I = 2$	10^{-6}	23	-2278.729636	-2278.644313	53.54
	10^{-7}	24	-2278.740240	-2278.654735	53.65
	10^{-8}	26	-2278.745398	-2278.659761	53.74
$I = 2$,	10^{-6}	32	-2278.728921	-2278.643872	53.37
MPA	10^{-7}	33	-2278.739525	-2278.654295	53.48
	10^{-8}	37	-2278.744682	-2278.659320	53.56

Neither the product nor the reagent for this dissociation reaction possess any MR character. SR theories, like local CC, can reproduce accurately this reaction's energy (reference value is 46.96 $kcal.mol^{-1}$ (*265*)). The CASSCF coefficients of the references confirmed furthermore the SR character. Thus, LCASPT2 does not improve the dissociation energy for this gold complex over other methods. We should however mention that even though chemically sensible, the active space found is very incomplete. The reaction energy at the CASSCF level proves itself. Increasing the size of the CAS reference certainly leads to improved energies. The obvious options to extend the active space are the carbene ligand and/or more d_{Au} orbitals. Furthermore, the orbitals used are not from fully optimized CASSCF references. We verified that this also plays a small role in the calculation of the reaction energies: using fully optimized CAS references for the reagent and the product reduces the reaction energies by 3 $kcal.mol^{-1}$, making the result closer to the reference values.

Table 6.17 resumes the main data collected for the excitation energies of the smaller

nickel complex presented in Fig. 6.9.

Table 6.17: Excitation energies (ΔE, in eV) and avg(PNO) (for CASSCF the dimension of the virtual space) for the small nickel complex in Fig. 6.9. Results presented for two different basis sets, using $I = 2$, $I = 2$ with the MPA and $I = 1$.

Method	CASSCF	LCASPT2					
Domain	—	$I = 2$		$I = 2$,MPA		$I = 1$	
thrpno_occ	—	10^{-6}	10^{-8}	10^{-6}	10^{-8}	10^{-6}	10^{-8}
avg(PNO) (aug-cc-pVDZ)	493	29	31	36	40	34	38
ΔE (aug-cc-pVDZ) (eV)	0.853	2.450	2.455	2.450	2.455	2.450	2.455
avg(PNO) (aug-cc-pVTZ)	1265	49	52	65	69	60	64
ΔE (aug-cc-pVTZ) (eV)	0.853	2.396	2.399	2.396	2.399	2.397	2.398

For this nickel complex the accuracy of LCASPT2 is also barely affected by the use of the MPA. The largest difference with and without this option is below 0.4 meV for both basis sets. The total number of P_2 pairs is reduced to 57.3% of the original value (4851) for aug-cc-pVDZ and to 60.4% for aug-cc-pVTZ. By comparing to the case of the gold complex it is possible to conclude that even though the total number of pairs discarded changes with the molecular size, savings in CPU time are not so sensible: they are also around a factor of 2 for cc-pVDZ. As for cc-pVTZ, we observed a reduction of CPU times to 75% by using the MPA (without the MPA the slowest calculation takes 12400 s).

The conclusions previously taken when comparing different PAO domain sizes are also confirmed here: the differences between the columns $I = 2$ and $I = 1$ are all within 1 meV. Thus, when looking at an excitation energy itself, and not to a plot of absolute errors, we realize that differences between $I = 2$ and $I = 1$ are barely noticeable. However, CPU times are reduced by a factor of 3 by choosing $I = 1$.

The two different values of *thrpno_occ* give a difference in excitation energies within 4.7 meV. This difference decreases for smaller PAO domain sizes and larger basis sets. Furthermore, in the case of this nickel complex, substitution spaces are reduced to 6-7% of the canonical dimensions, consistent with what was observed for the gold complexes. For the triple-ζ basis the reduction goes up to 4%. Comparing Table 6.16 with 6.17 confirms that avg(PNO) is independent of the molecular size, since the values for avg(PNO) barely change between these two examples.

Finally, we should analyze the results for consistency. Both basis sets yield consistent results. Differences amount to 55 meV. However, there is some discrepancy between the

CASPT2 and CASSCF results for both these cases. This means that the active space might still be incomplete and require some enlargement.

Last, we present the results for the larger nickel complex in Fig. 6.9, up to now the largest system tested at the LCASPT2 level. Table 6.18 presents absolute energies and the singlet-triplet splitting for this complex using $I = 2$ with the MPA and $I = 1$.

Table 6.18: Absolute energies and singlet-triplet splitting (ΔE, in eV) for the large nickel complex in Fig. 6.9. Results for CASSCF, DLPNO-NEVPT2 (*72*) and for LCASPT2 using $I = 2$ with the MPA and $I = 1$.

		$E_{triplet}$ (E_h)	$E_{singlet}$ (E_h)	ΔE (eV)
CASSCF	(*72*)	-6074.799651	-6074.720816	2.145
	This work	-6074.791411	-6074.707468	2.284
	Difference	0.0082	0.0133	—
LCASPT2	$I = 2$,MPA, 10^{-6}	-6093.822729	-6093.746928	2.063
	$I = 2$,MPA, 10^{-8}	-6093.875157	-6093.799350	2.063
	$I = 1$, 10^{-6}	-6093.758469	-6093.682608	2.064
	$I = 1$, 10^{-8}	-6093.810923	-6093.735026	2.065
	DLPNO-NEVPT2	-6093.840776	-6093.768594	1.964

The first result to analyze in this case is the CAS references. In ref. (*72*) a fully optimized CAS is used, which for this system takes too long to obtain. On the other hand, we use a partially optimized CAS reference, where only the active space is optimized at the CASSCF level. The closed-shell spaces of both states are expressed by the triplet state's IBOs. As Table 6.18 shows, this causes barely any effect on the triplet GS: the difference amounts to 8 meV. For the singlet state the difference increases to 13 meV, but it is still nevertheless negligible, especially when the time spent in obtaining the CAS reference is taken into account (2 to 2.5 hours). Then we should also analyze the singlet-triplet splitting. LCASPT2 predicts a larger splitting than DLPNO-NEVPT2 does, being that probably an artifact of the reference function used. Nevertheless, the differences between methods are very small (100 meV). Furthermore, all LCASPT2 results are consistent, even for different values of $iext$. We note here that we tried to perform this same calculation with $iext = 2$ but the memory requirements were very high. As for the relative sizes of the domains, for the calculations here presented avg(PNO) ranges between 42 and 53 PNOs. This is about 1.1 to 1.4% of the respective canonical virtual space (3761), and consistent with the other calculations presented in this section. Finally,

going to $iext = 1$ causes the reduction of CPU times to less than 50% of the timings for $iext = 2$ with MPA (the longest calculations took 7.6 hours for triplet and 9.5 hours for the singlet). This also agrees well with the rest of the results in this section. But the reduction of the number of pairs is for this case even larger than the cases before. With the MPA 66% of the pairs are treated as being distant (total of 42195 P_2 pairs). This result is in good agreement with the asymptotic linear scaling for the number of pairs we expect for the LCASPT2 theory.

6.6 Scaling

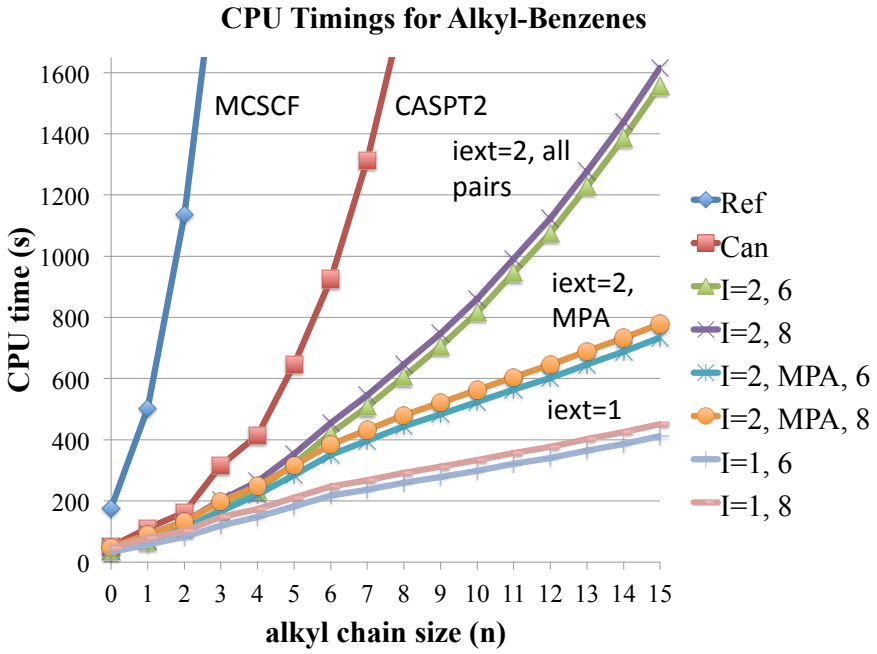

Figure 6.27: CPU timings for all the alkyl substituted benzenes. *Ref* stands for the calculation of the reference (CASSCF) and *Can* stands for ic-CASPT2. All other calculations are performed with LCASPT2. $I = 2$ is the short for $iext = 2$, $I = 1$ is the short for $iext = 1$ and the numbers 6 and 8 are the result of $-log_{10}(thrpno\_occ)$.

The present section analyzes the scaling of LCASPT2's computational costs with the molecular size. Fig. 6.27 plots CPU timings against the size of the alkyl chain for alkyl benzenes. Times are plotted for the full optimization of the reference, ic-CASPT2 and LCASPT2. Both $thrpno\_occ = 10^{-6}$ and $thrpno\_occ = 10^{-8}$ are used for the default PAO domain option ($I = 2$), for $I = 2$ with MPA and for $I = 1$. For each of these curves

two types of functions were fitted: a polynomial ($ax^3 + bx^2 + cx + d$); a power function ($ex^f + g$). While the former was obtained using Microsoft Excel's curve fitting function, demanding always that R^2 is at least 0.99, the latter was derived by least squares. The first approximation in the least squares fit were the polynomials from Microsoft Excel truncated to the last exponent and the constant. Table 6.19 present the best fit functions for ic-CASPT2 and for LCASPT2.

Table 6.19: Polynomials and power functions fitted to the scalings from Fig. 6.27.

Method		$ax^3 + bx^2 + cx + d$	$ex^f + g$
ic-CASPT2	—	$a = 5$, $b = -36$, $c = 189$, $d = -31$	$e = 4.7$, $f = 2.86$, $g = 30.5$
LCASPT2	10^{-6}	$a = 0.0$, $b = 4.3$, $c = 36.6$, $d = 28.9$	$e = 4.3$, $f = 2.49$, $g = 29.0$
$I = 2$	10^{-8}	$a = 0.0$, $b = 4.3$, $c = 40.0$, $d = 45.1$	$e = 3.5$, $f = 2.63$, $g = 43.3$
LCASPT2	10^{-6}	$a = 0.0$, $b = 0.0$, $c = 47.6$, $d = 37.6$	$e = 48.1$, $f = 1.01$, $g = 37.7$
$I = 2$,MPA	10^{-8}	$a = 0.0$, $b = 0.0$, $c = 49.5$, $d = 57.5$	$e = 50.0$, $f = 1.02$, $g = 57.7$
LCASPT2	10^{-6}	$a = 0.0$, $b = 0.0$, $c = 25.1$, $d = 45.5$	$e = 25.5$, $f = 1.03$, $g = 45.8$
$I = 1$	10^{-8}	$a = 0.0$, $b = 0.0$, $c = 26.6$, $d = 64.5$	$e = 27.1$, $f = 1.03$, $g = 65.2$

Both the optimization of the reference and the ic-CASPT2 calculation show scalings with higher powers of the molecular size. For ic-CASPT2 a cubic polynomial and a power function with exponent close to 3 were fitted. It is to expect that asymptotically ic-CASPT2 scales with the 5^{th} power of the molecular size. The difference between the expected and observed scalings is surely due to the restriction to small molecules. The optimization of the reference seems to scale with an even higher power of the molecular size and with a larger pre-factor. This leads us to point to the fact that the possible future applicability of LCASPT2 is going to depend on possible work to reduce the computational cost of the full optimization of CASSCF references. Even though approximations like the ones used in the section 6.5 made CASPT2 calculations on larger molecules possible, a critic eye and caution are always needed when looking at the results. Reducing the computational costs of CASSCF calculations is then of utmost importance.

As for the LCASPT2 calculations, we should start by noticing that using $thrpno\_occ = 10^{-6}$ or $thrpno\_occ = 10^{-8}$ leads to both similar scalings and CPU times. In fact, the difference in CPU times goes from 40 to 60 seconds for the largest case here studied ($n = 15$). The extra cost is of at most 10%. Of course that for very large systems this difference increases, but probably it will still not be significant enough. This is a consequence of the slow increase of the domain sizes with $thrpno\_occ$, as seen for picolinic

acid in section 6.4. Furthermore, for $I = 2$ no linear scaling is observed. The scaling goes even with a quadratic polynomial or with a power function with exponent of approximately 2.5. This behavior is expected, since no pair approximations are playing a role in the calculations. For the case $I = 2$ with the MPA, up to n-hexylbenzene the respective curve of CPU timings with the molecular size seems to follow a second degree polynomial. However, this behavior is rather smooth. From n-heptylbenzene this curve changes to a straight-line equation. We note that both fits performed were to the whole set of points and still we were able to obtain a coefficient of determination of at least 0.99. This shows that if there is a quadratic character in these curves, it has barely any weight on the whole curve: the behavior is dominantly linear. Finally, there is the case of $I = 1$, which seems to be described by two straight-line equations, one from benzene up to n-hexylbenzene, the other from n-heptylbenzene on. These results are justified by both the MPA (used also for this case) and the reduced PAO domain sizes. The latter are so restrictive on substitution spaces that the quadratic behavior becomes very smooth. Finally, with the current implementations, LCASPT2 is always faster than the parent canonical method. It can thus be stated that the borderline for which LCASPT2 and ic-CASPT2 have the same computational time cost is below the molecular size of benzene, if it exists. To be entirely fair, it should be pointed out again that the algorithm for ic-CASPT2 was not optimized in the way that LCASPT2 was.

Fig. 6.28 plots the CPU times for increasing sizes of the chain connecting the two thiophene radical cations. Appendix 8.9 presents a zoom-in of Fig. 6.28 for the region 0 to 60 seconds. These calculations involve only the GS of these chain molecules. All calculations were performed using $iext = 1$, $thrpno\_occ = 10^{-8}$ and $thrdist = 10^{-6}$ E_h.

The advantage of the bithiophene chains is that larger ranges of molecular sizes are reached when studying the scaling behavior of LCASPT2. Indeed, the conclusions taken from the alkyl benzenes example can be extrapolated for the case of the bithiophene chains. There are also two scaling behaviors, one for small enough systems, for which pair approximations play a minor role, and another for larger systems, for which pair approximations efficiently reduce the computational costs. Thus, up to 182 atoms and 2508 basis functions LCASPT2 shows the asymptotic linear scaling behavior.

Fig. 6.28 still represents the time costs of some parts of our code. We can verify that the CPU time spent in generating PNOs is negligible when compared to the calculation of the exchange integrals or the total CPU time spent in LITF. From the scaling behavior up to $n = 50$, the generation of PNOs should never be a bottleneck in LCASPT2 calculations. In this range of molecular sizes, LCASPT2 spends the most of CPU time in LITF, even

though at some point the calculation of integrals should become as "expensive" as LITF, or even more expensive. We note that LITF CPU times include not only the solving of residual matrices, which depend on the number of iterations, but also the calculation of all necessary intermediates, overlap matrices, *etc.*.

The most expensive individual step in LCASPT2 is however the calculation of integrals. We can still verify that the main effect of pair approximations is in the calculation of integrals, since LITF does not show the two types of behavior for small and larger molecular sizes. This can be easily understood by realizing that LITF spends a significant percentage of CPU time calculating intermediates and other quantities, not in solving the residuals for groups of configuration subspaces. For the largest chain example, LITF spends 49 s solving all residual equations, which corresponds to 12% of the total CPU required by LITF. Both the total LITF CPU times and the solving of the residuals scale linearly with the molecular size. More detail can be seen in the Fig. from Appendix 8.9.

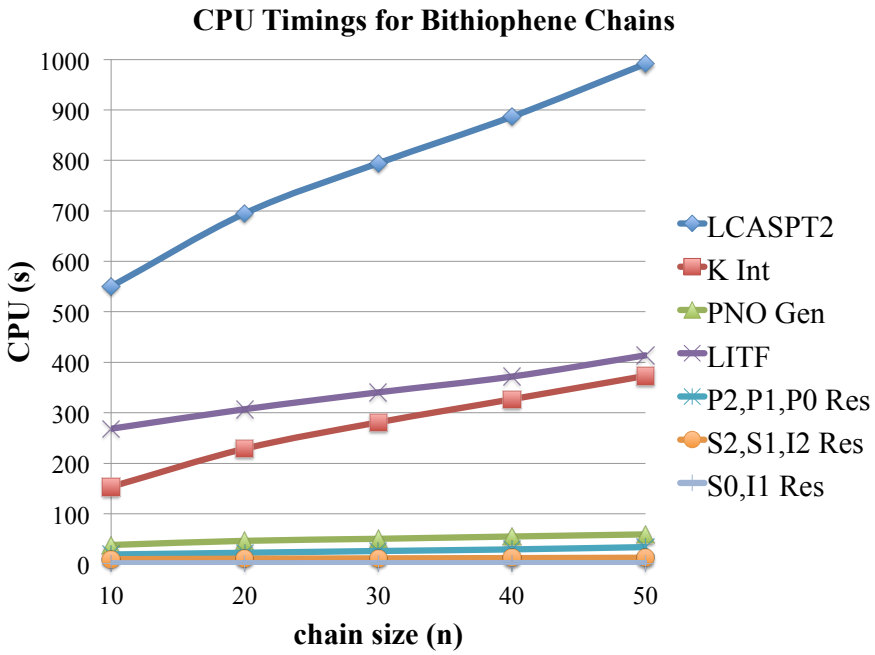

Figure 6.28: CPU timings for the bithiophene chains. *K Int* stands for the calculation of the exchange integrals, *PNO Gen* for the algorithm to generate PNOs and *Res* for the algorithms to solve the residual equations for groups of configuration subspaces.

Finally, we should look at Fig. 6.29, which shows how memory requirements of LCASPT2 increase with the molecular size. Using least squares a power function depending on the 1.1 power of the molecular size was found. We can thus conclude that

the LCASPT2 method implemented shows asymptotic linear scaling in CPU times and an almost linear scaling in memory demands.

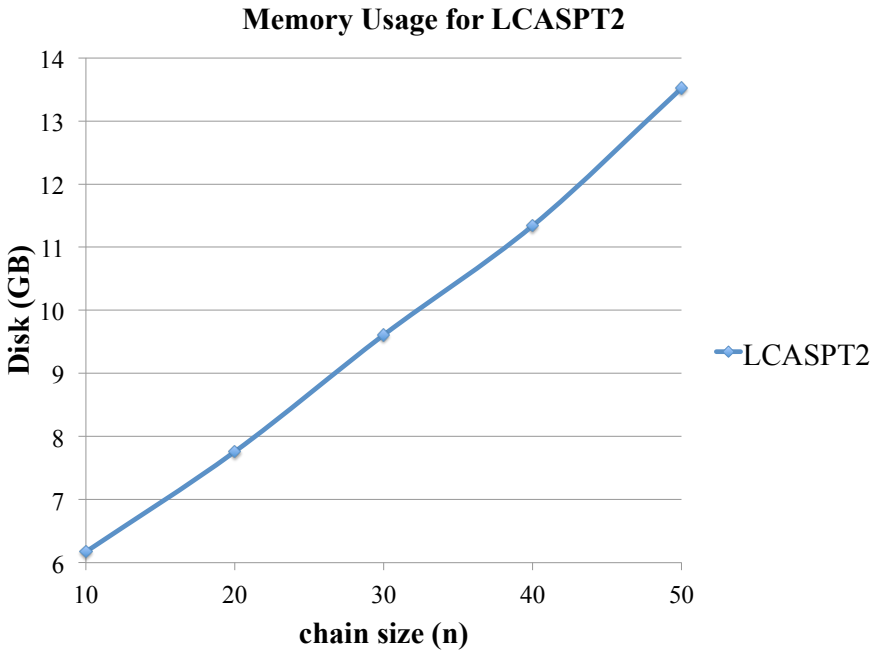

Figure 6.29: Memory usage in GB for the bithiophene chains using LCASPT2s.

6.7 Potential Energy Surfaces

This section presents and discusses the behavior of LCASPT2 in the description of PESs. The examples chosen can be easily calculated on a current personal computer, and the gaining in CPU timings when using LCASPT2 is surely not significant. However, these examples show how accurately the method behaves with respect to ic-CASPT2 for a wide range of geometries and in the application to conceptually more complex problems.

A PES is an electronic energy profile function of certain geometry changes. It provides an electronic potential on which the nuclei of a molecule will move. Variables can be bond distances and/or changes in the angles between three or four atoms. A PES plots how processes (*e.g.* reactions) are undertaken and which structures are possible for a certain combination of atoms (stable isomers, tautomers, conformations).

Fig. 6.30 presents the PES for the first singlet and triplet electronic states of ethylene (ethene). Both states follow the surface optimized for the singlet GS. In this PES the carbon-carbon bond distance changes by 0.025 Å, from 0.919 to 3.269 Å. All the energies here presented are relative to the minimum in the S0 surface calculated with ic-CASPT2.

This is the zero for all curves. The same PESs calculated with LCASPT2 are presented also for $thrpno\_occ = 10^{-6}$ and for $thrpno\_occ = 10^{-8}$. As can be seen, the LCASPT2 PESs follow closely the respective canonical curves. The LCASPT2 errors at the minimum of the S0 surface are of 0.3 mE_h for $thrpno\_occ = 10^{-8}$ and 0.8 mE_h for $thrpno\_occ = 10^{-6}$. At the same point but in the triplet surface both errors are larger by 0.1 mE_h. These errors are negligible and cannot be seen macroscopically on the PESs. However, orbital or pair domains typically change for different geometries (*213, 357, 406*). Consequently, the dimensions of the substitution spaces for a given orbital pair differ, even if the two geometries have the same pair lists. Hence, PESs calculated with local methods are not microscopically smooth. Microscopically, the errors of LCASPT2 with respect to ic-CASPT2 do not differ much from the errors already given. An average error of 0.79 mE_h was found for $thrpno\_occ = 10^{-6}$ and of 0.31 mE_h for $thrpno\_occ = 10^{-8}$. The maximum errors are relatively close to average errors, staying at 1.04 mE_h for $thrpno\_occ = 10^{-6}$ and 0.58 mE_h for $thrpno\_occ = 10^{-8}$. Both maxima occurred in the triplet PES. We can thus verify that both the accuracy and consistency of LCASPT2 are in average valid in any point in a PES, yielding macro- and microscopically consistent results.

Local PNO methods retrieve a certain amount of the Ecorr according to the number of PNOs used for each pair. This depends both on cut-off thresholds and on the spectrum of occupation numbers. Since PNO transformation matrices depend on pair amplitudes, which change with the geometry, then the PNO-transformation matrices depend also on the geometry of a molecule. It is thus to expect variability in avg(PNO) with geometrical changes. These changes should in principle not be abrupt. $\frac{P}{V} = \frac{avg(PNO)}{n_{virtual}}$ shows how the number of PNOs change along the ethylene PES. For most regions of the PES $\frac{P}{V}$ oscillates around a given value, consistent with the expected behavior. There might be tendencies on a larger scale, but in small scales $\frac{P}{V}$ just fluctuates. We see however that for certain parts of the PES there are some jumps in $\frac{P}{V}$. An example is when the singlet and the triplet states become degenerate at 2.119 Å. These jumps can happen if there are significant changes in the zeroth-iteration pair amplitudes, which in turn occur if the main composition of the reference is also changed (both in the orbitals or in the contribution of reference configurations). Just like the example given above, it might also be that other electronic state(s) become(s) degenerate with one of the states of interest around these jumps in the dimension of substitution spaces. Even though these details were not deeply investigated, as the results show, the quality of PESs is not affected. Nevertheless, these jumps cannot arise from PAO domains since these are full for the whole PES.

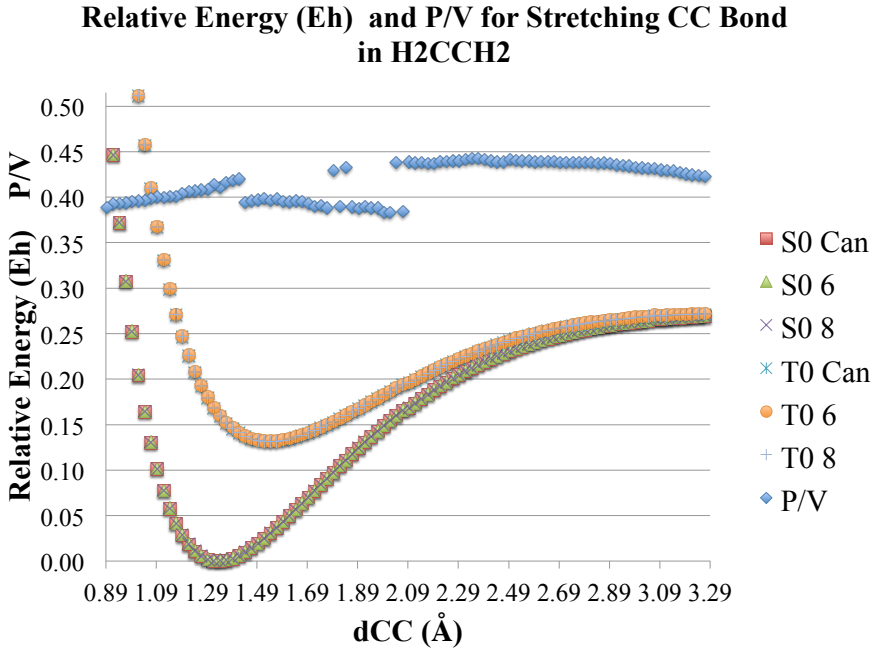

Figure 6.30: PES for the CC stretching in ethylene using ic-CASPT2 and LCASPT2 (6 stands for $thrpno\_occ = 10^{-6}$ and 8 for $thrpno\_occ = 10^{-8}$). Separate calculations on the singlet GS (S0) and the first triplet (T0). All plots presented by subtracting the minimum energy in the canonical S0 PES. The last curve ($\frac{P}{V}$) presents the ratio $\frac{avg(PNO)}{n_{virtual}}$.

Finally, these results should be compared with the literature. Table 6.20 presents some energies taken from the PES of ethylene and the respective experimental values.

Table 6.20: Main energies from the ethylene PES and the respective experimental values. Vertical S-T is the vertical transition from the minimum in the singlet GS to the triplet PES. Vertical T-S is the same difference but from the triplet PES to the GS, dissociation S is the dissociation energy for the singlet state and the Adiabatic S-T is the energy difference between the minima in both PESs. Corrected calculated values inside ().

	Calculated	Experimental
Vertical S-T (eV)	4.57 (—)	4.6 (*407*), 4.51 (*408*)
Vertical T-S (eV)	2.90 (0.06)	—
Adiabatic S-T (eV)	3.57 (2.78)	2.52 (*409*)
Dissociation S (eV)	7.40 (—)	7.55 (*410*), 7.52 (*411*)
Dissociation T (eV)	3.82 (4.61)	—

The vertical excitation energy taken from our PESs for the singlet-triplet excitation

energy is in very good agreement with the experimental values. The difference goes up to 0.06 eV for the values presented. The singlet state dissociation also agrees with the experimental values and also with other theoretical results (*42*). The experimental adiabatic excitation energy agrees reasonably well with other theoretical investigations (2.92 eV with the zero point energy correction (*408*)), but not with ours. The problem in the adiabatic energy difference we calculated lies in the fact that the absolute minimum in the triplet PES is not represented by any of the geometries considered. Therefore, the triplet dissociation energy calculated cannot be reasonable either. We decided thus to optimize the absolute minimum in the triplet PES to recalculate some quantities in Table 6.20. Using the optimized triplet geometry, which alike the singlet GS ethylene is not planar (each methylene is in its own plane, orthogonal to each other), new values were calculated for energies. These are inside () in Table 6.20. The new Adiabatic S-T energy difference is in much better agreement with the experimental value. Using the zero point energy of ethylene (0.14 eV (*408*)) we obtain an adiabatic excitation energy 0.12 eV apart from the experimental value (2.8 $kcal.mol^{-1}$). With the correct minimum in the triplet PES the Vertical T-S splitting was also recalculated, which is just slightly more than 1 $kcal.mol^{-1}$ (0.06 eV). Hence, at the minimum of the triplet well both the triplet and the singlet states are expected to be degenerate. For the dissociation of the triplet we found no value to compare to. But since the dissociation products should have a geometry similar to the dissociation products of the singlet state, we can also conclude we have a reasonable estimation for this dissociation energy.

Finally there is still the case of hexatriene's cis-trans isomerization. Like any other example here presented, LCASPT2's Ecorr converged towards the respective canonical energies. However, even for this small molecule the converged LCASPT2 Ecorr corresponded to 99.96% of the canonical correlation energy using the default PAO domain sizes. Excitation energies however, converged fully to the canonical result. For the default $thrpno\_occ = 10^{-8}$ absolute errors of 1.7 meV were observed.

Fig. 6.31 presents the reduction to one coordinate of the PESs for the cis-trans isomerization of hexatriene. We represent the S0 and S1 states. Table 6.21 compiles some relevant energies calculated from these PESs. It is known that the PES for the cis-trans isomerization of double bonds depends at least on two geometry coordinates: the distance between the two atoms forming the double bond; a dihedral angle involving those two atoms and bonded atoms from the largest substituents. In the case of hexatriene the two main geometry coordinates are the CC bond between carbons 3 and 4 (the middle carbons) and the dihedral angle formed by carbons 2, 3, 4 and 5 (middle carbons plus

the two adjacent carbons). Since only 8 points in each electronic state's PES were calculated, we opted for representing these two coordinates in just one variable. This variable is not accurate but chosen to represent in a chemical sensible way the process taking place. Therefore the abscissa is omitted in Fig. 6.31. Only structures along the bond flip pathway were considered, which consists in the rotation of one of the carbons along the middle bond axis.

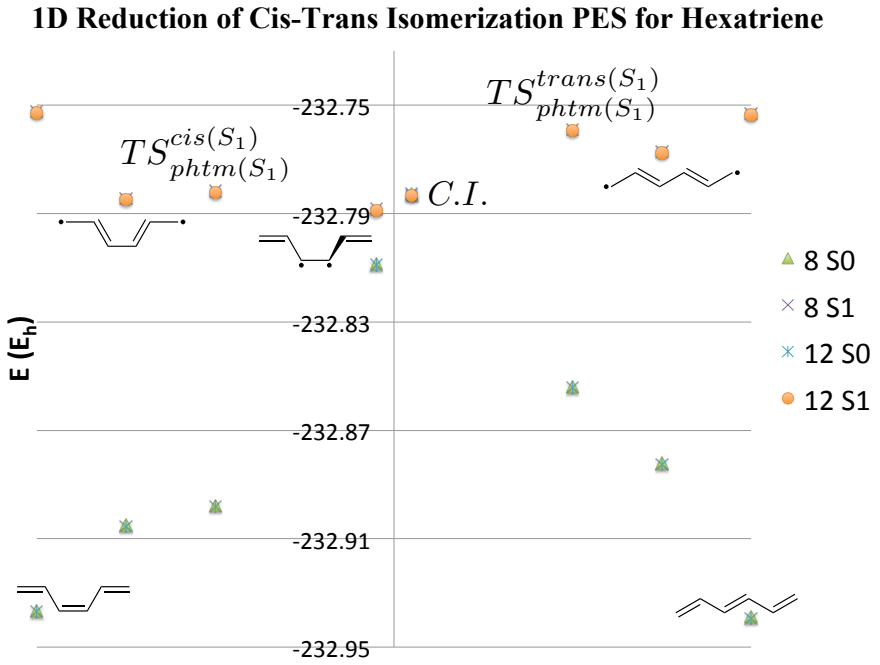

Figure 6.31: Reduction to one coordinate of the PES for the cis-trans isomerization of hexatriene. Results presented for the first two singlet electronic states, S0 and S1, for two values of *thrpno_occ*, 10^{-8} (8) and 10^{-12} (12).

The structures optimized are (from left to right, only the points with structure next to them in Fig. 6.31): cis-hexatriene in the GS; cis-hexatriene in the ES; minimum in the ES PES; trans-hexatriene in the ES; trans-hexatriene in the GS. Both the cis and trans isomers in the S1 PES have mostly a diradical character as showed in Fig. 6.31. The vertical excitation energies calculated are in good agreement with previously calculated excitation energies (*412*). But the vertical deexcitation energies calculated are significantly below the ones reported in (*412*) (approximately by 1 eV). There are however no CASPT2 nor experimental results for the deexcitation energies to compare to. The minimum in the S1 PES corresponds to the commonly known phantom state. We will refer from here on to this state as being the phantom isomer, in analogy to cis and trans isomers. In this

structure, one of the middle carbons (say carbon 3) showed a pyramidal geometry. The other carbon (4) still remained planar though. The dihedral angle between carbons 2, 3, 4 and 5 is of 99º. The structure of a Conical Intersection (C.I.) close to the phantom isomer was also optimized. As expected, the C.I. is geometrically close to the phantom isomer, with a dihedral angle of 97º. This dihedral angle differs by 20º from literature results (*382*). This does not mean that our results are inconsistent with the literature. First of all, different basis sets and optimization algorithms were used. But perhaps even more relevant is the fact that the region around the phantom isomer in these PESs is very flat. And not only is the C.I. geometrically close to the phantom isomer, these structures are also in the energetic proximity of each other: the phantom isomer is more stable by 0.16 eV (3.69 $kcal.mol^{-1}$) than the C.I.. The magnitude of this energy difference also agrees well with the values for other related systems (*413*). We should still mention the fact that the geometry found in (*382*) for the C.I. also showed the pyramidal C3 - planar C4 type of structure found for the phantom structure and the C.I..

Table 6.21: Main energies (eV) taken from the hexatriene PES for both the cis and trans hexatriene. V. (De)Exc. stands for vertical (de)excitation energy, A. Exc. stands for adiabatic excitation energy, Phan. (S1) is the energetic distance towards the phantom geometry, C.I. the energetic distance to the C.I. and E_a stands for the activation energy.

	V. Exc.	A. Exc.	V. Deexc.	Phan. (S1)	C.I.	E_a
cis	5.00	4.14	3.28	0.11	0.05	0.07
trans	5.05	4.67	3.13	0.58	0.42	0.22

We found also two Transition States (TSs) converting the cis and trans isomers into the C.I.. The TSs found had dihedral angles of 101º (trans) and 27º (cis). The cis TS here optimized differs also by 25-30º with respect to the literature results (*382*) and our optimized TS occurs earlier. The respective activation energy is in our case also lower (0.07 and 0.22 eV instead of 0.27 and 0.38 eV). However, as pointed out in reference (*382*), the activation energies in these systems are very small and sensitive to the basis set size. The activation energies there published are known to be above the experimental values. The authors furthermore remark that larger basis sets shift the cis TS towards the respective reagent, meaning the cis isomer in the S1 PES.

7. Conclusions

In this work a local variant of CASPT2 using both PNOs and PAOs was developed and implemented. At this moment this program is implemented in the development version of MOLPRO (*284, 362*). The method was named PNO-PAO Local Complete Active Space 2^{nd}-order Perturbation Theory (LCASPT2).

All the configuration subspaces used to express the correlated wavefunction are spanned using ICCs. Contravariant, singlet-triplet and covariant configurations are used according to what is most advantageous to simplify the residual equations and their structure for each configuration subspace. Closed-shell spaces are localized using the IBO scheme (*173*). IBOs are also used for the active space to help building PAO domains for active orbitals. However, with the orthogonalization of configuration subspaces the localization of the active space is no longer used. Unlike other localization schemes, IBOs yield very stable orbital charges, which build stable PAO domains. PAOs are built and used to span the substitution spaces of all pairs and singles (internals have no virtual orbitals in their substitution spaces). Domains of PAOs are built for each closed-shell orbital. For active orbitals, a single domain is assembled in order to achieve invariance for the respective PAO domain. This is important since we require orthogonal configuration subspaces to build PNOs. Using pair amplitudes in the PAO and orthogonal configuration bases, PNOs are generated for all types of pairs. Projection to the PNO basis is used for all pairs and also for S_2 configurations. The other configuration subspaces in the singles (S_1 and S_0) are left in the PAO basis. The orthogonal configuration basis is required to build PNOs because these require a uniquely defined set of configurations. Furthermore, solving the residual equations in MR theories requires the use of the perturbational update of amplitudes. PAOs are used as an intermediate stage before generating PNOs, which allows a significant reduction of the scaling to generate PNOs.

With this implementation, domain approximations take place at two stages: at the PAO level; at the PNO level. We explored the influence of the PAO domain sizes to verify that ideally the primary domains should be extended by adding two neighboring shells of atoms ($iext = 2$). We made these the default PAO domain sizes. With these domains, the average error in the calculation of excitation energies lies around 5 meV. Using just one neighboring layer ($iext = 1$) might be used for larger molecules. This does not lead to a significant loss in accuracy: the average error in excitation energies is 1-2 meV larger; for reaction energies, differences to the default option are below 1 $kcal.mol^{-1}$. Computational

times are significantly reduced by using $iext = 1$: 30% of the times for the default option. Besides the average error increasing, the drawback for this option is that the distribution of errors is not as uniform and consistent.

We observed that using a threshold of 10^{-8} for the PNO occupation numbers yields the most accurate and consistent results for double- and triple-ζ basis sets. This threshold is *thrpno_occ*, and with *thrpno_occ* $= 10^{-8}$ the accuracy is about 99.9% for the recovery of the correlation energy. Using this threshold there is an average of 60 PNOs per orbital pair. Domain sizes decrease for larger molecules. *thrpno_occ* $= 10^{-6}$ (*ca.* 50 PNOs per pair) yields also accurate and consistent results for those basis sets, if an energy consistency criterion is used to build the PNO domains. For those conditions and larger basis sets, *thrpno_occ* $= 10^{-6}$ actually surpassed the accuracy of *thrpno_occ* $= 10^{-8}$. These are however two cases and not a larger and more significant study. Since the computational time cost for both options is equivalent, *thrpno_occ* $= 10^{-8}$ is our default option. The energy completion threshold is on by default because it balances all pair energies.

Pair approximations were also implemented in LCASPT2. Distant and very distant pairs are distinguished from normal pairs. Exchange integrals associated to distant pairs are evaluated using the Multipole Approximation (MPA). This leads to a significant cut of the computational effort. It also reduces to linear the scaling of the number of pairs with the molecular size. In terms of energy differences, the MPA barely has any visible effect: for reaction energies the error here found is of 0.2 $kcal.mol^{-1}$; for excitation energies the error is around the meV. It was verified however that CPU times are reduced usually by a factor of $40 - 50\%$. For systems composed by many fragments the saving can be even more pronounced (75% for two separated fragments). Very distant pair approximations were not studied, but due to the similar implementation, we assume they behave like in other methods implemented in our institute.

Using domain and pair approximations, the implemented LCASPT2 showed asymptotical linear scaling behavior. In our studies, the linear scaling behavior begins early, already with systems with 33 atoms. If pair approximations are not used, the method will show a scaling behavior between quadratic and cubic.

Up to this date, the largest system studied with LCASPT2 was the singlet-triplet splitting of a nickel complex with more than 230 atoms and with 4175 basis functions. In reference (*242*) we present other examples of large systems. The bottleneck we found in our calculations was not at the CASPT2 level anymore, but rather in the optimization of the reference wavefunction. In our calculations we spent indeed a large amount of the time optimizing the CASSCF references. However, for some studies a fully optimized CASSCF

reference is not required. This simplifies getting the reference and extends significantly the applicability of CASPT2. We can safely state that if a reasonable CASSCF reference is possible to calculate, then also a treatment of dynamic correlation effects at the CASPT2 level using LCASPT2 is.

8. Appendix

8.1 P_2 Residuals using different types of Configurations

P_2 residuals in the canonical virtual and orthogonal configuration bases with contravariant P_2 configurations

$$\tilde{R}^{ij}_{ab} = K^{ij}_{ab} - \sum_k \left(f_{ik} c^{kj}_{ab} + c^{ik}_{ab} f_{kj} \right) + \left(\mathbf{F}^v \mathbf{c}^{ij} + \mathbf{c}^{ij} \mathbf{F}^v \right)_{ab}$$
$$-\frac{1}{2} \sum_{D_1} \sum_{tu} \left[f_{jt} D^{(1)}_{tu} T_{uD_1} c^{iD_1}_{ab} + f_{it} D^{(1)}_{tu} T_{uD_1} c^{jD_1}_{ba} \right] + \sum_{S_2} \sum_t c^{ij}_{aS_2} T_{tS_2} f_{tb}$$
$$+ \sum_{S_2} \sum_t c^{ji}_{bS_2} T_{tS_2} f_{ta} - \frac{1}{2} \sum_{S_2} \sum_{tu} c^{ij}_{aS_2} T_{tS_2} D^{(1)}_{tu} f_{ub} - \frac{1}{2} \sum_{S_2} \sum_{tu} c^{ji}_{bS_2} T_{tS_2} D^{(1)}_{tu} f_{ua}$$
$$+ f_{ai} \sum_{S_1} c^{jS_1}_b \left(X_{S_1} + T_{S_1} \right) + f_{bj} \sum_{S_1} c^{iS_1}_a \left(X_{S_1} + T_{S_1} \right)$$

P_2 residuals in the canonical virtual and orthogonal configuration bases with singlet-triplet configurations for P_2, P_1 and S_2

$$R^{ijp}_{ab} = (2-p) \left(K^{ij} + pK^{ji} \right)_{ab} + 2(2-p) \left(\mathbf{F}^v \mathbf{c}^{ijp} + \mathbf{c}^{ijp} \mathbf{F}^v \right)_{ab}$$
$$-2(2-p) \sum_k \left(f_{ik} c^{kjp}_{ab} + c^{ikp}_{ab} f_{kj} \right) + 2(2-p) \sum_{S_2} \sum_t \left(c^{ijp}_{aS_2} T^{(p)}_{tS_2} f_{tb} + p f_{ta} T^{(p)}_{tS_2} c^{ijp}_{bS_2} \right)$$
$$-\frac{1}{2}(2-p) \sum_{D_1} \sum_{tu} \left[f_{jt} D^{(1)}_{tu} T^{(p)}_{uD_1} c^{iD_1p}_{ab} + p f_{it} D^{(1)}_{tu} T^{(p)}_{uD_1} c^{jD_1p}_{ab} \right]$$
$$+(2-p) \sum_{S_2} \sum_{tu} \left(c^{ijp}_{aS_2} T^{(p)}_{tS_2} D^{(1)}_{tu} f_{ub} + p f_{ta} D^{(1)}_{tu} T^{(p)}_{uS_2} c^{ijp}_{bS_2} \right)$$
$$+(2-p) \sum_{S_1} \left[f_{ai} c^{jS_1}_b + p c^{jS_1}_a f_{ib} \right] \left(X_{S_1} + T_{S_1} \right) + (2-p) \sum_{S_1} \left[c^{iS_1}_a f_{jb} + p f_{aj} c^{iS_1}_b \right] \left(X_{S_1} + T_{S_1} \right)$$

8.2 α, β, σ, and ρ Coupling terms in Residuals

α terms:

$$\alpha^{(p)}_w (D_1, D_0) = \frac{1}{2} \sum_{tuv} T^{(p)}_{tu,D_0} S^{(p)}_{tu,vw} T_{vD_1}$$
$$\alpha^A_v (S_2, S_1) = 2 T_{vS_2} \sigma(S_1) - \sum_t T_{tS_2} D^{(1)}_{tv} T_{S_1}$$
$$- \sum_{tu} T_{tS_2} D^{(1)}_{uv} T_{ut,S_1} + \sum_{tuw} T_{tS_2} \left[\tilde{D}^{(2)}_{wv,ut} T'_{uw,S_1} - D^{(2)}_{wu,vt} T_{uw,S_1} \right]$$

$$\tilde{D}^{(2)}_{tu,vw} = \frac{1}{3}\left(2D^{(2)}_{tv,uw} + D^{(2)}_{tw,uv}\right)$$

$$\alpha^{B}_{v}\left(S_2, S_1\right) = \sum_{tu} T_{tS_2}\left[\sum_{w} D^{(2)}_{vw,ut} T^{'}_{uw,S_1} - D^{(1)}_{uv} T^{'}_{ut,S_1}\right]$$

$$\alpha^{C}_{t}\left(S_1, S_2\right) = 4X_{S_1} T_{tS_2} - \sum_{uv}\left(2T_{vu,S_1} - T^{'}_{vu,S_1}\right) D^{(1)}_{tv} T_{uS_2}$$

$$+2\sum_{u} T_{S_1}\left(\mathbf{S}^{S_2}\right)_{tu} T_{uS_2} - \sum_{uvw}\left(2T_{wu,S_1} - T^{'}_{wu,S_1}\right) D^{(2)}_{tv,uw} T_{vS_2}$$

$$\alpha^{D}_{t}\left(S_1, S_2\right) = 2X_{S_1} T_{tS_2} - \sum_{uv}\left(2T^{'}_{vu,S_1} - T_{vu,S_1}\right) D^{(1)}_{tv} T_{uS_2}$$

$$+\sum_{u} T_{S_1}\left(\mathbf{S}^{S_2}\right)_{tu} T_{uS_2} - \sum_{uvw} T_{wu,S_1} D^{(2)}_{tv,uw} T_{vS_2} - \sum_{uvw} T^{'}_{vu,S_1} D^{(2)}_{tv,uw} T_{wS_2}$$

β terms:

$$\beta^{B}_{v}\left(D_1, S_1\right) = \sum_{tu} T_{tD_1} D^{(1)}_{tu} T^{'}_{uv,S_1} - \sum_{tuw} T_{tD_1} \tilde{D}^{(2)}_{tw,uv} T^{'}_{uw,S_1}$$

$$\beta^{A}_{v}\left(D_1, S_1\right) = \sum_{tu} T_{tD_1} D^{(1)}_{tu} T_{uv,S_1} + \sum_{t} T_{tD_1} D^{(1)}_{tv} T_{S_1}$$

$$+\sum_{tuw} T_{tD_1} D^{(2)}_{tv,wu} T_{uw,S_1} - \sum_{tuw} T_{tD_1} \tilde{D}^{(2)}_{tw,vu} T^{'}_{uw,S_1}$$

$$\beta^{(p)}_{w}\left(S_2, I_2\right) = \frac{1}{2}\sum_{tuv} T_{tS_2}\left(\mathbf{S}^{I_2 p}\right)_{tw,vu} T^{(p)}_{uv,I_2}$$

$$\beta^{C}_{v}\left(S_1, D_1\right) = \sum_{tu}\left(2T_{tv,S_1} - T^{'}_{tv,S_1}\right) D^{(1)}_{tu} T_{uD_1}$$

$$+2\sum_{t} T_{S_1} D^{(1)}_{tv} T_{tD_1} + \sum_{tuw}\left(2T_{tu,S_1} - T^{'}_{tu,S_1}\right) D^{(2)}_{tu,vw} T_{wD_1}$$

$$\beta^{D}_{v}\left(S_1, D_1\right) = \sum_{tu}\left(2T^{'}_{tv,S_1} - T_{tv,S_1}\right) D^{(1)}_{tu} T_{uD_1} - \sum_{t} T_{S_1} D^{(1)}_{tv} T_{tD_1}$$

$$-\sum_{tuw} T_{tu,S_1} D^{(2)}_{tu,vw} T_{wD_1} - \sum_{tuw} T^{'}_{tu,S_1} D^{(2)}_{tw,vu} T_{wD_1}$$

σ terms:

$$\sigma\left(S_1\right) = \left(X_{S_1} + T_{S_1}\right)$$

ρ terms:

$$\rho_{tvu}\left(D_1\right) = \sum_{w} D^{(2)}_{tv,uw} T_{wD_1}$$

$$\rho^{(p)}_{wvxz}\left(D_0\right) = \sum_{tu} T^{(p)}_{tu,D_0}\left(\mathbf{S}^{S_0}\right)_{tuw,vxz}$$

$$\rho_{tuv}\left(S_2\right) = 2T_{tS_2} D^{(1)}_{uv} - T_{uS_2} D^{(1)}_{tv} - \sum_{w} D^{(2)}_{tw,uv} T_{wS_2}$$

$$\rho_{vwxz}\left(S_1\right) = T_{S_1} D^{(2)}_{zv,xw} - \sum_t \left(2T'_{tx,S_1} - T_{tx,S_1}\right) D^{(2)}_{tw,zv} + \sum_t T'_{tz,S_1} D^{(2)}_{tw,xv} + \sum_t T_{tz,S_1} D^{(2)}_{tv,xw} + \sum_{tu} T'_{tu,S_1} D^{(3)}_{tw,xu,zv} + \sum_{tu} T_{tu,S_1} D^{(3)}_{tu,zv,xw}$$

$$\rho^{(p)}_{tuvw}\left(I_2\right) = 2\left(2-p\right) T^{(p)}_{tw,I_2} D^{(1)}_{vu} - \left(2-p\right) T^{(p)}_{uw,I_2} D^{(1)}_{tv} - \left(2-p\right) T^{(p)}_{tu,I_2} D^{(1)}_{vw} - \left(2-p\right) \sum_x T^{(p)}_{xw,I_2} D^{(2)}_{tx,uv} - \left(2-p\right) \sum_x T^{(p)}_{tx,I_2} D^{(2)}_{wx,uv} + \sum_x T^{(p)}_{xu,I_2} \left(\mathbf{S}^{(p)}\right)_{tw,xv} + \frac{1}{2} \sum_{xz} T^{(p)}_{xz,I_2} \left(D^{(3)}_{tx,wz,uv} + pD^{(3)}_{tz,wx,uv}\right)$$

8.3 Tables Simulation

Table 8.1: %Ecorr against avg(PNO) and the respective values for $thrPNO_{occ}$ for cyclobutadiene. Comparison between converged ST PNOs, EndPNO ST, zero-iteration ST PNOs, IniPNO ST, and zero-iteration S,T PNOs, IniPNO S,T.

	EndPNO ST		IniPNO S,T		IniPNO ST	
$thrPNO_{occ}$	avg(PNO)	%Ecorr	avg(PNO)	%Ecorr	avg(PNO)	%Ecorr
10^{-5}	8	96.58	—	—	10	97.34
10^{-6}	18	99.38	10	98.93	19	99.37
10^{-7}	33	99.88	19	99.60	31	99.83
10^{-8}	53	99.97	31	99.85	46	99.94
10^{-9}	73	99.99	46	99.95	63	99.98
10^{-10}	89	100.00	61	99.98	80	99.99
10^{-11}	112	100.00	112	100.00	112	100.00
10^{-12}	112	100.00	112	100.00	112	100.00

Table 8.2: Absolute error in eV for the excitation energy of Pyrrole, ΔE, against avg(PNO), for many values of $thrPNO_{occ}$. Comparison between converged ST PNOs, EndPNO, and zero-iteration ST PNOs, IniPNO.

	IniPNO		EndPNO	
Threshold	avg(PNO)	ΔE	avg(PNO)	ΔE
10^{-5}	8	0.3251	8	0.2753
10^{-6}	18	0.0535	19	0.0427
10^{-7}	37	0.0014	40	0.0037
10^{-8}	64	0.0027	68	0.0003
10^{-9}	94	0.0014	101	0.0004
10^{-10}	127	0.0006	133	0.0002
10^{-11}	175	0.0000	175	0.0000
10^{-12}	175	0.0000	175	0.0000

8.4 Schematic Representation of the Active Spaces used for the many Families of Molecules

The scheme for the active spaces for the many groups of molecules is presented below.

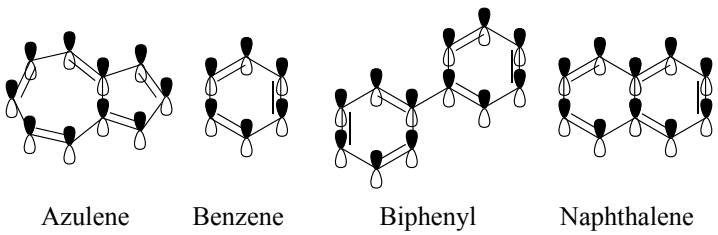

Figure 8.1: Scheme of the active space used for the family of aromatics.

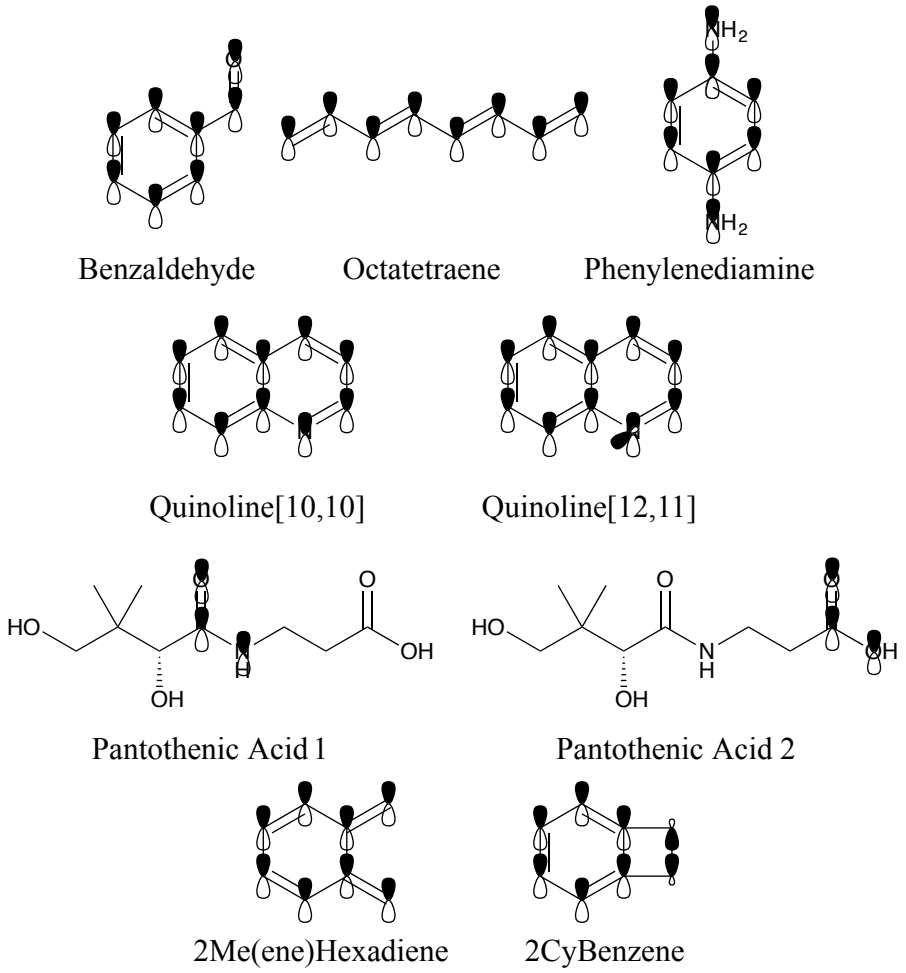

Figure 8.2: Scheme of the active space used for the family of "other" molecules.

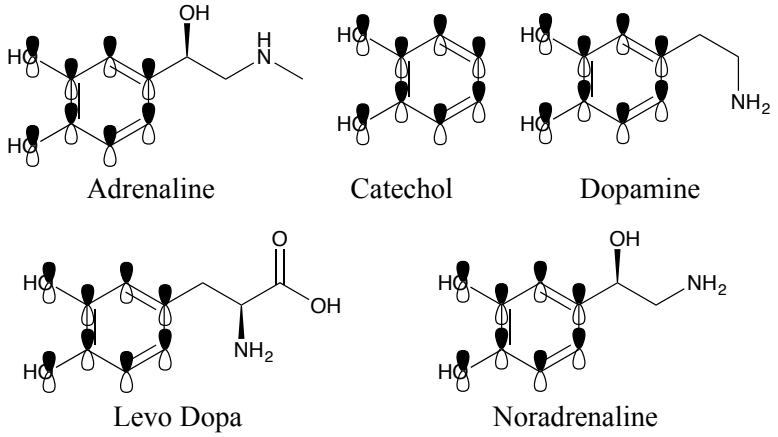

Figure 8.3: Scheme of the active space used for the family of catechols.

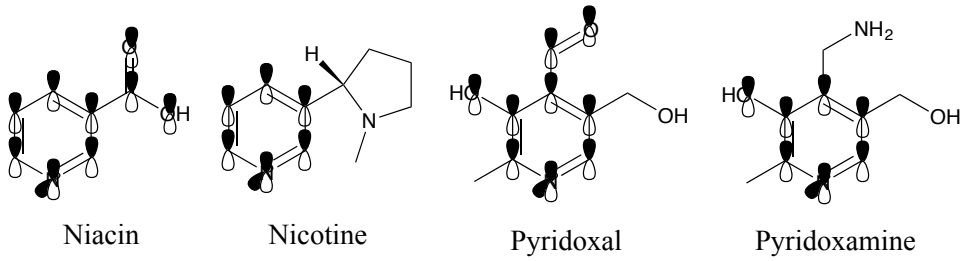

Figure 8.4: Scheme of the active 1 space used for the family of pyridines.

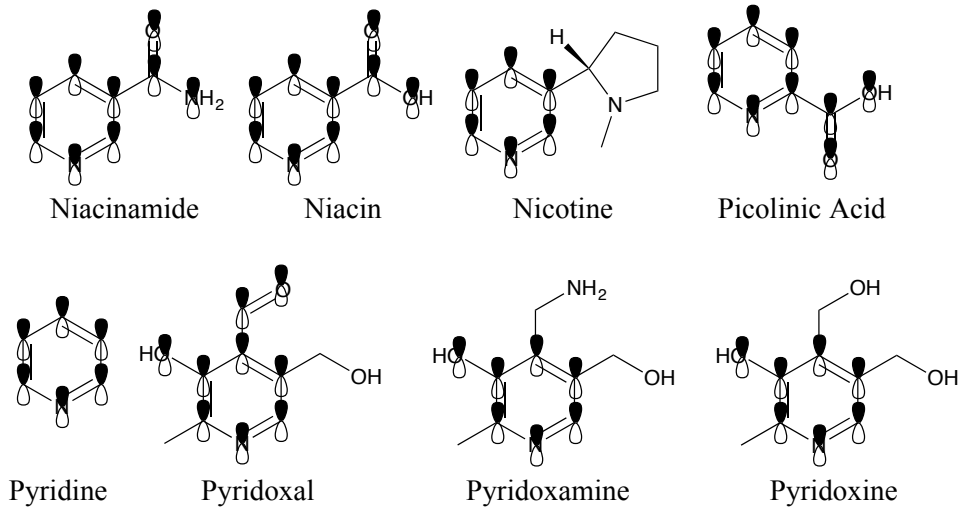

Figure 8.5: Scheme of the active 2 space used for the family of pyridines.

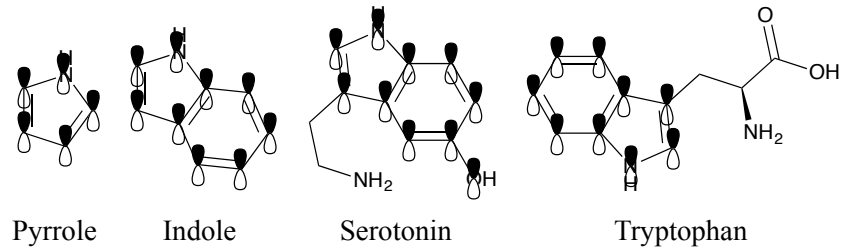

Figure 8.6: Scheme of the active space used for the family of pyrrole-indoles.

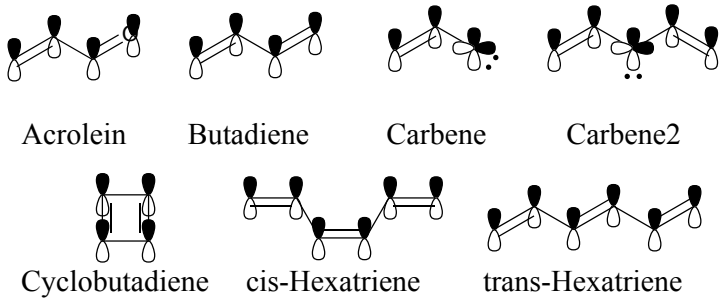

Figure 8.7: Scheme of the active space used for the family of small molecules.

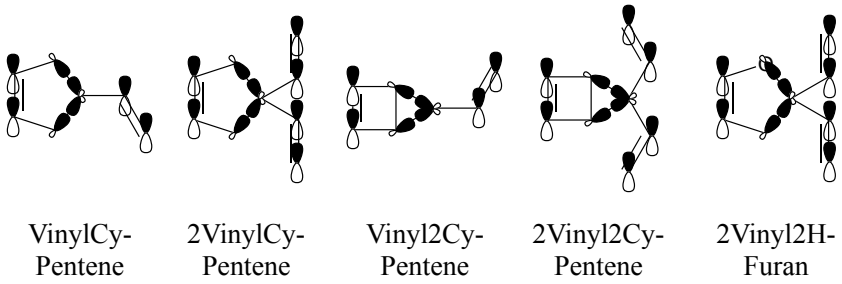

Figure 8.8: Scheme of the active space used for the family of "reaction" molecules.

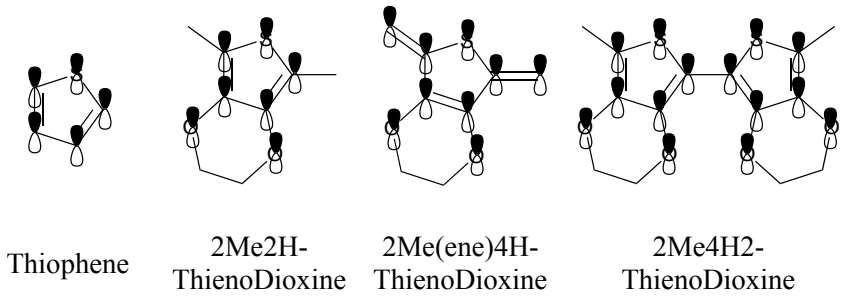

Figure 8.9: Scheme of the active space used for the family of thiophenes.

8.5 The Active Orbitals for the Family of "Reaction" Molecules

The optimized active orbitals for the family of reaction molecules are presented next.

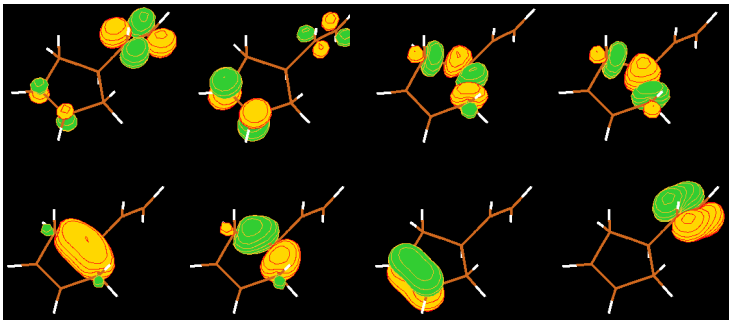

Figure 8.10: Active orbitals for VinylCyPentene.

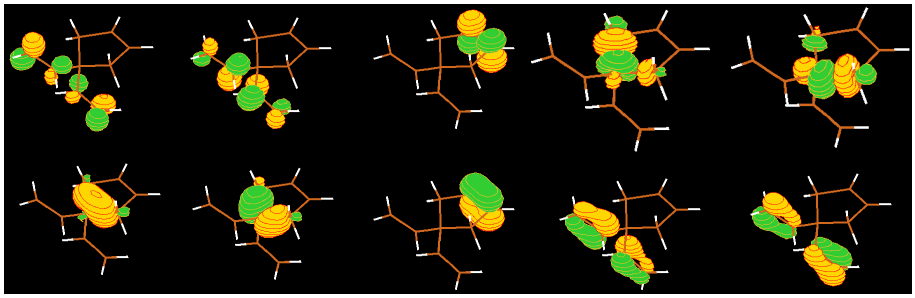

Figure 8.11: Active orbitals for 2VinylCyPentene.

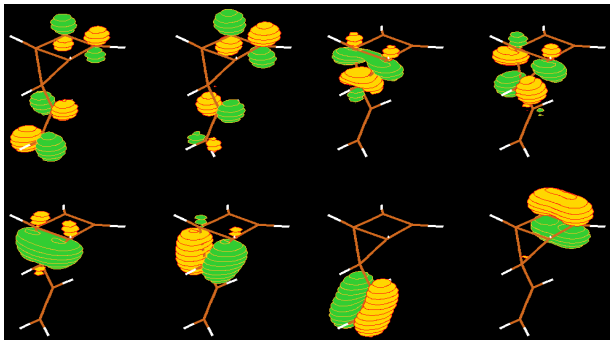

Figure 8.12: Active orbitals for Vinyl2CyPentene.

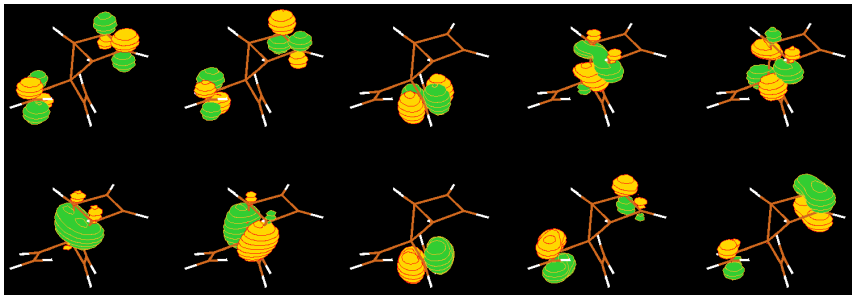

Figure 8.13: Active orbitals for 2Vinyl2CyPentene.

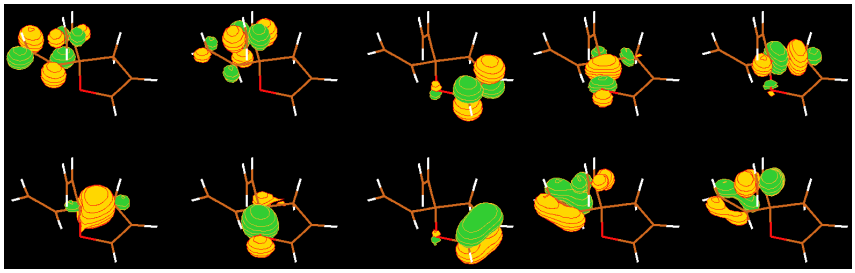

Figure 8.14: Active orbitals for 2Vinyl2HFuran.

8.6 Complementary Data Orbital Domains Results

Table 8.3: Average %Ecorr and the respective statistical data for $I = 1$ and $I = 2, RA$. σ multiplied by 100, c_v multiplied by 10^4.

		$I = 1$					$I = 2, RA$				
State	*thrpno_occ*	%Ecorr	σ	c_v	min	MAX	%Ecorr	σ	c_v	min	MAX
GS	10^{-6}	99.30	10.7	10.7	99.05	99.47	99.61	4.7	4.7	99.53	99.69
	10^{-7}	99.47	10.4	10.5	99.22	99.64	99.78	4.3	4.3	99.70	99.86
	10^{-8}	99.54	10.6	10.6	99.30	99.71	99.86	4.4	4.4	99.78	99.93
	10^{-9}	99.57	10.4	10.4	99.33	99.73	99.89	4.3	4.3	99.81	99.95
	10^{-10}	99.58	10.3	10.4	99.34	99.74	99.90	4.2	4.2	99.82	99.96
	10^{-11}	99.58	10.3	10.4	99.35	99.74	99.90	4.2	4.2	99.83	99.96
	10^{-12}	99.58	10.3	10.4	99.35	99.74	99.90	4.2	4.2	99.83	99.96
ES	10^{-6}	99.30	10.7	10.7	99.04	99.47	99.61	4.6	4.7	99.51	99.68
	10^{-7}	99.46	10.4	10.5	99.21	99.64	99.77	4.3	4.3	99.69	99.85
	10^{-8}	99.54	10.7	10.7	99.29	99.71	99.85	4.5	4.5	99.77	99.93
	10^{-9}	99.57	10.6	10.6	99.33	99.74	99.88	4.4	4.4	99.81	99.95
	10^{-10}	99.58	10.5	10.6	99.34	99.74	99.89	4.4	4.4	99.82	99.96
	10^{-11}	99.58	10.5	10.5	99.34	99.74	99.90	4.4	4.4	99.82	99.96
	10^{-12}	99.58	10.5	10.6	99.35	99.75	99.90	4.4	4.4	99.83	99.96

Table 8.4: Average %Ecorr and the respective statistical data for $I = 0$ PAO domains and the data without the energy completion criterion (off). σ multiplied by 100, c_v multiplied by 10^4.

		$I = 0$					off				
State	*thrpno_occ*	%Ecorr	σ	c_v	min	MAX	%Ecorr	σ	c_v	min	MAX
GS	10^{-6}	97.91	35.3	36.0	96.84	98.51	98.91	8.8	8.9	98.75	99.10
	10^{-7}	98.07	35.0	35.7	96.99	98.67	99.68	4.9	4.9	99.59	99.78
	10^{-8}	98.13	35.1	35.7	97.06	98.73	99.85	3.9	3.9	99.78	99.92
	10^{-9}	98.15	35.0	35.6	97.08	98.75	99.90	3.6	3.6	99.83	99.95
	10^{-10}	98.16	35.0	35.6	97.09	98.75	99.91	3.5	3.5	99.84	99.96
	10^{-11}	98.16	35.0	35.6	97.09	98.75	99.91	3.5	3.5	99.84	99.96
	10^{-12}	98.16	35.0	35.6	97.09	98.76	99.91	3.5	3.5	99.84	99.96
ES	10^{-6}	97.91	35.5	36.2	96.82	98.52	98.86	9.3	9.4	98.64	99.07
	10^{-7}	98.06	35.3	36.0	96.98	98.67	99.67	4.8	4.8	99.59	99.77
	10^{-8}	98.13	35.4	36.1	97.05	98.74	99.85	3.9	3.9	99.77	99.92
	10^{-9}	98.16	35.4	36.0	97.08	98.76	99.89	3.6	3.6	99.82	99.95
	10^{-10}	98.16	35.4	36.0	97.08	98.77	99.90	3.5	3.5	99.84	99.96
	10^{-11}	98.16	35.4	36.0	97.09	98.77	99.91	3.5	3.5	99.84	99.96
	10^{-12}	98.16	35.4	36.1	97.09	98.77	99.91	3.5	3.5	99.84	99.96

Table 8.5: avg(PNO) and the respective statistical data for $I = 1$ and $I = 2, RA$.

		$I = 1$					$I = 2, RA$				
State	*thrpno_occ*	avg(PNO)	σ	c_v	min	MAX	avg(PNO)	σ	c_v	min	MAX
GS	10^{-6}	48	3	0.06	43	55	50	3	0.05	45	56
	10^{-7}	51	3	0.06	46	58	53	3	0.05	49	59
	10^{-8}	61	5	0.08	53	70	63	4	0.06	56	71
	10^{-9}	81	7	0.09	69	93	83	6	0.07	73	94
	10^{-10}	110	9	0.08	94	126	115	8	0.07	100	130
	10^{-11}	142	11	0.08	126	163	153	10	0.07	136	173
	10^{-12}	205	19	0.09	177	258	252	27	0.11	200	296
ES	10^{-6}	48	3	0.06	44	56	50	3	0.06	44	57
	10^{-7}	51	3	0.06	46	59	53	3	0.05	49	60
	10^{-8}	63	5	0.08	55	72	65	4	0.07	58	74
	10^{-9}	85	8	0.09	73	99	88	7	0.08	76	101
	10^{-10}	116	10	0.08	99	134	121	9	0.07	105	137
	10^{-11}	148	11	0.07	133	170	159	11	0.07	141	178
	10^{-12}	205	19	0.09	177	258	252	27	0.11	200	296

Table 8.6: avg(PNO) and the respective statistical data for $I = 0$ and off, *i.e.*, without the energy completion threshold.

		off					*full*				
State	*thrpno_occ*	avg(PNO)	σ	c_v	min	MAX	avg(PNO)	σ	c_v	min	MAX
GS	10^{-6}	42	4	0.09	34	51	14	2	0.14	10	17
	10^{-7}	45	4	0.09	36	54	27	4	0.13	21	33
	10^{-8}	54	6	0.11	42	64	49	6	0.11	38	57
	10^{-9}	70	9	0.12	54	84	78	7	0.09	63	90
	10^{-10}	90	11	0.13	69	110	115	9	0.08	97	131
	10^{-11}	109	13	0.12	83	136	154	11	0.07	136	177
	10^{-12}	136	22	0.16	98	194	259	31	0.12	200	300
GS	10^{-6}	42	4	0.09	34	51	15	2	0.15	12	19
	10^{-7}	45	4	0.09	37	54	30	4	0.14	23	38
	10^{-8}	55	6	0.12	43	67	53	6	0.12	42	65
	10^{-9}	74	9	0.13	57	91	84	8	0.09	68	96
	10^{-10}	95	12	0.13	72	119	121	9	0.07	103	137
	10^{-11}	113	14	0.12	86	144	161	11	0.07	141	184
	10^{-12}	136	22	0.16	98	194	259	31	0.12	200	300

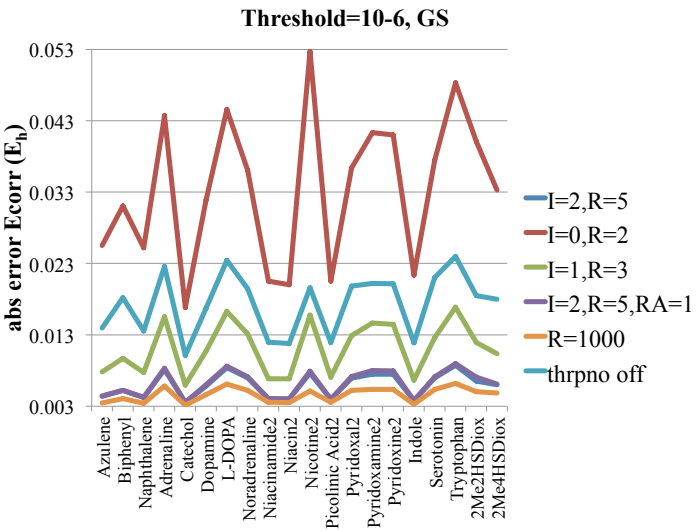

Figure 8.15: Absolute error on GS Ecorr in E_h for *thrpno_occ* $= 10^{-6}$. Comparison for different PAO domain sizes and for *thrpno* off.

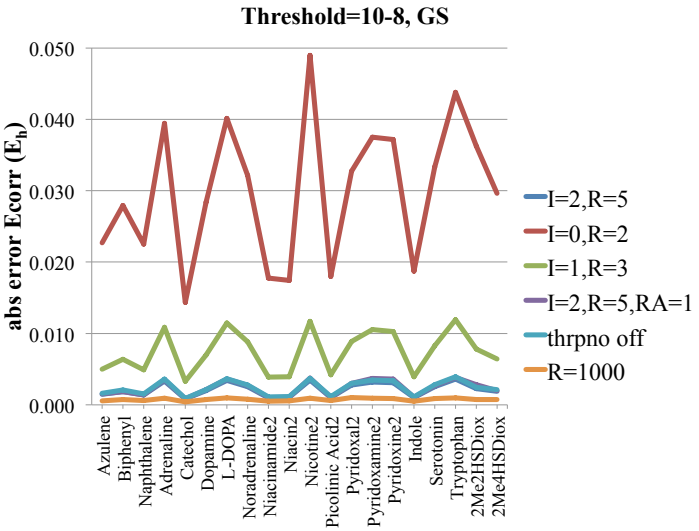

Figure 8.16: Absolute error on GS Ecorr in E_h for *thrpno_occ* $= 10^{-6}$. Comparison for different PAO domain sizes and for *thrpno* off.

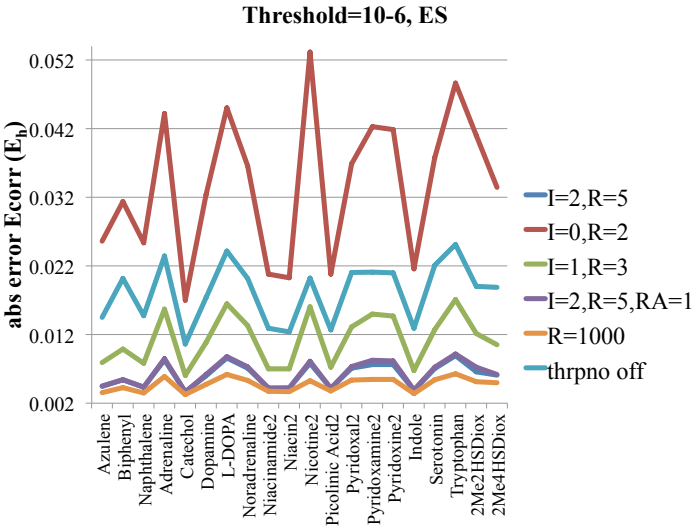

Figure 8.17: Absolute error on ES Ecorr in E_h for *thrpno_occ* $= 10^{-6}$. Comparison for different PAO domain sizes and for *thrpno* off.

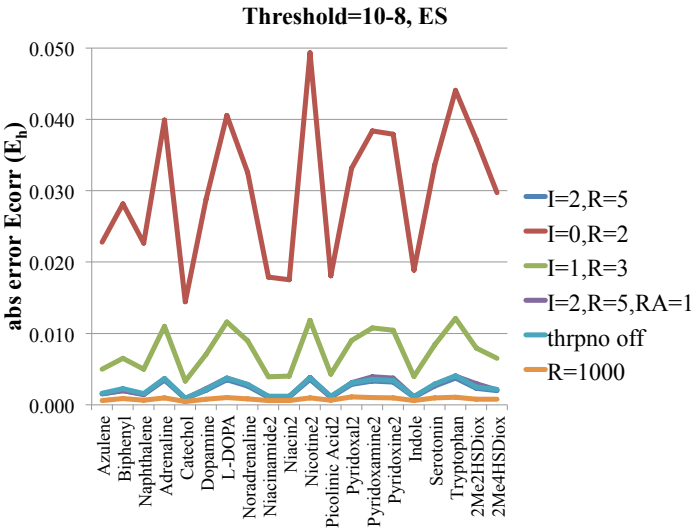

Figure 8.18: Absolute error on ES Ecorr in E_h for *thrpno_occ* $= 10^{-8}$. Comparison for different PAO domain sizes and for *thrpno* off.

8.7 Complementary Data Reaction Energies

To convert triplet reaction energies into singlet reaction energies we can use the following balance of energy

$$\begin{array}{ccccc} & & \Delta E_S^{rx} & & \\ & {}^1R_A + {}^1R_B & \longrightarrow & {}^1P & \\ \Delta E_{ST}^{R_B} & \downarrow & & \downarrow & \Delta E_{ST}^{P} \\ & {}^1R_A + {}^3R_B & \longrightarrow & {}^3P & \\ & & \Delta E_T^{rx} & & \end{array}$$

This allows us to write the following equation:

$$\Delta E_T^{rx} + \Delta E_{ST}^{R_B} = \Delta E_S^{rx} + \Delta E_{ST}^{P}$$

yielding

$$\begin{aligned} \Leftrightarrow \Delta E_S^{rx} &= \Delta E_T^{rx} - \Delta E_{ST}^{P} + \Delta E_{ST}^{R_B} \\ \Leftrightarrow \Delta E_S^{rx} &= E_T^{P} - E_T^{R_A} - E_T^{R_B} - \Delta E_{ST}^{P} + \Delta E_{ST}^{R_B} \\ \Leftrightarrow \Delta E_S^{rx} &= E_S^{P} - E_T^{R_A} - E_T^{R_B} + \Delta E_{ST}^{R_B} \end{aligned}$$

Any of the last three equations can be used to calculate ΔE_S^{rx}.

The orbital diagram for the electrocyclic reaction is presented below. The black horizontal lines represent qualitatively the orbital energies. The arrows (upwards and downwards) represent the electronic occupation of the orbitals and the blue lines connecting

orbitals represent the orbital changes from reagent to product. The letter S stands for symmetric orbital with respect to the symmetry plan conserved during the reaction and A for antisymmetric.

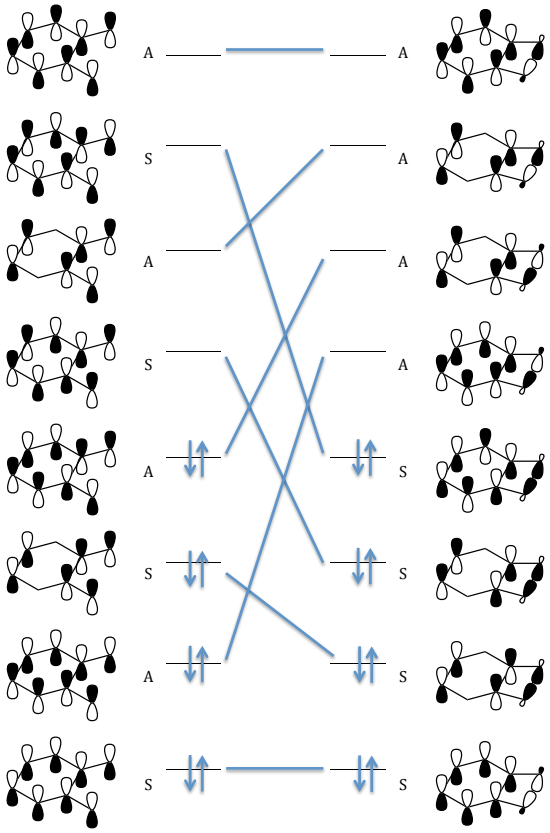

Figure 8.19: The MO diagram for the electrocyclic reaction presented in Figure 6.19.

8.8 Complementary Data Basis Sets Results

Table 8.7: Average %Ecorr, the respective standard deviation (σ), coefficients of variation (c_v; multiplied by 10^4), minima and maxima for aug-cc-pVDZ and aug-cc-pVTZ.

GS

	aug-cc-pVDZ					aug-cc-pVTZ				
thrpno_occ	avg	σ	c_v	min	MAX	avg	σ	c_v	min	MAX
10^{-6}	99.66	0.03	3.5	99.58	99.72	99.63	0.03	2.9	99.57	99.67
10^{-7}	99.82	0.03	3.5	99.76	99.88	99.78	0.02	2.4	99.75	99.82
10^{-8}	99.90	0.03	3.2	99.83	99.95	99.89	0.02	2.2	99.85	99.92
10^{-9}	99.93	0.03	3.0	99.86	99.97	99.93	0.02	2.0	99.89	99.96
10^{-10}	99.94	0.03	2.9	99.87	99.98	99.94	0.02	1.9	99.90	99.97
10^{-11}	99.94	0.03	2.9	99.87	99.98	99.94	0.02	1.8	99.91	99.97
10^{-12}	99.94	0.03	2.9	99.87	99.98	99.94	0.02	1.8	99.91	99.97

ES

	aug-cc-pVDZ					aug-cc-pVTZ				
thrpno_occ	avg	σ	c_v	min	MAX	avg	σ	c_v	min	MAX
10^{-6}	99.65	0.03	3.1	99.58	99.70	99.63	0.03	2.7	99.57	99.66
10^{-7}	99.81	0.03	3.3	99.75	99.87	99.77	0.02	2.2	99.73	99.81
10^{-8}	99.89	0.03	3.3	99.82	99.95	99.88	0.02	2.2	99.85	99.92
10^{-9}	99.93	0.03	3.1	99.86	99.97	99.92	0.02	2.0	99.89	99.95
10^{-10}	99.94	0.03	3.0	99.87	99.98	99.94	0.02	1.9	99.90	99.97
10^{-11}	99.94	0.03	3.0	99.87	99.98	99.94	0.02	1.9	99.91	99.97
10^{-12}	99.94	0.03	3.0	99.87	99.98	99.94	0.02	1.9	99.91	99.97

Table 8.8: avg(PNO), the respective standard deviation (σ), coefficients of variation, minima and maxima for aug-cc-pVDZ and aug-cc-pVTZ.

GS

	aug-cc-pVDZ					aug-cc-pVTZ				
thrpno_occ	avg	σ	c_v	min	MAX	avg	σ	c_v	min	MAX
10^{-6}	48	4	0.09	40	57	92	8	0.09	78	108
10^{-7}	52	4	0.07	47	60	96	7	0.07	83	110
10^{-8}	65	4	0.06	61	74	111	6	0.06	103	126
10^{-9}	88	5	0.06	83	101	147	9	0.06	138	166
10^{-10}	119	8	0.07	108	137	207	13	0.06	194	231
10^{-11}	152	14	0.09	127	177	282	19	0.07	254	319
10^{-12}	229	40	0.17	158	296	513	84	0.16	361	665

ES

	aug-cc-pVDZ					aug-cc-pVTZ				
thrpno_occ	avg	σ	c_v	min	MAX	avg	σ	c_v	min	MAX
10^{-6}	48	4	0.09	40	56	92	8	0.09	78	109
10^{-7}	52	4	0.07	46	60	95	7	0.07	84	111
10^{-8}	64	4	0.06	60	72	114	6	0.05	108	129
10^{-9}	86	5	0.06	81	98	155	10	0.06	142	175
10^{-10}	116	8	0.07	105	132	220	14	0.06	204	249
10^{-11}	149	13	0.09	125	172	297	21	0.07	268	342
10^{-12}	229	40	0.17	158	296	513	84	0.16	361	665

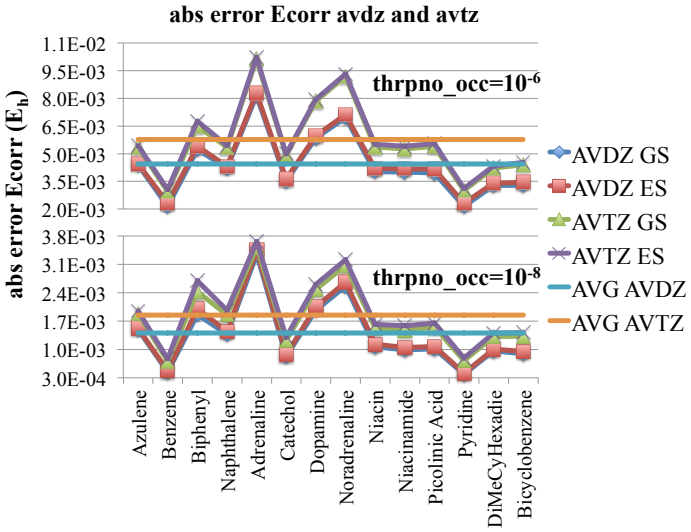

Figure 8.20: Absolute error on Ecorr in E_h for *thrpno_occ* $= 10^{-6}$ (6) and *thrpno_occ* $= 10^{-8}$ (8). Comparison between basis sets aug-cc-pVDZ and aug-cc-pVTZ.

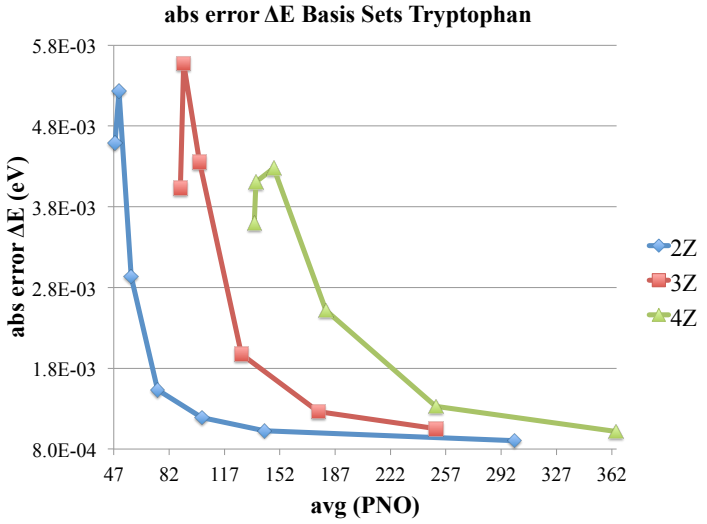

Figure 8.21: Convergence excitation energies for tryptophan using aug-cc-pVDZ (2Z), aug-cc-pVTZ (3Z) and aug-cc-pVQZ (4Z) basis sets. *thrpno_occ* ranges from 10^{-6} to 10^{-12} for 2Z and from 10^{-6} to 10^{-11} to 3Z and 4Z.

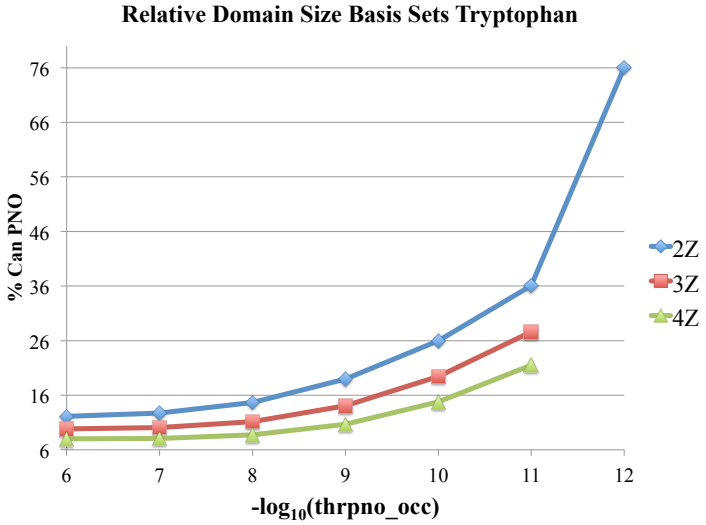

Figure 8.22: Relative PNO domain size against $-log_{10}(thrpno\_occ)$ for tryptophan. Data for basis sets aug-cc-pVDZ (2Z), aug-cc-pVTZ (3Z) and aug-cc-pVQZ (4Z). *thrpno_occ* ranges from 10^{-6} to 10^{-12} for 2Z and from 10^{-6} to 10^{-11} to 3Z and 4Z.

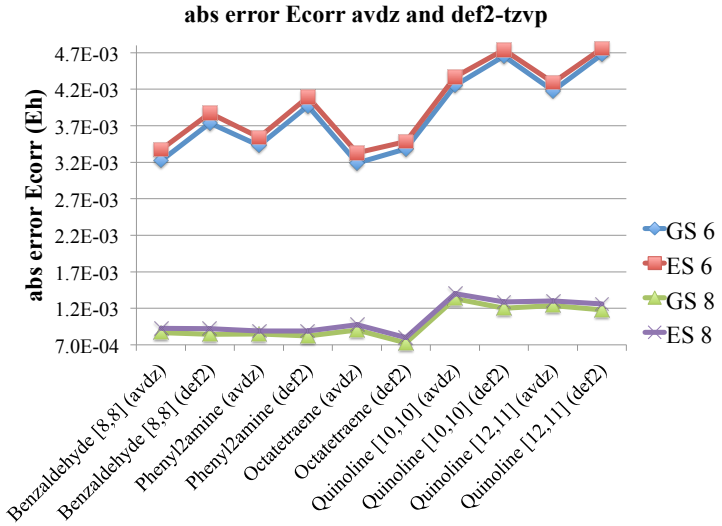

Figure 8.23: Absolute error on Ecorr in E_h for $thrpno\_occ = 10^{-6}$ (6) and $thrpno\_occ = 10^{-8}$ (8). Comparison between basis sets aug-cc-pVDZ and def2-tzvp.

Table 8.9: Average %Ecorr, the respective standard deviation (σ; multiplied by 10^2), coefficients of variation (c_v; multiplied by 10^4), minima and maxima for the basis sets aug-cc-pVDZ and def2-tzvp.

		GS									
		aug-cc-pVDZ					def2-tzvp				
State	*thrpno_occ*	avg	σ	c_v	min	MAX	avg	σ	c_v	min	MAX
GS	10^{-6}	99.67	1.3	1.3	99.66	99.69	99.69	1.1	1.1	99.68	99.71
	10^{-7}	99.83	1.7	1.7	99.81	99.85	99.83	1.6	1.6	99.81	99.85
	10^{-8}	99.91	1.1	1.1	99.89	99.92	99.93	0.85	0.85	99.92	99.94
	10^{-9}	99.94	0.84	0.84	99.92	99.95	99.96	0.44	0.44	99.95	99.97
	10^{-10}	99.94	0.77	0.77	99.93	99.96	99.97	0.29	0.29	99.97	99.97
	10^{-11}	99.95	0.76	0.76	99.94	99.96	99.97	0.24	0.24	99.97	99.98
	10^{-12}	99.95	0.75	0.75	99.94	99.96	99.97	0.23	0.23	99.97	99.98
ES	10^{-6}	99.67	1.3	1.3	99.65	99.69	99.68	1.1	1.1	99.67	99.70
	10^{-7}	99.82	1.7	1.7	99.80	99.84	99.82	1.7	1.7	99.80	99.84
	10^{-8}	99.90	1.2	1.2	99.89	99.92	99.92	0.87	0.87	99.91	99.93
	10^{-9}	99.93	0.86	0.86	99.92	99.95	99.96	0.46	0.46	99.95	99.96
	10^{-10}	99.94	0.79	0.79	99.93	99.96	99.97	0.29	0.29	99.97	99.97
	10^{-11}	99.95	0.77	0.77	99.94	99.96	99.97	0.25	0.25	99.97	99.98
	10^{-12}	99.95	0.76	0.76	99.94	99.96	99.97	0.24	0.24	99.97	99.98

Table 8.10: avg(PNO), the respective standard deviation (σ), coefficients of variation, minima and maxima for the basis sets aug-cc-pVDZ and def2-tzvp.

		aug-cc-pVDZ					def2-tzvp				
State	*thrpno_occ*	avg	σ	c_v	min	MAX	avg	σ	c_v	min	MAX
GS	10^{-6}	48	4	0.08	44	53	71	6	0.09	63	79
	10^{-7}	52	3	0.06	48	56	74	6	0.08	67	82
	10^{-8}	64	4	0.06	60	69	88	6	0.07	79	96
	10^{-9}	85	6	0.07	78	92	114	9	0.08	101	125
	10^{-10}	115	9	0.08	103	126	150	14	0.09	130	168
	10^{-11}	146	12	0.08	131	160	190	20	0.10	162	214
	10^{-12}	225	17	0.08	199	245	271	25	0.09	244	302
ES	10^{-6}	48	4	0.08	44	53	71	7	0.09	64	80
	10^{-7}	52	3	0.07	49	57	74	6	0.08	68	83
	10^{-8}	67	4	0.06	62	72	90	7	0.07	82	99
	10^{-9}	91	6	0.07	84	98	120	10	0.08	107	132
	10^{-10}	122	9	0.08	111	133	158	15	0.09	138	177
	10^{-11}	152	12	0.08	138	167	197	20	0.10	169	222
	10^{-12}	225	17	0.08	199	245	271	25	0.09	244	302

8.9 Complementary Data Scaling Results

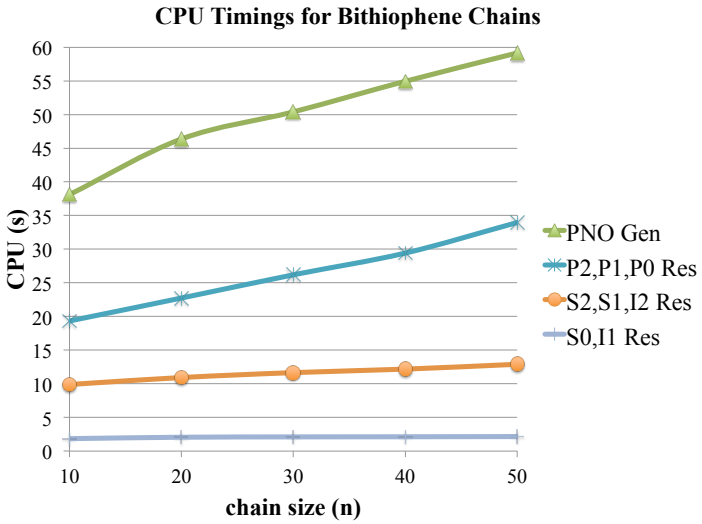

Figure 8.24: Zoom-in in CPU timings for the bithiophene chains. *PNO Gen* stands for the algorithm to generate PNOs and *Res* for the algorithms to solve the residual equations for groups of configuration subspaces. Zoom in for the region 0 to 60 s.

Bibliography

1. P. Pulay *Chem. Phys. Lett.*, vol. 100(2), p. 151, 1983.
2. M. Schütz, G. Hetzer, and H.-J. Werner *J. Chem. Phys.*, vol. 111(13), p. 5691, 1999.
3. H.-J. Werner and M. Schütz *J. Chem. Phys.*, vol. 135, p. 144116, 2011.
4. F. Neese, F. Wennmohs, and A. Hansen *J. Chem. Phys.*, vol. 130, p. 114108, 2009.
5. C. Møller and M. S. Plesset *Phys. Rev.*, vol. 46, p. 618, 1934.
6. F. Jensen, *Introduction to Computational Chemistry*. Wiley, 2007.
7. R. J. Bartlett and M. D. Silver *J. Chem. Phys.*, vol. 62, p. 325, 1975.
8. P. Pulay and S. Sæbø *Theor. Chim. Acta*, vol. 69, p. 357, 1986.
9. K. Hirao *Chem. Phys. Lett.*, vol. 196, p. 397, 1992.
10. T. Helgaker, P. Jørgensen, and J. Olsen, *Molecular Electronic-Structure Theory*. Wiley, 2014.
11. A. Szabo and N. S. Ostlund, *Modern Quantum Chemistry: Introduction to Advanced Electronic Structure Theory*, ch. Many-Body Perturbation Theory. In *Dover Books on Chemistry (414)*, 1996.
12. P. M. Kozlowski and E. R. Davidson *J. Chem. Phys.*, vol. 100, p. 3672, 1994.
13. K. Wolinski, H. L. Sellers, and P. Pulay *Chem. Phys. Lett.*, vol. 140, p. 225, 1987.
14. H.-J. Werner *Mol. Phys.*, vol. 89(2), p. 645, 1996.
15. P. Celani and H.-J. Werner *J. Chem. Phys.*, vol. 112(13), p. 5546, 2000.
16. J. A. Pople and R. K. Nesbet *J. Chem. Phys.*, vol. 22, p. 571, 1954.
17. R. Krishnan, M. J. Frisch, and J. A. Pople *J. Chem. Phys.*, vol. 72, p. 4244, 1980.
18. N. C. Handy, P. J. Knowles, and K. Somasundram *Theor. Chim. Acta*, vol. 68, p. 87, 1985.

19. P. J. Knowles, K. Somasundram, N. C. Handy, and K. Hirao *Chem. Phys. Lett.*, vol. 113, p. 8, 1985.

20. R. H. Nobes, J. A. Pople, L. Radom, N. C. Handy, and P. J. Knowles *Chem. Phys. Lett.*, vol. 138, p. 481, 1987.

21. J. S. Andrews, D. Jayatilaka, R. G. A. Bone, N. C. Handy, and R. D. Amos *Chem. Phys. Lett.*, vol. 183, p. 423, 1991.

22. M. S. Gordon and D. G. Truhlar *Theor. Chim. Acts*, vol. 71, p. 1, 1987.

23. P. M. Kozlowski and E. R. Davidson *Chem. Phys. Lett.*, vol. 222, p. 615, 1994.

24. H. B. Schlegel *J. Chem. Phys.*, vol. 84, p. 4530, 1986.

25. H. B. Schlegel *J. Phys. Chem.*, vol. 92, p. 3075, 1988.

26. P. J. Knowles and N. C. Handy *J. Phys. Chem.*, vol. 92, p. 3097, 1988.

27. P. J. Knowles and N. C. Handy *J. Chem. Phys.*, vol. 88, p. 6991, 1988.

28. I. Hubač and P. Čársk*i Phys. Rev. A*, vol. 22, p. 2392, 1980.

29. R. D. Amos, J. S. Andrews, N. C. Handy, and P. J. Knowles *Chem. Phys. Lett.*, vol. 185, p. 256, 1991.

30. P. J. Knowles, J. S. Andrews, R. D. Amos, N. C. Handy, and J. A. Pople *Chem. Phys. Lett.*, vol. 186, p. 1991, 130.

31. W. J. Lauderdale, J. F. Stanton, J. Gauss, J. D. Watts, and R. J. Bartlett *Chem. Phys. Lett.*, vol. 187, p. 21, 1991.

32. C. W. Murray and E. R. Davidson *Chem. Phys. Lett.*, vol. 187, p. 451, 1991.

33. C. W. Murray and E. R. Davidson *Int. J. Quantum Chem.*, vol. 43, p. 755, 1992.

34. C. W. Murray and N. C. Handy *J. Chem. Phys.*, vol. 97, p. 6509, 1992.

35. T. J. Lee and D. Jayatilaka *Chem. Phys. Lett.*, vol. 201, p. 1, 1993.

36. J. S. Andrews, C. W. Murray, and N. C. Handy *Chem. Phys. Lett.*, vol. 201, p. 458, 1993.

37. D. J. Tozer, N. C. Handy, R. D. Amos, J. A. Pople, R. H. Nobes, Y. Xie, and H. F. S. III *Mol. Phys.*, vol. 79, p. 777, 1993.

38. T. J. Lee, A. P. Rendell, K. Dyall, and D. Jayatilaka *J. Chem. Phys.*, vol. 100, p. 7400, 1993.

39. K. Andersson, P.-Å. Malmqvist, B. O. Roos, A. J. Sadlej, and K. Wolinski *J. Phys. Chem.*, vol. 94, p. 5483, 1990.

40. K. Hirao *Chem. Phys. Lett.*, vol. 190, p. 374, 1992.

41. R. B. Murphy and R. P. Messmer *Chem. Phys. Lett.*, vol. 183, p. 443, 1991.

42. R. B. Murphy and R. P. Messmer *J. Chem. Phys.*, vol. 97, p. 4170, 1992.

43. H.-J. Werner and P. J. Knowles *J. Chem. Phys.*, vol. 89(9), p. 5803, 1988.

44. K. Hirao *Chem. Phys. Lett.*, vol. 201, p. 59, 1993.

45. H.-J. Werner, *Ab Initio Methods in Quantum Chemistry II*, ch. Matrix-Formulated Direct Multiconfiguration Self-Consistent Field and Multiconfiguration Reference Configuration Interaction Methods. In Lawley (*415*), 1987.

46. B. O. Roos, *Ab Initio Methods in Quantum Chemistry II*, ch. The Complete Active Space Self-Consistent Field Method and its Applications in Electronic Structure Calculations. In Lawley (*415*), 1987.

47. R. Shepard, *Ab Initio Methods in Quantum Chemistry II*, ch. The Multiconfiguration Self-Consistent Field Method. In Lawley (*415*), 1987.

48. B. O. Roos, P. R. Taylor, and P. E. M. Siegbahn *Chem. Phys.*, vol. 48, p. 157, 1980.

49. P. E. M. Siegbahn, J. Almlöf, A. Heiberg, and B. O. Roos *J. Chem. Phys.*, vol. 74, p. 2384, 1981.

50. B. O. Roos *Int. J. Quantum Chem.*, vol. S14, p. 175, 1980.

51. K. Ruedenberg, M. W. Schmidt, M. M. Gilbert, and S. T. Elbert *Chem. Phys.*, vol. 71, p. 41, 1982.

52. K. Ruedenberg, L. M. Cheung, and S. T. Elbert *Int. J. Quant. Chem.*, vol. 16, p. 1069, 1979.

53. C. Bloch *Nuc. Phys.*, vol. 6, p. 329, 1958.

54. J. H. C. Bloch *Nuc. Phys.*, vol. 8, p. 91, 1958.

55. B. H. Brandow *Rev. Mod. Phys.*, vol. 39, p. 771, 1967.

56. H. P. Kelly *Adv. Chem. Phys.*, vol. 14, p. 129, 1969.

57. K. Wolinski and P. Pulay *J. Chem. Phys.*, vol. 90, p. 3647, 1989.

58. B. O. Roos, P. Linse, P. E. M. Siegbahn, and M. R. A. Blomberg *Chem. Phys.*, vol. 66, p. 197, 1982.

59. R. K. Nesbet *Proc. R. Soc. London Ser. A*, vol. 230, p. 312, 1955.

60. D. M. Silver, S. Wilson, and R. J. Bartlett *Phys. Rev. A*, vol. 16, p. 477, 1977.

61. E. R. Davidson and C. F. Bender *Chem. Phys. Lett.*, vol. 59, p. 369, 1978.

62. P. Celani and H.-J. Werner *J. Chem. Phys.*, vol. 119(10), p. 5044, 2003.

63. P. Pulay *Int. J. Quantum Chem.*, vol. 111, p. 3273, 2011.

64. K. Andersson, P.-Å. Malmqvist, and B. O. Roos *J. Chem. Phys.*, vol. 96, p. 1218, 1992.

65. P. Knowles, M. Schütz, and H.-J. Werner, *Modern Methods and Algorithms of Quantum Chemistry*, ch. Ab Initio Methods for Electron Correlation in Molecules. In Grotendorst (*354*), 2000.

66. S. Sæbø and P. Pulay *J. Chem. Phys.*, vol. 86(2), p. 914, 1987.

67. N. C. Handy, R. D. Amos, J. F. Gaw, J. E. Rice, and E. D. Simandiras *Chem. Phys. Lett.*, vol. 120, p. 151, 1985.

68. S. Sæbø *Int. J. Quantum Chem.*, vol. 38, p. 641, 1990.

69. C. Angeli, R. Cimiraglia, S. Evangelisti, T. Leininger, and J.-P. Malrieu *J. Chem. Phys.*, vol. 114, p. 10252, 2001.

70. C. Angeli, R. Cimiraglia, and J.-P. Malrieu *J. Chem. Phys.*, vol. 117, p. 9138, 2002.

71. C. Angeli, M. Pastore, and R. Cimiraglia *Theor. Chem. Acc.*, vol. 117, p. 743, 2007.

72. Y. Guo, K. Sivalingam, E. F. Valeev, and F. Neese *J. Chem. Phys.*, vol. 144, p. 094111, 2016.

73. P. M. Kozlowski and E. R. Davidson *Chem. Phys. Lett.*, vol. 226, p. 440, 1994.

74. T. Shiozaki, W. Győrffy, P. Celani, and H.-J. Werner *J. Chem. Phys.*, vol. 135, p. 081106, 2011.

75. K. Andersson and B. O. Roos *Chem. Phys. Lett.*, vol. 191(6), p. 507, 1992.

76. K. Andersson and B. O. Roos *Int. J. Quantum Chem.*, vol. 45, p. 591, 1993.

77. R. González-Luque, M. Merchán, and B. O. Roos *Chem. Phys.*, vol. 171, p. 107, 1993.

78. R. González-Luque, M. Merchán, and B. O. R. P. Borowski *Theor. Chim. Acta*, vol. 86, p. 467, 1993.

79. L. Serrano-Andrés, M. Merchán, I. Nebot-Gil, B. O. Roos, and M. Fülscher *J. Am. Chem. Soc.*, vol. 115, p. 6184, 1993.

80. M. Merchán, L. Serrano-Andrés, R. González-Luque, and M. R. B. O. Roos *J. Mol. Struct. THEOCHEM*, vol. 463, p. 201, 1998.

81. B. O. Roos, K. Andersson, M. P. Fülscher, P.-Å. Malmqvist, L. Serrano-Andrés, K. Pierloot, and M. Merchán *Adv. Chem. Phys.*, vol. 93, p. 219, 1996.

82. B. O. Roos *Acc. Chem. Res.*, vol. 32, p. 137, 1999.

83. B. O. Roos, M. P. Fülscher, P.-Å. Malmqvist, L. Serrano-Andrés, and M. Merchán, ch. Theoretical Studies of the Electronic Spectra of Organic Molecules.

84. M. Merchán, L. Serrano-Andrés, M. P. Fülscher, and B. O. Roos *Recent Adv. Comput. Chem.*, vol. 4, p. 161, 1999.

85. L. Serrano-Andrés and M. Merchán *J. Mol. Struct. THEOCHEM*, vol. 729, p. 99, 2005.

86. K. Andersson, B. O. Roos, P.-Å. Malmqvist, and P. O. Widmark *Chem. Phys. Lett.*, vol. 230, p. 391, 1994.

87. K. Andersson and B. O. Roos, *Modern Electronic Structure Theory*, ch. Multiconfigurational Second-Order Perturbation Theory. In Yarkony (*416*), 1994.

88. M. F. Rode and H.-J. Werner *Theor. Chem. Acc.*, vol. 114, p. 309, 2005.

89. J. Finley, P.-Å. Malmqvist, B. O. Roos, and L. Serrano-Andrés *Chem. Phys. Lett.*, vol. 288, p. 299, 1988.

90. J.-P. Malrieu, J.-L. Heully, and A. Zaitzevskii *Theor. Chim. Acta.*, vol. 90, p. 167, 1995.

91. B. O. Roos and K. Andersson *Chem. Phys. Lett.*, vol. 245, p. 215, 1995.

92. T. Shiozaki, C. Woywod, and H.-J. Werner *Phys. Chem. Chem. Phys.*, vol. 15, p. 262, 2013.

93. T. Shiozaki and H.-J. Werner *Mol. Phys.*, vol. 111(5), p. 607, 2013.

94. F. Aquilante, P.-Å. Malmqvist, T. B. Pedersen, A. Ghosh, and B. O. Roos *J. Chem. Theory Comput.*, vol. 4(5), p. 694, 2008.

95. F. Aquilante, R. L. T. B. Pedersen, B. O. Roos, A. S. de Merás, and H. Koch *J. Chem. Phys.*, vol. 129, p. 024113, 2008.

96. W. Győrffy, T. Shiozaki, G. Knizia, and H.-J. Werner *J. Chem. Phys.*, vol. 138, p. 104104, 2013.

97. T. Shiozaki and H.-J. Werner *J. Chem. Phys.*, vol. 133, p. 141103, 2010.

98. T. Shiozaki, G. Knizia, and H.-J. Werner *J. Chem. Phys.*, vol. 134, p. 034113, 2011.

99. T. Shiozaki and H.-J. Werner *J. Chem. Phys.*, vol. 134, p. 184104, 2011.

100. S. Ten-no *Chem. Phys. Lett.*, vol. 447, p. 175, 2007.

101. H. Fliegl, W. Klopper, and C. Hättig *J. Chem. Phys.*, vol. 122, p. 084107, 2005.

102. D. P. Tew, W. Klopper, C. Neiss, and C. Hättig *Phys. Chem. Chem. Phys.*, vol. 9, p. 1921, 2007.

103. T. B. Adler, G. Knizia, and H.-J. Werner *J. Chem. Phys.*, vol. 127, p. 221106, 2007.

104. H.-J. Werner, G. Knizia, and F. R. Manby *Mol. Phys.*, vol. 109, p. 407, 2011.

105. G. Knizia, T. B. Adler, and H.-J. Werner *Mol. Phys.*, vol. 130, p. 054104, 2009.

106. C. Hättig, D. P. Tew, and A. Köhn *J. Chem. Phys.*, vol. 132, p. 231102, 2010.

107. H.-J. Werner and E. A. Reinsch *J. Chem. Phys.*, vol. 76, p. 3144, 1982.

108. P. J. Knowles and H.-J. Werner *Chem. Phys. Lett.*, vol. 145(6), p. 514, 1988.

109. H.-J. Werner and P. J. Knowles *Theor. Chem. Acc.*, vol. 78, p. 175, 1990.

110. P. J. Knowles and H.-J. Werner *Theor. Chem. Acc.*, vol. 84, p. 95, 1992.

111. K. R. Shamasundar, G. Knizia, and H.-J. Werner *J. Chem. Phys.*, vol. 135, p. 054101, 2011.

112. B. O. Roos *Chem. Phys. Lett.*, vol. 15, p. 153, 1972.

113. B. O. Roos and P. E. M. Siegbahn, ch. The Direct Configuration Interaction Method from Molecular Integrals.

114. P. E. M. Siegbahn *Chem. Phys.*, vol. 25, p. 197, 1977.

115. R. Fink and V. Staemmler *Theor. Chim. Acta*, vol. 87, p. 129, 1993.

116. P. Celani, H. Stoll, H.-J. Werner, and P. J. Knowles *Mol. Phys.*, vol. 122, p. 2369, 2004.

117. T. J. Martinez and E. A. Carter *J. Chem. Phys.*, vol. 102, p. 7564, 1995.

118. P. E. M. Siegbahn *J. Chem. Phys.*, vol. 72, p. 1647, 1980.

119. V. R. Saunders and J. H. van Lenthe *Mol. Phys.*, vol. 48, p. 923, 1983.

120. H. Lischka, R. Shepard, F. B. Brown, and I. Shavitt *Int. J. Quant. Chem.*, vol. 20, p. 91, 1981.

121. A. Banerjee and J. Simons *Int. J. Quantum Chem.*, vol. 19, p. 207, 1981.

122. F. A. Evangelista and J. Gauss *J. Chem. Phys.*, vol. 134, p. 114102, 2011.

123. F. A. Evangelista, M. Hanauer, A. Köhn, and J. Gauss *J. Chem. Phys.*, vol. 136, p. 204108, 2012.

124. M. Hanauer and A. Köhn *J. Chem. Phys.*, vol. 136, p. 204107, 2012.

125. M. Hanauer and A. Köhn *Chem. Phys.*, vol. 401, p. 50, 2012.

126. M. Hanauer and A. Köhn *J. Chem. Phys.*, vol. 134, p. 204111, 2011.

127. W. Liu, M. Hanauer, and A. Köhn *Chem. Phys. Lett.*, vol. 565, p. 122, 2013.

128. P. K. Samanta, D. Mukherjee, M. Hanauer, and A. Köhn *J. Chem. Phys.*, vol. 140, p. 134108, 2014.

129. M. Hanauer and A. Köhn *J. Chem. Phys.*, vol. 137, p. 131103, 2012.

130. U. S. Mahapatra, B. Datta, B. Bandyopadhyay, and D. Mukherjee *Adv. Quant. Chem.*, vol. 30, p. 163, 1998.

131. J. Yang, G. K.-L. Chan, F. R. Manby, M. Schütz, and H.-J. Werner *J. Chem. Phys.*, vol. 136(14), p. 144105, 2012.

132. S. Sæbø and P. Pulay *Ann. Rev. Phys. Chem.*, vol. 44, p. 213, 1993.

133. M. Schütz and H.-J. Werner *J. Chem. Phys.*, vol. 114(2), p. 661, 2001.

134. S. Sæbø *Int. J. Quantum Chem.*, vol. 42, p. 217, 1992.

135. I. Shavitt, ch. The Method Of Configuration Interaction.

136. S. Sæbø and P. Pulay *J. Chem. Phys.*, vol. 88(3), p. 1884, 1988.

137. C. Riplinger and F. Neese *J. Chem. Phys.*, vol. 138, p. 034106, 2013.

138. T. D. Crawford and H. F. S. III, "Introduction to coupled-cluster theory for computational chemists." [Online; accessed 12-January-2016].

139. C. Riplinger, B. Sandhoefer, A. Hansen, and F. Neese *J. Chem. Phys.*, vol. 139, p. 134101, 2013.

140. S. Sæbø and P. Pulay *Chem. Phys. Lett.*, vol. 113, p. 13, 1985.

141. O. Sinanoğlu *Adv. Chem. Phys.*, vol. 6, p. 315, 1964.

142. R. K. Nesbet *Adv. Chem. Phys.*, vol. 9, p. 321, 1965.

143. P. Otto and J. Ladik *Int. J. Quantum Chem.*, vol. 22, p. 169, 1982.

144. W. D. Laidig, G. D. P. III, and R. J. Bartlett *Int. J. Quantum Chem. Symp.*, vol. 6, p. 561, 1982.

145. W. D. Laidig, G. D. P. III, and R. J. Bartlett *Chem. Phys. Lett.*, vol. 97, p. 209, 1983.

146. W. D. Laidig, G. D. P. III, and R. J. Bartlett *J. Phys. Chem.*, vol. 89, p. 2161, 1985.

147. C. Hampel and H.-J. Werner *J. Chem. Phys.*, vol. 104, p. 6286, 1996.

148. H.-J. Werner, G. Knizia, C. Krause, M. Schwilk, and M. Dornbach *J. Chem. Theor. Comp.*, vol. 11, p. 484, 2015.

149. C. Krause and H.-J. Werner *Phys. Chem. Chem. Phys.*, vol. 14, p. 7591, 2012.

150. T. B. Adler and H.-J. Werner *J. Chem. Phys.*, vol. 135, p. 144117, 2011.

151. W. Meyer *Int. J. Quantum Chem. Symp.*, vol. 5S, p. 341, 1971.

152. W. Meyer *J. Chem. Phys.*, vol. 58, p. 1017, 1973.

153. F. Neese, A. Hansen, and D. G. Liakos *J. Chem. Phys.*, vol. 131, p. 064103, 2009.

154. L. M. J. Huntington, A. Hansen, F. Neese, and M. Nooijen *J. Chem. Phys.*, vol. 136, p. 064101, 2012.

155. J. Yang, Y. Kurashige, F. R. Manby, and G. K. L. Chan *J. Chem. Phys.*, vol. 134, p. 044123, 2011.

156. W. Förner, J. Ladik, P. Otto, and J. Čížek *Chem. Phys.*, vol. 97, p. 251, 1985.

157. J. E. Subotnik, A. D. Dutoi, and M. Head-Gordon *J. Chem. Phys.*, vol. 123, p. 114108, 2005.

158. B. Jansìk, S. Høst, K. Kristensen, and P. Jørgensen *J. Chem. Phys.*, vol. 134, p. 194104, 2011.

159. E. Kapuy, Csépes, and C. Kozmutza *Int. J. Quantum Chem.*, vol. 23, p. 981, 1983.

160. C. Edmiston and M. Krauss *J. Chem. Phys.*, vol. 45, p. 1833, 1966.

161. W. Kutzelnigg *Theor. Chim. Acta (Berl.)*, vol. 1, p. 327, 1963.

162. P. R. Taylor, G. B. Backskay, N. S. Hush, and A. C. Hurley *Chem. Phys. Lett.*, vol. 41, p. 444, 1976.

163. M. Schütz, J. Yang, G. K.-L. Chan, F. R. Manby, and H.-J. Werner *J. Chem. Phys.*, vol. 138, p. 054109, 2013.

164. C. Kozmutza and E. Kapuy *Int. J. Quantum Chem.*, vol. 38, p. 665, 1990.

165. E. Kapuy, F. Bogar, F. Bartha, and C. Kozmutza *J. Mol. Struct.*, vol. 79, p. 61, 1991.

166. E. Kapuy and C. Kozmutza *J. Chem. Phys.*, vol. 94, p. 5565, 1991.

167. C. Kozmutza and E. Kapuy *J. Comp. Chem.*, vol. 12, p. 953, 1991.

168. D. B. Krisiloff and E. A. Carter *Phys. Chem. Chem. Phys.*, vol. 14, p. 7710, 2012.

169. S. F. Boys *Rev. Mod. Phys.*, vol. 32(2), p. 296, 1960.

170. S. F. Boys, *Quantum Theory of Atoms, Molecules, and the Solid State.* Academic Press, 1966.

171. J. M. Foster and S. F. Boys *Rev. Mod. Phys.*, vol. 32(2), p. 300, 1960.

172. J. Pipek and P. G. Mezey *J. Chem. Phys.*, vol. 90(9), p. 4916, 1989.

173. G. Knizia *J. Chem. Theory Comput.*, vol. 9, p. 4834, 2013.

174. J. Čížek and J. Paldus *Int. J. Quantum Chem.*, vol. 5, p. 359, 1971.

175. G. Stollhoff and P. Fulde *J. Chem. Phys.*, vol. 73, p. 4548, 1980.

176. G. Stollhoff and P. Vasilopulos *J. Chem. Phys.*, vol. 84, p. 2744, 1986.

177. G. Konig and G. Stollhoff *J. Phys. Chem.*, vol. 91, p. 2993, 1990.

178. T. Nagata, D. G. Fedorov, H. Li, and K. Kitaura *J. Chem. Phys.*, vol. 136, p. 204112, 2012.

179. G. D. Fletcher, D. G. Fedorov, S. R. Pruitt, T. L. Windus, and M. S. Gordon *J. Chem. Theo. Comp.*, vol. 8, p. 75, 2012.

180. T. Nagata, D. G. Fedorov, K. Ishimura, and K. Kitaura *J. Chem. Phys.*, vol. 135, p. 044110, 2011.

181. D. G. Fedorov, K. Ishimura, T. Ishida, K. Kitaura, P. Pulay, and S. Nagase *J. Comput. Chem.*, vol. 28, p. 1476, 2007.

182. A. D. Findlater, F. Zahariev, and M. S. Gordon *J. Phys. Chem. A*, vol. 119, p. 3587, 2015.

183. D. G. Fedorov and K. J. Kitaura *J. Chem. Phys.*, vol. 123, p. 134103, 2005.

184. W. Li and P. Piecuch *J. Phys. Chem. A*, vol. 114, p. 8644, 2010.

185. W. Li, P. Piecuch, J. R. Gour, and S. Li. *J. Chem. Phys.*, vol. 131, p. 114109, 2009.

186. W. Li and P. Piecuch *J. Phys. Chem. A*, vol. 114, p. 6721, 2010.

187. J. Friedrich and M. Dolg *J. Chem. Theory Comput.*, vol. 5, p. 287, 2009.

188. J. Friedrich, D. P. Tew, W. Klopper, and M. Dolg *J. Chem. Phys.*, vol. 132, p. 164114, 2010.

189. K. Walczak, J. Friedrich, and M. Dolg *Chem. Phys.*, vol. 376, p. 36, 2010.

190. J. Friedrich, M. Hanrath, and M. Dolg *J. Chem. Phys.*, vol. 126, p. 154110, 2007.

191. J. Friedrich and M. Dolg *J. Chem. Phys.*, vol. 129, p. 244105, 2008.

192. J. Friedrich, S. Coriani, T. Helgaker, and M. Dolg *J. Chem. Phys.*, vol. 131, p. 154102, 2009.

193. J. Friedrich and J. Hänchen *J. Chem. Theory Comput.*, vol. 9, p. 5381, 2013.

194. M. Ziółlkowski, B. Jansì, T. Kjærgaard, and P. Jørgensen *J. Chem. Phys.*, vol. 133, p. 014107, 2010.

195. K. Kristensen, M. Ziółlkowski, B. Jansìk, T. Kjærgaard, and P. Jørgensen *J. Chem. Theory Comput.*, vol. 7, p. 1677, 2011.

196. K. Kristensen, P. Jørgensen, B. Jansìk, T. Kjærgaard, and S. Reine *J. Chem. Phys.*, vol. 137, p. 114102, 2012.

197. J. J. Eriksen, P. Baudin, P. Ettenhuber, K. Kristensen, T. Kjærgaard, and P. Jørgensen *J. Chem. Theory Comput.*, vol. 11, p. 2984, 2015.

198. P. Y. Ayala and G. E. Scuseria *J. Chem. Phys.*, vol. 110, p. 3660, 1999.

199. J. Almlöf *Chem. Phys. Lett.*, vol. 181, p. 319, 1991.

200. M. Häser and J. Almlöf *J. Chem. Phys.*, vol. 96, p. 489, 1992.

201. M. Häser *Theor. Chim. Acta*, vol. 87, p. 147, 1993.

202. S. Sæbø, W. Tong, and P. Pulay *J. Chem. Phys.*, vol. 98, p. 2170, 1993.

203. M. Schütz, G. Rauhut, and H.-J. Werner *J. Phys. Chem. A*, vol. 102, p. 5997, 1998.

204. N. Runeberg, M. Schütz, and H.-J. Werner *J. Chem. Phys.*, vol. 110, p. 7210, 1999.

205. R. A. Chiles and C. E. Dykstra *Chem. Phys. Lett.*, vol. 80, p. 69, 1981.

206. P. Pulay *Int. J. Quantum Chem. Symp.*, vol. 17, p. 257, 1983.

207. P. Pulay and S. Sæbø *Chem. Phys. Lett.*, vol. 117, p. 37, 1985.

208. J. A. Pople, R. Krishnan, H. B. Schlegel, and J. S. Binkley *Int. J. Quantum Chem.*, vol. 14, p. 91, 1978.

209. R. J. Bartlett and G. D. P. III *Int. J. Quantum Chem.*, vol. 14, p. 561, 1978.

210. A. ElAzhary, G. Rauhut, P. Pulay, and H.-J. Werner *J. Chem. Phys.*, vol. 108, p. 5185, 1998.

211. G. Rauhut and H.-J. Werner *Phys. Chem. Chem. Phys.*, vol. 3, p. 4853, 2001.

212. N. J. Russ and T. D. Crawford *Chem. Phys. Lett.*, vol. 400, p. 104, 2004.

213. N. J. Russ and T. D. Crawford *J. Chem. Phys.*, vol. 121, p. 691, 2004.

214. G. Hetzer, P. Pulay, and H.-J. Werner *Chem. Phys. Lett.*, vol. 290, p. 143, 1998.

215. M. Schütz *Phys. Chem. Chem. Phys.*, vol. 4, p. 3941, 2002.

216. M. Schütz and H.-J. Werner *Chem. Phys. Lett.*, vol. 318, p. 370, 2000.

217. M. Schütz, G. Hetzer, and H.-J. Werner *J. Chem. Phys.*, vol. 111, p. 5691, 1999.

218. M. Schütz *J. Chem. Phys.*, vol. 113, p. 9986, 2000.

219. M. Schütz *J. Chem. Phys.*, vol. 116, p. 8772, 2002.

220. T. Korona and H.-J. Werner *J. Chem. Phys.*, vol. 118, p. 3006, 2003.

221. D. Kats, T. Korona, and M. Schütz *J. Chem. Phys.*, vol. 127, p. 064107, 2007.

222. D. Kats, T. Korona, and M. Schütz *J. Chem. Phys.*, vol. 125, p. 104106, 2006.

223. D. Kats and M. Schütz *Z. Phys. Chem.*, vol. 224, p. 601, 2010.

224. K. Freundorfer, D. Kats, T. Korona, and M. Schütz *J. Chem. Phys.*, vol. 133, p. 244110, 2010.

225. D. Kats and M. Schütz *J. Chem. Phys.*, vol. 131, p. 124117, 2009.

226. O. Vahtras, J. Almlöf, and M. W. Feyereisen *Chem. Phys. Lett.*, vol. 213, p. 514, 1993.

227. M. W. Feyereisen, G. Fitzgerald, and A. Komonicki *Chem. Phys. Lett.*, vol. 208, p. 359, 1993.

228. M. Schütz and F. R. Manby *Phys. Chem. Chem. Phys.*, vol. 5, p. 3349, 2003.

229. H.-J. Werner, F. R. Manby, and P. Knowles *J. Chem. Phys.*, vol. 118, p. 8149, 2003.

230. H.-J. Werner and F. R. Manby *J. Chem. Phys.*, vol. 124, p. 054114, 2006.

231. T. B. Adler, H.-J. Werner, and F. R. Manby *J. Chem. Phys.*, vol. 130, p. 054106, 2009.

232. R. Polly, H.-J. Werner, F. R. Manby, and P. J. Knowles *Mol. Phys.*, vol. 102, p. 2311, 2004.

233. M. Schütz, H.-J. Werner, R. Lindh, and F. R. Manby *J. Chem. Phys.*, vol. 121, p. 737, 2004.

234. F. R. Manby, H.-J. Werner, T. B. Adler, and A. J. May *J. Chem. Phys.*, vol. 124, p. 094103, 2006.

235. Q. Ma and H.-J. Werner *J. Chem. Theory Comput.*, vol. 11, p. 5291, 2015.

236. H.-J. Werner *J. Chem. Phys.*, vol. 129, p. 101103, 2008.

237. T. B. Adler and H.-J. Werner *J. Chem. Phys.*, vol. 130, p. 241101, 2009.

238. T. B. Adler, *Local explicitly correlated methods for the treatment of large molecules close to the basis set limit*. PhD thesis, Stuttgart Universität, 2010.

239. Y. Liu and H.-J. Werner *Unpublished*.

240. Y. Liu, *A local coupled-cluster method for open-shell molecules: DF-LUCCSDD(T)*. PhD thesis, Stuttgart Universität, 2011.

241. F. Agapito and H.-J. Werner *Unpublished*.

242. F. Menezes, D. Kats, and H.-J. Werner *J. Chem. Phys.*, vol. 145(12), p. 124115, 2016.

243. C. Edmiston and M. Krauss *J. Chem. Phys.*, vol. 42, p. 1119, 1965.

244. W. Meyer *Theor. Chim. Acta*, vol. 35, p. 277, 1974.

245. W. Meyer and P. Rosmus *J. Chem. Phys.*, vol. 63, p. 2356, 1975.

246. H.-J. Werner and W. Meyer *Mol. Phys.*, vol. 31, p. 855, 1976.

247. P. Botschwina and W. Meyer *J. Chem. Phys.*, vol. 67, p. 2390, 1977.

248. P. Botschwina and W. Meyer *Chem. Phys.*, vol. 20, p. 43, 1977.

249. P. Rosmus and W. Meyer *J. Chem. Phys.*, vol. 69, p. 2745, 1978.

250. W. Meyer *J. Chem. Phys.*, vol. 64, p. 2901, 1976.

251. W. Meyer, W. Jakubetz, and P. Schuster *Chem. Phys. Lett.*, vol. 21, p. 97, 1973.

252. W. Kutzelnigg *Theor. Chim. Acta (Berl.)*, vol. 1, p. 343, 1963.

253. R. Ahlrichs and F. Dreissler *Theor. Chim. Acta (Berl.)*, vol. 36, p. 275, 1975.

254. R. Ahlrichs, F. Driessler, H. Lischka, V. Staemmler, and W. Kutzelnigg *J. Chem. Phys.*, vol. 62, p. 1235, 1975.

255. R. Ahlrichs and W. Kutzelnigg *J. Chem. Phys.*, vol. 48, p. 1819, 1968.

256. R. Ahlrichs, H. Lischka, and V. Staemmler *J. Chem. Phys.*, vol. 62(4), p. 1225, 1975.

257. P. R. Taylor *J. Chem. Phys.*, vol. 74, p. 1256, 1981.

258. P. O. Löwdin *Phys. Rev.*, vol. 97, p. 1474, 1955.

259. D. G. Liakos and F. Neese *J. Phys. Chem. A*, vol. 116, p. 4801, 2012.

260. D. G. Liakos, A. Hansen, and F. Neese *J. Chem. Theory Comput.*, vol. 7, p. 76, 2011.

261. A. Hansen, D. G. Liakos, and F. Neese *J. Chem. Phys.*, vol. 135, p. 214102, 2011.

262. F. Neese, A. Hansen, and D. G. Liakos *J. Chem. Phys.*, vol. 131, p. 064103, 2009.

263. L. M. J. Huntington and M. Nooijen *J. Chem. Phys.*, vol. 133, p. 184109, 2010.

264. C. Riplinger, P. Pinski, U. Becker, E. F. Valeev, and F. Neese *J. Chem. Phys.*, vol. 144, p. 024109, 2016.

265. M. Schwilk, D. Usvyat, and H.-J. Werner *J. Chem. Phys.*, vol. 142(12), p. 121102, 2015.

266. C. Hättig, D. P. Tew, and B. Helmich *J. Chem. Phys.*, vol. 136, p. 204105, 2012.

267. D. P. Tew, B. Helmich, and C. Hättig *J. Chem. Phys.*, vol. 135, p. 074107, 2011.

268. D. P. Tew and C. Hättig *Int. J. Quantum Chem.*, vol. 113, p. 224, 2013.

269. G. Schmitz, C. Hättig, and D. P. Tew *Phys. Chem. Chem. Phys.*, vol. 16, p. 22167, 2014.

270. F. Pavošević, F. Neese, and E. F. Valeev *J. Chem. Phys.*, vol. 141, p. 054106, 2014.

271. B. Helmich and C. Hättig *J. Chem. Phys.*, vol. 135, p. 104111, 2011.

272. B. Helmich and C. Hättig *J. Chem. Phys.*, vol. 135, p. 214106, 2011.

273. B. Helmich and C. Hättig *J. Chem. Phys.*, vol. 139, p. 084114, 2013.

274. B. Helmich and C. Hättig *Comput. Theor. Chem.*, vol. 35, p. 1040, 2014.

275. D. Walter, A. Venkatnathan, and E. A. Carter *J. Chem. Phys.*, vol. 118, p. 8127, 2003.

276. D. Walter, A. B. Szilva, K. Niedfeldt, and E. A. Carter *J. Chem. Phys.*, vol. 117, p. 1982, 2002.

277. D. Walter and E. A. Carter *Chem. Phys. Lett.*, vol. 346, p. 177, 2001.

278. G. Reynolds and E. A. Carter *Chem. Phys. Lett.*, vol. 265, p. 660, 1997.

279. G. Reynolds, T. J. Martinez, and E. A. Carter *J. Chem. Phys.*, vol. 105, p. 6455, 1996.

280. T. S. Chwee, A. B. Szilva, R. Lindh, and E. A. Carter *J. Chem. Phys.*, vol. 128, p. 224106, 2008.

281. D. B. Krisiloff, C. M. Krauter, F. J. Ricci, and E. A. Carter *J. Chem. Theory Comput.*, vol. 11, p. 5242, 2015.

282. S. Hoyau, D. Maynau, and J. P. Malrieu *J. Chem. Phys.*, vol. 134, p. 054125, 2011.

283. O. Demel, J. Pittner, and F. Neese *J. Chem. Theory Comput.*, vol. 11, p. 3104, 2015.

284. H.-J. Werner, P. J. Knowles, G. Knizia, F. R. Manby, and M. Schütz *WIREs Comput. Mol. Sci.*, vol. 2, p. 242, 2012.

285. K. R. Shamasundar, G. Knizia, and H.-J. Werner, "The integrated tensor framework (itf)," 2011. [Online; accessed 22-May-2016].

286. D. Kats and F. R. Manby *J. Chem. Phys.*, vol. 138, p. 144101, 2013.

287. D. Kats *J. Chem. Phys.*, vol. 141, p. 244101, 2014.

288. A. Szabo and N. S. Ostlund, *Modern Quantum Chemistry: Introduction to Advanced Electronic Structure Theory*, ch. Maathematical Review. In *Dover Books on Chemistry* (*414*), 1996.

289. A. Szabo and N. S. Ostlund, *Modern Quantum Chemistry: Introduction to Advanced Electronic Structure Theory*, ch. Many-Electron Wave Functions and Operators. In *Dover Books on Chemistry* (*414*), 1996.

290. A. Szabo and N. S. Ostlund, *Modern Quantum Chemistry: Introduction to Advanced Electronic Structure Theory*, ch. The Hartree-Fock Approximation. In *Dover Books on Chemistry* (*414*), 1996.

291. B. T. Colegrove and H. H. S. III *J. Phys. Chem.*, vol. 94(14), p. 5593, 1990.

292. A. Szabo and N. S. Ostlund, *Modern Quantum Chemistry: Introduction to Advanced Electronic Structure Theory*, ch. Configuration Interaction. In *Dover Books on Chemistry* (*414*), 1996.

293. A. Szabo and N. S. Ostlund, *Modern Quantum Chemistry: Introduction to Advanced Electronic Structure Theory*, ch. Pair and Coupled-Pair Theories. In *Dover Books on Chemistry (414)*, 1996.

294. E. Davidson *J. Comp. Phys.*, vol. 17, p. 87, 1975.

295. T. D. Crawford, "Size-extensivity and size-consistency," 1996. [Online; accessed 7-January-2016].

296. O. Christiansen, H. Koch, and P. Jørgensen *Chem. Phys. Lett.*, vol. 243, p. 409, 1995.

297. D. C. Comeau and R. J. Bartlett *Chem. Phys. Lett.*, vol. 207, p. 414, 1993.

298. S. A. Kucharski, M. Włoch, M. Musiał, and R. Bartlett *J. Chem. Phys.*, vol. 115, p. 8263, 2001.

299. K. Kowalski and P. Piecuch *J. Chem. Phys.*, vol. 113(19), p. 8490, 2000.

300. K. Kowalski and P. Piecuch *J. Chem. Phys.*, vol. 115(2), p. 643, 2001.

301. P. Piecuch and R. J. Bartlett *Adv. Quantum Chem.*, vol. 34, p. 295, 1999.

302. D. Kats and F. R. Manby *J. Chem. Phys.*, vol. 139, p. 021102, 2013.

303. D. F. Feller, M. W. Schmidt, and K. Ruedenberg *J. Am. Chem. Soc.*, vol. 104, p. 960, 1982.

304. K. Ruedenberg, M. W. Schmidt, and M. M. Gilbert *Chem. Phys.*, vol. 71, p. 51, 1982.

305. K. Ruedenberg, M. W. Schmidt, M. M. Gilbert, and S. T. Elbert *Chem. Phys.*, vol. 71, p. 65, 1982.

306. L. M. Cheung, K. R. Sundeberg, and K. Ruedenberg *J. Am. Chem. Soc.*, vol. 100, p. 8024, 1978.

307. L. M. Cheung, K. R. Sundeberg, and K. Ruedenberg *Int. J. Quant. Chem.*, vol. 16, p. 1103, 1979.

308. J. Olsen, B. O. Roos, P. Jørgensen, and H. J. Jensen *J. Chem. Phys.*, vol. 89, p. 2185, 1988.

309. H.-J. Werner and M. Meyer *J. Chem. Phys.*, vol. 74, p. 5794, 1981.

310. P. Pulay *Chem. Phys. Lett.*, vol. 73, p. 393, 1980.

311. P. Pulay *J. Comput. Chem.*, vol. 3, p. 556, 1982.

312. K. K. Docken and J. Hinze *J. Chem. Phys.*, vol. 57, p. 4928, 1972.

313. M. W. Schmidt and M. S. Gordon *Ann. Rev. Phys. Chem.*, vol. 49, p. 233, 1998.

314. U. Kaldor *J. Chem. Phys.*, vol. 63(5), p. 2199, 1975.

315. C. Edmiston and K. Ruedenberg *J. Chem. Phys.*, vol. 43, p. S97, 1965.

316. S. Dubillard, J.-B. Rota, T. Saue, and K. Faegri *J. Chem. Phys.*, vol. 124, p. 154307, 2006.

317. W. C. Lu, C. Z. Wang, M. W. Schmidt, L. Bytautas, K. M. Ho, and K. Ruedenberg *J. Chem. Phys.*, vol. 120, p. 2629, 2004.

318. A. C. West, M. W. Schmidt, M. S. Gordon, and K. Ruedenberg *J. Chem. Phys.*, vol. 139, p. 234107, 2013.

319. T. Janowski *J. Chem. Theory Comput.*, vol. 10, p. 3085, 2014.

320. D. E. Bernholdt and R. J. Harrison *Chem. Phys. Lett.*, vol. 250, p. 477, 1996.

321. J. L. Whitten *J. Chem. Phys.*, vol. 58, p. 4496, 1973.

322. F. Weigend *Phys. Chem. Chem. Phys.*, vol. 4, p. 4285, 2002.

323. F. Weigend, A. Köhn, and C. Häattig *J. Chem. Phys.*, vol. 116, p. 3175, 2002.

324. F. Weigend, M. Häser, H. Patzelt, and R. Ahlrichs *Chem. Phys. Lett.*, vol. 294, p. 143, 1998.

325. G. Hetzer, M. Schütz, H. Stoll, and H.-J. Werner *J. Chem. Phys.*, vol. 113, p. 9443, 2000.

326. T. B. Adler, H.-J. Werner, and F. R. Manby *J. Chem. Phys.*, vol. 135, p. 144117, 2011.

327. W. Boughton and P. Pulay *J. Comput. Chem.*, vol. 14, p. 736, 1993.

328. H.-J. Werner and K. Pflüger *Ann. Rep. Comp. Chem.*, vol. 2, p. 53, 2006.

329. R. Mata and H.-J. Werner *Mol. Phys.*, vol. 105, p. 2753, 2007.

330. A. E. Reed, R. B. Weinstock, and F. Weinhold *J. Chem. Phys.*, vol. 83, p. 735, 1985.

331. H.-J. Werner and K. Pflüger *Ann. Reports in Comp. Chem.*, vol. 2, p. 53, 2006.

332. M. Rintelman, I. Adamovic, S. Varganov, and M. S. Gordon *J. Chem. Phys.*, vol. 122(4), p. 044105, 2005.

333. Y. Kurashige and T. Yanai *J. Chem. Phys.*, vol. 135, p. 094104, 2011.

334. N. Forsberg and P.-Å. Malmqvist *Chem. Phys. Lett.*, vol. 274, p. 196, 1997.

335. H. Nakano *J. Chem. Phys.*, vol. 99(10), p. 7983, 1993.

336. H. Nakano *Chem. Phys. Lett.*, vol. 207, p. 372, 1993.

337. P. J. Knowles and H.-J. Werner *Chem. Phys. Lett.*, vol. 145, p. 514, 1988.

338. W. Meyer, *Methods of Electronic Structure Theory*, ch. Configuration Expansion by Means of Pseudonatural Orbitals. Plenum, 1977.

339. P. E. M. Siegbahn *Int. J. Quantum Chem.*, vol. 18, p. 1229, 1980.

340. B. O. Roos *Adv. Chem. Phys.*, vol. 69, p. 399, 1987.

341. T. Yanai, Y. Kurashige, E. Neuscamman, and G. K.-L. Chan *Phys. Chem. Chem. Phys.*, vol. 14, p. 7809, 2012.

342. T. Yanai and G. K.-L. Chan *J. Chem. Phys.*, vol. 124, p. 194106, 2006.

343. E. Neuscamman, T. Yanai, and G. K.-L. Chan *Int. Rev. Phys. Chem.*, vol. 29, p. 231, 2010.

344. T. Yanai and G. K.-L. Chan *J. Chem. Phys.*, vol. 127, p. 104107, 2007.

345. G. K.-L. Chan and T. Yanai *Adv. Chem. Phys.*, vol. 134, p. 343, 2007.

346. E. Neuscamman, T. Yanai, and G. K.-L. Chan *J. Chem. Phys.*, vol. 130, p. 124102, 2009.

347. E. Neuscamman, T. Yanai, and G. K.-L. Chan *J. Chem. Phys.*, vol. 132, p. 024106, 2010.

348. T. Yanai, Y. Kurashige, E. Neuscamman, and G. K.-L. Chan *J. Chem. Phys.*, vol. 132, p. 024105, 2010.

349. K. Sivalingam, M. Krupicka, A. A. Auer, and F. Neese *J. Chem. Phys.*, vol. 145, p. 054104, 2016.

350. C. Hampel, K. A. Peterson, and H.-J. Werner *Chem. Phys. Lett.*, vol. 190, p. 1, 1992.

351. P. Pulay, S. Saebø, and W. Meyer *J. Chem. Phys.*, vol. 81, p. 1901, 1984.

352. G. E. Scuseria, C. L. Janssen, and H. F. S. III *J. Chem. Phys.*, vol. 89, p. 7382, 1988.

353. W. Meyer *J. Chem. Phys.*, vol. 64, p. 2901, 1976.

354. J. Grotendorst, ed., *Modern Methods and Algorithms of Quantum Chemistry*. Dover Books on Chemistry, John von Neumann Institute for Computing, 2000.

355. P. O. Löwdin *J. Chem. Phys.*, vol. 18, p. 365, 1950.

356. P. O. Löwdin *Adv. Phys.*, vol. 5(17), p. 1, 1956.

357. R. Mata and H.-J. Werner *J. Chem. Phys.*, vol. 125, p. 184110, 2006.

358. G. Schmitz, B. Helmich, and C. Hättig *Mol. Phys.*, vol. 111, p. 2463, 2013.

359. D. Kats, "Quantwo." Unpublished, 2012-2016.

360. E. A. Hylleraas *Z. Phys.*, vol. 65, p. 209, 1930.

361. K. Andersson *Chem. Phys. Lett.*, vol. 237, p. 212, 1995.

362. H.-J. Werner, P. J. Knowles, G. Knizia, F. R. Manby, M. Schütz, P. Celani, W. Györffy, D. Kats, T. Korona, R. Lindh, A. Mitrushenkov, G. Rauhut, K. R. Shamasundar, T. B. Adler, R. D. Amos, A. Bernhardsson, A. Berning, D. L. Cooper, M. J. O. Deegan, A. J. Dobbyn, F. Eckert, E. Goll, C. Hampel, A. Hesselmann, G. Hetzer, T. Hrenar, G. Jansen, C. Köppl, Y. Liu, A. W. Lloyd, R. A. Mata, A. J. May, S. J. McNicholas, W. Meyer, M. E. Mura, A. Nicklass, D. P. O'Neill, P. Palmieri, D. Peng, K. Pflüger, R. Pitzer, M. Reiher, T. Shiozaki, H. Stoll, A. J.

Stone, R. Tarroni, T. Thorsteinsson, and M. Wang, "Molpro, version 2015.1, a package of ab initio programs," 2015. see.

363. J. Nieplocha, B. Palmer, V. Tipparaju, M. Krishnan, H. Trease, and E. Aprà *Int. J. High Perform. Comp. App.*, vol. 20, p. 203, 2006.

364. T. H. Dunning *J. Chem. Phys.*, vol. 90, p. 1007, 1989.

365. R. A. Kendall, T. H. Dunning, and R. J. Harrison *J. Chem. Phys.*, vol. 96, p. 6796, 1992.

366. T. H. Dunning, K. A. Peterson, and A. Wilson *J. Chem. Phys.*, vol. 114, p. 9244, 2001.

367. D. E. Woon and T. H. Dunning *J. Chem. Phys.*, vol. 98, p. 1358, 1993.

368. K. A. Peterson, D. E. Woon, and T. H. Dunning *J. Chem. Phys.*, vol. 100, p. 7410, 1994.

369. A. K. Wilson, T. van Mourik, and T. H. Dunning *J. Mol. Struct. THEOCHEM*, vol. 388, p. 339, 1996.

370. F. Weigend and R. Ahlrichs *Phys. Chem. Chem. Phys.*, vol. 7, p. 3297, 2005.

371. H.-J. Werner and P. J. Knowles *J. Chem. Phys.*, vol. 82, p. 5053, 1985.

372. P. J. Knowles and H.-J. Werner *Chem. Phys. Lett.*, vol. 115, p. 259, 1985.

373. C. Köppl and H.-J. Werner *J. Chem. Theory Comput.*, 2016.

374. P. J. Knowles, C. Hampel, and H.-J. Werner *J. Chem. Phys.*, vol. 99, p. 5219, 1993.

375. C. Hampel, K. Peterson, and H.-J. Werner *Chem. Phys. Lett.*, vol. 190, p. 1, 1992.

376. M. J. O. Deegan and P. J. Knowles *Chem. Phys. Lett.*, vol. 227, p. 321, 1994.

377. L. Groenendaal, F. Jonas, D. Freitag, H. Pielartzik, and J. R. Reynolds *Adv. Mater.*, vol. 12, p. 481, 2000.

378. J. Y. Kim, J. H. Jung, D. E. Lee, and J. Joo *Synth. Met.*, vol. 126, p. 311, 2002.

379. J. Ouyang, Q. Xu, C.-W. Chu, Y. Yang, G. Li, and J. Shinar *Pol.*, vol. 45, p. 8443, 2004.

380. M. Döbbelin, R. Marcilla, M. Salsamendi, C. Pozo-Gonzalo, P. M. Carrasco, J. A. Pomposo, and D. Mecerreyes *Chem. Mater.*, vol. 19, p. 2147, 2007.

381. B. Fan, X. Mei, and J. Ouyang *Macromol.*, vol. 41, p. 5971, 2008.

382. M. Olivucci, F. Bernardi, P. Celani, I. Ragazos, and M. A. Robb *J. Am. Chem. Soc.*, vol. 116(3), p. 1077, 1994.

383. A. Fedorov, L. Batiste, E. P. A. Couzijn, and P. Chen *ChemPhysChem*, vol. 11, p. 1002, 2010.

384. T. Madrakian, A. Afkhami, M. Borazjani, and M. Bahram *Bull. Kor. Chem. Soc.*, vol. 25, p. 12, 2004.

385. R. Bersohn, U. Even, and J. Jortner *J. Chem. Phys.*, vol. 80, p. 1050, 1984.

386. S. Siva, G. Venkatesh, A. A. M. Prabhu, R. K. Sankaranarayanan, and N. Rejendiran *Phys. Chem. Liq.*, vol. 50, p. 434, 2012.

387. T. A. LeGreve, E. E. Baquero, and T. S. Zwier *J. Am. Chem. Soc.*, vol. 129(13), p. 4028, 2007.

388. T. Madrakian, A. Afkhami, M. Borazjani, and M. Bahram *Bull. Korean Chem. Soc.*, vol. 25(12), p. 1764, 2004.

389. H. Edelhoch *Biochem.*, vol. 6(7), p. 1948, 1967.

390. P. Foggi, F. V. R. Neuwahl, L. Moroni, and P. R. Salvi *J. Phys. Chem. A*, vol. 107, p. 1689, 2003.

391. [Online; accessed 8-May-2016].

392. P. J. S. Gomes, C. Serpa, and L. G. Arnaut *J. Photochem. Photobiol. A: Chem*, vol. 184, p. 228, 2006.

393. G. A. George and G. C. Morris *J. Mol. Spectrosc.*, vol. 26, p. 67, 1968.

394. P. K. Jha and G. P. Halada *Chem. Cent. J.*, vol. 5, p. 12, 2011.

395. A. M. El-Zohry and E. Y. Hashem *J. Spec.*, vol. 2013, 2013.

396. A. Bartecki, J. Szoke, G. Varsanyi, and M. Vizesy, *Absorption Spectra in the Ultraviolet and Visible Region, Vol. 3.* Academic Press, 1966.

397. P. M. Clayton, C. A. Vas, T. T. T. Bui, A. F. Drake, and K. Mcadam *Chir.*, vol. 25, p. 288, 2013.

398. R. F. Evans, E. F. G. Herington, and W. Kynaston *Trans. Faraday Soc.*, vol. 49, p. 1284, 1953.

399. E. B. Hughes, H. H. G. Jellinek, and B. A. Ambrose *J. Phys. Chem.*, vol. 53(3), p. 410, 1949.

400. K. O. Honikel and N. B. Madsen *J. Biol. Chem.*, vol. 247(4), p. 1057, 1972.

401. M. Adrover, J. Frau, C. Caldeés, B. Vilanova, J. Donoso, and F. Muñoz *J. Photochem. Photobiol. A: Chem*, vol. 209, p. 19, 2010.

402. M. Aranda and G. Morlock *J. Chrom. A*, vol. 1131(1), p. 253, 2006.

403. R. A. Jones, ed., *The Chemistry of Heterocyclic Compounds, Pyrroles*. Wiley, 1990.

404. F. S. Boig, G. W. Costa, and I. Osvar *J. Org. Chem.*, vol. 18(7), p. 775, 1953.

405. R. Pacios, R. Marcilla, C. Pozo-Gonzalo, J. A. Pomposo, H. Grande, J. Aizpurua, and D. Mecerreyes *J. Nanosc. Nanotech.*, vol. 7, p. 2938, 2007.

406. J. E. Subotnik and M. Head-Gordon *J. Chem. Phys.*, vol. 123, p. 064108, 2005.

407. T. H. Dunning and V. McKoy *J. Chem. Phys.*, vol. 47(5), p. 1735, 1967.

408. M. T. Nguyen, M. H. Matus, W. A. Lester, and D. A. Dixon *J. Phys. Chem. A*, vol. 112(10), p. 2082, 2008.

409. F. Qi, O. Sorkhabi, and A. G. Suits *J. Chem. Phys.*, vol. 112, p. 10707, 2000.

410. S. J. Blanksby and G. B. Ellison *Acc. Chem. Res.*, vol. 36(4), p. 255, 2003.

411. K. M. Ervin, S. Gronert, S. E. Barlow, M. K. Gilles, A. G. Harrison, V. M. Bierbaum, C. H. DePuy, W. C. Lineberger, and G. B. Ellison *J. Am. Chem. Soc.*, vol. 112, p. 5750, 1990.

412. K. Nakayama, H. Nakano, and K. Hirao *Int. J. Quantum Chem.*, vol. 66, p. 157, 1998.

413. J. Quenneville and T. J. Martinez *J. Phys. Chem. A*, vol. 107, p. 829, 2003.

414. A. Szabo and N. S. Ostlund, *Modern Quantum Chemistry: Introduction to Advanced Electronic Structure Theory.* Dover Books on Chemistry, Dover Publications, 1996.

415. K. P. Lawley, ed., *Ab Initio Methods in Quantum Chemistry II.* Wiley, 1987.

416. D. R. Yarkony, ed., *Modern Electronic Structure Theory.* World Scientific, 1994.